Techno-economic modeling and robust optimization of power systems planning under a high share of renewable energy sources and extreme weather events

Adam Abdin

université PARIS-SACLAY

CentraleSupélec

NNT : 2019SACLC046

Techno-economic modeling and robust optimization of power systems planning under a high share of renewable energy sources and extreme weather events

Thèse de doctorat de l'Université Paris-Saclay
préparée à CentraleSupélec

École doctorale n°573 Interfaces : Approches Interdisciplinaires / Fondements, Application et Innovation (Interfaces)
Spécialité de doctorat: Ingénierie des Systèmes Complexes

Thèse présentée et soutenue à Gif-sur-Yvette, le 23/07/2019, par

ISLAM F. ABDIN

Composition du Jury :

Guillaume Sandou Professor, CentraleSupélec, Control Department	President
Jay Apt Professor, Carnegie Mellon University, College of Engineering	Rapporteur
Antonio Conejo Professor, Ohio State University, College of Engineering	Rapporteur
Michel-Alexandre Cardin Associate Professor, Imperial College London, Faculty of Engineering	Rapporteur
Paola Girdinio Professeur, Universita degli Studi di Genova Department of Electrical Engineering	Examinateur
Yi Ding Professor, Zhejiang University, College of Electrical Engineering	Examinateur
Wim van Ackooij Ingénieur de Recherche (HDR), Electricité De France R&D	Examinateur
Enrico Zio Professor, Mines Paristech, PSL Research University Politecnico di Milano, Department of Energy	Directeur de thèse

Thèse de doctorat

CentraleSupelec, Université Paris-Saclay

Doctoral Thesis

Techno-economic modeling and robust optimization of power systems planning under a high share of renewable energy sources and extreme weather events

---

Author:
Islam F. Abdin

Supervisor:
Prof. Enrico Zio

August 02, 2019

To M. F. Abdin (Prof. Dr.-Ing.)
my dear father

Acknowledgements

I would like to express my sincere gratitude to my thesis advisor, Prof. Enrico Zio, for his generous support in developing this research work, for his constant encouragement and for his significant efforts in ensuring its scientific rigor. Thank you, also, for constantly spreading enthusiasm in our attempts to contribute to scientific research.

I extend my appreciation to Dr. Aakil Caunhye and Dr. Yiping Fang for our collaborations and their contributions to some of the methods developed in this thesis and for the many interesting discussions we had around its themes. I would also like to thank Dr. Sebastien Lepaul from EDF R& D for his support and encouragement and for his efforts in organizing the different workshops and seminars where we had the chance to discuss the work with our industrial partners in EDF.

My sincere gratitude for Prof. Michel-Alexandre Cardin, Dr. Aakil Caunhye and Dr. Elizaveta Kuznetsova for welcoming me within their team at the Future Resilient Systems laboratory - Singapore-ETH Centre (SEC), National University of Singapore, where I got the chance to expand my knowledge on resilience of complex systems and robust optimization methods.

To the honorable jury members: Prof. Jay Apt, Prof. Antonio J. Conejo, Prof. Michel-Alexandre Cardin, Prof. Guillaume Sandou, Prof. Paola Girdinio, Prof. Yi Ding and Dr. Wim van Akooij, my sincere gratitude for your time and consideration. It was an absolute privilege having defended this thesis before such excelled academics and professionals who are real references in their domains. I am very grateful for the constructive remarks, comments, suggestions and your kind encouragement.

My warmest feelings to all my colleagues and the supporting staff at the Laboratory of Industrial Engineering, CentraleSupelec, Universite Paris-Saclay, where I have started and completed this Ph.D. thesis. Every one of them contributed to my personal and scientific growth and to the amazing time I had during those years.

My deepest gratitude to my family.

Abstract

Recent objectives for power systems sustainability and mitigation of climate change threats are modifying the breadth of power systems planning requirements. On one hand, sustainable low carbon power systems which have a high share of intermittent renewable energy sources (IRES) are characterized by a sharp increase in inter-temporal variability, and require flexible systems able to cope and ensure the security of electricity supply. On the other hand, the increased frequency and severity of extreme weather events threatens the reliability of power systems operation, and require resilient systems able to withstand those potential impacts. All of which while ensuring that the inherent system uncertainties are adequately accounted for directly at the issuance of the long-term planning decisions.

In this context, the present thesis aims at developing a techno-economic modeling and robust optimization framework for multi-period power systems planning considering a high share of IRES and resilience against extreme weather events. The specific planning problem considered is that of selecting the technology choice, size and commissioning schedule of conventional and renewable generation units under technical, economical, environmental and operational constraints. Within this problem, key research questions to be addressed are: (i) the proper integration and assessment of the operational flexibility needs due to the increased variability of the high shares of IRES production, (ii) the appropriate modeling and incorporation of the resilience requirements against extreme weather events within the power system planning problem and (iii) the representation and treatment of the inherent uncertainties in the system supply and demand within this planning context.

To this end, we first introduce an integrated framework for operational flexibility assessment in power system planning with a significant share of IRES. The framework stands on: (i) the formulation of an integrated generation expansion planning (GEP) and unit commitment (UC) model accounting for key short-term technical constraints, (ii) the elaboration of accurate and systematic horizon reduction methods to alleviate the computational burden of the resulting large-sized optimization problem and (iii) the definition of suitable metrics for the operational flexibility assessment of the obtained plans. The framework is applied to the multi-annual planning horizon of a realistically sized case study, under several scenarios of IRES penetration levels and carbon limits to validate its superiority in accounting for the needs of operational flexibility compared to conventional planning methods.

The framework proposed is, then, extended to incorporate the system resilience against extreme weather events. Specifically, a set of piece-wise linear models are developed to calculate the impact of extreme heat waves and drought events on the performance of the power generation units and on the system load. A method for integrating this impact within a resilient planning approach is, then, proposed

and the results are analyzed for case studies under real future climate projections obtained from the Coupled Model Intercomparison Project phase 5.

Finally, to account for the various supply and demand uncertainties, the power system planning model with dynamic constraints is treated within a multi-stage adaptive robust optimization. The uncertainty of electricity demand and renewable power generation is taken into account through distribution-free bounded intervals, with parameters that permit control over the level of conservatism of the solution. A solution method based on linear decision rules and information-level approximation is also presented. The method is, then, applied to the case study and the results confirm the effectiveness of the proposed approach especially in coping with multi-fold short-term ramping uncertainties in power systems planning.

In summary, the original contributions of this thesis are:

- Proposing a computationally efficient multi-period integrated generation expansion planning and unit commitment model that accounts for key short-term constraints and chronological system representation to derive the planning decisions under a high share of renewable energy penetration.
- Introducing the expected flexibility shortfall metric for operational flexibility assessment.
- Proposing a set of piece-wise linear models to quantify the impact of extreme heat waves and water availability on the derating of thermal and nuclear power generation units, renewable generation production and system load.
- Presenting a method for explicitly incorporating the impact of the extreme weather events in a modified power system planning model.
- Treating the inherent uncertainties in the electric power system planning parameters via a novel implementation of a multi-stage adaptive robust optimization model.
- Proposing a novel solution method based on "information basis" approximation for the linear decision rules of the affinely adjustable robust planning model.
- Applying the framework proposed to a practical size case studies based on realistic climate projections and under several scenarios of renewable penetration levels and carbon limits to validate the relevance of the overall modeling for real applications.

Résumé

Les objectifs récents en ce qui concerne la durabilité des systèmes électriques et l'atténuation des menaces liées au changement climatique modifient la portée des exigences de planification des systèmes électriques. D'une part, les systèmes durables d'énergie à faible émission de carbone qui comportent une part élevée de sources d'énergie renouvelables intermittentes (IRES) se caractérisent par une forte augmentation de la variabilité intertemporelle et nécessitent des systèmes flexibles capables d'assurer la sécurité de l'approvisionnement électrique. D'autre part, la fréquence et la gravité accrues des phénomènes climatiques extrêmes menacent la fiabilité du fonctionnement des réseaux électriques et exigent des systèmes résilients capables de résister à ces impacts potentiels. Tout en s'assurant que les incertitudes inhérentes au système sont bien prises en compte directement au moment de la prise des décisions de planification à long terme.

Dans ce contexte, la présente thèse vise à développer une modélisation technico-économique et un cadre d'optimisation robuste pour la planification des systèmes électriques multi-périodes en considérant une part élevée d'IRES et la résilience aux phénomènes climatiques extrêmes. Le problème spécifique de planification considéré est celui du choix de la technologie, de la taille et du programme de mise en service des unités de production conventionnelles et renouvelables sous des contraintes techniques, économiques, environnementales et opérationnelles. Dans le cadre de ce problème, les principales questions de recherche à aborder sont : (i) l'intégration et l'évaluation appropriées des besoins de flexibilité opérationnelle en raison de la variabilité accrue des parts élevées de la production d'IRES, (ii) la modélisation et l'intégration appropriées des exigences de résilience contre les phénomènes climatiques extrêmes dans la planification du système électrique et (iii) le traitement des incertitudes inhérentes de l'offre et la demande dans ce cadre de planification.

Dans ce but, nous introduisons d'abord un cadre intégré pour l'évaluation de la flexibilité opérationnelle dans la planification des systèmes électriques avec une part élevée de l'IRES. Le cadre comprend : (i) la formulation d'un modèle intégré de planification de l'expansion de la production (GEP) et d'engagement unitaire (UC) tenant compte des principales contraintes techniques à court terme, (ii) l'élaboration de méthodes précises et systématiques de réduction de l'horizon pour alléger la charge de calcul du problème d'optimisation à grande échelle qui en résulte et (iii) la définition des métriques adaptées pour évaluer la flexibilité opérationnelle des plans. Le cadre est appliqué à une période de planification pluriannuelle d'une étude de cas de taille réaliste, dans le cadre de plusieurs scénarios de taux de pénétration IRES et de limites de carbone, afin de valider sa supériorité pour tenir compte des besoins de flexibilité opérationnelle par rapport aux méthodes de planification classiques.

Le cadre proposé est ensuite prolongé pour intégrer la résilience du système face aux phénomènes climatiques extrêmes. Plus précisément, un ensemble de modèles linéaires sont développés pour calculer l'impact des vagues de chaleur extrême et des épisodes de sécheresse sur la performance des générateurs électriques et sur la demande du système. Une méthode d'intégration de cet impact dans le model de planification est ensuite proposée et les résultats sont analysés pour des études de cas sous des projections climatiques futures réelles obtenues de la Coupled Model Intercomparison Project phase 5 .

Enfin, pour prendre en compte les différentes incertitudes de l'offre et de la demande, le modèle de planification du système électrique à contraintes dynamiques est traité dans une optimisation adaptative robuste et multi-étape. L'incertitude de la demande d'électricité et de la production d'énergie renouvelable est prise en compte par le biais d'intervalles délimités sans distribution, avec des paramètres qui permettent de contrôler le niveau de conservatisme de la solution. Une méthode de solution basée sur des règles de décision linéaires et une approximation au niveau de l'information est également présentée. La méthode est ensuite appliquée à l'étude de cas et les résultats confirment l'efficacité de l'approche proposée, en particulier pour ce qui est de faire face aux incertitudes à court terme de la planification des systèmes électriques qui sont multiples et variables.

En résumé, les contributions originales de cette thèse sont :

- Proposer un modèle de planification du système électrique intégré multipériode avec des contraintes dynamiques et en considérant un pourcentage élevé de pénétration des énergies renouvelables.
- Introduire la mesure du déficit de flexibilité prévu pour l'évaluation de la flexibilité opérationnelle.
- Proposer un ensemble de modèles linéaires pour quantifier l'impact des vagues de chaleur extrêmes et de la disponibilité de l'eau sur le déclassement des unités de production d'énergie thermique et nucléaire, la production d'énergie renouvelable et la consommation électrique du système.
- Présenter une méthode permettant d'intégrer explicitement l'impact des phénomènes climatiques extrêmes dans le modèle de planification du système électrique.
- Traiter les incertitudes inhérentes aux paramètres de planification du système électrique par la mise en œuvre d'un nouveau modèle d'optimisation adaptatif robuste à plusieurs phases.
- Proposer une nouvelle méthode de solution basée sur l'approximation des règles de décision linéaires du modèle de planification robuste.
- Appliquer le cadre proposé à des études de cas de taille pratique basées sur des projections climatiques réalistes et selon plusieurs scénarios de niveaux de pénétration des énergies renouvelables et de limites de carbone pour valider la pertinence de la modélisation globale pour des applications réelles.

Contents

List of Figures

List of Tables

Nomenclature

Indexes:

b	index of bin in the LDC segmentation
c	index of LDC being approximated
d	index of days
i	index of power plant technology cluster
m	index of load-levels
n	index of approximation step for step-function approximation
s	index of sub-periods (weeks or days)
t	index of hours
w	index of weeks
y	index of planning year

Sets:

Θ	set of investment decision variables
Ω	set of operating decision variables
B	set of bins for the LDC segmentation
C	set of LDCs of the planning horizon
D	set of days within a year
I	set of power plant technology clusters
I^{new}	subset of new power plants cluster
I^{res}	subset of renewable power plants
I^{th}	subset of thermal and nuclear power plants
M	set of load-levels
S	set of weekly or daily sub-periods
T	set of hourly sub-periods
$\mathcal{U}_{yst}(\Gamma)$	polyhedral uncertainty set for uncertain parameters
W	set of weeks within a year
Y	set of years in the planning horizon

Parameters:

α	share of waste heat released into the air	(%)
β	efficiency degrading rate when T'^{in_w} is in the range of $[T'_{health}, T'_{risk}]$	(%)
ϵ_i	Expected forced outage rate of power plant technology i	(%)
Γ	parameter to control the level of conservatism of the decision maker (uncertainty budget)	/

$\mu_{(c,b,d)}$	share of time for day (d) during which the time-series has a value greater than or equal to the lowest value in the range corresponding to bin (b)	(hours)
$\vartheta_{(c,b)}$	share of time for LDC (c) during which the time-series has a value greater than or equal to the lowest value in the range corresponding to bin (b)	(hours)
ζ_{it}^{ewe}	power supply efficiency of power plant (i) at time (t) under the respective temperature and water availability conditions	(%)
a^{res}	percentage of the variable generation output covered by secondary reserve	(%)
A_{it}	hourly availability of intake cooling flow at plant (i), time (t)	(%)
B_y^{max}	maximum budget available for investment in generation expansion for year (y)	(M€)
C_i^{inv}	investment cost of power plants of technology (i)	(M€)
C_i^{fom}	fixed O&M costs of power plant technology (i)	(€)
C_i^{stup}	start-up cost of power plant technology (i)	(€)
$C_{i,y}^{mrgl}$	marginal cost of power plant (i) including the variable O&M and CO_2 costs, considering inflation	(€/ MWh)
C^l	temperature sensitivity coefficient of electricity load	(MW/°C)
C^{lns}	cost of load not served	(€/ MWh)
$CF_{i,y,*}$	capacity factor of renewable energy sources ($i \in I^{res}$) at load-level (h) or sub-period (s) hour (t) in year (y)	/
DR_y	discount rate for year (y)	(%)
$Dur_{y,m}$	duration of load-level (h) in year (y)	(hours)
E_i	amount of carbon emission per MWh of power plant technology (i)	(tCO_2 / MWh)
E_y^{max}	maximum total allowable emission per year (y)	(tCO_2)
h	parameter to represent the information level of the affinely adjustable robust optimization model	/
$L_{y,*}$	demand at load-level (h) or sub-period (s) hour (t) in year (y)	(MW)
LS^{max}	maximum allowable load shedding	(MWh)
M_i^u	minimum up-time for power plant technology ($i \in I^{th}$)	(hours)
M_i^d	minimum down-time of power plant technology($i \in I^{th}$)	(hours)
N_{step}	total number of steps specified for the step-function approximation	/
N_{days}	total number of days specified for the sample days approximation	/
N_{weeks}	total number of weeks specified for the sample weeks approximation	/
P_i^{max}	maximum capacity of power plant belonging to technology (i)	(MW)
P_i^{min}	minimum stable power output of power plant $i \in I^{th}$	(MW/h)
P_i^{start}	maximum output of power plant ($i \in I^{th}$) when started	(MW)
Pen_y^{lvl}	annual renewable penetration level requirement	(%)
Pr_i^{max}	maximum available primary reserve capability of power plant technology (i)	(MW)
Prr	percentage of the load required to be covered by primary reserve	(%)
r^{min}	minimum planning reserve margin	(MW)

R_i^{Umax}	maximum upwards ramping capability of power plant of technology ($i \in I^{th}$)	(MW/h)
R_i^{Dmax}	maximum downwards ramping capability of power plant of tecnology ($i \in I^{th}$)	(MW/h)
R_{sds}	solar surface-downwelling shortwave radiation	(μm)
$Sr_i^{max,up}$	maximum available upwards secondary reserve capability of power plant technology (i)	(MW)
$Sr_i^{max,dn}$	maximum available downwards secondary reserve capability of power plant technology (i)	(MW)
Srr^{up}	percentage of the load required to be covered by the secondary upwards reserve	(%)
Srr^{dn}	percentage of the load required to be covered by the secondary downwards reserve	(%)
t'^{min}	minimum water stream temperature	(°C)
t'^{max}	maximum water stream temperature	(°C)
t'^{ip}	air temperature at the inflection point	(°C)
$\Delta T'$	permissible temperature increase of the cooling water	(°C)
$\Delta T'^{max}$	regulated maximum permissible temperature increase of the cooling water	(°C)
T'_{as}	air temperature at surface	(°C)
T'_{cell}	solar-pv cell temperature	(°C)
T'_{health}	temperature when the maximum discharge of waste heat is in normal operating range	(°C)
T'_{risk}	temperature when the actual maximum discharge of waste heat is equal to the designed value	(°C)
T'^{in_c}	temperature of cooling water circulated back to the condenser	(°C)
T'^{in_w}	power plant intake water temperature	(°C)
T'^{out_max}	regulated maximum permissible temperature of the discharged cooling water	(°C)
$\overline{T'}_t$	geographical aerage values of the projected air temperature at time (t)	(°C)
$\overline{T'}_t^{ref}$	historical reference air temperature at time (t)	(°C)
T_i^{life}	expected life-time of new power plant of technology (i)	(years)
T_i^{const}	construction time of power plant of technology (i)	(years)
V_0	cut-out velocity of the wind turbine	(m/s)
V_l	cut-in velocity of the wind turbine	(m/s)
V_H	wind speed at wind turbine height	(m/s)
V_R	rated velocity of the wind turbine	(m/s)
V_{10m}	near-surface wind speeds at 10 meters height	(m/s)
V^{req}	required volume of cooling water for operating a thermal power plant at its maximum capacity	(m^3)
V_i^{cpty}	cooling water extraction capacity of plant (i)	(m^3/s)
V_{it}^{src}	permissible amount of water flow that can be taken from the water source for plant (i) at time (t)	(m^3/s)
Y^{end}	end year of the planning horizon	/
Y^{res}	first year during which the IRES quota target is binding	/

Continuous Variables:

π	vector of all dual variables associated to the respective bounds of the uncertainty set	(variable dependent)
$error_{c,b}$	error variable of the sample day approximation for LDC (c) and for bin (b)	/
h_n	load-level (step height) for the step-function approximation at step (n)	(MW)
$lns_{y,*}$	load not served at load-level h or sub-period (s) hour (t) in year (y)	(MWh)
LS^{ewe}_{yst}	load not served during extreme weater event (ewe) at sub-period (s), hour (t) of year (y)	(MWh)
$p_{i,y,*}$	power output of power plant (i) at load-level (h) or sub-period (s) hour (t) in year (y)	(MWh)
$pr_{i,y,s,t}$	primary reserve of unit (i) at sub-period (s) hour (t) in year (y)	(MWh)
$\boldsymbol{R}_{yst}(\mathcal{V}^t_{ys})$	recourse variable definition for uncertainty realization ($\mathcal{V}^t_{ys}$) at sub-period (s), hour (t) of year (y)	(variable dependent)
$(\boldsymbol{R^0}_{yst}, \boldsymbol{R^L}_{ystt'}, \boldsymbol{R^C}_{i'ystt'})$	coefficients of the linear decision rule for affinely adjustable robust counterpart	(variable dependent)
$sr^{up}_{i,y,s,t}$	secondary upwards reserve of unit (i) at sub-period (s) hour (t) in year (y)	(MWh)
$sr^{dn}_{i,y,s,t}$	secondary downwards reserve of unit (i) at sub-period (s) hour (t) in year (y)	(MWh)
$v_{i,y,s,t}$	shut-down decision of power plant of technology (i) at sub-period(s) hour (t) in year (y)	/

Discrete Variables:

λ_d	selection decision for the sample day (d) in the time horizon approximation (1 if selected and 0 otherwise)
ϕ_w	selection decision for the sample week (w) in the time horizon approximation (1 if selected and 0 otherwise)
k_n	breakpoint at which the approximated LDC step-function changes value from step (n) to step ($n+1$)
$q_{i,y}$	commissioning decision of power plant of technology (i) in year y
$u_{i,y,s,t}$	commitment status of power plant of technology (i) at sub-period (s) hour (t) in year (y)
$x_{i,y}$	availability (commissioning) state of power plant of technology (i) in year y
$z_{i,y,s,t}$	start-up decision of power plant of technology (i) at sub-period (s) hour (t) in year (y)

Acronyms:

AARC	Affinely Adjustable Robust Counterpart
AARO	Affinely Adjustable Robust Optimization
C-GEP	Integrated GEP and UC model
CCGT	Combined Cycle Gas Turbine
CF	Capacity Factor
CLC	Closed-Loop Cooling
CMIP5	Coupled Model Intercomparison Project Phase 5
CP	Conventional Planning
EAC	Equivalent Annual Cost
EFS	Expected Flexibility Shortfall
ewe	Extreme weather event
GEP	Generation Expansion Planning
HUA	Hourly Unit Availability
IRES	Intermittent Renewable Energy Sources
IRRE	Insufficient Ramping Resources Expectation
LDC	Load Duration Curve
LHS	Left Hand Side
LNS	Load Not Served
MILP	Mixed Integer Linear Programming
NRMSE	Normalized Root Mean Squared Error
O&M	Operation and Maintenance
OCGT	Open Cycle Gas Turbine
OTC	Once-Through Cooling
PV	Photo Voltaic
RCP	Representative Concentration Pathway
RHS	Right Hand Side
RMSE	Root Mean Squared Error
RP	Resilient Planning
S-GEP	Soft-linked GEP and UC model
UC	Unit Commitment
VaR	Value at Risk
WCD	Worst Case Deterministic

Part I

Thesis

1 Introduction

Electric power systems are at the heart of any modern society. These are inherently large-scale dynamic systems with a high degree of spatio-temporal complexity. Their reliability and security of supply are central considerations in any regional or global energy-related policy. Methods for power systems planning have typically ensured key operational reliability aspects under normal operating conditions and in response to anticipated demand variability, uncertainty and supply disruptions, e.g. due to errors in load forecasts and to unexpected generation units outages. Solutions have been commonly built on capacity adequacy and operating reserves requirements, among others. However, recent objectives for environmental sustainability and the threats of climate change are challenging the reliability requirements of power systems in various new ways and necessitate adapted planning methods.

The present thesis describes the research work done towards the development of an integrated techno-economic modeling and robust optimization framework for power systems planning adapted to this new context. Specifically, the planning framework seeks to address the challenges associated with the sustainability targets of future power systems, most notably: ensuring operational flexibility against the variability of renewable energy sources, ensuring resilience against extreme weather events and ensuring robustness against the uncertainties inherent in both the electric power supply and system load.

This introductory chapter will present to the reader the context and contributions of this work, and is organized as follows. Section (1.1) summarizes the main sustainability drivers for the current (and future) power systems planning and operation. These well-known sustainability targets have become a worldwide imperative in all sectors of economic activity, and are embedded within almost any regulatory or policy dialogue. Section (1.2) briefly reviews the particular transformation related to the electric power sector planning, not only driven by the sustainability goals, but also by the more general technological and/or regulatory advancements. In section (1.3) the main power systems planning challenges addressed in this work are detailed, along with a thorough review of previous research works and research gaps. Then, section (1.4) formulates the key research questions and ensuing objectives as well as the original contributions of the work. Finally, a schematic representation of the overall structure of the thesis is provided in section (1.5).

1.1 Sustainability of future electric power systems

The electric power industry is both a major contributor to climate change and a sector that will be deeply disrupted by the effects of climate change. The role of the power sector towards climate change stems from the fact that it is the largest contributor to global green house gas (GHG) emissions. From 2000 to 2010, the increase in the power sector emissions outpaced the increase in overall emissions by around 1% per year [1]. In 2018, global energy-related CO2 emissions rose 1.7% to a historic high of 33.1 Gt CO2. The power sector accounted for nearly two-thirds of this emissions growth [2]. To reduce emissions to levels

equivalent with the internationally agreed goal of keeping the temperature increase below 2°C of that of pre-industrial levels, the share of low-carbon electricity generation will need to triple or quadruple by 2050 [2].

Moreover, over the coming decades, the power sector may be disrupted by climate change impacts. For example, power plants, especially those in coastal areas, may be affected by extreme weather events and rising sea levels. Electricity grids may be impacted by storms, and the rise in global temperature may affect electricity generation including thermal and hydroelectric stations in many locations. And while the industry may have options for adapting to climatic changes, significant costs are likely to be incurred [3]. Several actions are, therefore, urgently needed if the reliability and sustainability targets for the power sector are to be achieved.

1.1.1 Greenhouse gas emissions

Controlling GHG emissions ultimately requires "de-carbonizing" the power sector, both by reducing the high demand for energy and by supplying power that generates much less GHG. A clear path for de-carbonizing power production is through what the Intergovernmental Panel on Climate Change (IPCC) describes as a fundamental shift in global investment from fossil fuel to renewable energy [1]. Renewable energy sources have significant potential for reducing GHG emissions and are becoming mainstream investment choices as they are becoming more competitive. In 2012, they accounted for just over half of the new electricity-generating capacity investments globally while electricity generation from renewable sources increased by over 7% in 2018 alone [2]. Yet only a small fraction of renewable potential has been exploited so far; estimates suggest that in different regions of the world, renewable energy sources can produce more than 2.6 times the energy demand [1]. Another path for supporting the reduction of GHG is placing more stringent limits on carbon emissions for existing or new thermal plants. This can be possibly achieved by a wider implementation of carbon capture and storage (CCS) technology.

1.1.2 Climate change

Ensuring the resilience of the power system against the adverse effects of climate change is another key element for ensuring the sustainability and reliability of power supply. The past decade has seen a rising frequency in weather-related natural disasters. Damage and loss associated with these extreme events resulted in millions of victims and billions of dollars in losses. There are various ways in which climate change affects the power sector [4]:

- Extreme weather events such as storms, floods and extreme temperatures can impact the power production and delivery, causing supply disruptions and infrastructure damage.
- The reduction in water availability can constrain hydropower as well as the operation of the thermal power plants (fossil fuel and nuclear) which require water for cooling.
- Unusual seasonal temperatures can impact the electricity demand patterns due to the increased need for cooling during summer heat waves, or the increased demand for heating in excessively cold winters.

Although thermal power plants are designed to operate under diverse climatic conditions, they will be particularly affected by the decreasing efficiency of thermal conversion as a result of rising ambient temperatures. In addition, in many regions, decreasing volumes of

water available for cooling and increasing water temperatures could lead to reduced power operations, operations at reduced capacity or even temporary shutdowns [5]. The rising temperatures also create challenges for meeting river temperature regulations. For example, in 2009, the French power system at one time lost one third of its nuclear capacity, to respect thermal discharge limits [4].

Within this context, it is clear that current power system planning efforts must be able to account for these future challenges or, otherwise, they run the risk of leading to inadequate and unreliable investments.

1.2 Electric power systems planning

Power system planning is an important techno-economic problem, which has been addressed extensively both by the sector stakeholders and by academics. Research on power system planning is carried out by governments and power system operators for future system-wide expansion, and for deciding on optimal policies and regulations. It is also carried out within privately owned power utilities in countries which have liberalized the energy sector, to plan for future investments.

Electric power systems planning can be divided into two main problems: generation expansion planning (GEP) and network expansion planning (NEP). Both are typically formulated as optimization problems, seeking to determine the optimal technology mix, location and construction time of new generation units, as well as the optimal size and location of the power lines. Albeit being highly intertwined, the complexity and scale of each problem has led research work to often focus on addressing each of them separately [6].

The present work focuses on the modeling of the GEP problem and the optimization of its solution, as it is considered most critically affected by the future context, both from the economic (costs) and technical (service provision) aspects. In literature, GEP modeling in a centralized planning context can be traced back to the seminal paper [7]. With the power sector being constantly subjected to changes driven by economical, technical, technological and environmental issues, the body of GEP literature has persistently expanded to accommodate the new requirements, through a variety of modeling and solution methods. Some of the developments include: improvements in the details considered, such as reserve requirements [8, 9], reliability and maintenance [8, 10–12], policy developments such as the restructuring of the power sector and the introduction of competition [10, 13–15], CO_2 mitigation solutions [16, 17], renewable energy resources integration and support schemes [15, 18–21], uncertainty and stochasticity in generation production and demand [10, 19, 22–25], demand side management (DSM) [26, 27], and smart-grids [28], among others. Reviews of the GEP problem can be found in [29–31], and a comprehensive recent review in [32].

In particular, as noted in the previous section, the need to combat climate through the de-carbonizatoin of the sector, as well as the advancements in the information and communication technology (ICT) has paved the way to fundamental transformations in both the electricity supply and demand of electricity (schematically illustrated in Figure (1.1)):

On the supply side:

- There is an increased shift from large synchronous generators to light-weight decentralized ones.
- There is an increased penetration of intermittent renewable energy sources (IRES), for which the investments are getting cheaper and the remuneration programs are becoming more attractive.

- There is an increased threat of power disruption due to extreme weather events.

On the demand side:

- There is a growing number of distributed variable generation resources, in the form of electric vehicles, electric solar production roof-tops, micro-grids, energy storage systems, among others.
- There is a usage shift of the demand from being passive (pure consumers) to being active (both consumers and small-scale producers, i.e. "prosumers").
- There is a strong potential for unusual demand patterns due to climate change effects.

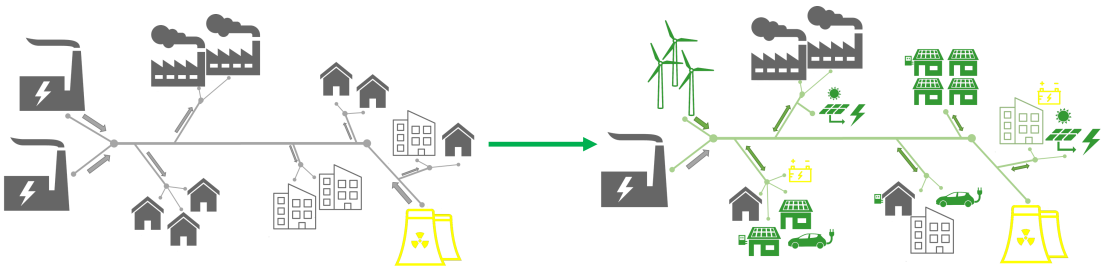

FIGURE 1.1 – Schematic illustration of power systems transformation towards decentralized power generation and bi-directional power flow

These developments are posing a number of pressing challenges that need to be adequately and methodologically incorporated and addressed within the power systems planning framework. The next section details the key challenges addressed in this work and reviews the relevant studies that have previously treated them.

1.3 Electric power systems planning challenges

1.3.1 Operational flexibility

One of the most recent concerns in power systems planning with high shares of IRES penetration is whether or not these systems are able to answer to the operational flexibility requirements, generally described as the ability of the system to respond to the inter-temporal variability rising from both intermittent IRES production and demand. The variability in the net load (demand minus RES production), requires that the remainder of the hydro-thermal [1] units cope with tighter flexibility requirements [33–37]. Answering to such requirements is clearly a function of the short-term operational status of these units and their technical abilities: ramping rates, unit commitment states, minimum up and down times, start-up time and minimum stable load, to name a few. In this respect, traditional long term GEP models that do not consider the chronological representation of net load variations, nor these short term technical constraints, but instead rely on merit order dispatch, would fail to provide any information on whether the investment plans obtained are sufficiently sensible and flexible to these variations. This type of evaluation is, instead, typically performed by the well known unit commitment (UC) problem, which does not consider investment decisions [38–40].

[1] In the remainder of the thesis, the term "thermal" is used to refer to oil, gas, coal as well as nuclear generation technologies

Traditional GEP models, based on step-wise load duration curves or other non chronological approximations, have for long been appropriate for power systems planning, especially in systems dominated by dispatchable hydro-thermal units and with the primary concern of generation adequacy (e.g. [41–43]). These models have the main advantage of being computationally cheap, and therefore large sized systems and long term planning horizons up to several decades can be easily optimized. However, when it comes to planning for system flexibility under IRES penetration, recent studies have started to show the importance of integrating the UC short-term constraints within the long-term planning model [44–52].

Study [44] considers a combined GEP-UC model for planning over a single year, reduced to 4 weeks with chronological hourly representation, each week representing a season. In [45] a detailed formulation of the combined GEP-UC problem is provided and employed for the analysis of the Greek power system, under several scenarios of carbon emission pricing, emission caps, and IRES penetration targets. A multi-annual planning horizon is considered, where the year is approximated to 12 days, each one representing a month. The results reveal the correlation between significant IRES penetration with large amounts of natural gas production, which offers more flexibility to the power system. Similarly, in [46] a combined model for multi-annual planning is proposed and a clustering representation of the units in integer variables is presented. Several planning horizons are considered, where annual demand is reduced to a number of representative weeks selected in an ad-hoc manner. The comparison on the case study shows that when short-term constraints are considered, higher investments are driven to flexible peaking plants. In [47], a soft-linking between long-term and short-term models is implemented. The framework is to solve a long-term low resolution model to obtain a generation portfolio under a single IRES penetration scenario and to embed this portfolio in a short-term chronological model, which is solved multiple times with increasing level of technical constraints. It considers a case study for a single year and uses the number of units start-ups as a proxy for flexibility evaluation. A very similar approach is implemented in [48], but also varying the IRES penetration level. The impact of including several short-term constraints (most notably: startups/shutdowns, minimum stable load, ramping rates and operating reserves) is analyzed for a future planning year. Study [49] solves a planning model based on a basic screening curve method and proposes a perturbation algorithm with embedded short-term constraints to improve the plans obtained. A single future year is considered under different IRES penetration scenarios. A brief comparison of the results obtained pre and post the implementation of the perturbation algorithm, in terms of the installed capacity, is discussed. It shows that considering the short-term constraints results in less installation of base load capacity compared to mid and peak load ones. Finally, studies [50] and [51] compare the results of a fully integrated model to those of a traditional planning only model. The former work considers only a single future planning year, whereas the latter considers a multi-annual planning horizon of 10 years, where each year is approximated to 4 days in an ad-hoc manner. The comparison is based on the costs and emission levels resulting from both models, and shows that neglecting these constraints underestimates both attributes. A summary of the main differences among the reviewed literature is given in Table (1.1).

TABLE 1.1 – Summary of the relevant literature regarding the integrated electric power system planning models

Reference	Horizon considered	Horizon reduction	Model type	Scenarios considered	System considered
[44]	Single year	4 weeks, each representing a season	Integrated GEP-UC	Different wind production profiles	Grey-field
[45]	Multi-annual	12 days per year, each representing a month	Integrated GEP-UC	RES penetration levels, carbon pricing, carbon cap	Grey-field
[46]	Multi-annual	13 typical weeks per year, one for each month plus one containing the peak load	Integrated GEP-UC	Different time horizons	Grey-field
[47]	Single year	Full representation	Soft linking between GEP and UC	Single RES penetration level, increased consideration of short-term technical constraints	Grey-field
[48]	Single year	Full representation	Soft linking between GEP and UC	Different RES penetration levels	Grey-field
[49]	Single year	Full representation	Integrated GEP-UC	Different wind penetration levels	Grey-field
[50]	Single year	Full representation	Integrated GEP-UC	RES penetration levels, carbon pricing	Grey-field
[51]	Multi-annual	4 days per year, each representing a season	Integrated GEP-UC	Wind penetration levels, carbon emission	Grey-field

Operational flexibility

Properly quantifying operational flexibility is critical for evaluating the overall system reliability. Whereas reliability relates to the fact that sufficient firm-capacity[2] is available at each time period to satisfy the system load, as measured by typical metrics, such as loss of load expectation (LOLE) and expected energy not supplied (EENS), operational flexibility considers how a specific operational state of the system at a given period would contribute to (or hinder) its ability to deploy its resources for accommodating variations in subsequent periods: for this, no time period can be assessed in isolation of the others, nor without detailed knowledge of the exact system state and technical characteristics at the given period. Therefore, metrics to describe operational flexibility have been proposed in the literature, varying in the degree of complexity and in the data required for their estimation. The work in [53] proposes a probabilistic metric that takes into account key technical characteristics of the generation units and aggregates them for a system-level assessment. In [54], a number of interdependent metrics are defined for individual generation units to assess their available flexibility in real time. Study [55] proposes two flexibility indices to provide an offline estimation of the flexibility level of power systems. The first metric is obtained by analyzing the

[2] Available generation capacity excluding failed units, units in maintenance, offline units, etc.

adjustable space of generators, whereas the second assesses the flexibility level of a system by its capability for accommodating wind. Finally, [56] proposes a metric which additionally considers the impacts of the transmission network on the flexibility levels.

Research gap

As shown, most of the studies reviewed argue for the benefit of including the short-term unit-commitment constraints within the long-term planning framework, especially in terms of answering to the flexibility requirements under increased IRES penetration, by analyzing the differences in capacity installation, production profile, emission and curtailment levels, system costs, or a combination of these. Those studies, however, do not resolve to using quantitative flexibility metrics to formally assess and compare the benefits of their proposed approaches. On the other hand, studies that have proposed quantitative flexibility metrics have often considered existing systems for the application and do not integrate those methods within the expansion planning problem itself. Furthermore, since the resulting expansion problem with unit-commitment constraints is computationally intensive, each study has resorted to a different combination of horizons reduction or ad-hoc approximation, neglecting to address the bias that this can impose on the results.

1.3.2 Resilience

Increasingly frequent and extreme weather events, such as heat waves, droughts, floods and storms, significantly affect the operational status of power systems. Evidence of power generation disruptions due to such events highlights the fragility of the existing systems and the need of considering resilience within the planning of future power systems [57].

Particularly, heat waves are among the most worrying weather extremes, due to the expected increase in their frequency and severity in the 21st century [58, 59]. For example, France was particularly impacted by the 2003 summer heat wave, which caused an excess of about 15,000 deaths from 4th to 18th August directly attributable to the heat [60]. By combining peaks of extreme temperature and severe soil and hydrological droughts, this event also affected significantly the energy production sector (mainly because of the cooling process of thermal power plants). These last years, numerous regions of the world experienced severe heat waves with comparable effects: Russia in 2010, Texas in 2011, Australia in 2012, India and Southern Pakistan in 2015. Therefore, it is of great importance to design the ability of the energy systems for coping with future heat wave events.

Among the research that studied the impacts of extreme weather events on power systems, [61] presents a multi-objective optimization of distributed power generation systems considering extreme wind and lightning events. [62] proposes a probabilistic methodology to assess the resilience degradation of transmission networks subject to extreme wind events. In [63], an extreme weather stochastic model is applied to a realistic cascading failure simulator of power grids, accounting for the operating conditions that a repair crew may encounter during an extreme weather event. The impacts of water availability on the generation capacity expansion planning is investigated in [64] and the electricity sector growth is compared under different scenarios of water rights. [65] proposes an integrated electricity and natural gas planning model taking into consideration the power grid resilience against storms, earthquakes and floods. [66] studies the potential impacts of heat waves on power grid operation, by quantifying the capacity of thermal power plants as a function of ambient temperature.

Research gap

Whereas most of those studies focus on evaluating the impact of extreme weather threats on the operation of power systems, there exist very few studies that incorporate resilience within the power system planning problem itself. Moreover, no study explicitly considers flexibility and resilience within a unified planning and assessment framework.

1.3.3 Uncertainties

Accounting for the inherent uncertainties in IRES supply and system load is another significant concern for ensuring reliable system performance. Two popular approaches have been often applied to address the uncertainties for the GEP and UC problems, separately. One is stochastic optimization (SO) [67–71], which models uncertain parameters by means of scenarios generated from probability distribution functions. This method may be suitable if the probability functions are available, which is not always the case, and especially when considering long-term uncertainties such as in a GEP problem. Moreover, SO does not guarantee the feasibility of the solution under *any* uncertainty realization within the uncertainty range [72], which is a significant limitation in addressing the operational flexibility attribute that depends on the specific realization of uncertainties among time-coupled constraints. The other popular approach is robust optimization (RO) [73], which models uncertain parameters by means of distribution-free bounded intervals. RO is attractive in that it avoids the above-mentioned limitations of SO, but, it has been often criticized for resulting in over-conservative solutions and for being computationally intensive. State-of-the art RO methods deal with these problems by introducing an uncertainty budget parameter to control the conservatism of the solution and by resorting to efficient solution methods (such as Column and Constraint Generation (CCG) [74] or affine simplification of the recourse action [75]) to accelerate the solution.

Research gap

Some research works have focused on RO-based approaches to handle uncertainties and address operational flexibility in power systems planning and operation. In [76], a two-stage adaptive RO model is proposed for long term generation and transmission expansion under generator output uncertainties but with no explicit consideration of the ramping requirements. Ramping was considered in [77] for power system planning but only through an approximated hourly load ramping uncertainty that is based on average net-load levels. Detailed ramping constraints were considered in robust unit commitment models such as in [78–81], but without considering the impact on power systems planning. Moreover, [80] has demonstrated how the two-stage robust UC model can lead to infeasibility in the dispatch problem when the generation ramping capability is limited. This showed the importance of considering non-anticipativity constraints in power systems operations within a multistage robust optimization. Yet, these results were not extended to investigate their impact on the power systems investment decisions.

1.4 Thesis objectives and original contributions

To address the above-mentioned challenges, the present thesis aims at developing a techno-economic modeling and robust optimization framework for multi-period generation expansion planning considering a high share of IRES and resilience against extreme weather

events. The specific planning problem considered is that of selecting the technology choice, size and commissioning schedule of conventional and renewable generation units under technical, economical, environmental and operational constraints. Within this problem, key research objectives addressed are (Figure (1.2): (i) the proper integration and assessment of the operational flexibility needs due to the increased variability from the high shares of IRES penetration, (ii) the appropriate modeling and incorporation of the resilience requirements against extreme weather events within the power system planning model and (iii) the representation and treatment of the inherent uncertainties in the system supply and demand within this planning context.

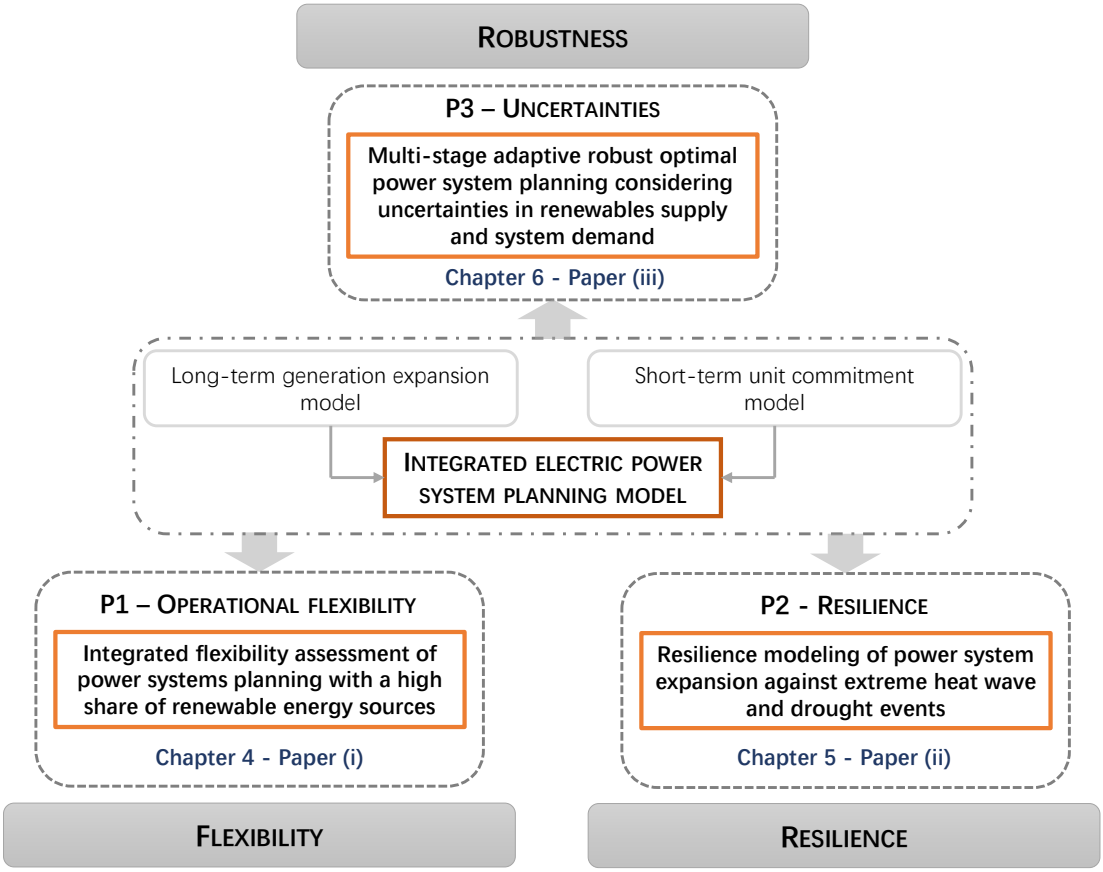

FIGURE 1.2 – Research objectives of the present thesis

1.4.1 Thesis contributions

To overcome the above mentioned limitations and fill the research gaps, the original contributions towards each of the ensuing objectives are summarized below:

Managing operational flexibility in GEP: [Chapter 4, Paper (i)]

- The thesis contributes to electric power systems planning with high shares of IRES penetration and stringent carbon targets, by proposing a computationally efficient, multi-period integrated GEP-UC model that accounts for key short-term constraints and chronological net load representation. In particular:

  * The importance of considering these constraints to account for operational flexibility under high IRES penetration is demonstrated quantitatively by comparing the output of the integrated model to that of the traditional GEP, which leads to investment decisions based on average system operating conditions.
  * For computational tractability, horizon reduction is introduced by systematic optimization, to avoid biases on the results obtained by ad-hoc methods.

- The thesis introduces the expected flexibility shortfall (EFS) metric for operational flexibility assessment to capture the expected amount of load loss specifically due to insufficient flexibility. We analyze the complementarity of this metric to other metrics of literature, most notably the insufficient ramping resource expectation (IRRE) proposed in [53], which considers the expected frequency of flexibility shortage rather than its magnitude.
- The relevance of the overall modeling for real applications is shown by its application to a realistic case study representing the national system of France, with load and IRES capacity-factor data spanning a 10-years planning period. Sensitivity to key supply and demand parameters is also performed.
- The results of the framework for a wide range of IRES penetration targets and carbon emission limits allows highlighting the importance of relying on suitable metrics for the operational flexibility assessment rather than on quantities typically considered for power system planning, like generation mixes, system costs and amount of renewable curtailment, which are not capable to reflect the true flexibility levels of the obtained plans.

Ensuring resilience against extreme weather events in GEP: [Chapter 5, Paper (ii)]

- The thesis proposes a set of piece-wise linear models to describe the impact of different scenarios of extreme heat waves and water availability on the derating of thermal power units operation, renewable generation production and system load.
- The work presents a method for explicitly incorporating the extreme weather impact in a modified mixed integer linear programming (MILP) power system planning model to derive adequate system investment decisions.
- The work extends the previously proposed quantitative framework for operational flexibility assessment of power systems with a high share of IRES penetration to also include their resilience against extreme heat waves and drought events.
- The framework is applied to a practical-sized power system planning problem with realistic future climate projections obtained from the Coupled Model Intercomparison Project Phase 5 (CMIP5), for demonstrating the relevance of the proposed planning approach in terms of system costs and technology choices.

Treatment of uncertainties in the GEP: [Chapter 6, Paper (iii)]

- The thesis presents a multiperiod multi-stage affinely adjustable robust optimization (AARO) model for long-term integrated generation expansion planning and unit commitment to explicitly account for detailed ramping uncertainties. The uncertainty characterization of the system load and IRES capacity factor (IRES-CF) takes the form of a deterministic uncertainty set with a controllable level of conservatism.

- The thesis discusses the dimensionality problem of the fully adjustable model along with the concept of "information basis level" of the resulting problem.
- To resolve the dimensionality issue, a novel approximation method is proposed by introducing a new parameter which controls the level of affine dependency (information level) of the problem. A sensitivity analysis is conducted on this parameter and it is shown that significant computational gains can be achieved while keeping the significance of the results.
- The proposed approach is applied for investment decisions in a practical-sized case study with a high share of IRES penetration, under realistic assumptions. The importance of explicitly considering the detailed ramping constraints for robust long-term planning is shown and discussed in details. The superiority of considering multi-stage AARO over other methods to account for ramping effects in power systems planning with high shares of IRES production is demonstrated.

1.5 Thesis structure

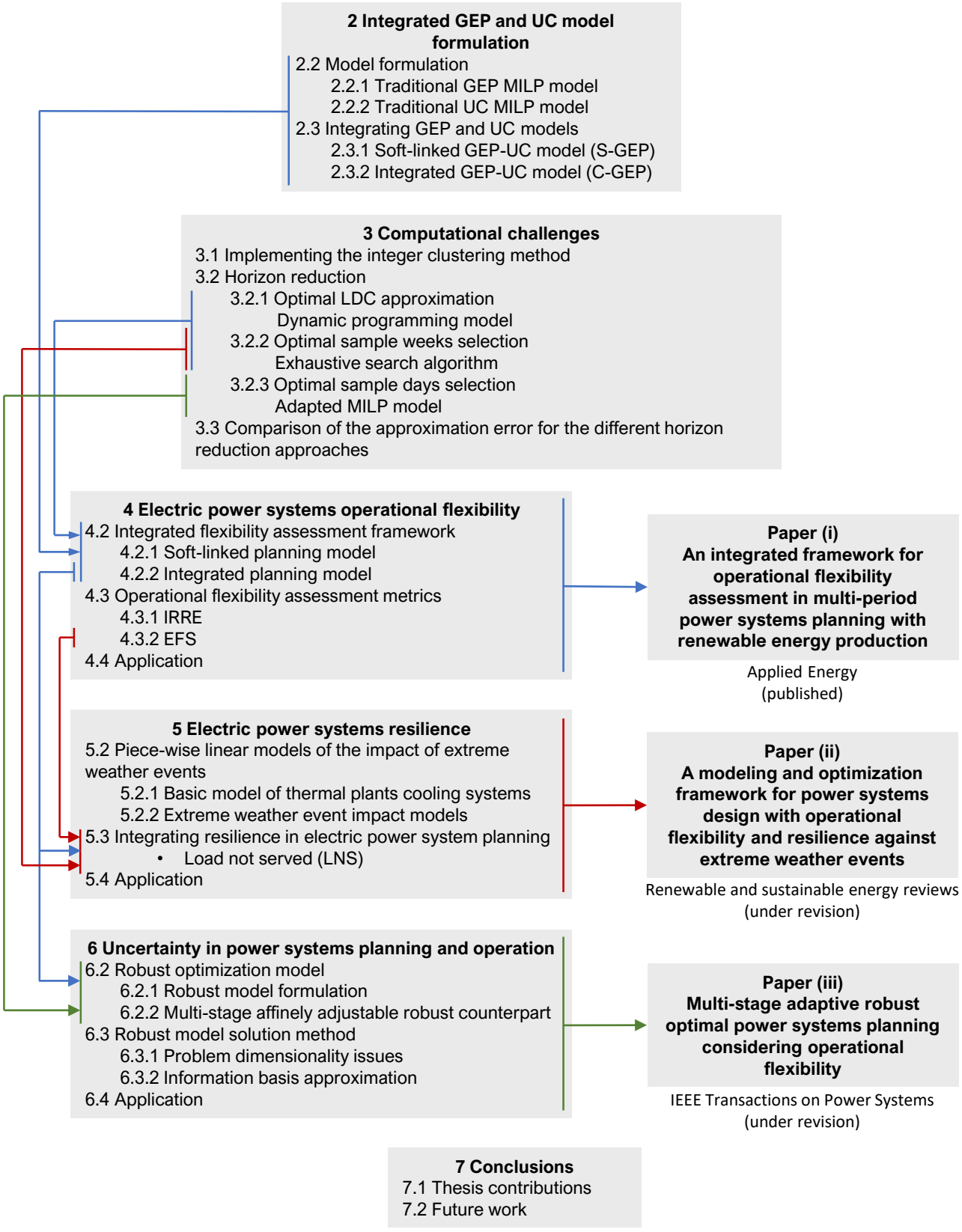

FIGURE 1.3 – Thesis structure diagram

2 Integrated model for multi-period generation expansion planning (GEP) and unit commitment (UC)

2.1 Overview

In this chapter, the formulation of the integrated multi-period power system planning model proposed and used throughout this thesis is presented. First, a typical formulation of the long-term generation expansion planning (GEP) model is described. This model derives investment decisions based on an approximated step-function of the load duration curve (LDC). Hence, no short-term related constraints are directly incorporated and the chronological order of load and dispatch data is ignored. Second, a short-term unit-commitment (UC) model is formulated. This model accounts for the chronological evolution of the system operation and includes key short-term commitment and dispatch constraints, such as the minimum up and down times and the thermal units ramping capabilities. The UC model by itself, however, does not consider the generation units investment and commissioning decisions.

Two methods for integrating the GEP and UC models are, then, described: the first is the soft-linking of the models and the second is their full integration in a single optimization model. In Chapter (4), the two methods will be compared for power systems planning under a high share of IRES penetration to show the superiority of the integrated model with respect to the different key performance indicators considered, most notably also with respect to operational flexibility.

2.2 Model formulation

2.2.1 Traditional GEP mixed integer linear programming model

The long-term GEP model has the objective of minimizing the total discounted cost over the planning horizon under typical long-term simplified constraints. No hourly chronological order is considered and load is represented as load blocks derived from the LDC with duration ($Dur_{y,h}$) and load levels ($L_{y,h}$). This model is formulated as a mixed integer linear program (MILP) and is described as follows:

GEP objective function

The objective function seeks to minimize the total discounted costs over the planning horizon. Equation (2.1) represents the total investment costs in new units, equation (2.2) represents the total production costs calculated on the basis of the yearly LDCs, and equation (2.3) represents the fixed operation and maintenance (O&M) costs:

$$\min_{\Omega} \sum_{y \in Y} (1+DR)^{-y} \cdot \sum_{i \in I} C_i^{inv} \cdot P_i^{max} \cdot q_{i,y} \tag{2.1}$$

$$+ \sum_{y \in Y} (1+DR)^{-y} \cdot \sum_{m \in M} Dur_{y,m} \cdot \left[\sum_{i \in I} \left(C_{i,y}^{mrgl} \cdot p_{i,y,m} \right) + C^{lns} \cdot lns_{y,m} \right] \tag{2.2}$$

$$+ \sum_{y \in Y} (1+DR)^{-y} \cdot \sum_{i \in I} C_{i,y}^{fom} \cdot P_i^{max} \cdot \sum_{l=1}^{y} q_{i,l} \tag{2.3}$$

where $\Omega \ni \{q_{i,y},\ x_{i,y},\ p_{i,y,m},\ lns_{y,m}\}$.

GEP constraints

1. Units availability and construction time: units are only available to operate if they are commissioned:

$$x_{i,y} \leq \sum_{l=1}^{y} q_{i,l}, \quad \forall i \in I^{new}, y \in Y \tag{2.4}$$

2. Annual budget constraint: an upper limit is imposed on the annual budget:

$$\sum_{i \in I^{new}} C_i^{inv} \cdot P_i^{max} \cdot q_{i,y} \leq B_y^{max}, \quad \forall y \in Y \tag{2.5}$$

3. Supply-demand balance constraint: the total energy generated plus the load not served (LNS) should be equal to the respective load level, for each block n of the annual LDC:

$$Dur_{y,m} \cdot \left(\sum_{i \in I} p_{i,y,m} + lns_{y,m} \right) = Dur_{y,m} \cdot L_{y,m}, \quad \forall m \in M, y \in Y \tag{2.6}$$

4. Maximum output levels: thermal units power output is limited by the maximum capacity and the expected forced outage rate ϵ:

$$p_{i,y,m} \leq (1-\epsilon_i) \cdot P_i^{max} \cdot x_{i,y}, \quad \forall i \in I^{th}, m \in M, y \in Y \tag{2.7}$$

5. Design reserve margin (system adequacy): yearly available capacity should be greater than the maximum load level plus a reserve margin, for adequacy considerations:

$$\sum_{i \in I} \left(P_i^{max} \cdot x_{i,y} \right) \geq \left(1 + r^{min} \right) \cdot \max_{m \in M} (L_{y,m}), \quad \forall y \in Y \tag{2.8}$$

6. Minimum annual renewable penetration: annual IRES production should be higher than the required penetration level, effective from the desired year Y^{res}:

$$\sum_{i \in I^{res}} \sum_{m \in M} \left(Dur_{y,m} \cdot p_{i,y,m} \right) \geq Pen_y^{lvl} \cdot \sum_{m \in M} \left(Dur_{y,m} \cdot L_{y,m} \right), \quad \forall y \in [Y^{res}, Y^{end}] \tag{2.9}$$

7. Renewable energy production: IRES production is typically represented through an hourly availability or hourly capacity factor (CF). Since in the GEP problem no hourly representation is considered, an approximation method is used to obtain what we refer to as the IRES capacity factor duration curve (IRES-CFDC):

$$Dur_{y,m} \cdot p_{i,y,m} \leq x_{i,y} \cdot P_i^{max} \cdot Dur_{y,m} \cdot CF_{i,y,m} \quad \forall i \in I^{res}, m \in M, y \in Y \tag{2.10}$$

8. Allowable emission: yearly carbon emission for thermal units production is limited to a maximum amount:

$$\sum_{i \in I^{th}} \left(E_i \cdot \sum_{m \in M} \left(Dur_{y,m} \cdot p_{i,y,m} \right) \right) \leq E_y^{max}, \quad \forall y \in Y \tag{2.11}$$

It should be noted that since the penetration of IRES by itself might not necessarily correspond to lower carbon emissions in the system (as the choice of the remaining investments may fall on highly emitting technologies), it is important to set an emission target. There are two main ways to do so: either by setting a carbon cost/tax in the objective function to be minimized or by setting an emission limit as a constraint. The former might not be suitable for long-term, system-wide planning, as it presupposes the main aim of ensuring a certain limit on these emissions from which the carbon tax is derived, and could be more meaningful within a multi-objective optimization framework where sensitivity to different carbon tax can be investigated. We, therefore, opt for the latter and explore the effect of setting a carbon emission limit as constrained by Eq. (2.11)

2.2.2 Traditional UC mixed integer linear programming model

The UC model, which has the objective of minimizing the short-term operational costs, takes into account the detailed hourly technical capabilities of the units, the chronological demand and the IRES availability (IRES-CF). All the units commissioning decisions are considered to have been taken beforehand (from the GEP model) and the model seeks only to find the optimal short-term commitment and dispatch decisions. The model is formulated as an MILP problem as follows:

UC objective function

The objective function seeks to minimize the total discounted operating costs of the systems, including the hourly variable production cost, start-up cost and LNS cost:

$$\min_{\Theta} \sum_{y \in Y} (1 + DR)^{-y} \cdot \sum_{s \in S} \sum_{t \in T} \left[\sum_{i \in I} \left(C_{i,y}^{mrgl} \cdot p_{i,y,s,t} + C_i^{stup} \cdot z_{i,y,s,t} \right) + C^{lns} \cdot lns_{y,s,t} \right] \tag{2.12}$$

where $\Theta \ni \left\{ p_{i,y,s,t},\ lns_{y,s,t},\ u_{i,y,s,t},\ z_{i,y,s,t},\ v_{i,y,s,t},\ pr_{i,y,s,t},\ sr_{i,y,s,t}^{up},\ sr_{i,y,s,t}^{dn} \right\}$.

UC constraints

1. Only units commissioned can be operated: for thermal units, only existing units in year y are available to be committed for year y, sub-period s, hour t:

$$u_{i,y,s,t} \leq x_{i,y}^*, \quad \forall i \in I^{th}, y \in Y, s \in S, t \in T \tag{2.13}$$

2. Supply-demand balance constraint:

$$\sum_{i \in I} p_{i,y,s,t} + lns_{y,s,t} = L_{y,s,t}, \quad \forall y \in Y, s \in S, t \in T \tag{2.14}$$

3. Unit-commitment constraint: this constraint regulates and keeps track of the start-up and shut-down decisions of the thermal power plants:

$$u_{i,y,s,t} - u_{i,y,s,t-1} = z_{i,y,s,t} - v_{i,y,s,t}, \forall i \in I^{th}, y \in Y, s \in S, t \in T \setminus \{1\} \tag{2.15}$$

4. Minimum up-time and down-time: thermal power plants can only be turned off after their minimum up time has elapsed (2.16). Similarly, units can only start-up when their minimum down time has elapsed (2.17):

$$u_{i,y,s,t} \geq \sum_{\tau \geq t - M_i^u}^{t} z_{i,y,s,\tau}, \forall i \in I^{th}, y \in Y, s \in S, t \in T \setminus \{1, ..., M_i^u\} \tag{2.16}$$

$$x_{i,y}^{*} - u_{i,y,s,t} \geq \sum_{\tau \geq t - M_i^d}^{t} v_{i,y,s,\tau}, \forall i \in I^{th}, y \in Y, s \in S, t \in T \setminus \{1, ..., M_i^d\} \tag{2.17}$$

5. Ramping constraints: system flexibility is directly affected by how fast the existing thermal units can adjust their production levels to accommodate for changes in net load variation; these changes are limited by each generation technology ramping capabilities, both upwards (2.18) and downwards (2.19):

$$p_{i,y,s,t} - p_{i,y,s,t-1} \leq u_{i,y,s,t-1} \cdot R_i^{Umax} + z_{i,y,s,t} \cdot P_i^{start}, \forall i \in I^{th}, \quad y \in Y, s \in S, t \in T \setminus \{1\} \tag{2.18}$$

$$p_{i,y,s,t-1} - p_{i,y,s,t} \leq u_{i,y,s,t-1} \cdot R_i^{Dmax}, \forall i \in I^{th}, y \in Y, \quad s \in S, t \in T \setminus \{1\} \tag{2.19}$$

6. Maximum, minimum output levels: thermal units output, including reserve requirements, is limited by their maximum capacity (2.20) and their minimum stable production level (2.21):

$$p_{i,y,s,t} + pr_{i,y,s,t} + sr_{i,y,s,t}^{up} \leq (1 - \epsilon_i) \cdot P_i^{max} \cdot u_{i,y,s,t}, \forall i \in I^{th}, \quad y \in Y, s \in S, t \in T \tag{2.20}$$

$$p_{i,y,s,t} \geq u_{i,y,s,t} \cdot P_i^{min} + sr_{i,y,s,t}^{dn}, \quad \forall i \in I^{th}, y \in Y, s \in S, t \in T \tag{2.21}$$

7. Operating reserves: three types of operating reserves are considered, according to a defined percentage of hourly load and of renewable generation: those are primary reserve (2.22), secondary upwards reserve (2.23), and secondary downwards reserve (2.24):

$$\sum_{i \in I^{th}} pr_{i,y,s,t} \geq Prr \cdot L_{y,s,t}, \forall y \in Y, s \in S, t \in T \tag{2.22}$$

$$\sum_{i \in I^{th}} sr_{i,y,s,t}^{up} \geq Srr^{up} \cdot L_{y,s,t} + \sum_{i \in I^{res}} \left(a^{res} \cdot p_{i,y,s,t}\right), \forall y \in Y, s \in S, t \in T \tag{2.23}$$

$$\sum_{i \in I^{th}} sr_{i,y,s,t}^{dn} \geq Srr^{dn} \cdot L_{y,s,t} + \sum_{i \in I^{res}} \left(a^{res} \cdot p_{i,y,s,t}\right), \forall y \in Y, s \in S, t \in T \tag{2.24}$$

8. Reserve capabilities: Each unit hourly reserve provision is limited by a maximum technical limit:

$$pr_{i,y,s,t} \leq u_{i,y,s,t} \cdot Pr_i^{max}, \quad \forall i \in I^{th}, y \in Y, s \in S, t \in T \tag{2.25}$$
$$sr_{i,y,s,t}^{up} \leq u_{i,y,s,t} \cdot Sr_i^{max,up}, \quad \forall i \in I^{th}, y \in Y, s \in S, t \in T \tag{2.26}$$
$$sr_{i,y,s,t}^{dn} \leq u_{i,y,s,t} \cdot Sr_i^{max,dn}, \quad \forall i \in I^{th}, y \in Y, s \in S, t \in T \tag{2.27}$$

9. Renewable energy production: IRES production is limited by the hourly capacity factor CF and the commissioning of the units [1]

$$p_{i,y,s,t} \leq x_{i,y}^{*} \cdot P_i^{max} \cdot CF_{i,y,s,t}, \quad \forall i \in I^{res}, y \in Y, s \in S, t \in T \tag{2.28}$$

10. Maximum allowable emissions: The maximum emission constraint is also similarly implemented in the UC model but with hourly resolution:

$$\sum_{i \in I^{th}} \left(E_i \cdot \sum_{s \in S} \sum_{t \in T} p_{i,y,s,t} \right) \leq E_y^{max}, \quad \forall y \in Y \tag{2.29}$$

2.3 Integrating GEP and UC models

Below we describe two different schemes for coupling the long-term GEP and short-term UC models: i) via soft-linking the two models (S-GEP), and ii) via fully integrating the two models within a single optimization problem (C-GEP).

2.3.1 Soft-linked GEP-UC model (S-GEP)

The S-GEP model consists of two mixed integer linear programming problems which are successively solved:

1. The long-term GEP model, which has the objective of minimizing the total discounted cost over the planning horizon under typical long-term simplified constraints. No hourly chronological order is considered and load is represented as load blocks.
2. The short-term UC model, which has the objective of minimizing the short-term operational costs, taking into account the detailed short-term technical capabilities of the units, the chronological demand and IRES availability.

The soft linking of the two problems is achieved by:

1. Solving the long-term GEP problem first, under the simplified system representation;
2. Populating the obtained investment plans within the UC problem, which is, then, solved to obtain the detailed operation of these plans.

2.3.2 Integrated GEP-UC model (C-GEP)

The C-GEP model is the straightforward integration of the two models described above into a single optimization model, with the following adjustments:

[1] Notice that this constraint is formulated as an inequality and allows for IRES shedding.

- The load-duration step representation indexed by (m) in the GEP model is replaced by the sub-period index (s) and the hourly chronological index (t), for all parameters and decision variables.
- The detailed operating cost equation of the UC objective function replaces that of the traditional GEP model.
- It should be noted that the investment cost considered in the integrated model should be adjusted to ensures the proper relationship between the annual investment and operational costs and the correct evaluation of the different investment options having different life spans $Tlife_i$. This is achieved by adjusting the investment cost C_i^{inv} to represent the Equivalent Annual Cost (EAC) that is obtained by multiplying the $AnnuityFactor_i$ calculated as: $AnnuityFactor_i = \frac{1-(1+DR)^{-Tlife_i}}{DR}$.

2.4 Model implementation

All optimization problems are modeled in the Python programming language. The MILP problems are programmed using the Pyomo software package [82, 83] and solved on a PC with Intel Core i7 at 3.2GHz and 8GB memory using IBM ILOG-CPLEX with an optimality gap of 0.01%.

As can be seen, the integrated high resolution MILP problem is computationally challenging, especially when considering a multi-annual planning horizon. The next Chapter describes methods to address the computational complexity by systematic and accurate simplifications of the model.

3 Computational challenges

3.1 Overview

The integrated multi-annual planning problem proposed in this work is a very large MILP and solving it with over-the-counter solvers can be computationally challenging at best, if not infeasible. This is specifically because of the hourly decisions resolutions within the long-term planning horizon. For this, efficient approximation methods are needed to alleviate the computational burden while ensuring that the integrity of the results are maintained. This chapter summarizes the different methods developed in this work or adapted from the existing literature to address this issue. Although these methods are not the main focus of the work, they remain important to handle the computational complexity of the model proposed and its computation for practical application. To this end, in Section (3.2) the integer clustering method implemented in the planning model to handle the discrete decision variables is described. Then, in Section (3.3), three different approaches for the optimal horizon reduction are described: i) a dynamic programming model for the optimal LDC step-function approximation, ii) an optimal sample weeks selection reliant on an exhaustive search algorithm, and iii) an optimal sample days selection model.

3.2 Power generation units clustering

The integrated power system planning model formulated in the previous chapter employs the integer clustering method to handle discrete decision variables [84]. In the literature, this method has been primarily developed to reduce the computational complexity in UC problems and has found applications for the power systems planning models. Typically, many decision variables, such as the commissioning and commitment decisions, start-up and shut-down decisions, are binary variables that consider each generation unit individually. Even for moderate size planning or operational horizon, this can quickly scale up to significantly large MILP problems that are computationally infeasible. The integer clustering method addresses this issue by grouping the decisions for similar and/or identical units in a single integer variable, instead of many binary ones. The generation units clustering can follow different approaches: for example, grouping only identical units, grouping units by location and/or by some specific economic or technical criteria, such as the production costs or technical ramping rates. Clustering can be most directly achieved by grouping generation units belonging to the same technology type (i.e. nuclear, combined cycle gas turbine (CCGT), solar-pv, etc.) as those units would share, on average, many similar characteristics. The cluster characteristics are, then, defined as the means of the technical and economic parameters values of the units within the cluster. Clearly, this would lead to losing specific plant-level information in exchange to significantly improving the calculation time. One can argue, however, that while detailed plant-level characteristics are significant for decisions related to short-term operation, they are less relevant for long-term planning, where the mean

values of the parameters would still reasonably represent the units in the cluster, with little trade-off in the solution accuracy [84].

Computationally, the integer clustering of the discrete decisions variables provides a problem structure that significantly reduces the combinatorial state space. The number of possible discrete combinations of the typical binary variables scales exponentially 2^{N_i} with the number of units per cluster N_i, whereas clustering scales as the product of the cluster sizes $\prod N_i$, where i is the index representing each cluster. For example, a CCGT cluster comprising 20 individual units only contains 21 possible states for any discrete decision variable in the clustered model, whereas the number of the potential binary states is approximately $2^{20} \approx 1 \cdot 10^6$, with an exponential growth for each additional unit. In addition, clustering also reduces the number of continuous constraints and variables, since all relations apply over the smaller set of clusters [85].

For the mathematical formulation, little of the traditional GEP or UC formulation changes with clustering. The key exceptions is to represent each technology cluster with the cluster identifier. Discrete variables in the problem are, then, no longer binary but can take any positive integer value:

$$q_{i,y}, x_{i,y}, u_{i,y,s,t}, z_{i,y,s,t}, v_{i,y,s,t} \in \mathbb{W}, \quad \forall i \in I, y \in Y, s \in S, t \in T \tag{3.1}$$

where $\mathbb{W}$ is the set of whole numbers (including 0).

Notice that according to that definition, each unit is still represented individually within each decision variable (such as commitment or commissioning state), but handled collectively within the cluster in the optimization model. Some small adjustments are, then, necessary within the respective constraints compared to the non-clustered formulations, as applied in the model formulation proposed in the previous chapter. All of the other continuous variables, such as power output level, reserves contribution, etc., and constraints, are also aggregated for the entire cluster i.

3.3 Time horizon reduction

Another approach to reduce the computational complexity of the integrated planning and operational problems is to resort to a simplification of the time horizon considered. Within the multi-annual integrated planning model, even a single planning year fully represented via 8760 hours scales up immensely with the number of discrete and continuous decisions required to be taken for each time step. However, there is no need to consider the full horizon as it is reasonable to expect that many of those hours are identical or very similar in the load levels or the IRES-CF levels.

Indeed, for the typical GEP problem without short-term constraints, the decisions are typically derived based on average values for the system load. The so called LDC for these systems is approximated via a step-function, where the number of steps and their values are often selected in an ad-hoc manner. This approach significantly simplifies the system representation, with the main disadvantage being that it loses all chronological information related to the load or IRES-CF evolution. However, this approach has many relevant applications and in the next section we describe an optimization model that optimally finds this step-function approximation.

However, the aim of the integrated planning model is to preserve the chronological order of the load and IRES-CF evolution, especially for capturing the realistic ramping evolution of the system. Two methods are, then, presented that optimally approximate the yearly load

by selecting a subset of weeks or days representative of the full horizon, while preserving the chronological order.

It should be noted that the *optimal approximation* in this context refers to minimizing the error between the original LDC and the approximated LDC obtained from the subset of selected weeks or days, as will be explained in the next sections. In this sense, the error definition remains consistent among all the different approaches proposed in the next sections.

3.3.1 Optimal load duration curve approximation

To obtain the investment decisions in the traditional GEP model, the yearly load is typically sorted to be represented as a LDC, which is approximated by a step-function, where each step represents an average load-level and duration. This function is typically obtained by deciding in an ad-hoc manner the number of steps and segmenting the LDC accordingly. Depending on the choice of segmentation, the outcome of the model can greatly differ, for instance, if more steps are introduced for the peak load hours or the base ones. Moreover, in a multi-annual planning context the LDC forecast varies among the different years, so that a segmentation strategy for a year might not be optimal for other years. A consistent method for the LDC approximation is, therefore, necessary.

Dynamic programming model

The seminal work of [86] is one of very few studies in power systems planning found to address this issue. We define a similar optimization problem where the objective of the step function approximation is the minimization of the energy mismatch between each approximated step and its actual corresponding segment in the original LDC. The optimization problem can be formulated as:

$$\min_{\mathbf{k}} \sum_{n=1}^{N_{step}} \sum_{\xi=k_{n-1}}^{k_n} \left(F(\xi) - h_n\right)^2 \tag{3.2}$$

subject to:

$$h_n = \frac{1}{k_n - k_{n-1}} \cdot \sum_{\xi=k_{n-1}}^{k_n} F(\xi), \quad n = 1, 2, ..., N_{step} \tag{3.3}$$

where $F(\xi)$ represents the actual LDC function, N_{step} is the total number of steps specified for the approximation, n is the index of the current approximation step, h_n is the height (load level) of the step function for step n and k_n is the breakpoint at which the step function changes value from step n to step $n+1$. A schematic illustration of the LDC step-function approximation is given in Figure (3.1).

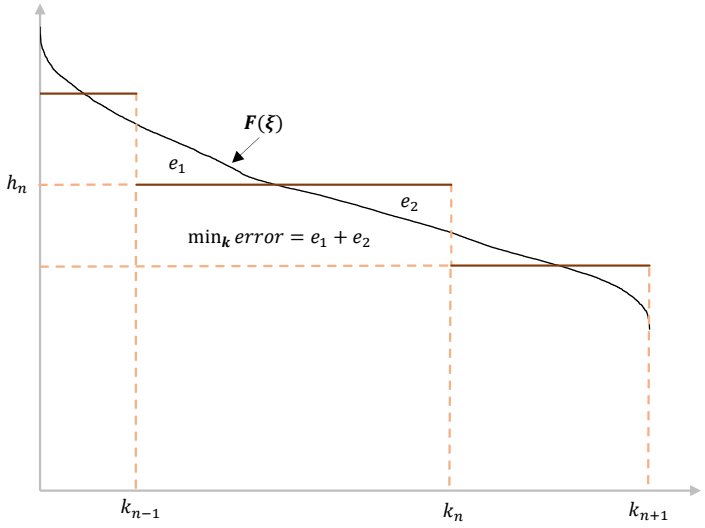

FIGURE 3.1 – Illustrative example of LDC step function approximation

Notice that the breakpoint vector **k**, which indicates the point at which the height of the step-function changes, fully defines the step-function. This is because as soon as k_n is defined, the step height h_n is simply calculated as the mean value of the segment $F(\xi), \xi \in [k_{n-1}, k_n]$. The objective is, then, to find the breakpoints vector **k**, which fully defines the approximated step function and is such to minimize the mismatch of equation (3.2). This problem can be stated as a dynamic programming problem, where the backward recursive functional equation is defined as:

$$f_n(\chi) = \min_{\chi \leq k \leq T} \left[\sum_{\xi=\chi}^{k} \left(F(\xi) - h_{N_{step}-n+1} \right)^2 + f_{n-1}(k) \right], \quad n = 1, 2, ..., N_{step} \tag{3.4}$$

for which $h_{N_{step}-n+1}$ can be calculated as given in equation (3.3).

For the simplified GEP model, it is important to note that since we consider the investment in IRES capacity as a decision variable, the average capacity factor (CF) of each IRES technology should be properly represented. Neglecting this consideration within the simplified long-term GEP problem is equivalent to assuming that wind and solar technologies are fully dispatchable. Constraint (2.9) in the model formulation is, therefore, introduced to avoid this inaccuracy. Similar to the LDC approximation, the CF of each IRES technology can be approximated by a level and a duration. However, the real average correlation between the load and the IRES-CF should be maintained to avoid unrealistic and biased results. An illustration of the approach followed in this work to account for this correlation is given in Appendix (A).

3.3.2 Optimal sample weeks selection

The horizon reduction for the integrated GEP-UC models need to maintain the real hourly chronological order of both the load and the IRES-CF. This is typically achieved by approximating the full year to a number of days, weeks or months while preserving the sub-period chronological order. To approximate a year by a number of sampled weeks, the optimal

weeks can be obtained by solving an optimization problem similar to that proposed in [87], which reported superior approximations than other ad-hoc methods.

Exhaustive search algorithm

The weeks are selected with the objective of minimizing the energy mismatch between the original LDC and the approximated one (LDC^{aprox}), obtained through scaling up the weeks sampled to the full year length. Mathematically, this is represented by [87]:

$$\boldsymbol{\phi}^* \in arg\min_{\boldsymbol{\phi}} \sum_{\tau=1}^{T} (LDC_\tau - LDC^{aprox}_{\boldsymbol{\phi},\tau})^2 \tag{3.5}$$

where T is the total number of hours in each planning year and $\boldsymbol{\phi}$ is a vector representing the set of decisions of the selected weeks ($\phi_w \in \{0,1\}$ for each week w). For a reasonably low number of weeks, the optimization can be solved using an exhaustive search algorithm that evaluates all possible combinations of the N_{weeks} specified weeks and selects those that minimize the LDC energy mismatch. Once the optimal weeks are obtained for the load, the same weeks are selected for the IRES-CF data to ensure that the correlation between the two is maintained.

3.3.3 Optimal sample days selection

In many cases, even a representative number of weeks can be computationally challenging for finding a solution to the integrated planning problem. In these cases, a more compact time horizon that captures the same essential features is needed. While it can be argued that in these cases a simple reduction in the number of weeks considered is sufficient (e.g. 1 sample week instead of 4), it is obvious that such a solution is sub-optimal compared to selecting a similar number of days independently. However, it is computationally infeasible to use the same exhaustive search method to select a number of days instead of weeks. As an example, the number of possible solutions for different reduction intervals is:

- for 4 weeks approximation: 1,326 possible solutions
- for 4 days approximation: 727,441,715 possible solutions
- for 5 days or more: > 52 billions possible solutions

The work in [88] proposes another method for selection of number of days which relies on altering the original definition of the optimization problem so that it can be solved using MILP techniques. The alternative formulation is important since obtaining the approximation of the LDC requires sorting the hourly load-level values of the selected days in an ascending order, to compare the error to the original LDC. This sorting is difficult to integrate within a MILP problem. The solution proposed for this problem relies on segmenting the LDC into a number of bins $b \in B$. Each of these bins represent the share of time during which the time series has a value greater than or equal to the lowest value in the range corresponding to bin b. These values can be easily calculated for any range of bins segmentation and can be represented by a parameter $\vartheta_{(c,b)}$, where c denotes the respective LDC being approximated. Similarly, for every potential representative day, the share of time in day d during which the time series exceeds the lowest value of the range corresponding to the same bin b can be calculated. This information is represented by the parameter $\mu_{(c,b,d)}$.

Note that, when selecting the set of representative days, a weight should be assigned to each of them as to scale them up to be equivalent to the total energy of the original LDC. While this can be set as a decision variable (as in [88]), we adapt the formulation to assume a constant weight pre-defined for the set of representative days. For this, we assume a uniform weight calculated as the ratio between the number of days indicated for the approximation and the total number of days of the respective LDC (365 days for a yearly LDC). Now, assuming that a subset of representative days $D' \subset D$ is selected and is represented by a variable $\lambda_d = 1$, the share of the time during which the approximated LDC has a value greater than or equal to the lowest value in the range of bin b is also known and is equal to $\sum_{d \in D} (weight_d \cdot \lambda_d \cdot \mu_{c,b,d})$. For clarity, an illustration of these descriptions is shown in Figure (3.2)[1].

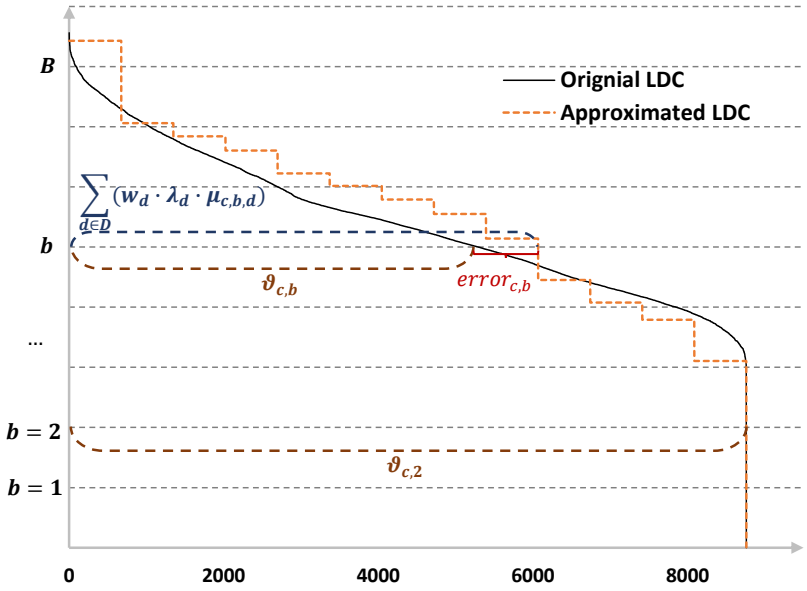

FIGURE 3.2 – Illustrative example of approximation error based on the definition of the partitioning bins.

Then, the error to be minimized can be described as the difference between the original and the approximated LDC *in the share of time that the lowest value in the range of bin b is exceeded*. This eliminates the need to sort the data of the selected days within the optimization. Mathematically, this error function is defined as:

$$error_{c,b} = \mid \vartheta_{c,b} - \sum_{d \in D} (weight_d \cdot \lambda_d \cdot \mu_{c,b,d}) \mid, \quad \forall c \in C, b \in B \tag{3.6}$$

from which the MILP problem that follows can be formulated.

Adapted mixed integer linear programming model

The sample days selection optimization problem following the above adaptations can be formulated as:

[1]Figure adapted from [88]

$$\min_{\lambda_d} \sum_{c\in C}\sum_{b\in B}\left(error^{+}_{c,b} + error^{-}_{c,b}\right)^2, \tag{3.7}$$

s.t.,

$$error^{+}_{c,b} - error^{-}_{c,b} = \vartheta_{c,b} - \sum_{d\in D}\left(weight_d \cdot \lambda_d \cdot \mu_{c,b,d}\right), \quad \forall c \in C, b \in B \tag{3.8}$$

$$\sum_{d\in D} \lambda_d = N_{days}, \tag{3.9}$$

$$\lambda_d \in \{0,1\}, \quad \forall d \in D; \tag{3.10}$$

$$error^{+}_{c,b}, error^{-}_{c,b} \in \mathbb{R}^{+}_{0}, \quad \forall c \in C, b \in B. \tag{3.11}$$

Note that the variables $error^{+}$ and $error^{-}$ are used for the proper handling of the *absolute* term in equation (3.6).

The MILP model seeks to find the vector of selected days ($\lambda_d = 1$) with the objective of minimizing the mismatch error (3.7). Equation (3.8) defines the mismatch error considered and described in the previous section. Equation (3.9) imposes the number of selected days which corresponds to the predefined number of periods required N_{days}. Equations (3.10) and (3.11) restrict the domains of the respective variables. The MILP model can, then, be solved with over-the-counter solvers and is able to optimize a reasonable set of days selection (up to 11 days, in our experience) in the order of hours.

3.4 Comparison of the horizon reduction methods

This section provides a brief illustration and comparison between the approximations achieved using the three different horizon reduction approaches described in this chapter. The aim of this comparison is to provide an overview of the approximation quality and an overall validation for the use of these approaches within the context of the thesis.

To effectively quantify the accuracy of the different approximations by a step-function or a set of representative periods, appropriate metrics should be used. Most notably, the approximation should preserve the annual electricity load (and IRES-CF) for each planning year. Moreover, the metric should evaluate the information regarding the distribution of load (and IRES-CF) and their respective frequency of occurrence. This is especially important when considering high inter-temporal variations, such as the case with a high share of IRES penetration [89]. This information can be evaluated by comparing the original and approximated time series in terms of the LDC approximation accuracy (i.e. by sorting the data from high to low and evaluating the sorted data). To this end, the normalized-root-mean-square-error ($NRMSE$) metric is used to evaluate the quality of the approximation relative to the original LDC. The root-mean-square error ($RMSE$) is first calculated, from which the ($NRMSE$) can be obtained:

$$RMSE = \sqrt{\frac{\sum_{t\in T}\left(LDC_t - LDC_t^{aprox}\right)^2}{\mid T \mid}} \tag{3.12}$$

$$NRMSE = \frac{RMSE}{\max\left(LDC\right) - \min\left(LDC\right)} \cdot 100\ [\%] \tag{3.13}$$

Next, we evaluate and compare the error of the approximations achieved by the three above-mentioned approaches. Most notably:

- Step-function approximation (12 steps)
- Sample days approximation (4 days)
- Sample weeks approximation (4 weeks)

The results are given for the approximations of the 10 planning years considered in this work (more details on the system description can be found in Chapter (4.4.1)). Table (3.1) summarizes the $NRMSE$ value for each approximated, as given by the three approaches: step-function approximation, optimal representative days and optimal representative weeks. The mean and standard deviations of the results across the whole planning horizon are also given.

	NRMSE											
	Year 1	Year 2	Year 3	Year 4	Year 5	Year 6	Year 7	Year 8	Year 9	Year 10	Mean	Std. Dev
Step-Aproximation (12 steps)	4.09%	4.11%	4.29%	3.87%	3.81%	3.86%	3.49%	3.78%	4.10%	3.75%	3.91%	0.23%
Representative days (4 days)	1.50%	1.73%	1.40%	2.13%	1.57%	2.03%	3.07%	1.34%	1.51%	2.02%	1.83%	0.52%
Representative weeks (4 weeks)	0.76%	0.96%	0.63%	1.05%	0.92%	1.46%	1.63%	0.80%	0.64%	0.75%	0.96%	0.34%

TABLE 3.1 – Comparison of the NRMSE for the different approximation methods and for all planning years considered.

It can be seen that, in the worst case, the error of the approximations obtained does not exceed 4.3% for -low resolution- step-approximation. As expected, the error improves as a higher resolution approximation is used, reaching levels as low as 0.63% for the 4 weeks approximation of year 3. The mean value across the whole planning horizon confirms these results, with a significant improvement the higher the approximation time-step considered. Notice how the standard deviation of the $NRMSE$ across the whole planning horizon is reasonably low, confirming the consistency of these results for a wide range of LDC characteristics. As an example, Figure (3.3) visually illustrates the quality of the approximations and compares it for the three approaches proposed and for two different planning years.

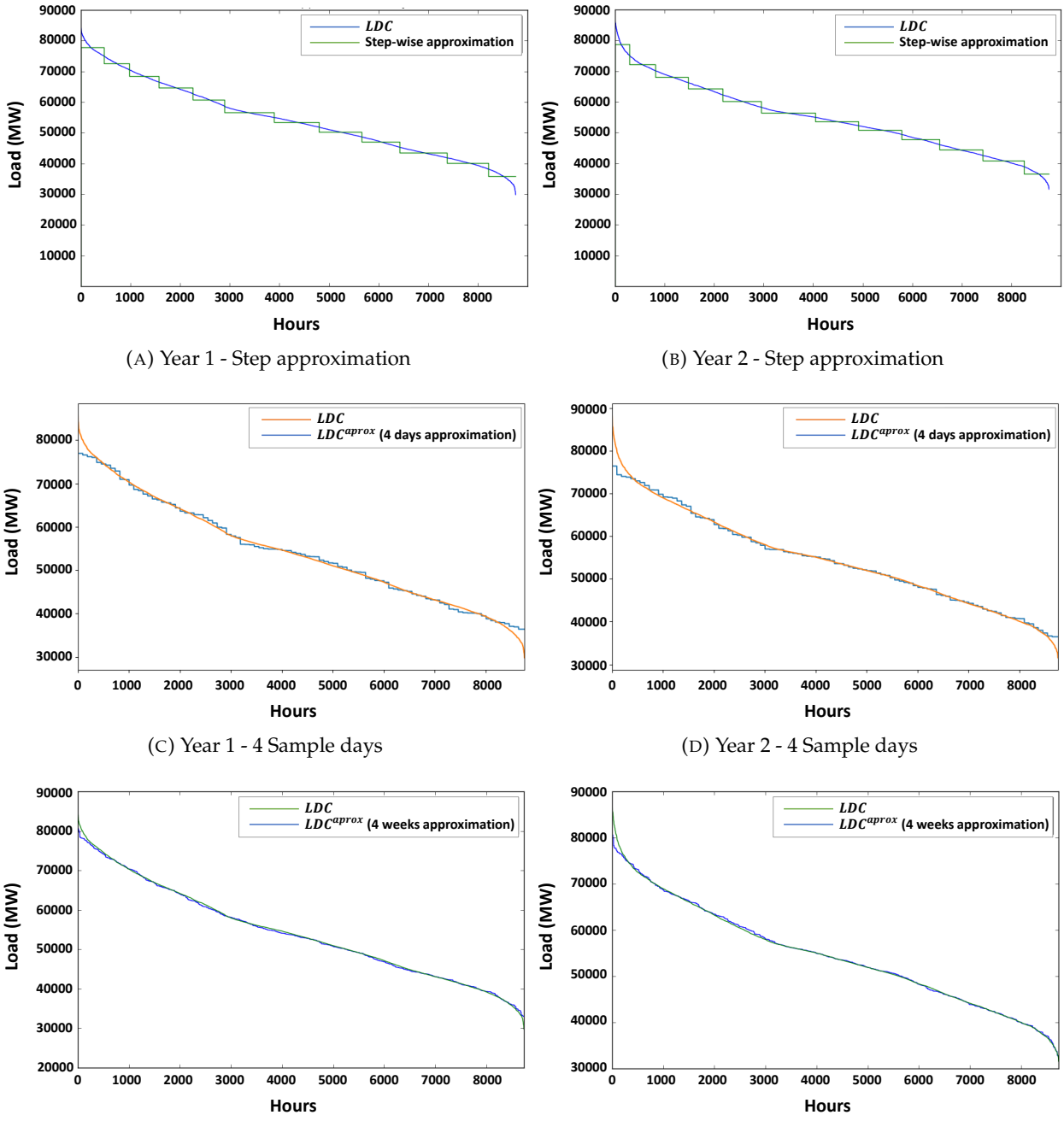

(A) Year 1 - Step approximation

(B) Year 2 - Step approximation

(C) Year 1 - 4 Sample days

(D) Year 2 - 4 Sample days

(E) Year 1 - 4 Sample weeks

(F) Year 2 - 4 Sample weeks

FIGURE 3.3 – Graphical illustration for the comparison of the quality of the approximations obtained by the different horizon reduction approaches and for two distinct planning years (Year 1 and Year 2)

4 An integrated planning and assessment method for electric power systems operational flexibility

4.1 Overview

This chapter details the integrated framework for operational flexibility assessment in power systems planning and its application to a realistically sized case study to derive the system investment decisions under a high share of IRES penetration. Most notably, two probabilistic metrics are introduced in this chapter for the quantitative operational flexibility assessment, : the insufficient ramping resource expectation (IRRE) proposed in [53] and the originally introduced expected flexibility shortfall (EFS) metric, which quantifies the expected load loss when the system is not able to adequately respond to the inter-temporal variability.

The numerical example considers a single-region green-field planning problem. On one hand, this is done to avoid any bias that existing units may impose on the expansion plans and, therefore, to be able to focus solely on the models outcomes; on the other hand, it is done to validate the framework capability for efficiently addressing large-sized instances. The framework, however, is straightforwardly applicable to grey-field planning problems, where some of the decision variables related to the unit commissioning decisions will be set as fixed parameters representing the existing system units. Those will be only considered for the operational decisions, such as, commitment and production levels. In the same way, the framework is, also, easily extendable to multi-regional planning, where a set of regions would be defined and commissioning and commitment decisions would be taken for each region separately. In this case, additional power flow constraints between the regions should be defined, as widely discussed in the literature. Finally, a wide range of IRES penetration levels (0% to 50%), most notably wind and solar, is considered, as well as different scenarios for carbon emission limits.

The results highlight the importance of relying on suitable quantitative metrics for operational flexibility assessment in power systems planning rather than solely relying on generic performance measures, such as system costs and mixes of power plants technologies, which are shown not to sufficiently reflect the flexibility levels of the obtained plans.

4.2 Integrated flexibility assessment framework

The integrated operational flexibility assessment framework proposed is described in the next sections. For comparison purposes, it will be applied to the two types of power system

planning models formulated in Chapter (2): the traditional GEP model soft-linked with a UC model (denoted S-GEP) and the integrated GEP-UC model solved as a single optimization (denoted C-GEP). Section (4.2.1) describes the assessment framework applied to the former, and Section (4.2.2) that applied to the latter. The comparison aims at validating and quantifying the superiority of the C-GEP planning model in accounting for the short-term ramping variability, compared to classical planning models in a systematic manner. For both cases, the framework stands: i) the formulation of the optimization planning models, ii) the application of accurate horizon reduction approximation methods and iii) the application of quantitative metrics for assessment of the operational flexibility of the of the obtained plans.

4.2.1 Assessment framework for soft-linked planning model

For the S-GEP model, the integrated planning and assessment framework follows:

1. Solving the simplified GEP model (2.1)-(2.11). This model derives the system investment decisions from the traditional LDC approximation. For this, instead of relying on ad-hoc methods to approximate the LDC, the dynamic programming algorithm (3.4) is used. This guarantees the optimal representation of the different load levels for evaluation and comparison purposes.
2. The optimal yearly investment decisions (Ω^*) are, therefore, obtained. Those include the optimal annual commissioning decisions per generation technology ($q^*_{i,y}$) and subsequently the availability of the generation units per technology and per year ($x^*_{i,y}$).
3. The UC model (2.12)-(2.29) is, then, solved considering the generation units availability as a parameter to obtain their optimal operational decisions throughout the planning horizon.
4. To solve the UC model in a tractable and consistent manner, the approximation methods described in (3.3.2) and (3.3.3) are used for the optimal sample weeks or days selection to represent the system load and IRES-CF. The solution of the UC problem results in the optimal system operational decisions (Θ^*).
5. The flexibility of the investment and operational decisions (Ω, Θ) are, then, evaluated by the quantitative metrics ($IRRE, EFS$), described in this section, to obtain the flexibility levels of the plans.
6. The process can, then, be repeated to plan and evaluate the flexibility under different scenarios (e.g. IRES penetration levels, emission limits, system costs, etc.). This framework is schematically illustrated in Figure (4.1).

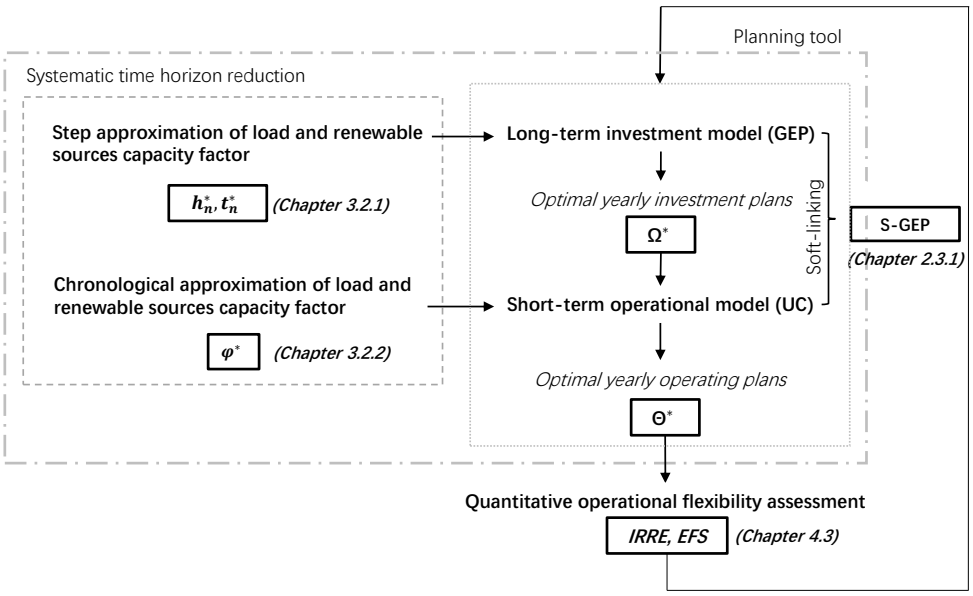

FIGURE 4.1 – Operational flexibility assessment framework: Soft-linked planning model

4.2.2 Assessment framework for integrated planning model

The framework for the integrated planning model follows the same steps as described above, with the exception that both the investment and operational decisions are optimized within the same problem. This means that only the chronological horizon approximation method is used as illustrated in Figure (4.2).

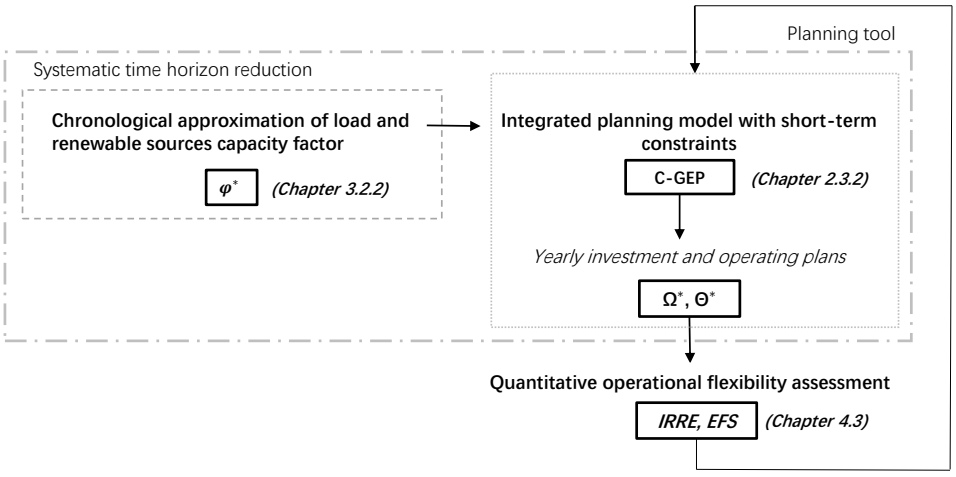

FIGURE 4.2 – Operational flexibility assessment framework: Integrated planning model

4.3 Operational flexibility assessment metrics

4.3.1 Insufficient ramping resource expectations (IRRE)

The IRRE is the expected number of instances in which the generation units in a power system cannot answer to the changes in net load. The metric is generally obtained by [53]:

1. Calculating the net load ramping time series for the whole planning horizon in both upwards (up) and downwards (dn) directions.
2. Calculating the up/dn available flexible resources within a specified time horizon of interest (e.g. one hour), given the availability and commitment status of each generation unit, its start-up time, its actual production level and its total upwards or downwards ramping capabilities for the next period.
3. Aggregating all the time series for all resources to obtain the total up/dn available flexibility time series.
4. Calculating the up/dn available flexibility empirical cumulative distribution function from the total available flexibility time series.
5. Calculating the probability of insufficient ramping by substituting the required net load ramping in the obtained distribution function. The sum of the up/down probabilities time series gives the IRRE+/-.

4.3.2 Expected flexibility shortfall (EFS)

While the IRRE indicates the expected frequency for not meeting the flexibility requirements, it does not give any information about how short the system is on average when not able to meet these requirements. This can be calculated through the expected flexibility shortfall (EFS) metric.

The EFS metric builds on the value-at-risk (VaR) measure defined as the "possible maximum loss over a given holding period within a fixed confidence level" [90]. Mathematically, this is defined as:

$$VAR_{\alpha}(X) = \sup\{x \mid P[X \geq x] > \alpha\} \tag{4.1}$$

where X in our context is a variable denoting the loss of load due to insufficient flexibility and $\sup\{x \mid P[X \geq x] > \alpha\}$ indicates the highest 100α percentile of the loss distribution. The expected flexibility shortfall (EFS) is, thus, the conditional expectation of load loss due to insufficient flexibility, given that it is beyond the VaR level, or:

$$EFS_{\alpha}(X) = E\left[X \mid X \geq VaR_{\alpha}(X)\right] \tag{4.2}$$

The EFS is calculated by performing steps (1) to (3) of the IRRE calculations, followed by:

4. Calculating the up/dn losses time series as the absolute difference between the up/dn net load ramping series and the respective total available flexibility resources.
5. Calculating the VaR at the desired $100(1-\alpha)\%$ confidence levels.
6. Calculating the EFS as the average loss for observations exceeding the VaR level, at the respective confidence levels.

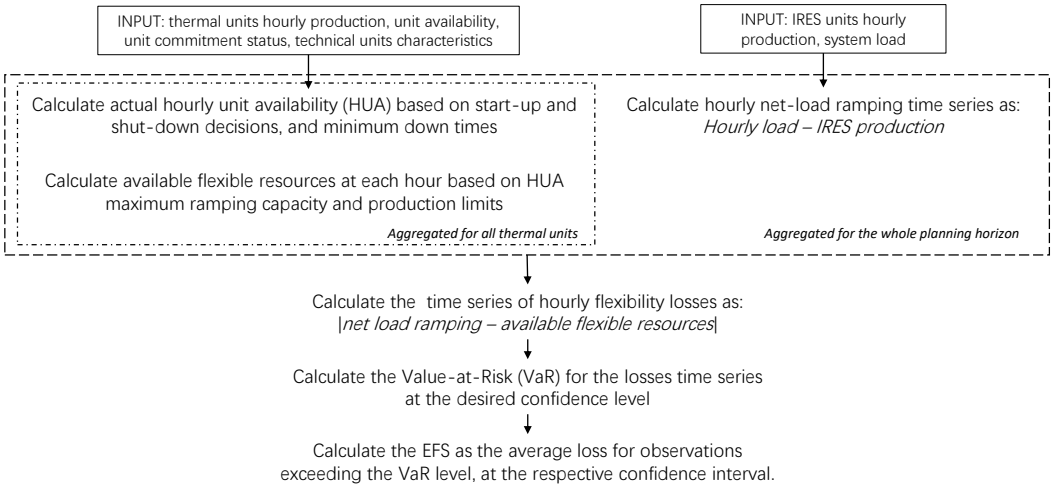

FIGURE 4.3 – Schematic illustration for the EFS calculation steps

4.4 Application

4.4.1 System description and implementation notes

For the multi-annual demand representation, we have taken the 10 years load data of France, from 2006 to 2015, which are publicly available at [91], to represent a realistic system demand for 10 planning years. We have similarly calculated the IRES-CF, namely wind and solar power, from the actual yearly production time series, by dividing each hourly production by the total installed capacity of each technology. This results in the hourly CF time series per renewable technology and for each year. Forecasting methods for long-term data prediction can be used to estimate these parameters, but is beyond the objectives of this work, instead we focus on showing the accuracy and relevance of the assessment results when applied to realistic data that do not require further validation.

Table 4.1 summarizes the technical and cost data for the generation technologies considered in the expansion planning. The cost data and units capacities are obtained from the IEA/NEA Projected Costs of Generating Electricity report (2015 edition) [92]; the remaining technical characteristics are largely based on data described in [93] to maintain consistency with characteristics relevant to the French power system. The discount rate is assumed to be 3% in accordance to the IEA/NEA estimations for government-owned utilities in countries with good bond ratings or ones with stable rate-of-return regulation, such as the case in most developed economies. The minimum design reserve margin r^{min} is set to 15% of the maximum annual load, operating reserves are set to cover 1% of the hourly load for primary and secondary reserves, and 10% of the hourly IRES production for upwards and downwards secondary reserves. The penalty for not meeting demand (C^{lns}) is set to 4k€/MWh to discourage load shedding. Finally, the construction time of new units is neglected , as we are considering a relatively concise planning horizon.

TABLE 4.1 – Technical and economic characteristics for the different generation technologies

Technology $[i]$	P_i^{max} $[MW]$	P_i^{min} $[MW]$	R_i^{Umax} $[MWh/min]$	R_i^{Dmax} $[MWh/min]$	M_i^u $[hours]$	M_i^d $[hours]$	E_i $[tCO_2/MWh]$	ϵ_i	C_i^{inv} $[M€]$	C_i^{mrgl} $[€/MWh]$	C_i^s $[k€]$
Nuclear	1400	700	$0.5\%P_n$/min	$0.5\%P_n$/min	12	48	0	0.01	3.95	9.33	15.0
Fossil Hard Coal	1100	550	$1.5\%P_n$/min	$1.5\%P_n$/min	6	10	0.96	0.06	2.08	36.67	11.26
Fossil Gas (CCGT)	550	165	$5\%P_n$/min	$5\%P_n$/min	3	5	0.46	0.04	1.02	69.00	7.53
Fossil Gas (OCGT)	270	54	$20\%P_n$/min	$20\%P_n$/min	1	2	0.67	0.08	0.7	110.00	3.79
On-Shore Wind	80	0	/	/	/	/	0	*	1.9	0	/
Solar-PV	60	0	/	/	/	/	0	*	1.5	0	/

4.5 Results and discussion

4.5.1 IRES penetration and carbon emission policy scenarios

We first explore 12 scenarios covering a wide range of IRES penetration and carbon emission targets: a base case with no IRES nor emission targets, in addition to all remaining combinations of 0%, 25%, 35% and 50% binding IRES penetration targets (represented as a percentage of total electricity demand) and 0%, 75% and 50% emission limit (calculated as a percentage of each corresponding no emission limit scenario). We apply the assessment framework on the two types of planning models considered (C-GEP and S-GEP), for comparing the effect of integrating the short-term constraints within the long-term investment planning problem and primarily in terms of operational flexibility. For the S-GEP model, each annual LDC is approximated by twelve load-duration steps, while for the C-GEP model, each year is approximated by four optimal weeks.

Base case

For the base case, Figure (4.4) illustrates the total capacity installed of each generation technology, at the end of each year, obtained by each model. The bulk of the investments is done in the first year, where 82.01 GW and 80.59 GW total capacities are installed by the S-GEP and the C-GEP model, respectively, and gradually increase to the end of the planning horizon. The final total capacities installed are 87.14 GW and 85.72 GW for S-GEP and C-GEP, respectively. The additional capacities in both cases are in the Fossil OCGT technology. It can be observed that, in the case with no requirement on IRES penetration, the capacity investments given by both models are very similar.

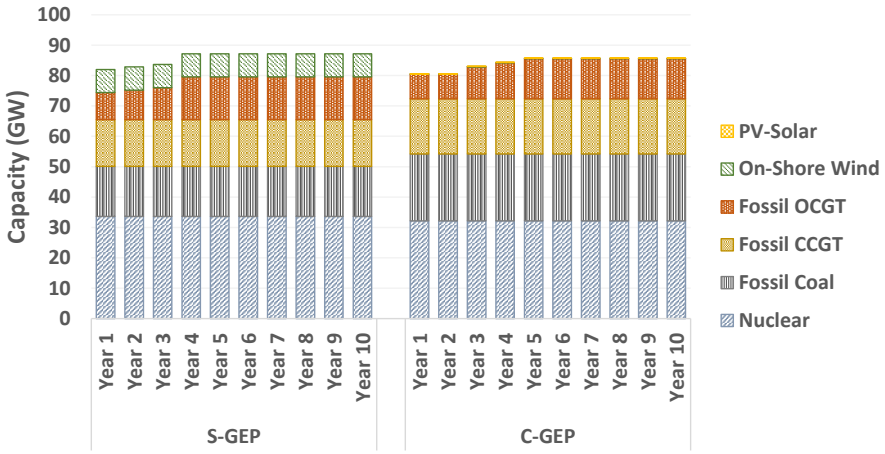

FIGURE 4.4 – Cumulative yearly installed capacity for the base case obtained through the S-GEP (left) and C-GEP (right) models

TABLE 4.2 – Results of different performance measures and operational flexibility metrics for the plans obtained through the S-GEP and C-GEP models for the base case (No IRES requirement, no carbon limits) (worse performance highlighted).

(A) Installed capacities and generic performance measures results

	S-GEP	C-GEP	
Total IRES Installed Capacity [GW]	7.60	0.14	**Difference [%]**
Total Installed Capacity [GW]	87.14	85.72	**(C-GEP relative to S-GEP)**
Total Cost (excluding LNS) [B€]	313.00	310.59	-0.77%
Load Not Served [% of total load]	0.12%	0.01%	-89.38%
RES shedding [% of total IRES]	0.00%	0.00%	/
Carbon Emission [Mtons]	1379.60	1699.93	+23.22%

(B) Operational flexibility metrics results

		S-GEP	C-GEP	**Difference [%] (C-GEP relative to S-GEP)**
IRRE+ (% of upwards ramps)		7.38%	2.20%	-70.13%
EFS+ (MW)	**EFS+ (95%)**	512.70	90.53	-82.22%
	EFS+ (99%)	2402.85	451.31	-38.08%
IRRE- (% of downwards ramps)		0.01%	0.00%	-42.52%
EFS- (MW)	**EFS- (95%)**	0.00	0.00	/
	EFS- (99%)	0.00	0.00	/

To better assess the S-GEP and C-GEP obtained plans, a number of performance measures are compared. Most notably, we compare the amount of load not served (LNS), the amount of IRES shedding, the total carbon emission and the total cost (investment + operating costs)[1] of the plans obtained through each model for the whole planning horizon. Table (4.2a) summarizes the results of the different measures for the base case. The C-GEP model outperforms the S-GEP in the resulting LNS, amounting to only 0.01% of the total load for the former as opposed to 0.12% for the latter. Since only a small fraction of the capacities installed are in IRES technologies, no amount of IRES shedding was required. Wind

[1] excluding the cost of LNS to avoid redundancy

and solar shedding would typically be decided if large energy quantities are produced, leading to very large inter-temporal variability so that it becomes more cost effective to shed the cheap IRES energy than to adapt the rest of the thermal units (e.g. turn on or shut down some of those units). Regarding carbon emission, operating the C-GEP obtained plan evidently results in higher total emission ($\approx$ 1700 Mtons compared to $\approx$ 1380 Mtons by the S-GEP model), which is explained by the overall higher fossil capacities installed. The total investment and operating cost is lower for the C-GEP plan (310.59 Bn€) compared to the S-GEP one (313.00 Bn€). This, together with the lower amount of LNS, indicates that the C-GEP plan is better adapted to satisfy the load at lower cost, but results in higher carbon emission than the S-GEP one.

The operational flexibility assessment of the resulting plans using the proposed metrics is summarized in Table (4.2b) . The IRRE and EFS results (at the 95% and 99% confidence intervals) are reported for the total increasing (+) and decreasing (-) net load variations. The results show that operating the S-GEP obtained plan is expected not to satisfy 7.38% of the total number of upwards ramps (IRRE+) as opposed to only 2.20% for the C-GEP plan. Moreover, the EFS is more than 5 times higher for the S-GEP plan, averaging around 512.00 MW and 2400 MW, at the 95% and the 99% confidence intervals, respectively, as opposed to an expectation of only 90 MW and 450 MW for the C-GEP obtained plan, at the respective confidence intervals. Regarding the negative ramps, it is shown that the operational flexibility shortages are of much less significance for both models plans, albeit still being slightly worse for the S-GEP one.

Increased IRES penetration and emission limit policies

Table (4.3) summarizes the results of the different performance measures analyzed for the base-case scenario (top-left corner), along with the different combinations of IRES penetration (horizontally) and emission limit (vertically) policies considered. First, we notice how an increased IRES penetration requirement leads to a significant difference in the final capacity mix given by the S-GEP and the C-GEP models compared to when such requirement is not imposed. Moving horizontally across the Table, i.e. to higher IRES requirements, the "short-term aware" C-GEP model results in mixes with much higher fossil capacities and much less nuclear than to the S-GEP one. These fossil technologies possess overall better short-term dynamic properties, such as ramping capabilities and shorter minimum up and down times. Such an investment choice can be, therefore, attributed to the ability of the integrated C-GEP model to derive decisions better adapted to the increased short-term variations imposed by the IRES penetration. Moreover, the total capacity installed increases significantly for the C-GEP plans compared to the S-GEP ones. The S-GEP model overestimates the actual IRES availability since it considers average capacity factor values, so it invests in overall less capacities in the other technologies. This gap increases with higher IRES penetration, from around 10 GW difference for the 25% IRES cases, to 15 GW for those with 35% IRES and up to 30 GW difference for the 50% IRES penetration plans. It is clear that such capacity differences are non-negligible and that they would significantly affect the reliability of the power system, if not adequately accounted for.

This becomes even clearer as we consider the resulting LNS percentage. There is a steep increase in the amount of LNS for the S-GEP plans with higher IRES levels, from 0.12% of the total load on average and up to 2.7% for the highest IRES penetration levels. As predicted from the capacity difference, this represents an unacceptably high level of LNS and defies the security of supply of the plans. The C-GEP plans, on the other hand, maintain

a low average LNS percentage of 0.02%, with negligible variation across all scenarios. IRES shedding exhibits a similar steep increase with the higher IRES penetration levels; however, it remains comparable for both the C-GEP and S-GEP plans with only a few percentage points difference in each respective scenario. As previously explained, shedding decisions are taken when they are more cost effective, the C-GEP model accounts for these sheds when deciding on the investment plans, and ensures that the plans obtained would still meet the IRES quota requirements. This is not the case for the S-GEP plans, which could lead to final plans that are theoretically meeting these requirements, but practically are not.

By looking at the differences in the performance measures of the C-GEP and S-GEP plans, especially the total installed capacities, one would expect a much higher total cost (not including LNS cost) for the C-GEP plans compared to the S-GEP ones. This is in fact not the case: while indeed the C-GEP plans with significant IRES penetrations result in higher costs, these are not proportional to the additional investments made and the amount of LNS avoided. The maximum cost difference reached at 50% IRES penetration averaged around only +6.31% more for the C-GEP plans than for the S-GEP ones, whereas the capacities were on average +20% higher.

Again, the amount of carbon emission is consistently higher for all C-GEP plans compared to the S-GEP ones, which is not surprising as the amount of fossil capacity installed is higher in those plans. This was optimally obtained through the C-GEP model as those units possess faster dynamic capabilities that are needed to counterbalance the higher net load variability as more IRES penetrate the system. Furthermore, this leads to the observation that increasing IRES penetration levels by itself does not necessarily indicate lower carbon emission levels in the system, since the rest of the investments are counterbalancing with more dynamic yet more emitting units. In this respect, the S-GEP model can be considered to be underestimating the actual emission levels as higher IRES penetrate the systems. For our numerical example, these underestimations are found to be in the range of 14% (No IRES, 50% emission limit case) to 60% (35% IRES, no emission limit case).

Imposing carbon emission limits, as shown by moving vertically across the table does not have a significant impact on most of these measures. It does, however, considerably affect the capacity mix obtained through the different models. Evidently, as more stringent carbon limits are imposed, the capacity mix shifts towards less emitting technologies and, most notably, nuclear. Most of the fossil capacity reduction is in the fossil coal capacity since it is the most emitting one; the total capacity installed, however, remains almost constant. Furthermore, despite the large differences in the capacity mixes, the total costs of the plans do not heavily vary, averaging around +1% increase in most cases, as higher emission limits are imposed.

TABLE 4.3 – Results of the different performance measures for the plans obtained through the S-GEP and C-GEP models for the range of IRES penetration and carbon emission limits considered (worse performance highlighted)

			No IRES		25% IRES		35% IRES		50% IRES	
			S-GEP	C-GEP	S-GEP	C-GEP	S-GEP	C-GEP	S-GEP	C-GEP
No emission limit	Installed Capacity (GW)	Nuclear	33.60	32.20	23.80	2.80	19.60	0.00	12.60	0.00
		Fossil Coal	16.50	22.00	15.40	39.60	13.20	37.40	11.00	28.60
		Fossil CCGT	15.40	18.15	13.20	17.05	12.65	18.70	10.45	19.80
		Fossil OCGT	14.04	13.23	17.28	21.06	17.01	22.41	18.09	25.65
		On-Shore Wind	7.60	0.08	56.96	54.48	79.76	75.20	113.92	108.24
		PV-Solar	0.00	0.06	0.00	0.06	0.00	3.12	0.00	18.00
	Total IRES Installed Capacity [GW]		7.60	0.14	56.96	54.54	79.76	78.32	113.92	126.24
	Total Installed Capacity [GW]		87.14	85.72	126.64	135.05	142.22	156.83	166.06	200.29
	Load Not Served [%]		0.12%	0.01%	0.61%	0.01%	1.21%	0.02%	1.62%	0.02%
	RES Shedding [%]		0.00%	0.00%	2.31%	0.44%	5.89%	2.48%	12.59%	9.56%
	Carbon Emission [Mtons]		1379.60	1699.93	1177.23	2920.81	1074.35	2648.64	1007.95	1876.63
	Total Cost (excluding LNS) [B€]		313.00	310.59	354.19	359.68	375.28	383.58	409.32	435.14
75% emission limit	Installed Capacity (GW)	Nuclear	37.80	37.80	28.00	11.20	22.40	8.40	15.40	4.20
		Fossil Coal	12.10	17.60	11.00	28.60	8.80	27.50	7.70	16.50
		Fossil CCGT	15.40	16.50	13.20	19.80	14.30	19.80	11.00	28.05
		Fossil OCGT	14.31	14.04	17.28	21.33	17.01	22.95	18.09	25.11
		On-Shore Wind	7.52	0.08	56.96	54.56	79.76	74.88	113.92	107.44
		PV-Solar	0.06	0.06	0.00	0.06	0.00	3.84	0.00	19.02
	Total IRES Installed Capacity [GW]		7.58	0.14	56.96	54.62	79.76	78.72	113.92	126.46
	Total Installed Capacity [GW]		87.19	86.08	126.44	135.55	142.27	157.37	166.11	200.32
	Load Not Served [%]		0.11%	0.01%	1.19%	0.02%	2.71%	0.02%	2.71%	0.03%
	RES Shedding [%]		0.00%	0.00%	2.81%	0.91%	6.25%	3.41%	13.06%	9.70%
	Carbon Emission [Mtons]		1047.78	1272.76	890.20	2180.01	857.71	1966.52	831.14	1407.10
	Total Cost (excluding LNS) [B€]		313.63	311.11	355.75	360.35	377.05	385.04	411.22	439.54
50% emission limit	Installed Capacity (GW)	Nuclear	40.60	43.40	30.80	22.40	26.60	18.20	18.20	12.60
		Fossil Coal	5.50	12.10	6.60	20.90	5.50	19.80	4.40	9.90
		Fossil CCGT	18.70	19.80	16.50	15.95	13.20	17.60	11.55	26.40
		Fossil OCGT	14.85	10.80	15.66	21.06	17.28	22.68	17.82	25.11
		On-Shore Wind	7.52	0.16	56.96	54.16	79.76	74.00	113.92	106.40
		PV-Solar	0.06	0.00	0.00	0.06	0.00	4.92	0.00	20.64
	Total IRES Installed Capacity [GW]		7.58	0.16	56.96	54.32	79.76	78.92	113.92	127.04
	Total Installed Capacity [GW]		87.23	86.26	126.52	135.07	142.34	157.20	165.89	201.05
	Load Not Served [%]		0.11%	0.02%	0.60%	0.02%	1.19%	0.02%	2.70%	0.01%
	RES Shedding [%]		0.00%	0.00%	3.04%	1.77%	6.72%	4.47%	13.47%	11.34%
	Carbon Emission [Mtons]		737.05	849.79	670.82	1392.25	631.64	1323.82	660.86	937.32
	Total Cost (excluding LNS) [B€]		315.71	312.59	356.99	361.39	379.31	387.85	413.05	442.17

Let us now analyze how increased IRES penetration and stringent emission limit policies impact the operational flexibility of the capacity expansion plans. The operational flexibility metrics values for all cases considered are summarized in Table (4.4)

For the upwards ramping requirements, the results show that the S-GEP plans become significantly short on flexibility as higher percentages of IRES penetrate the system. A linear and steep increasing trend of the flexibility shortage, reaching an IRRE+ of up to 47% (for the 50% IRES case), represents a failure to answer to almost half of the number of times the system is expected to provide upwards flexibility. The EFS+ similarly reaches multiples of its value for the plan with lower IRES penetrations (e.g. EFS value of 8157.30 MW compared to 2402.85 MW with 99% confidence, for the 50% and 0% IRES cases, respectively). For the C-GEP plans, the different metrics indicate very low expected shortages compared to the S-GEP ones. The IRRE+ does not exceed 2.20% for all cases considered and remains almost constant at an average of 1.30%. On the other hand, the EFS+ does not exceed a comparatively smaller value up to the 99% confidence, for all cases considered.

For the downwards ramping requirements, as with the base case, the results are much less significant, with no shortage expected in most of the cases. This is reasonably justified since we consider a single-region planning where as a consequence of considering all generation units sitting at the same region, at any given moment, enough generation units are online and can reduce their production to answer to downward ramps. It is still seen through the IRRE- metric results that systems with very large IRES presence would exhibit

some flexibility shortage. Generally, it should be noted that the downwards flexibility shortage would become more relevant considering multi-regional planning, since the available downwards resources will be limited to those belonging to the same region.

It is shown that the flexibility shortage of the C-GEP plans remain low and almost constant across all the different cases considered, while that of the S-GEP plans are much more affected by the IRES penetration levels than by carbon emission limits. The consistently low C-CEP shortage values do not only indicate this model superior adequacy in accounting for the different IRES and carbon requirements, but that it is also able to fully cope to the variations in the different policy requirements, while ensuring adequate operational flexibility levels.

TABLE 4.4 – Results of the operational flexibility metrics for the plans obtained through the S-GEP and C-GEP models for the range of IRES penetration and carbon emission limits considered (worse performance highlighted).

			No IRES		25% IRES		35% IRES		50% IRES	
			S-GEP	C-GEP	S-GEP	C-GEP	S-GEP	C-GEP	S-GEP	C-GEP
No emission limit	IRRE+ (% of upwards ramps)		7.38%	2.20%	16.13%	1.20%	26.74%	1.12%	46.71%	1.13%
	EFS+ (MW)	EFS+ (95%)	512.70	90.53	1681.61	34.37	3118.14	38.76	4275.79	70.53
		EFS+ (99%)	2402.85	451.31	5781.33	171.33	8670.87	193.24	8157.30	351.60
		EFS+ (99.9%)	5212.17	3227.19	10704.63	1278.89	17876.77	1602.35	14674.80	2977.76
	IRRE- (% of downwards ramps)		0.01%	0.01%	0.01%	0.01%	0.04%	0.04%	0.23%	0.2%
	EFS- (MW)	EFS- (95%)	0.00	0.00	0.00	0.00	0.00	0.00	0.00	0.00
		EFS- (99%)	0.00	0.00	0.00	0.00	0.00	0.00	0.00	0.00
		EFS- (99.9%)	0.00	0.00	0.00	0.00	0.00	0.00	0.00	0.00
75% emission limit	IRRE+ (% of upwards ramps)		7.27%	2.15%	16.30%	1.07%	26.82%	1.02%	46.86%	1.17%
	EFS+ (MW)	EFS+ (95%)	497.39	84.57	1862.13	24.49	3128.12	35.51	4782.05	77.56
		EFS+ (99%)	2345.28	421.59	6587.33	122.06	8725.54	177.04	8983.71	386.65
		EFS+ (99.9%)	5117.10	3061.18	13561.78	1049.74	19269.63	1521.26	15706.40	3169.95
	IRRE- (% of downwards ramps)		0.01%	0.01%	0.01%	0.01%	0.04%	0.04%	0.23%	0.22%
	EFS- (MW)	EFS- (95%)	0.00	0.00	0.00	0.00	0.00	0.00	0.00	0.00
		EFS- (99%)	0.00	0.00	0.00	0.00	0.00	0.00	0.00	0.00
		EFS- (99.9%)	0.00	0.00	0.00	0.00	0.00	0.00	0.00	0.00
50% emission limit	IRRE+ (% of upwards ramps)		7.24%	2.04%	16.43%	1.37%	27.34%	1.43%	47.56%	1.23%
	EFS+ (MW)	EFS+ (95%)	484.50	75.20	1927.50	37.60	3586.40	179.40	5107.20	132.00
		EFS+ (99%)	2293.33	374.74	6702.66	187.55	9670.93	894.45	9969.54	658.18
		EFS+ (99.9%)	5069.55	2963.69	14665.06	1359.96	20659.63	5378.26	16145.05	3692.00
	IRRE- (% of downwards ramps)		0.01%	0.01%	0.01%	0.01%	0.05%	0.03%	0.22%	0.19%
	EFS- (MW)	EFS- (95%)	0.00	0.00	0.00	0.00	0.00	0.00	0.00	0.00
		EFS- (99%)	0.00	0.00	0.00	0.00	0.00	0.00	0.00	0.00
		EFS- (99.9%)	0.00	0.00	0.00	0.00	0.00	0.00	0.00	0.00

These results are consistent with those of the other studies reviewed. Most notably, in Palmintier and Webster [50] where an overall similar investigation was conducted to compare two model types similar to those presented in this work which considers a grey-field planning framework. The following similarities also highlights the relevance and consistency of the framework considered in this thesis for the grey-field system planning problems. Their investigation over a range of IRES and carbon levels revealed the same trends in the capacity mixes obtained, most notably, that with higher IRES penetration, the mix shifts to include more units with faster dynamic properties (typically fossil peaking units). They also showed that carbon emission can be underestimated by 30-60% by planning models that do not consider short-term system representation. However, they considered only a single-period optimization problem with wind penetration as an exogenous parameter, and did not consider quantitative metrics for the operational flexibility assessment. The multi-period planning considered here allows more realistic planning paradigms, where investment decisions can be optimally taken at different periods, and allows a wide variation in the system parameters at the different periods (see for example the wide spectrum of inter-temporal load variations of the four weeks sampled per year in Appendix (B)). Moreover,

it is observed in the results, that although the resulting capacity mixes give an indication of the flexibility levels of the plans obtained, they do not capture to what extent these plans are short on operational flexibility. Which becomes more clear when suitable quantitative metrics are used, as shown in these results.

4.5.2 Effect of fuel cost on operational flexibility

The investment plans obtained are evidently dependent on the set of system parameters initially chosen. Since we consider a deterministic problem, the variation in those parameters could admittedly alter the results obtained, most notably, the uncertainties regarding fuel costs and load evolution trend. We, therefore, opt for exploring selected scenarios representing a wide variation in those parameters, and investigating their effect on the operational flexibility levels of the plans obtained. In this section two scenarios of fuel costs (coal and natural gas costs) are explored: 50% increase and 50% decrease, to cover a wide variation of the base case, and consistent with the percentages considered in the IEA report for sensitivity analysis [92]. For clarity, only the results of the C-GEP model are reported for the median 35% IRES penetration level. However, all emission limit scenarios are investigated, since it is reasonable to assume that fuel costs could have a higher impact on the plans obtained when combined with stringent emission limits.

The installed capacities for all fuel cost and emission limit scenarios are illustrated in Figure (4.5). For the highest fuel cost scenario, much of the coal and -to a lesser extent- CCGT capacities are substituted by the less emitting nuclear units, more so as tighter emission limits are enforced. For the lower prices, the coal capacity is still substituted, but this time by the peaking CCGT and OCGT units. The lower emission requirements are attained through progressive substitution of fossil units by nuclear ones, as can be observed within each fuel cost scenario. The total installed capacity across all scenarios, however, remain constant.

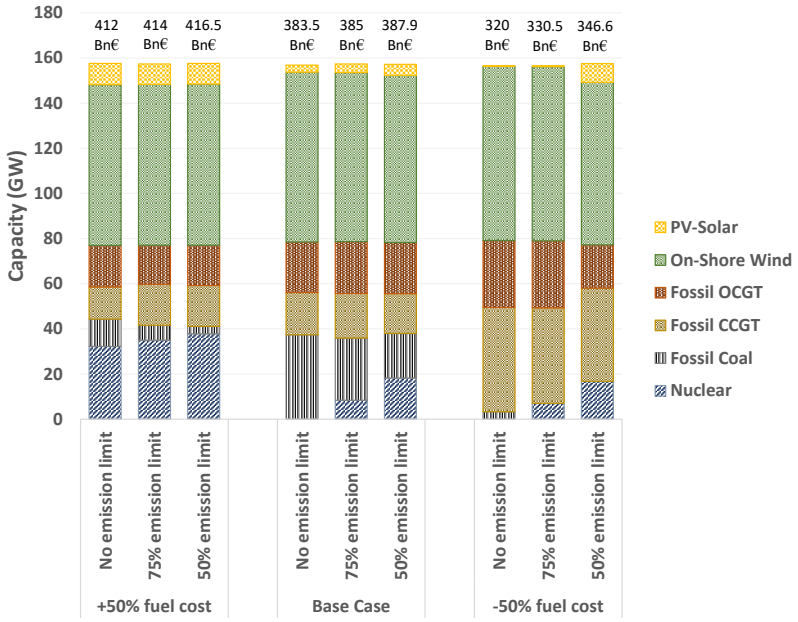

FIGURE 4.5 – Total installed capacity as given by the C-GEP model under 35% IRES penetration and for the different fuel cost scenarios

In terms of operational flexibility, Figures (4.6a) and (4.6b) illustrate the results for the IRRE+ and EFS+, respectively. As can be expected, plans obtained under the highest fuel

cost have the highest expectation of upwards flexibility shortages. This is because much of the fossil units, which possess better dynamic properties, are replaced by the less flexible nuclear ones. The opposite is observed for the plans obtained at the lowest fuel cost driven by the higher capacities of those peaking units. Notice, again, that despite this significant variation in the capacity mix across the different fuel scenarios, the IRRE of the integrated C-GEP model plans did not exceed 2.05% of the total number of upwards ramps, with a quasi-linear decreasing trend as a function of less stringent emission limits and decreasing fuel costs. This remains a very small percentage point relative to any shortage value observed for the S-GEP model under IRES penetrations. The EFS+ confirms the trends observed using the IRRE metric, however, at the highest fuel cost scenario it signaled a relatively high shortage expectations that could go up to the order of several GWs at the 99% confidence level. Such a magnitude is significant and would be important to account for, and highlights the complementarity of the two measurement approaches for giving an accurate assessment.

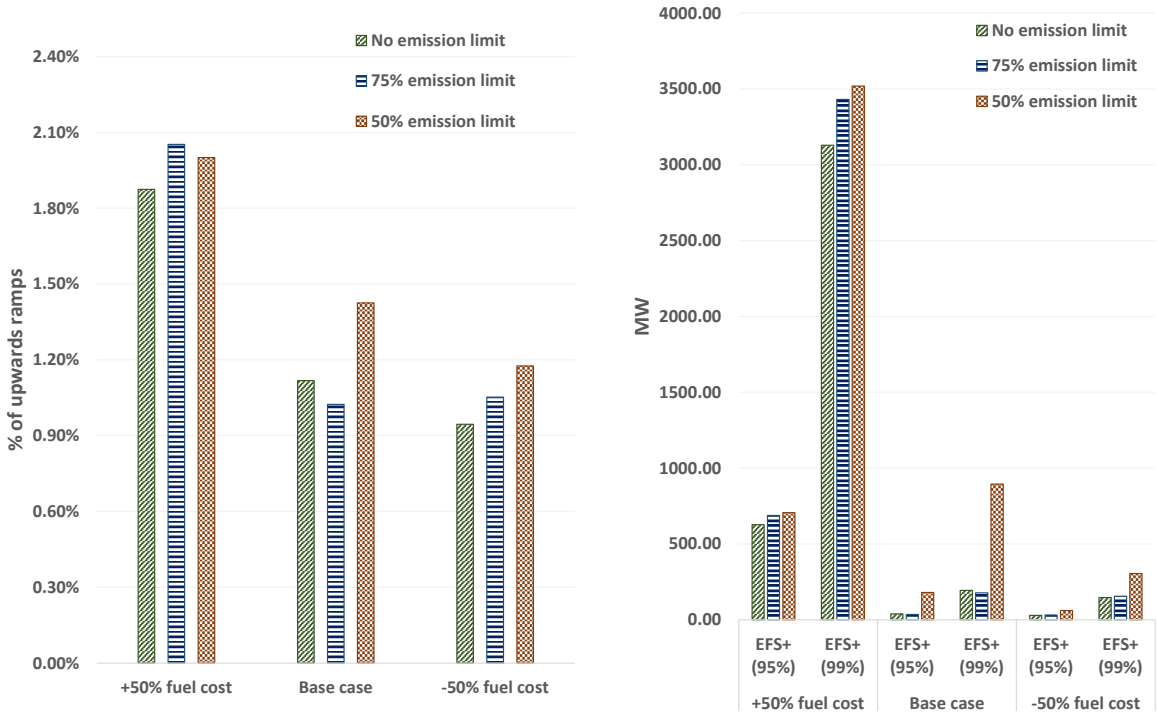

(A) IRRE+ (B) EFS+

FIGURE 4.6 – Results of operational flexibility assessment on the plans obtained through the C-GEP model under 35% IRES penetration and for the different fuel cost scenarios

4.5.3 Effect of load evolution on operational flexibility

The load evolution trends could be another source of influence on the plans obtained. In this respect, in their 2016 "Generation Adequacy Report", RTE [94] presented future load projections for France and Europe, with high and low growth scenarios of roughly +2% and -1%, respectively, accounting for all different sectors. For the purpose of sensitivity analysis, for the high an low load scenarios, we have amplified these values considering a +20% and a -10% linear load growth starting of the fifth year of the planning horizon. The negative scenario being a proxy for stringent energy efficiency driven policies. For clarity, only the results of the C-GEP model are reported for the median 35% IRES penetration level and for

the no emission limit policy. It should also be noted that no changes are assumed for the hourly load patterns compared to the previous cases considered.

The total power generation per technology and per load evolution scenario is illustrated in Figure (4.7). The Figure shows that, overall, there are no changes in the capacity mixes obtained, but that only the total capacities and production quantities vary per technology. Naturally, the installed capacities and power generation decrease as the total system load decreases. The reduction is mostly in the IRES technologies amounting to more than 50% of the total generation decrease across scenarios. This can be explained through two effects: lower load means that less IRES is required to satisfy the 35% penetration requirement, and it is more cost efficient (subject to the given assumptions) to reduce the IRES levels than to answer to the increased net load variability by cycling thermal units.

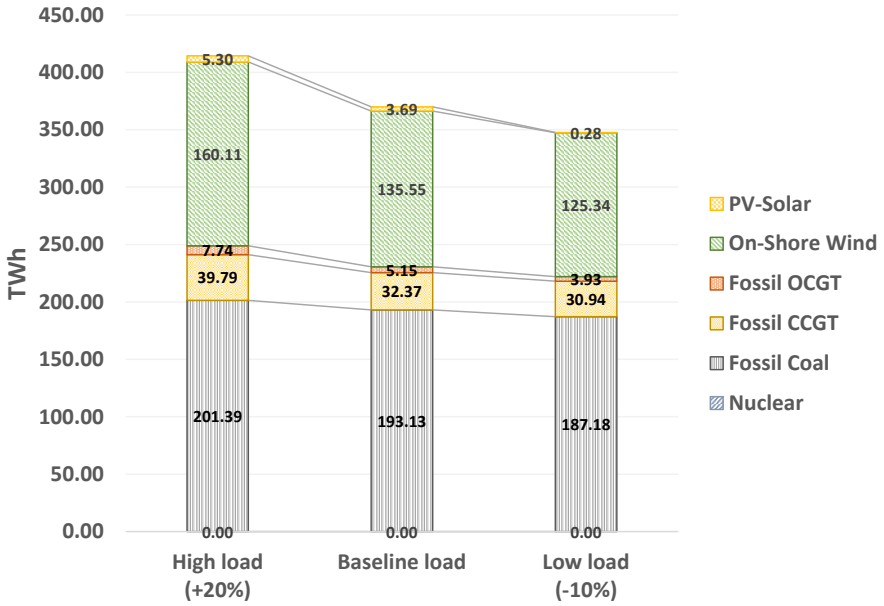

FIGURE 4.7 – Total energy production per technology for the plans obtained by the C-GEP model under 35% IRES penetration and for the different load growth scenarios

Regarding how the load evolution trend affects the obtained plans, Table (4.5a) summarizes the results of some of the performance measures previously considered. Overall, a gradual decreasing trend can be observed in all measurements with respect to the decreasing load scenario. This is also true for the operational flexibility results reported in Table (4.5b). While the absolute difference in those results would be important to consider for actual system planning, the linear gradual trend found suggests that the overall load evolution exhibits a less significant effect on the operational flexibility of the plans than the variations in the inter-temporal load patterns.

TABLE 4.5 – Results of different performance measures and operational flexibility metrics for the plans obtained through the C-GEP models under 35% IRES penetration for the different load growth scenarios

(A) Generic performance measures results

	High load (+20%)	Baseline load	Low load (-10%)
Total IRES Installed Capacity [GW]	94.24	78.32	69.6
Total Installed Capacity [GW]	188.52	156.83	142.15
Load Not Served [% of total load]	0.02%	0.02%	0.02%
RES shedding [% of total IRES]	3.43%	2.48%	2.25%
Carbon Emission [Mtons]	2818.70	2648.64	2555.18
Total Cost [Bn€]	439.67	383.58	357.42%

(B) Operational flexibility metrics results

		High load (+20%)	Baseline load	Low load (-10%)
IRRE+ [% of upwards ramps]		1.16%	1.12%	1.05%
EFS+ [MW]	**EFS+ [95%]**	51.10	38.76	32.30
	EFS+ [99%]	254.70	193.24	161.10
IRRE- [% of downwards ramps]		0.08%	0.04%	0.04%
EFS- [MW]	**EFS- [95%]**	0.00	0.00	0.00
	EFS- [99%]	0.00	0.00	0.00

5 Electric power systems resilience against extreme weather events

5.1 Overview

In the previous chapters, the integrated modeling and optimization framework used to account for the systems operational flexibility under a high share of IRES penetration has been developed. The results analyzed in Chapter (4) have shown how the integrated C-GEP model outperforms the traditional simplified S-GEP one in accounting for the high variability in the net-load. In this Chapter, we extend the integrated planning framework to also include system resilience against the impact of extreme weather events. Most notably, we consider the extreme heat wave and drought events that affect both the thermal generation units and the system load.

5.2 Piece-wise linear models of the impact of extreme weather events

Extreme heat waves affect thermal power plants by reducing their efficiency due to the derating of their cooling capabilities during the event. Load is sensitive to heat waves as it can significantly increase during periods of high temperatures due to increased air conditioning usage. The following section describes the set of piece-wise linear models to quantify these impacts and integrate them within the power system design problem.

5.2.1 Basic model of thermal plants cooling systems

Different cooling technologies exist for thermal power generation units. In the event of extreme heat waves, the impact on the different technologies can vary. In a power systems planning model the choice among the different cooling technologies is a decision variable. In this work, we consider two main cooling technologies:

- Once-through Cooling (OTC) system: the heated cooling water is returned to the water source. A large volume of water from the water source is required.

- Closed-loop cooling (CLC) system: water is circulated in the cooling loop including a cooling tower, where a small portion of cooling water evaporates and is released to atmosphere. Only a small volume of water has to be withdrawn from the water source.

The required volume of cooling water V^{req} for operating a thermal power plant at its maximum capacity P^{max} is proportional to P^{max} and inversely proportional to the increase of the temperature in the cooling water $\Delta T'$ [95–97], as follows:

$$V^{req} \propto \frac{P^{max}(1-\alpha)}{\Delta T'} \tag{5.1}$$

$$\Delta T' = max\left(min\left(T^{'out\_max} - T^{'in\_w}, \Delta T^{'max}\right), 0\right) \tag{5.2}$$

where α is the share of waste heat released into the air [%]; this share is small for OTC systems ($\alpha \to 0$) and large for CLC ones ($\alpha \to 1$). The permissible temperature increase of the cooling water $\Delta T'$ is limited by: 1) the regulated maximum permissible temperature increase of the cooling water $\Delta T^{'max}$, and 2) the regulated maximum permissible temperature of the discharged cooling water $T^{'out\_max}$ [95].

We can see that when $T^{'in\_w} \leq T^{'out\_max} - \Delta T^{'max}$, the maximum permissible temperature increase of the cooling water is only limited by $\Delta T^{'max}$, and the required volume of cooling water V^{req} is, thus, a constant value ($V^{req} = V^*$) for $\Delta T' = \Delta T^{'max}$. However, a high value of $T^{'in\_w}$ generally leads to an increase in V^{req} for operating the plant at its maximum capacity. This increase is significant for OTC systems, whereas it is moderate for CLC ones.

For thermal power plants with CLC systems, it is acceptable to assume that such plants are robust to water shortages and are independent from water availability [95, 96]. Also, the dependency to source water temperature can be neglected since any rise in the water temperature can be compensated by increasing the volume of cooling water V^{req} [96]. Instead, CLC systems are mainly affected by the temperature of cooling water circulated back to the condenser, $T^{'in\_c}$, which can be assumed to be close to air temperature [96].

5.2.2 Extreme weather event impact models

We consider extreme heat waves and drought events during summer time (JJAS, 21 June-20 September) that may force thermal power plants to reduce production owing to scarcity and high temperature of the cooling water. The intensity of the extreme weather event (ewe) of heat wave and drought is modeled by:

$$ewe = [T'_{it}, A_{it}], \forall i \in I, t \in T \tag{5.3}$$

where T'_{it} is the hourly air temperature at plant i, from which we can calculate the related stream temperature $T_i^{'in\_w}$ based on air-water interaction as follows [97]:

$$T_{it}^{'in\_w} = t^{'min} + \frac{t^{'max} - t^{'min}}{1 + e^{\gamma(t^{'ip} - T'_{it})}} \tag{5.4}$$

The parameters for the air/water temperature relationship are derived from the literature [95, 98, 99]: the minimum stream temperature is assessed to be $t^{'min} = 0$°C, the maximum stream temperature to be $t^{max} = 30.4$°C, the steepest slope to be $\gamma = 0.14$ and the air temperature at the inflection point to be $t^{'ip} = 16.5$°C [100]. The parameter of the extreme weather event A_{it} represents the hourly availability (percentage) of intake cooling flow at plant i, time t and is defined by:

$$A_{it} = \frac{\min(V_{it}^{src}, V_i^{cpty})}{V_i^*} \tag{5.5}$$

where V_{it}^{src} is the permissible amount of water flow that can be taken from the water source at plant i at time t, V_i^{cpty} represents the water extraction capacity of the plant and V_i^* is the

constant amount of the required volume of intake cooling water for plant i when the intake water temperature $T_{it}^{'in\_w} \leq T^{'out\_max} - \Delta T^{'max}$, as previously explained in Section (5.2.1).

Thermal units

For thermal power plants using the OTC system, $\forall i \in I^{th\_otc}$, the ratio of P_{it}^{usable} to P_i^{max} as a function of T'_{it} and A_{it} can be expressed by the following piece-wise linear equations for different ranges of T'_{it}:

$$\zeta_{it}^{ewe} = \begin{cases} P_{it}^{usable}/P_i^{max} = min(1, A_{it}), & T_{it}^{'in\_w} \leq T'_{health} \\ \min(1, A_{it}) \cdot \left[1 - \beta \cdot \left(T^{'in\_w} - T'_{health}\right)\right], & T'_{health} \leq T_{it}^{'in\_w} \leq T'_{risk} \\ \min(1, A_{it}) \cdot \delta \cdot \dfrac{\left(T^{'out\_max} - T_{it}^{'in\_w}\right)}{\Delta T^{'max}}, & T'_{risk} \leq T_{it}^{'in\_w} \leq T'_{shutdown} \\ 0, & T_{it}^{'in\_w} \geq T'_{shutdown} \end{cases} \tag{5.6}$$

where β is the efficiency degrading rate when $T^{'in\_w}$ is in the range of $[T'_{health}, T'_{risk}]$ and T'_{risk} is defined to represent the temperature when the actual maximum discharge of waste of heat is equal to the designed value and is given by:

$$T'_{risk} = T^{'out\_max} - \Delta T^{'max} \cdot \frac{1}{A_{it}} \tag{5.7}$$

Coefficient δ can be calculated based on the continuation of the piece-wise linear functions (5.6) at $T_{it}^{'in\_w} = T'_{risk}$ and is given by:

$$\delta = A_{it} + \beta \cdot \Delta T^{'max} - \beta \cdot A_{it} \cdot (T^{'out\_max} - T'_{health}) \tag{5.8}$$

The above piece-wise linear equations (5.6) hold when $T'_{risk} \geq T'_{health}$, i.e., $A_i \geq \Delta T^{'max}/(T^{'out\_max} - T'_{health})$. For the case where $T'_{risk} \leq T'_{health}$, i.e., $A_i \leq \Delta T^{'max}/(T^{'out\_max} - T'_{health}) \triangleq A_{it}^{shtg}$, we can simplify the piece-wise linear functions (5.6) as follows:

$$\zeta_{it}^{ewe} = \begin{cases} \min(1, A_{it}), & T_{it}^{'in\_w} \leq T'_{health} \\ \min(1, A_{it}) \cdot A_{it}^{shtg} \cdot \dfrac{(T^{'out\_max} - T_{it}^{'in\_w})}{\Delta T^{'max}}, & T'_{health} \leq T_{it}^{'in\_w} \leq T'_{shutdown} \\ 0, & T_{it}^{'in\_w} \geq T'_{shutdown} \end{cases} \tag{5.9}$$

For a thermal plant using the CLC system, $\forall i \in I^{th\_clc}$, the following piece-wise linear functions are used to describe the impact of the air temperature ($T'_{it} \approx T_{it}^{'in\_c}$) on the usable power capacity:

$$\zeta_{it}^{ewe} = \begin{cases} 1, & T'_{it} \leq T'_{health\_air} \\ 1 - \rho \cdot (T'_{it} - T'_{health\_air}), & T'_{it} \geq T'_{health\_air} \end{cases} \tag{5.10}$$

Renewable energy units

For renewable generation units, wind power and solar photovoltaic (PV) systems do not require water to generate electricity and, thus, the capacity of renewable generation will not be affected largely by an extreme heat wave and drought event. To obtain the future PV and wind power potential capacity factor (CF), we use the recent CMIP5 data of high-resolution

climate projections (fully described in section (5.4.2)), together with the wind and PV power production models proposed in the literature.

Since the wind speed at the turbine height is not a standard output of the climate projection model, we use near-surface wind speeds at 10 meters V_{10m} and assume a power-law relationship for extrapolating the vertical wind profile [101, 102]. The velocity at hub height H is calculated as:

$$V_H = V_{10m} \cdot \left(\frac{H}{10}\right)^{\frac{1}{7}} \tag{5.11}$$

Then, the wind speed V_H is converted into turbine-generated electric power capacity factor $\zeta_{it}, \forall i \in I^{res-wind}, t \in T$ using a standard power curve, described as follows:

$$\forall i \in I^{res-wind},\ CF_{wind,t} = \begin{cases} 0, & \text{if } V_H < V_l \text{ or } V_H > V_0 \\ \dfrac{V_H^3 - V_l^3}{V_R^3 - V_l^3}, & \text{if } V_l \leq V_H < V_R \\ 1, & \text{if } V_R \leq V_H < V_0 \end{cases} \tag{5.12}$$

where V_l, V_R and V_0 are the cut-in, rated and cut-out velocity of a wind turbine, respectively. Wind power capacity factor is calculated at the grid cell level (defined in the climate projection model) assuming a unique turbine model for all grid cells ($H = 80$ m, $V_l = 3.5$ m/s, $V_R = 12$ m/s, $V_0 = 25$ m/s), as in [103, 104]

PV power generation potential depends on solar irradiance, named surface-downwelling shortwave (i.e., wavelength interval 0.2-4.0 μm) radiation (R_{sds}) in the climate models, and other atmospheric variables affecting panel efficiency, i.e., surface air temperature (T'_{as}) and surface wind velocity (V_{10m}). The PV power generation can be expressed as [105, 106]:

$$\forall i \in I^{res-pv}, CF_{solar,t} = \left[1 + \gamma\ \left(T'_{cell} - T'^{0}\right)\right] \cdot \frac{R_{sds}}{R^0_{sds}} \tag{5.13}$$

where the upper script 0 refers to standard test conditions for which the nominal capacity of a PV device is determined as its measured power output ($R^0_{sds} = 1000$ Wm^{-2}, $T'^{0} = 25$°C). Parameter γ is set at -0.005°C^{-1}, considering the typical temperature efficiency of monocrystalline silicon solar panels [105]. Finally, the PV cell temperature T'_{cell} is obtained as:

$$T'_{cell} = c_1 + c_2 T'_{as} + c_3 R_{sds} + c_4 V_{10m} \tag{5.14}$$

where c_1 = 4.3°C, c_2 = 0.943, c_3 = 0.028°Cm^{2}W^{-1} and c_4 = -1.528°Csm^{-1} [105, 107].

After obtaining the grid cell level renewable (wind and PV) power capacity factors, then, the regional renewable power potentials can be obtained by averaging all the grid cell levels inside a given region.

System load

Power demand is usually sensitive to weather conditions. To capture this, the power demand in the extreme weather event is represented by:

$$L^{ewe}_t = L_t + C^l \cdot (\overline{T'}_t - \overline{T'}^{ref}_t) \tag{5.15}$$

where C^l is the temperature sensitivity coefficient of power load, e.g., it is around $+500MW/+1°C$ during the summer time in France [108]. Here $\overline{T'}_t$ and $\overline{T'}_t^{ref}$ represent the geographical average values of the projected air temperature and historical reference air temperature, respectively.

5.3 Integrating resilience requirements in electric power systems planning model

The impact of an extreme weather event to the power generation system is measured by the decrease of the generation capacity of affected thermal and PV plants, and the increase of power demand, as given above. Then, the power generation system resilience is evaluated by a deterministic metric, which is referred to as the total load not served (LNS) during the period of the extreme weather event, and is defined as:

$$LS_{yst}^{ewe} = \left(L_{yst}^{ewe} - \sum_{i \in I} p_{iyst}^{ewe} \right), \quad \forall y \in Y, s \in S, t \in T^{ewe} \tag{5.16}$$

$$p_{iyst}^{ewe} \leq \zeta_{iyst}^{ewe} \cdot P_i^{max} \cdot u_{iyst}, \quad \forall i \in I, y \in Y, s \in S, t \in T^{ewe} \tag{5.17}$$

$$\sum_{s \in S} \sum_{t \in T^{ewe}} LS_{yst}^{ewe} \leq LS^{max}, \quad \forall y \in Y \tag{5.18}$$

where u_{iyst} is the unit commitment state of generation units of technology i at time t, subperiod s in year y, and ζ_{iyst}^{ewe} is the efficiency factor of the generation units of technology i during the extreme weather event, calculated using the above piece-wise linear equations (5.6)-(5.14), and T^{ewe} is the total duration of the event. Equation (5.16) calculates the total amount of load shedding LS_{yst}^{ewe} in each year y during the extreme weather event as the difference between the hourly demand and the total power generation from all power units. Equation (5.17) limits the power generation output p_{iyst}^{ewe} of generation units of technology i at year y during the extreme weather event $s \in S, t \in T^{ewe}$ to the efficiency factor ζ_{iyst}^{ewe}. Finally, constraint (5.18) limits the amount of load shedding allowed during the extreme weather event LS_{yst}^{ewe} to a maximum limit LS^{max}.

It should be noted that the resilience metric used here is focused on the ability of the power system to mitigate the impact of the extreme heat wave and drought events and not on the recovery from those events. This is because in these specific extreme weather events the main action is to reduce the thermal units production levels or to shut them down completely to avoid overheating and further damages to the units, so that recovery of normal operation is immediate once weather conditions go back to normal.

5.4 Application

5.4.1 System description

To apply the extended modeling and optimization framework considering system resilience, we consider the multi-annual planning horizon representing the period between the year 2041 to 2046. Linear regression is used to obtain the system hourly load from the historical electricity load time series of France from the year 2008 to 2012 (previously described in Section (4.4.1)), assuming a growth of 1% to 1.5% from the beginning to the end of the planning horizon. Technical and cost data for the generation technologies considered for the

expansion planning are also based on the same case study considered in Section (4.4.1) and are summarized in Table (4.1).

Thermal generation units can be equipped with one of two different cooling technologies, that have different cost and technical characteristics. Under normal conditions, cooling towers with recirculating water (CLC) reduce the overall efficiency of power plants by $2-5\%$ compared to once-through use of water from lakes or large streams (OTC). Thus, these towers are associated with larger operational/marginal costs compared to OTC systems. Moreover, the investment costs of CLC systems are around 20% higher than those for OTC systems. Table (5.1) summarizes the specific technical and cost parameters of the generation units equipped with each cooling technology [96, 109, 110].

TABLE 5.1 – Technical and economic characteristics for the power generation units with different cooling technologies

Technology $[i]$	$\beta/\rho/\ C^{pv}$ [%]	$T'_{health}/^{ref\_pv}$ [°C]	$T'_{shutdown}$ [°C]	T'^{out_max} [°C]	$\Delta T'^{max}$ [°C]	C_i^{inv} $[M€/MW]$	C_i^{mrgl} $[€/MWh]$
Nuclear-OTC	0.44	15	32	32	10	3.95	13.84
Nuclear-CLC	0.44	10	/	/	/	4.74	14.11
Coal-OTC	0.97	15	32	32	10	2.08	38.97
Coal-CLC	0.94	10	/	/	/	2.60	39.75
CCGT-OTC	0.31	15	32	32	10	1.02	70.16
CCGT-CLC	0.30	10	/	/	/	1.22	71.50
Solar-PV	0.50	25	/	/	/	1.5	1.71
On-Shore Wind	/	/	/	/	/	1.9	2.16

Similar to the framework followed in the previous chapter, the yearly load is optimally approximated by four representative weeks and the chronological order within each week is maintained. For each planning year, an additional week corresponding to that containing the peak summer load is, then, added to simulate the impact of the heat wave and drought events during summer time.

5.4.2 Climate projections data of heat wave and drought events

Historical baseline temperature as well as future temperature projections for the years 2041 to 2046 are based on data obtained from the Coupled Model Intercomparison Project (CMIP5) experiments [111]. Similarly, wind speeds and solar irradiance data used to calculate the wind and solar CF are obtained from the CMIP5 experiments, following the models proposed in section (5.2.2). We consider three Representative Concentration Pathways (RCPs) that cover the impact of different trajectories of greenhouse gas concentration on future climate, compared to pre-industrial levels. In particular, we consider the RCP 8.5, RCP 4.5 and RCP 2.6, which represent an increased in radiative forcing of +8.5 Wm^{-2}, +4.5 Wm^{-2} and +2.6 Wm^{-2} respectively, compared to pre-industrial values. Table (5.2) summarizes the details of the CMIP5 experiments used for the different climate projections.

TABLE 5.2 – Details of the experiments used for the historical and projected temperature scenarios

Experiment type	Modeling Center (or group)	Institute ID	Model Name	Experiment	Period	Variable	Frequency
Historical (baseline)	Meteorological Research Institute	MRI	MRI-CGCM3	historicalEXT	2008-2012	tas	3hr
Projection	Centre National de Recherches Météorologiques	CNRM	CNRM-CM5	rcp85, rcp45, rcp26	2041-2046	tas	3hr
Projection	Meteorological Research Institute	MRI	MRI-CGCM3	rcp85, rcp45, rcp26	2041-2046	uas, vas, rsds	3hr

Since we are primarily interested in extreme weather scenarios related to the region of southern France, the climate data considered have been limited to the geographical scope of interest: that is, data spanning the longitudinal and latitudinal scope of approximately $(W2°35'00'' - E8°10'00'')$ and $(N46°06'00'' - N41°19'00'')$, respectively. To quantify the impact of an extreme heat wave, the average temperature time series as well as the average wind and solar CF are, then, computed for the geographical area considered, for each projected climate scenarios. Regarding water availability levels, different water level scenarios during the heat wave events are assumed to cover: high availability levels (A $>$ 1), normal levels (A = 1) and low availability levels (A $<$ 1).

5.5 Results and discussion

5.5.1 Impact of extreme heat wave and drought events on system load and efficiency of power generation

We start our investigation with a focus on future climate parameters obtained from the RCP 8.5 experiments, which is the representative concentration pathway assuming no decrease in current carbon emission trends throughout the 21st century. Significant temperature increase during the summer period is observed under the Representative Concentration Pathway (RCP 8.5), compared to the historical baseline scenario. The impact of this temperature increase on the load and power generation units are computed for a typical summer week for each year of the planning horizon. As an example, Figure (5.1) illustrates the projected temperature increase and its impact on system load during the period between the 30th of July and the 6th of August for the year 2041 in southern France, compared to the historical average levels in the same period and location. The temperature difference is seen to reach levels of $+9.2$°C, while its impact on the system load (calculated as per the proposed impact model) can increase up to $+1840$ MWh. Similar order of differences are observed for the other planning years considered.

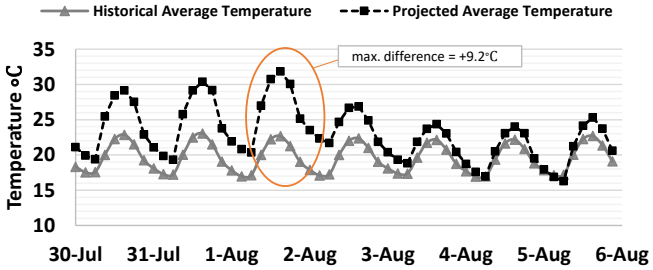

(A) Temperature difference

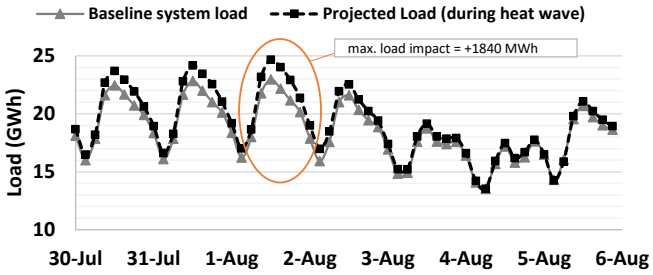

(B) Load difference

FIGURE 5.1 – Temperature difference and its impact on system load during the period between the 5th and the 12th of August, for both the baseline and the projected scenarios

The effect of heat wave and water shortages on the efficiency of thermal units depends on the cooling technology deployed. We consider three different levels of water availability and calculate their impact on the efficiency of thermal units during the heat wave event. Figure (5.2) illustrates the resulting efficiency for nuclear power plants during a heat wave and under different water availability levels, using data for the year 2041. It can be seen that OTC-based generators are highly affected by water shortages, compared with CLC units, which are impacted by the heat wave but maintain the same efficiency levels regardless of the water availability level.

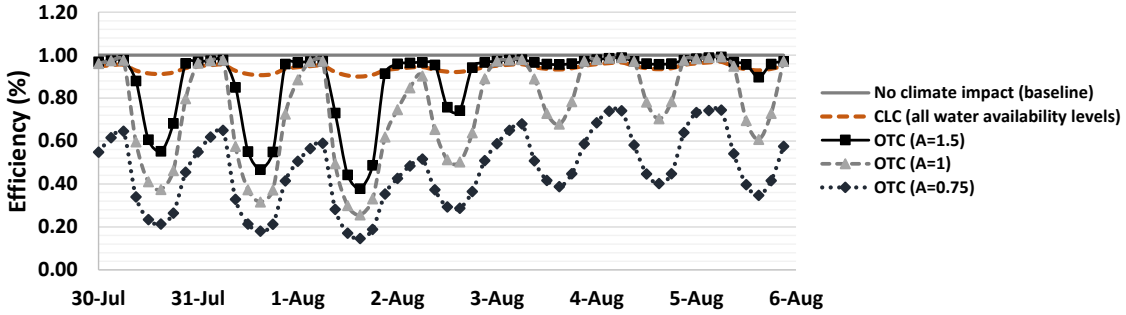

FIGURE 5.2 – Example of nuclear generation units efficiency derating during a heat wave event for different cooling technologies (OTC and CLC) and under different water availability scenarios (high availability: A $>$ 1, normal availability: A = 1, low availability A $<$ 1)

5.5.2 Resilient planning vs conventional planning

Resilient power systems planning should account for the impact of extreme weather events as an integral part of the planning problem, as discussed in the previous sections. We compare the resilient plans (denoted RP) to conventional plans (CP), obtained assuming no climate impact on the efficiency of the generation units. CP future investment plans are, then, used to simulate operation under different realizations of climate scenarios, to assess operational performance. We focus first on the results obtained under no IRES penetration level requirements.

The total amount of load not served (LNS) during the heat wave period is taken as the primary performance measure for the plans obtained. Figure (5.3) illustrates the resulting LNS for both RP and CP under the extreme weather events. The results show a significant load loss for the conventionally planned systems, that sharply increases with the worsening of the climate conditions. The loss reaches up to 851 GWh under the worst scenario of climate impact. This is not the case for the RP, which are shown to suffer an LNS significantly lower than CP, with a maximum of 17 GWh under the worst scenario of climate impact.

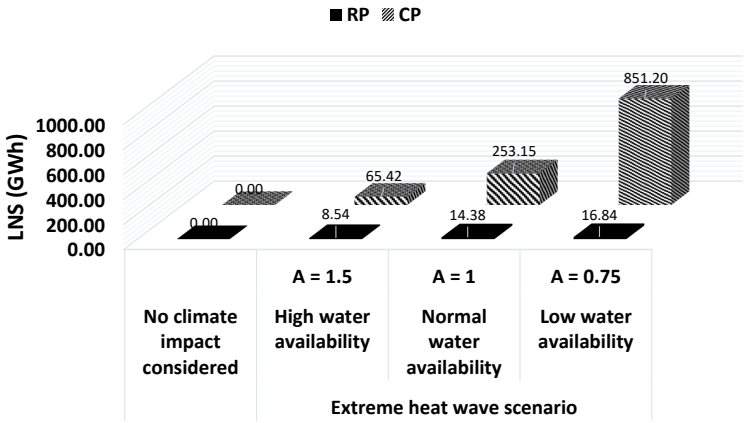

FIGURE 5.3 – LNS during different extreme weather events. Comparison between RP and CP under no IRES penetration.

In terms of system costs, RP have overall higher annualized investment and operational costs compared to CP, as can be seen in Figure (5.4). This is directly related to the fact that for RP the extreme weather impact on the power system is taken into account and so the plan compensates the lower thermal units efficiency by investing in more and better performing units. The slightly higher investment and operational costs, however, are fully offset by the reductions in LNS costs, as can be seen in Figure (5.4). The maximum difference between the total annualized investment and operation costs of the RP compared to the CP is equal to 1.23 B€ (low water availability scenario in Figure (5.4)), while the LNS cost saving for the same scenario is around 9.52 B€.

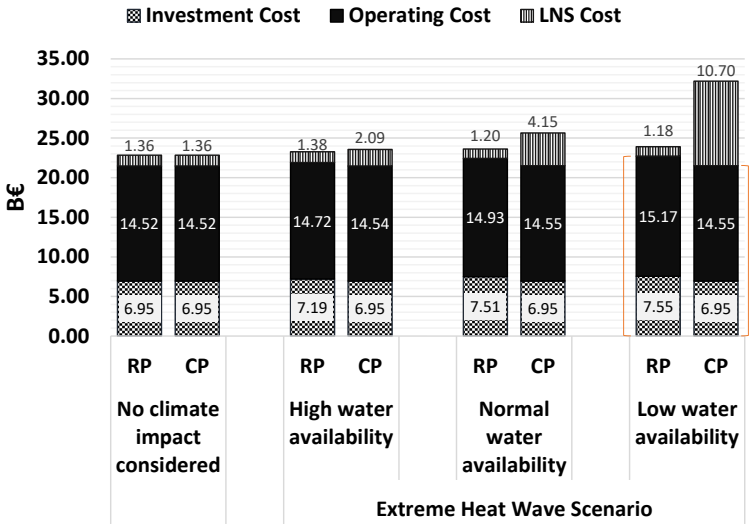

FIGURE 5.4 – Comparison between RP and CP costs subject to different extreme weather events under no IRES penetration.

Next, we extend the analysis to evaluate the impact of increasing IRES penetration levels on the system performance. Most notably we consider 0%, 25% and 50% IRES energy penetration levels (percentages of total system load) and solve the optimization problems under all extreme weather events, for both the RP and CP.

Figure (5.5) shows the impact of the increasing share of IRES levels on the LNS of the system during the extreme weather events, for RP and CP. Higher IRES penetration has a clear effect on reducing the amount of LNS during the extreme events. RP maintain low LNS levels in all cases considered, and slightly improves with increasing IRES levels, while CP show a significant decrease in LNS as IRES power compensates for the lack of system resilience.

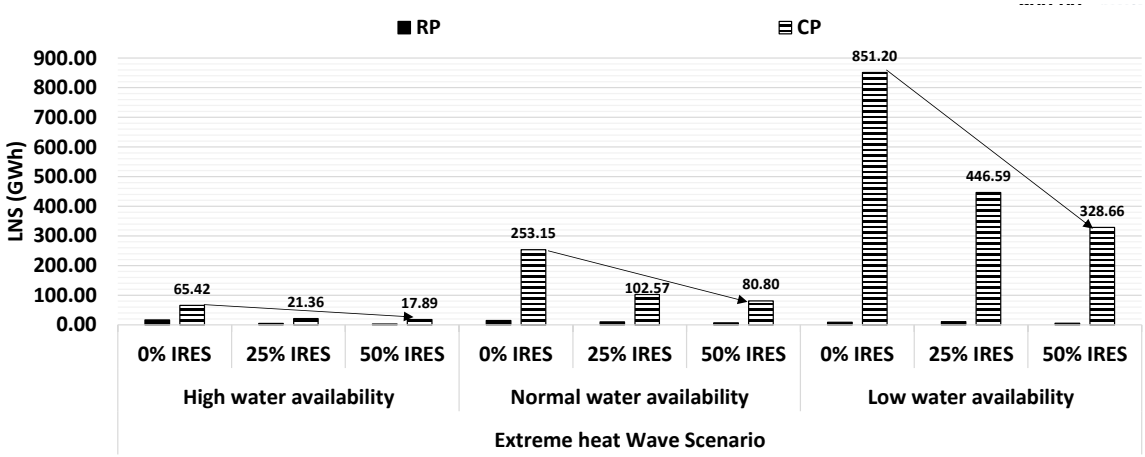

FIGURE 5.5 – Impact of high IRES penetration on LNS during different extreme weather events.

Moreover, it is shown that the increased IRES capacity reduces the gap between RP and CP, in terms of annualized investment and operational costs. For example, the difference in the total annualized investment and operation costs between the RP and CP plans decreases from +5.70% to +1.60% under the 0% and 50% IRES levels respectively, under the "Extreme

heat wave - Low water availability" scenario in Table (5.3). The same trends are also found under the other extreme weather scenarios considered.

			Annualized Investment Cost [BEuro]			Operating Cost (excluding LNS) [BEuro]			Total inv + op costs [BEuro]		
			RP	CP	Difference (% wrt CP)	RP	CP	Difference (% wrt CP)	RP	CP	Difference (% wrt CP)
Extreme heat wave scenario	High water availability	0% IRES	7.19	6.95	3.52%	14.72	14.54	1.20%	21.91	21.49	1.95%
		25% IRES	9.37	9.37	0.05%	14.12	13.99	0.95%	23.49	23.35	0.59%
		50% IRES	12.92	12.92	0.04%	14.29	14.14	1.03%	27.21	27.06	0.56%
	Normal water availability	0% IRES	7.51	6.95	8.02%	14.93	14.55	2.57%	22.43	21.50	4.33%
		25% IRES	9.55	9.37	2.00%	14.13	14.00	0.95%	23.69	23.37	1.37%
		50% IRES	13.05	12.92	0.99%	14.30	14.15	1.04%	27.34	27.07	1.01%
	Low water availability	0% IRES	7.55	6.95	8.63%	15.17	14.55	4.30%	22.72	21.50	5.70%
		25% IRES	9.66	9.37	3.09%	14.30	14.01	2.03%	23.95	23.38	2.46%
		50% IRES	13.17	12.92	1.92%	14.35	14.17	1.32%	27.52	27.08	1.60%

TABLE 5.3 – Comparison of RP and CP costs under different IRES penetration levels and extreme weather events.

5.5.3 Impact of extreme weather events on technology choice and system flexibility

The previous section has illustrated how power system RP cope with the detrimental impact of extreme weather events, with no significant increase in the system cost. We analyze in details the choices in the RP under the different scenarios. Most notably, the generation technology choice and capacity installed are major contributors to the system performance. Figure (5.6) summarizes the investment capacities and technologies choices under the different extreme weather events and IRES penetration levels. For clarity, the results illustrate the total capacity installed per each cooling technology type (OTC-based capacity vs CLC-based capacity) summed over all thermal power plants installed, under each scenario.

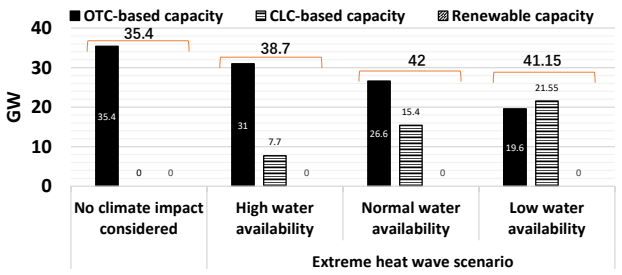

(A) 0% IRES penetration

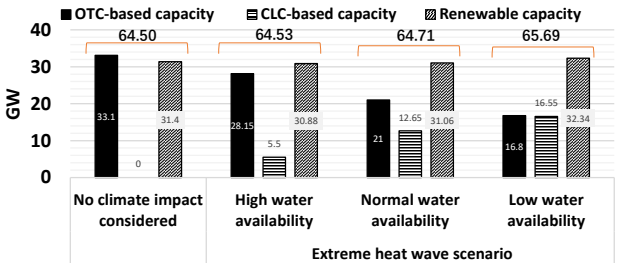

(B) 25% IRES penetration

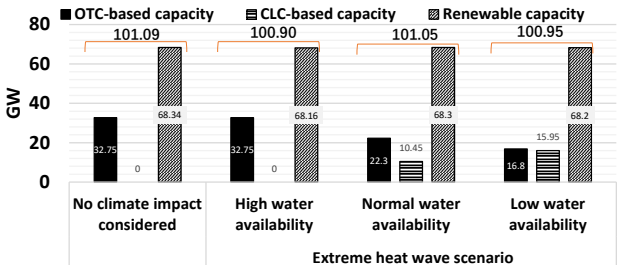

(C) 50% IRES penetration

FIGURE 5.6 – RP technology choice and capacity installed under different IRES penetration levels and extreme weather events.

The results show a clear shift from (the cheaper) OTC-based capacities to the (more expensive) CLC-based technology when the heat wave event is accounted for, primarily as

a result of internalizing in the system design the impact of the extreme event. This shift to CLC-based units further increases considering lower water availability levels during the heat wave event. The results also show that the total capacity of all technologies installed does not in fact vary in response to different extreme weather events but is rather significantly impacted by the amount of IRES penetration in the system, for an average of 39.3GW, 64.8GW and 101GW for the 0%, 25% and 50% IRES penetration scenarios, respectively, with low standard deviations of 2.9, 0.5 and 0.08 within each IRES scenario. On the other hand, the significant increase of capacity installed across different IRES penetration scenarios is directly attributed to the increased capacity required to satisfy the operational flexibility needs of the system under these scenarios, as has been discussed in previous work [112].

We finally explore how the operational flexibility of the RP and CP plans are affected by the different extreme climate events. Table (5.4) summarizes the EFS results at the 99% confidence level, for all IRES and climate scenarios. It can be seen that when the extreme weather events are not taken into account in the planning phase (as per the CP), the operational flexibility shortage is multiple times that of its RP counterpart under the same extreme weather events. This flexibility shortage difference further increases considering higher levels of IRES penetration. For instance, the EFS reaches approximately 7355 MW for CP compared to 2655 MW for RP, during the extreme weather event for a system with 50% share of IRES capacity. The flexibility shortages, however, are significantly lower than the load losses for the CP due to the lack of resilience, which were shown to be in the order of several hundred GWh in the previous sections. This is important to note since both RP and CP accommodate the operational flexibility attribute.

			EFS [MW] (99% condifdence level)	
			RP	CP
Extreme heat wave scenario	0% IRES	High water availability	28.84	3359.03
		Normal water availability	785.57	4588.56
		Low water availability	1933.98	5375.94
	25% IRES	High water availability	752.57	1732.63
		Normal water availability	1472.30	5050.12
		Low water availability	1621.71	4435.47
	50% IRES	High water availability	618.18	1281.81
		Normal water availability	1038.70	3981.68
		Low water availability	2655.01	7354.27

TABLE 5.4 – Expected Flexibility Shortfall (EFS) of RP under different IRES penetration levels and climate scenarios.

5.5.4 Sensitivity of the results for different climate projections (RCP8.5, RCP4.5 and RCP2.6)

In the previous sections, we have shown the improvements achieved by RP which account for extreme heat waves and drought events. Both RP and CP were optimized and/or evaluated under the climate parameters of the RCP 8.5, that is the most pessimistic radiative concentration pathway for the 21st century. In this section, we perform a sensitivity analysis considering other RCP projections from the CMIP5 climate experiments to confirm the relevance of the planning framework proposed under less pessimistic concentration pathways.

RCP 2.6 and 4.5 climate data are used to calculate future power system operating conditions. Most notably, solar irradiance and wind speed data are used to obtain wind and solar-PV CF, and temperature data during the summer period are used to simulate the future heat wave scenarios and their impact on thermal generators. We, then, use the RP and

CP under the RCP 8.5 scenario to check their operational performance under the other RCP scenarios.

Figure (5.7) shows the performance of the RP and CP obtained under the RCP 8.5, in terms of LNS during the extreme heat event under all RCP pathways considered. The values shown are the average LNS amounts for all water availability scenarios per each RCP. The results confirm the consistently lower LNS for the RP under all RCP scenarios and for all IRES penetration levels. In addition, as expected, the LNS decreases as less pessimistic RCP scenarios are considered. For example, the average LNS for the RP under 0% IRES penetration decreases from 10 GWh for the RCP 8.5 to 0.05 GWh for the RCP 2.6 scenarios.

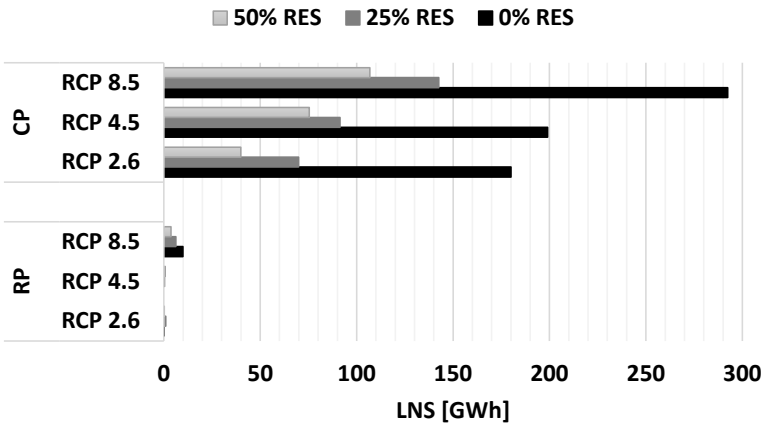

FIGURE 5.7 – Average amount of LNS under each RCP scenario (8.5, 4.5 and 2.6) and IRES penetration levels (0%, 25% and 50%). Comparison between the results for RP and CP.

With regards to the operational flexibility, the results reported in Figure (5.8) show the average EFS of the plans obtained under all extreme weather events for different IRES penetration levels. Less obvious trends can be found for the operational flexibility levels of the obtained plans across the different RCPs, as measured by the EFS metric. It can be confirmed, however, that RP consistently outperform CP also in terms of flexibility, as can be seen in the overall lower shortage levels illustrated in Figure (5.8). The improved flexibility performance of the RP highlights an important interaction between the resilience of the system and its flexibility, and the compound impact of failing to consider either aspect in the power system design phase.

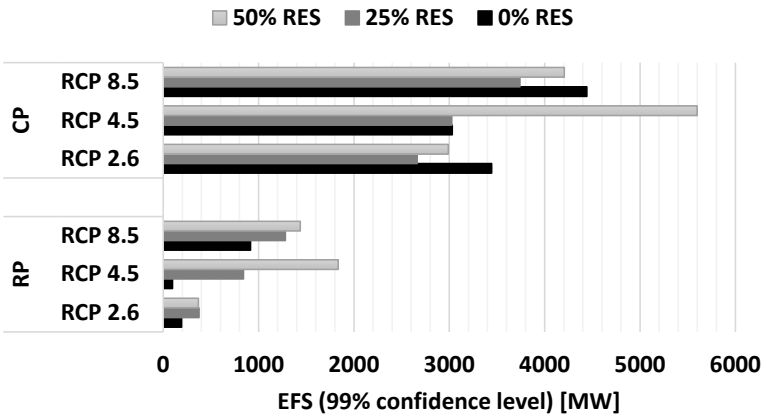

FIGURE 5.8 – Average amount of EFS under each RCP scenario (8.5, 4.5 and 2.6) and IRES penetration levels (0%, 25% and 50%). Comparison between the results for the RP and CP.

6 Uncertainty in electric power systems planning and operation

6.1 Overview

The integrated planning and assessment framework developed for electric power systems operational flexibility and resilience, thus far, has only considered deterministic optimization. While the results obtained have clearly shown the advantages of the framework proposed, it falls short of accounting for the inherent uncertainties characterizing the system parameters. This is especially significant in a long-term planning context under a high share of IRES penetration and extreme weather impacts, where it is obvious that the uncertainties surrounding the IRES availability, the system load and the efficiency of thermal supply may greatly influence the optimal investment decisions and their robustness against those uncertainties.

This chapter presents the methodology developed in this thesis to treat the uncertainties within the integrated power system planning problem. The long-term GEP model with short-term UC constraints is treated via a state-of-the-art multi-stage adaptive robust optimization (AARO) modeling technique. Most notably, the uncertainty characterizing the system load and IRES-CF, takes the form of a deterministic uncertainty set with a controllable level of conservatism. The AARO model accounts for the *here-and-now* commissioning and commitment decisions made robust against the uncertainties, and the *wait-and-see* dispatch decisions subject to uncertainty realization. The dimensionality issue of the resulting model is discussed in details and a novel approximation method based on "information basis" approximation is proposed. The method is, then, applied for the practical-size case study considered throughout the thesis. The results validate the superiority of considering the proposed robust optimization approach over other stochastic methods to account for uncertainties.

6.2 Robust optimization model

The distribution-free characterization of both load and IRES supply uncertainties is described as follows: the sub-period load vector, $\boldsymbol{L}$, takes on a range of possible values given by $\underline{\boldsymbol{L}} \leq \boldsymbol{L} \leq \bar{\boldsymbol{L}}$ and the capacity factor, $\boldsymbol{CF}$, which models IRES supply uncertainty, varies in the range $\underline{\boldsymbol{CF}} \leq \boldsymbol{CF} \leq \bar{\boldsymbol{CF}}$. A polyhedral uncertainty characterization is defined as follows:

$$\mathcal{U}_{yst}(\Gamma) = \Bigg\{ L_{yst} \in \mathbb{R}_{+}, \boldsymbol{CF}_{yst} \in \mathbb{R}_{+}^{|I^{res}|} : \underline{\mathrm{L}}_{yst} \leq L_{yst} \leq \bar{L}_{yst}, \underline{\mathrm{CF}}_{iyst} \leq CF_{iyst} \leq \bar{CF}_{iyst},$$

$$\forall i \in I^{res}, L_{yst} - \sum_{i \in I^{res}} CF_{iyst} \leq \Gamma \cdot (\bar{L}_{yst} - \sum_{i \in I^{res}} \underline{\mathrm{CF}}_{iyst}) \Bigg\}, \forall y \in Y, s \in S, t \in T \tag{6.1}$$

where $\Gamma(\leq 1)$, represents the level of conservatism of the decision maker. It is clear that when $\Gamma = 1$, the load and IRES-CF can take on their full range of possible values. When $\Gamma < 1$, the uncertainty set excludes the absolute worst-case situation, which is where all sub-period load are at their highest values and all IRES-CF are at their lowest values. Indeed, by varying Γ, the decision maker can control the level of conservatism in planning. Moreover, the uncertainty set is non-anticipative, in the sense that in sub-period t of year y the decision maker only has information about current and past uncertainty realizations. The lower bound of the uncertainty budget Γ can be derived through the observation that: $\underline{L}_{yst} - \sum_{i \in I^{res}} \bar{CF}_{iyst} \leq L_{yst} - \sum_{i \in I^{res}} CF_{iyst} \leq \Gamma \cdot (\bar{L}_{yst} - \sum_{i \in I^{res}} \underline{CF}_{iyst})$, $\forall y, s, t$. This implies that $\underline{L}_{yst} - \sum_{i \in I^{res}} \bar{CF}_{iyst} \leq \Gamma \cdot (\bar{L}_{yst} - \sum_{i \in I^{res}} \underline{CF}_{iyst})$, $\forall y, s, t$. Therefore, $\Gamma \geq \frac{\underline{L}_{yst} - \sum_{i \in I^{res}} \bar{CF}_{iyst}}{\bar{L}_{yst} - \sum_{i \in I^{res}} \underline{CF}_{iyst}}$, $\forall y, s, t$, from which we can calculate the lower bound of Γ:

$$\Gamma \geq \max_{y \in Y, s \in S, t \in T} \left\{ \frac{\underline{L}_{yst} - \sum_{i \in I^{res}} \bar{CF}_{iyst}}{\bar{L}_{yst} - \sum_{i \in I^{res}} \underline{CF}_{iyst}} \right\}. \tag{6.2}$$

6.2.1 Robust model formulation

The model under uncertainty is represented by a multistage adaptive robust optimization model, where decisions related to unit commitment, commissioning and start-up are *here-and-now* decisions made robust to uncertainty realizations and the dispatch decisions are *wait-and-see* decisions made subject to (and thus, flexible to) uncertainty realizations. For simplicity and clarity, some constraints, such as the operating reserve constraints (2.22)-(2.27), are ignored as they do not affect the core concepts addressed in this chapter. Those can be similarly processed using the same approach described in the next sections.

The objective of the model is to minimize the total cost of here-and-now decisions plus the worst-case total cost of wait-and-see decisions, also known as recourse decisions. Another important component of the model is full immunization, meaning the maintenance of feasibility over all possible uncertainty realizations in the polyhedral uncertainty sets. Letting $\mathcal{V}^t_{ys}$ $(= \{\boldsymbol{L}^t_{ys}, \boldsymbol{CF}^t_{ys}\})$, $\forall y \in Y, s \in S, t \in T$, and given that recourse decisions made in a time period t depend on the full history of the load L and IRES-CF CF from the first time period up to t, the formulation of the robust counterpart (RC) is:

$$\min_{\Omega, \Theta} \sum_{y \in Y} (1 + DR)^{-y} \cdot \sum_{i \in I^{new}} C^{inv}_i \cdot P^{max}_i \cdot q_{iy} \tag{6.3a}$$

$$+ \sum_{y \in Y} (1 + DR)^{-y} \cdot \sum_{s \in S} \cdot \sum_{t \in T} \sum_{i \in I^{th}} \left(C^{stup}_i \cdot z_{iyst} \right) \tag{6.3b}$$

$$+ \sum_{y \in Y} (1 + DR)^{-y} \cdot \sum_{i \in I} C^{fom}_{iy} \cdot P^{max}_i \cdot \sum_{l=1}^{y} q_{il} \tag{6.3c}$$

$$+ \max_{\substack{\mathcal{V}^t_{ys} \in \mathcal{U}^t_{ys} \\ t \in T}} \sum_{y \in Y} (1 + DR)^{-y} \cdot \sum_{s \in S} \sum_{t \in T} \left[\sum_{i \in I} \left(C^{mrgl}_{iy} \cdot p_{iyst}(\mathcal{V}^t_{ys}) \right) + C^{lns} \cdot lns_{yst}(\mathcal{V}^t_{ys}) \right] \tag{6.3d}$$

s.t.

Commissioning and commitment constraints

$$x_{iy} \leq \sum_{l=1}^{y} q_{il}, \forall i \in I^{new}, \forall y \in Y \tag{6.4}$$

$$\sum_{i \in I^{new}} C_i^{inv} \cdot P_i^{max} \cdot q_{iy} \leq B_y^{max}, \forall y \in Y \tag{6.5}$$

$$\sum_{i \in I} \left(P_i^{max} \cdot x_{iy}\right) \geq \left(1 + r^{min}\right) \cdot L^{max}, \forall y \in Y \tag{6.6}$$

$$\sum_{i \in I^{res}} x_{iy} \cdot P_i^{max} \geq Pen_y^{lvl} \cdot \sum_{i \in I} x_{iy} \cdot P_i^{max}, \forall y \in Y \tag{6.7}$$

$$u_{iyst} \leq x_{iy}, \forall i^{th} \in I, y \in Y, s \in S, t \in T \tag{6.8}$$

$$u_{iyst} - u_{iyst-1} = z_{iyst} - v_{iyst}, \forall i \in I^{th}, y \in Y, s \in S, t \in T \setminus \{1\} \tag{6.9}$$

$$u_{iyst} \geq \sum_{\tau \geq t - M_i^u}^{t} z_{iys\tau}, \forall i \in I^{th}, y \in Y, s \in S, t \in T \setminus \{1, ..., M_i^u\} \tag{6.10}$$

$$x_{iy} - u_{iyst} \geq \sum_{\tau \geq t - M_i^d}^{t} v_{iys\tau}, \forall i \in I^{th}, y \in Y, s \in S, t \in T \setminus \{1, ..., M_i^d\} \tag{6.11}$$

Full immunization

$$\forall \mathcal{V}_{ys}^t \in \prod_{t' \in [t]} \mathcal{U}_{ys}^{t'}, [t] \triangleq \{1, ..., t\}, \exists p_{iyst}(.), lns_{yst}(.) \in \mathbb{R}_+, \forall i \in I, y \in Y, s \in S, t \in T \tag{6.12}$$

Dispatch constraints

$$\sum_{i \in I} p_{iyst}(\mathcal{V}_{ys}^t) + lns_{yst}(\mathcal{V}_{ys}^t) = L_{yst}, \forall y \in Y, s \in S, t \in T \tag{6.13}$$

$$p_{iyst}(\mathcal{V}_{ys}^t) \leq u_{iyst} \cdot P_i^{max} \cdot (1 - \epsilon_i), \forall i \in I^{th}, y \in Y, s \in S, t \in T \tag{6.14}$$

$$p_{iyst}(\mathcal{V}_{ys}^t) \geq u_{iyst} \cdot P_i^{min}, \forall i \in I^{th}, y \in Y, s \in S, t \in T \tag{6.15}$$

$$p_{iyst}(\mathcal{V}_{ys}^t) \leq x_{iy} \cdot P_i^{max} \cdot CF_{iyst}, \forall i \in I^{res}, y \in Y, s \in S, t \in T \tag{6.16}$$

$$p_{iyst}(\mathcal{V}_{ys}^t) - p_{iyst-1}(\mathcal{V}_{ys}^{t-1}) \leq u_{iyst-1} \cdot R_i^{Umax} + z_{iyst} \cdot P_i^{start}, \forall i \in I^{th}, y \in Y, s \in S, t \in T \setminus \{1\} \tag{6.17}$$

$$p_{iyst-1}(\mathcal{V}_{ys}^{t-1}) - p_{iyst}(\mathcal{V}_{ys}^t) \leq u_{iyst-1} \cdot R_i^{Dmax}, \forall i \in I^{th}, y \in Y, s \in S, t \in T \setminus \{1\} \tag{6.18}$$

$$p_{iyst}(\mathcal{V}_{ys}^t), lns_{yst}(\mathcal{V}_{ys}^t) \geq 0, \forall i \in I, y \in Y, s \in S, t \in T \tag{6.19}$$

6.2.2 Multi-stage affinely adjustable robust counterpart

Because of the full immunization constraint (6.12) and the fact that the uncertain parameters are real-valued, the robust counterpart is semi-infinite. We propose to consider linear decision rules to make the problem tractable. This method, which results in what is known as a multistage affinely adjustable robust counterpart (AARC), is appealing in that it results in a linear model that can be solved using over-the-counter solvers and does not require significant tailor-made implementation efforts. The AARC is obtained by replacing the vector of

recourse variables using the following affine relationship:

$$\boldsymbol{R}_{yst}(\mathcal{V}_{ys}^{t}) = \boldsymbol{R}_{yst}^{\boldsymbol{0}} + \sum_{t' \in [t]} \boldsymbol{R}_{ystt'}^{\boldsymbol{L}} \cdot L_{yst'} + \sum_{i' \in I^{res}} \sum_{t' \in [t]} \boldsymbol{R}_{i'ystt'}^{\boldsymbol{C}} \cdot CF_{i'yst'} \tag{6.20}$$

where $[t] \triangleq \{1, ..., t\}$ and $(\boldsymbol{R}_{yst}^{\boldsymbol{0}}, \boldsymbol{R}_{ystt'}^{\boldsymbol{L}}, \boldsymbol{R}_{i'ystt'}^{\boldsymbol{C}})$ are the coefficients of the linear decision rule. Then, in the model with linear decision rules, the constraints can be processed into a finite number of linear constraints, relying on a duality-based reformulation to obtain the final MILP problem. Below we illustrate how the processing is achieved for one equality and one inequality constraint.

Equality constraint: Consider the supply-demand equality constraint (6.13). Replacing the uncertainty dependent variables $p_{iyst}(\mathcal{V}_{ys}^{t})$ and $lns_{yst}(\mathcal{V}_{ys}^{t})$ following equation (6.20), and re-arranging the terms, we obtain:

$$\left(\sum_{i \in I} p_{iyst}^{0} + lns_{yst}^{0}\right) + \sum_{t' \in [t-1]} \left(\sum_{i \in I} p_{iystt'}^{L} + lns_{ystt'}^{L}\right) \cdot L_{yst'} + \left(\sum_{i \in I} p_{iystt}^{L} + lns_{ystt}^{L} - 1\right)$$
$$\cdot L_{yst} + \sum_{i' \in I^{res}} \sum_{t' \in [t]} \left(\sum_{i \in I} p_{ii'ystt'}^{C} + lns_{ystt'}^{C}\right) \cdot CF_{i'yst'} = 0, \forall \mathcal{V}_{ys}^{t} \in \mathcal{U}_{ys}^{t}, y \in Y, s \in S, t \in T \tag{6.21a}$$

From this we know that equality (6.21a) is valid *if and only if* equations (6.21b)-(6.21e) are satisfied.

$$\sum_{i \in I} p_{iyst}^{0} + lns_{yst}^{0} = 0, \forall y \in Y, s \in S, t \in T \tag{6.21b}$$

$$\sum_{i \in I} p_{iystt'}^{L} + lns_{ystt'}^{L} = 0, \forall y \in Y, s \in S, t' \in [t-1], t \in T \tag{6.21c}$$

$$\sum_{i \in I} p_{iystt'}^{L} + lns_{ystt'}^{L} = 1, \forall y \in Y, s \in S, t' = t, t \in T \tag{6.21d}$$

$$\sum_{i \in I} p_{ii'ystt'}^{C} + lns_{ystt'}^{C} = 0, \forall i' \in I^{res}, y \in Y, s \in S, t' \in [t], t \in T \tag{6.21e}$$

Inequality constraint: Consider the maximum production limit inequality (6.14). The constraint, after applying the affine relationship (6.20), becomes:

$$\left(p_{iyst}^{0} + \sum_{t' \in [t]} p_{iystt'}^{L} \cdot L_{yst'} + \sum_{i' \in I^{res}} \sum_{t' \in [t]} p_{i'iystt'}^{C} \cdot CF_{i'yst'}\right) \leq u_{iyst} \cdot P_{i}^{max} \cdot (1 - \epsilon_{i}),$$
$$\forall i \in I^{th}, y \in Y, s \in S, t \in T \tag{6.22a}$$

Re-arranging the terms of the the constraint, given that an uncertainty-affected constraint $\text{LHS}_{ys} \leq \text{RHS}_{ys}$, where LHS contains all uncertainty terms and RHS contains the rest, is valid $\forall \mathcal{V}_{ys}^{t} \in \mathcal{U}_{ys}^{t}, t \in T$, *if and only if* $\max_{\mathcal{V}_{ys}^{t} \in \mathcal{U}_{ys}^{t}, t \in T} \text{LHS}_{ys} \leq \text{RHS}_{ys}$. Notice that any ($\geq$) constraint can easily be transformed to a ($\leq$) one and can follow the same above logic. Applying this logic to inequality (6.22a) we get:

$$\max_{\mathcal{V}_{ys}^{t} \in \mathcal{U}_{ys}^{t}} \sum_{t' \in [t]} \left(p_{iystt'}^{L} \cdot L_{yst'}\right) + \sum_{i' \in I^{res}} \sum_{t' \in [t]} \left(p_{ii'ystt'}^{C} \cdot CF_{i'yst'}\right) \leq (1 - \epsilon_{i}) \cdot P_{i}^{max} \cdot$$
$$u_{iyst} - p_{iyst}^{0}, \forall i \in I^{th}, y \in Y, s \in S, t \in T \tag{6.22b}$$

$$\sum_{t' \in [t]} (\pi^{A}_{iystt'} \cdot \bar{L}_{yst'} - \pi^{B}_{iystt'} \cdot \underline{L}_{yst'}) + \sum_{t' \in [t]} \sum_{i' \in I^{res}} (\pi^{C}_{ii'ystt'} \cdot \bar{CF}_{i'yst'} - \pi^{D}_{ii'ystt'} \cdot \underline{CF}_{i'yst'}) + \sum_{t' \in [t]} \pi^{E}_{iystt'} \cdot$$

$$\Gamma \cdot (\bar{L}_{yst'} - \sum_{i' \in I^{res}} \underline{CF}_{i'yst'}) \leq (1 - \epsilon_i) \cdot P^{max}_{i} \cdot u_{iyst} - p^{0}_{iyst}, \forall i \in I^{th}, y \in Y, s \in S, t \in T \quad (6.22c)$$

$$\pi^{A}_{iystt'} - \pi^{B}_{iystt'} + \pi^{E}_{ystt'} \geq p^{L}_{iystt'}, \forall i \in I^{th}, y \in Y, s \in S, t^{'} \in [t], t \in T \quad (6.22d)$$

$$\pi^{C}_{ii'ystt'} - \pi^{D}_{ii'ystt'} - \pi^{E}_{ystt'} \geq p^{C}_{ii'ystt'}, \forall i^{'} \in I^{res}, i \in I^{th}, y \in Y, s \in S, t^{'} \in [t], t \in T \quad (6.22e)$$

$$\pi^{A}_{iystt'}, \pi^{B}_{iystt'}, \pi^{C}_{ii'ystt'}, \pi^{D}_{ii'ystt'}, \pi^{E}_{iystt'} \geq 0, \forall i^{'} \in I^{res}, i \in I^{th}, y \in Y, s \in S, t^{'} \in [t], t \in T \quad (6.22f)$$

Dualizing the left-hand side of the constraint and because of strong duality, this set of non-linear inequalities can be replaced by the set of linear inequalities (6.22c)-(6.22f), where π is the vector of dual variables associated with the bounds of the uncertainty set (6.1). Applying the same principle to all inequality and equality constraints, the semi-infinite robust counterpart is converted into a finite mixed integer linear programming problem.

6.3 Robust model solution method

6.3.1 Problem dimensionality issues

As shown in the previous section, recourse decisions made in a time period, t, depend on $\mathcal{V}^t$ $(= \{\mathcal{V}_1, ..., \mathcal{V}_t\})$, i.e., the history of load and IRES-CF realizations from the first time period up to t. The duality-based approach used to define the equivalent deterministic problem, therefore, leads to an extremely large MILP reformulation. Take for example the maximum production limit constraint (6.14): in the deterministic formulation, this constraint would have a dimension of $\mid I^{th} \mid \times \mid Y \mid \times \mid S \mid \times \mid T \mid$, which we can denote as $\mid det. \mid$. On the other hand, the set of inequalities defining the AARC of this constraint (i.e., inequalities (6.22c)-(6.22f) have a dimension of $\mid det. \mid \times \left(1 + \frac{|T|+1}{2} \cdot (1 + \mid I^{res} \mid)\right)$, according to the definition of the uncertainty set (6.1). That is, the dimension of each robust constraint is multiplied by a strictly positive factor which is a function of the number of time periods T and number of IRES units I^{res}, considered. Even for a moderate size problem, this can quickly lead to extremely large and intractable MILP instances. For example, if we consider a time periods set T with a magnitude of 24 hours and an IRES units set I^{res} with a magnitude of 2 (e.g. wind and solar), the number of AARC constraints would be 38.5 multiples of the same set of constraints in the original deterministic formulation. The same applies for the number of variables, were each AARC constraints set would require an additional $5 \times \left(|I| + |Y| + |S| + \frac{|T|(|T|+1)}{2}\right) + 2|I^{res}|$ dual variables and an additional $|I| \times |Y| \times |S| \times \frac{|T|(|T|+1)}{2} \times (1 + |I^{res}|)$ affine coefficient variables, compared to the original deterministic constraint formulation.

6.3.2 Information basis approximation

Notice that one of the most important contributors to the above dimensionality issue is the appearance of the triangular number $\frac{|T| \cdot (|T|+1)}{2}$ which exponentially increases with the number of periods considered. This factor arises since in the defined linear decision rule,

the recourse variables depend on the entire history of realized uncertainty at every time period up to t, $\forall t \in T$. Following [75], we call this full affine dependency the "on-line information basis" since it -reasonably- considers that the decision maker takes into account all historical information revealed about the uncertainty realizations to adapt the recourse decision variables at the current time period.

We propose and investigate a solution method based on information basis level approximation, where, instead of considering the full affine dependency, only the most recent uncertainty realizations are taken into account to adjust the recourse variables at the current time period t. For this, we introduce a new parameter representing the information level, denoted h ($\leq |T|$), which will allow us to control how *early* the model accounts for information on uncertainty realization, to adjust the recourse variable at the current period. In this sense, the h parameter represents the number of most recent time periods that will be taken into account in the linear decision rule. If $h = |T|$, the full historical periods will be taken into account, which is equivalent to full affine dependency. If $h < |T|$, both the size of the equivalent AARC set of constraints, the associated dual variables and the affine coefficient variables will be reduced.

To implement this approximation method, the running index $[t]$ needs to be re-defined such as: $[t] \triangleq \begin{cases} \{1, ..., t\}, & \text{if } t \leq h \\ \{t-h, ..., t\}, & \text{if } t > h \end{cases}$. As an example, the number of AARC constraints defining inequalities (6.22c)-(6.22f) will have a dimension of: $|\ det.\ | \times \left(1 + 1/|T| \cdot (h+1) \cdot \left(|T| - \frac{h}{2}\right) \cdot (1 + |I^{res}|)\right)$, compared to the previously calculated value. This leads to a reduction in the number of constraints by a total of: $|det.| \times |I^{res}| \times \left((0.5|T| - h - 0.5) + \frac{h^2+h}{2|T|}\right)$ constraints, for each robust constraint reformulation. The same calculations can be made for the reduction in the number of variables. Notice that, as logical, the reduction in the number of constraints (and variables) increases as h decreases, i.e. as we take into account less historical information. However, the relationship is non-linear and indeed is negligeable for h values that are close to $|T|$, and is only significant around low values of h. Hence, there is a clear trade-off in the level of adjustability of the recourse variables and the computational complexity. This might lead to the expectation that using this method, we considerably sacrifice optimality for computational simplicity. Indeed, we show in the next section that this is not necessarily the case: by conducting a sensitivity analysis on the quality of solutions obtained by varying the h parameter, we show that significant computational gains can be achieved while still maintaining high quality of the solution.

6.4 Application

6.4.1 Power system description and implementation notes

For the application, we consider the same generation units characteristics (technical and economic) used for previous analysis described in Section (4.4.1), and same projections for the system load and IRES-CF for the years 2041-2046 calculated in Section (5.4.1) . To solve the integrated multi-stage AARO model, each full year is approximated by 4 days optimally obtained using the method proposed in Section (3.3.3). Hourly load uncertainty is set to vary within 10% of the nominal values, while hourly IRES uncertainty is set to vary within 20% around the nominal values. Experimental testing showed that the interior-point method

(Barrier algorithm) should be used to find the root relaxation of the MILP, to avoid primal-dual degeneracy.

6.5 Results and discussion

6.5.1 Sensitivity analysis on information basis approximation

We start with a reduced-size instance to conduct a sensitivity analysis on the impact of varying the information level parameter h on the planning problem solution time and quality. The horizon considered for this purpose covers only two planning years, each represented by 4 days of 24 hours. The parameter h, therefore, can vary from 1 to 24, representing the lowest to the highest information levels taken into account in the linear decision rule, respectively. Furthermore, since the ramping up and down constraints (6.17) and (6.18) are the only second-level constraints that are time-coupling, and where the full value of considering detailed commitment decisions appear, we compare two variations of the problems solution: one where we relax the ramping constraints and conduct the sensitivity, and the other where the ramping constraints are enforced. To ensure the proper evaluation of the quality of the solutions obtained, the integer-relaxed, fully affine dependent problem is solved as a guaranteed lower bound solution for both the ramping-relaxed and ramping-enforced MILP problems. A schematic description of how the optimality gap is compared for the purpose of the sensitivity analysis is shown in Fig. (6.1).

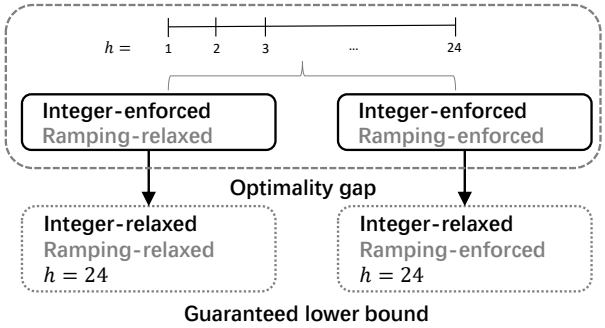

FIGURE 6.1 – Schematic illustration of the process for calculating the optimality gap for both ramping-relaxed and ramping-enforced MILP problems.

Table (6.1) shows the optimality gap obtained for solving the problem under different values of information level parameter h, for both the ramping-relaxed and the ramping-enforced MILP problems. It is shown that in all cases, the objective function (total cost) gap is at most 1%, which is an indicator of a strong performance even for low values of h. These results are consistent with the investment decisions obtained as is shown in Table (6.2). These decisions are identical for the solution under the lowest ($h = 1$) and the highest ($h = 24$) information basis levels. Moreover, the standard deviation of these investment decisions across all instances is very low, indicating the consistency of these results across all problem instances. Moreover, we have found that these observations hold across the h sensitivity variations performed under different values of uncertainty budget (Γ). With respect to the computational performance, Figure (6.2) shows that indeed the computational time significantly decreases as we consider lower values of h. For both ramping-relaxed and

ramping-enforced cases, the solution for the lowest h values is obtained within 10 to 40 seconds. Notice that this range remains consistent for the ramping-relaxed problem across all values of h, slightly increasing to a maximum of 38 seconds. For the ramping-enforced problem, a clear and significant solution time increase can be observed. For the fully adjustable problem ($h = 24$), the solution time is 4375 seconds, compared to 11, 15 and 31 seconds for the three lowest h values considered, respectively. This confirms that significant improvements can be gained in computational time while maintaining good results by using the proposed approximated linear decision rule.

TABLE 6.1 – Guaranteed optimality gap for the solutions obtained with respect to the sensitivity on the h parameter, for both the ramping-relaxed and the ramping-enforced MILP problems.

Information level (h)	1	2	3	4	5	6	7	8	9	10	11	12
Ramping-relaxed	0.37%	0.36%	0.70%	0.24%	0.40%	0.75%	0.75%	0.75%	0.16%	0.06%	0.87%	0.88%
Ramping-enforced	0.94%	0.95%	0.31%	0.50%	0.23%	0.05%	0.04%	0.49%	0.04%	0.48%	0.51%	0.26%
Information level (h)	13	14	15	16	17	18	19	20	21	22	23	24
Ramping-relaxed	0.47%	0.95%	0.80%	1.01%	0.53%	0.11%	0.26%	0.92%	0.54%	0.62%	0.40%	0.40%
Ramping-enforced	0.01%	0.03%	0.95%	0.48%	0.67%	0.61%	0.95%	0.50%	0.02%	0.97%	0.03%	0.03%

TABLE 6.2 – Number of units installed as per the ramping-enforced robust MILP problem under the lowest and highest information levels h.

	Number of units			
	$h = 1$	$h = 24$	all h	
Technology			Mean	Std. dev.
Nuclear Units	31	31	31	0
Coal Units	12	12	12	0
CCGT Units	27	27	27	0
Wind Units	298	298	298.8	3.97
Solar Units	0	0	0.33	0.48

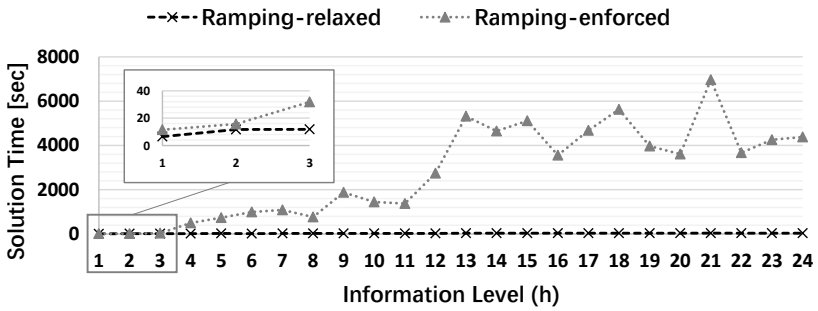

FIGURE 6.2 – Impact of varying the information level parameter h on the computational time of the ramping-relaxed and ramping-enforced robust MILP problems.

It should be noted that the variation in the solution time across different information level (h) problems is not strictly increasing. This is due to the differences in the time taken for the generic solver to solve the MILPs. Many factors, other than the problem size, can impact the solution time; for example the quality of the initial heuristic solution and the quality of

the cuts generated by the solver. Notice also how by considering the ramping constraints, the computational time of the problem increases significantly even for these reduced case studies. It is, then, worthy to investigate what value are these constraints adding to the solutions of the robust power system planning problem.

6.5.2 Worst-case analysis for robust power systems planning with ramping constraints

Notice that according to the definition of the uncertainty set (6.1) and letting the uncertain parameters take on their full range of values ($\Gamma = 1$), the robust solution should be expected to be trivial and simply equivalent to the worst-case deterministic solution. This is since any solution that satisfies the highest hourly load ($\bar{L}$) and lowest IRES-CF ($\underline{CF}$) should be -readily- feasible to satisfy any combination of lower load and higher IRES-CF in the uncertainty range. We show that this is, indeed, the case if the time-coupling ramping constraints are ignored. However, enforcing the ramping constraints implicitly re-defines the worst-case dispatch decisions in the AARC problem so that they are no longer simply satisfying the worst load and IRES-CF, but rather also ensuring the ramping feasibility under all other uncertainty realizations of those parameters. A simple example for this effect would be to satisfy the ramping between the lowest load ($\underline{L}_t$) at t and the successive highest load ($\bar{L}_{t+1}$) at $t+1$, if the uncertainties are to be realized in such a way. More complex interactions would occur if, in addition, we consider the uncertainty of the IRES-CF. In this case, unlike the AARC method, no straightforward method exists to ensure the feasibility of these complex interactions within the deterministic nor the stochastic models.

To illustrate this effect on the system investment and operation decisions, we will consider the whole 5 years planning horizon previously described for the case study and analysis. To further highlight the impact of the detailed ramping constraints on the robust solution obtained, we expand the hourly uncertainty of load and IRES-CF to be within 20% and 50% of their nominal values, respectively. Finally, we will deploy the information basis approximation method described in the previous section to find the solution to the AARC problem. The results will be compared to the worst-case deterministic problem solution (denoted WCD), both for the ramping-relaxed and ramping-enforced cases.

Let us first consider the ramping-relaxed case; as expected, both WCD and worst-case AARC solutions are identical. The total objective value in both cases amounts to 63.36Billion€. The breakdown of the (annualized) investment, operational and load not served (LNS) costs is shown in Fig. (6.3). By enforcing the ramping constraints, indeed, we find that the solutions of both problems are no longer identical. Clearly, the WCD objective value in this case is higher than the one with no ramping considered. Yet, interestingly, these values are even higher for the AARC worst-case solution with a $+3.10\%$ and $+12.43\%$ increase in the investment and operational costs, respectively, and a -17.25% decrease in the LNS cost, compared to the WCD solution, as shown in Fig. (6.3). It is clear that properly accounting for the uncertainty withing the AARC model significantly increases the investment and operational costs of the system because of the "implicit" worst-case ramping requirements.

To further understand how the uncertainties are driving the investment decisions within the ramping-enforced problems, Table (6.3) compares the total capacities installed per technology type for all cases considered. First, it is shown that the capacities installed are identical for both WCD and AARC solutions when the ramping is relaxed. Then, enforcing the ramping constraints leads to a clear shift in the installed capacities under the WCD solution, most notably, a shift from the least flexible nuclear capacity, to the most flexible CCGT

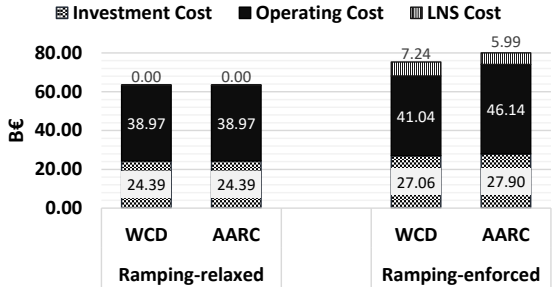

FIGURE 6.3 – Breakdown of (annualized) investment, operational and LNS solution costs for the ramping-relaxed and ramping-enforced problems. Comparison between the WCD and AARC solutions.

capacity. However, the ramping-enforced AARC solution confirms that neglecting the load and IRES-CF uncertainties underestimates the actual flexible capacity needed to account for the implicit worst case rampings. This is verified as per the investment decisions in a lower nuclear capacity and higher coal and CCGT ones, compared to the WCD solution.

TABLE 6.3 – Breakdown of total installed capacity per technology type for the ramping-relaxed and ramping-enforced problems. Comparison between the WCD and AARC solutions.

	Capacity Installed [GW]			
	Ramping-relaxed		Ramping-enforced	
Technology	WCD	AARC	WCD	AARC
Nuclear capacity	67.2	67.2	64.4	56
Coal capacity	7.7	7.7	6.6	15.4
CCGT capacity	12.1	12.1	20.3	25.3
Wind capacity	1.68	1.68	61.7	78.9
Solar capacity	85.32	85.32	29.7	19.62

Another indicator of the superiority of the AARC solution in accounting for ramping uncertainty, is the amount of IRES shedding attained for the worst-case solution. This is because IRES shedding is another mean for managing inter-temporal ramping variability next to thermal units ramping capacity and load shedding. Notice in Table (6.4) how the WCD and AARC shedding amounts are identical for the ramping-relaxed case, and the improved IRES shedding amounts as given by the AARC (total of 0.76%) compared to WCD solution (total of 4.47%), for the ramping-enforced case.

TABLE 6.4 – Breakdown of IRES shedding for the ramping-relaxed and ramping-enforced problems. Comparison between the WCD and AARC solutions.

	Ramping-relaxed		Ramping-enforced	
	WCD	AARC	WCD	AARC
Wind power shedding	2.15%	2.15%	3.02%	0.82%
Solar power shedding	1.47%	1.47%	8.67%	0.56%
Total IRES shedding	1.49%	1.49%	4.47%	0.76%

We finally discuss the solution times taken for the WCD and AARC problems. The WCD problem takes few seconds to be solved, whereas, even for a moderate h value ($h = 8$),

the AARC problem can take several hours as can be seen in Table (6.5). Clearly, accounting for the uncertainties under the AARC approach comes at a significant computational price. It is important to note, however, how the proposed information basis approximation method proposed allows for tractable and high-quality solutions, whereas considering the full AARC formulation for the ramping-enforced case does not allow us to find a root-relaxation solution even after 40 hours of run-time.

TABLE 6.5 – Computational time for the ramping-relaxed and ramping-enforced problems. Comparison between the WCD and AARC solutions.

	Ramping-relaxed		Ramping-enforced	
	WCD	AARC ($h = 8$)	WCD	AARC ($h = 8$)
Computation time [sec]	12	3060	13.3	25657.8

7 Conclusions

Planning power systems for providing secure and reliable electricity to users is key in any energy strategy. This is being challenged by several recent developments, most notably, the increased penetration of variable intermittent renewable energy sources (IRES), which is raising concerns about the ability of future power systems to effectively respond to the high net-load variations, a system property which is referred to as operational flexibility. Moreover, climate change threats and, particularly, the increased frequency and severity of extreme weather events, are threatening to disrupt electric power supply and require the consideration of system resilience right from the planning stage. Also, the inherent uncertainties characterizing those systems must be inevitably considered.

In the present thesis, the research work done for developing a techno-economic modeling and robust optimization framework for multi-period power systems planning considering a high share of IRES and resilience against extreme weather events has been presented. The specific planning problem considered is that of selecting the technology choice, size and commissioning schedule of conventional and renewable generation units under technical, economical, environmental and operational constraints. Within this problem, key research questions addressed have been:

(i) the proper integration and assessment of the operational flexibility needs due to the increased variability of the high shares of IRES within the power system planning problem,

(ii) the appropriate modeling and incorporation of the requirements of resilience against extreme weather events within the power system planning problem,

(iii) the representation and treatment of the uncertainties inherent in the system supply and demand, within the planning context.

The next section discusses the original research contributions of the thesis with respect to the identified research gaps as well as to the originality of the results obtained and the significance of the conclusions drawn. These contributions are presented in three subsections, each with regards to the respective objective of the thesis.

7.1 Thesis contributions (extended with respect to the originality of the results and analysis)

7.1.1 Operational Flexibility [Chapter 4, Paper (i)]

With respect to operational flexibility, an integrated framework for the quantitative assessment of operational flexibility in power systems planning has been developed. The framework stands on: (i) the development of a computationally efficient, multi-period integrated GEP-UC model that accounts for key short-term constraints and chronological net load representation, (ii) the elaboration of accurate and systematic horizon reduction methods to

alleviate the computational burden of the resulting large-sized optimization problem and (iii) the novel definition of suitable metrics for the operational flexibility assessment of the obtained plans. A realistic size case study has been investigated under several scenarios of IRES penetration levels and carbon reduction targets. Moreover, an investigation of the effect of varying the fuel costs and load growth has been conducted to comprehensively identify the most significant parameters that can affect the system operational flexibility.

The application of the framework to the case studies has shown its ability to provide transparent and objective results for obtaining and assessing different expansion plans across a wide range of policy requirements. The study has also allowed to highlight the importance of integrating short-term technical constraints and chronological load patterns, within long-term planning models and especially under significant renewable energy penetration levels.

Through the analysis of the results of the case studies considered, the following general conclusions can be drawn:

1. The results confirm those presented in other works and, most notably, that neglecting short-term constraints within long-term planning leads to an underestimation of the investment required in peaking fossil units, unrealistic production schedules with high amounts of load not served and an underestimation of carbon emissions.

2. Insights were gained by employing quantitative flexibility metrics for the assessment, most notably that expansion plans obtained through the integrated model are robust to the different renewable energy penetration and emission scenario realizations, in terms of flexibility shortage, i.e., they maintain a constant low shortage level regardless of the different requirements imposed.

3. On the other hand, flexibility-neglecting generation expansion planning models have shown a linear and significant trend of flexibility shortage with respect to the different renewable energy sources penetration requirements, enough to offset any computational advantage they have when such requirements are binding.

4. The complementarity of the two metrics considered, with regards to the frequency of flexibility shortage (IRRE) and its magnitude (EFS), is highlighted. It is shown that the sensitivity of one with respect to the different scenarios can be more significant than the other, which is important to consider for real applications.

5. Moreover, the results emphasize the importance of the use of suitable quantitative metrics for operational flexibility assessment, as opposed to relying on other generic indicators, such as the generation technology mix or system costs, which are not capable of reflecting the true flexibility levels of the obtained plans.

6. For real applications, the integrated framework can be used by power system planners to rapidly and accurately evaluate the impact of different system parameters and policy requirements on the resulting generation expansion plans, most notably in terms of operational flexibility. The planner can, then, adapt the policy requirements to ensure generation plans with an adequate flexibility level or set proper expectations on which levels are attainable under a specific set of parameters and requirements.

7. Finally, several remarks are highlighted in the relevant sections regarding the proper treatment of IRES investments as decision variables within the simplified GEP model as well as the horizon reduction methods, which can prove useful for practitioners if similar types of models are to be considered.

7.1.2 Resilience [Chapter 5, Paper (ii)]

With respect to planning for resilience against extreme weather events, a set of piece-wise linear models to quantify the impact of extreme heat waves and drought events have been proposed, as well as a method to integrate their impacts within the power system planning model. A practically sized case study based on realistic climate projections obtained from the Coupled Model Intercomparison Project Phase 5 (CMIP5) and system attributes representatives of the southern French geographical area has been investigated. Several extreme climate scenarios related to heat waves and water shortages are investigated and the results are compared between the resilience-driven planning framework proposed and the conventional planning results.

Through the analysis of the results of the case studies considered, the following general conclusions can be drawn:

1. The results show that significant improvements in terms of load supply during an extreme heat wave and drought events can be achieved under the resilient planning framework, compared to conventional planning.
2. Moreover, it is shown that although these improvements come at higher investment and operational costs, they are fully offset by the economic savings achieved by reducing the amount of load loss during those events.
3. With respect to the interaction between system resilience and operational flexibility, the results illustrate that although the plans obtained have higher flexibility shortage levels, they keep at least an order of magnitude lower than the load losses due to the lack of system resilience. This further highlights the advantage of extending the modeling to adopt a more comprehensive planning framework.

7.1.3 Uncertainties [Chapter 6, Paper (iii)]

To account for the uncertainty and intermittency of high shares of renewable energy production and system load, the power system planning model, which accounts for detailed short-term unit commitment and ramping constraints, has been treated via a multi-stage adaptive robust optimization model. The model accounts for the *here-and-now* commissionning and commitment decisions made robust against load and renewable generation uncertainties, and the *wait-and-see* dispatch decisions subject to uncertainty realization. To alleviate the computational burden, a novel solution method based on "information basis" level approximation for the linear decision rules has been proposed and a sensitivity analysis has been performed to confirm the effectiveness of this solution approach. A realistic-size case study is investigated to compare the significance of using the developed approach on the results, even in comparison to worst-case analysis of the deterministic model or other stochastic methods.

Through the analysis of the results of the case studies considered, the following general conclusions can be drawn:

1. the results show how the multi-stage affinely adjustable robust optimization model can be formulated and effectively implemented to handle load and IRES uncertainties in power system planning problems.
2. the sensitivity analysis conducted on the "information level" parameter introduced in the proposed solution method shows how significant computational gains are achieved using this method, with negligible loss in the solution accuracy.

3. the results of the worst-case analysis conducted show how considering the detailed ramping constraints within a multistage robust model significantly improves the plans obtained in terms of operational flexibility; this is because those uncertainties re-define the worst-case ramping requirements in such a way that would not be captured within stochastic or non-causal planning models.

7.2 Future work

A limitation of the work presented in this thesis lies in the mixed integer linear optimization models considered. Indeed, the economic planning parameters and the technical behavior of energy generation are affected by nonlinear conditions. For instance, production costs and ramping rates are nonlinear functions of the variations in partial-load levels, whereas start-up costs and times are nonlinear functions of the shut-down duration. These conditions become particularly relevant when short-term capabilities and operational flexibility are considered in the model. In this regard, future work will be devoted to the extension of the optimization model for accounting of nonlinearities in the system.

Moreover, the modeling and optimization framework presented here can be directly extended to multi-regional planning, to account for the differences in weather conditions across the different regions. Additionally, since extreme weather events are uncertain and stochastic in nature, the presented deterministic metric for resilience can be improved by accounting for the uncertainties within a probabilistic framework.

Finally, a natural extension of the present framework could explore the potential benefits of considering demand-side management policies, and/or different storage options as operational flexibility and resilience enabling resources for future power systems.

A Approximating the IRES-CF for the long-term GEP model

One way to approximate the IRES-CF is to re-order the chronological CF values in descending order and divide them into CF-blocks, each having a level and duration. A fundamental problem with this approach is that it presumes that the highest IRES-CF is concurrent with the highest load level and, analogously, the lowest IRES-CF is concurrent with the lowest load level. This imposes a significant and unrealistic bias in the results. We, thus, propose to approximate the IRES capacity factor duration curve (RES-CFDC) in a way that maintains the real hourly correlation between the load and the IRES availability, when both chronological time-series are available.

(A) LDC step function approximation

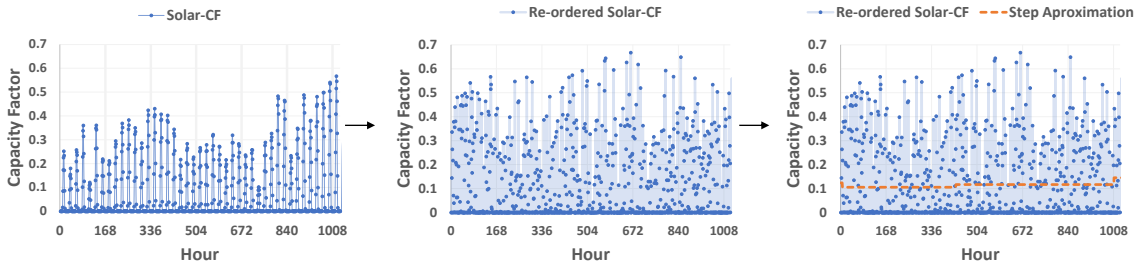

(B) Solar-CF step function approximation

FIGURE A.1 – 6 weeks representation of load and Solar CF yearly data and their step function approximation

This can be best illustrated by means of an example: consider a 6 weeks representation of hourly load and solar CF time series, such as that shown in Figure (A.1). This can be a forecasted time-series or historically monitored data. Each hourly load level corresponds to a specific solar CF for the same hour. When the load is re-ordered in descending order into a LDC, the solar-CF is re-ordered by maintaining each CF respective value relative to its original hourly load level. When the LDC is, then, approximated by a step-function to

obtain average load levels and durations, the same duration blocks are used to segment and find corresponding average values for the solar CF time-series.

B Illustration of the high temporal variability in the load profiles used

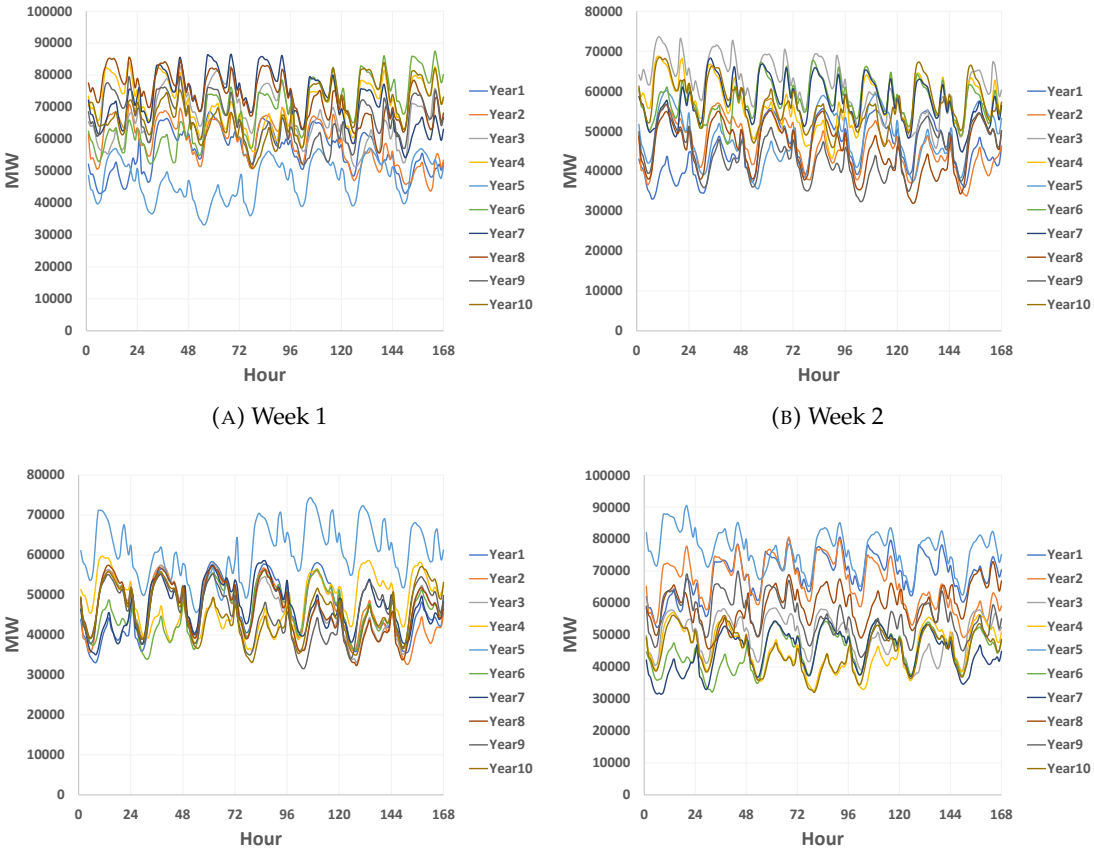

(A) Week 1

(B) Week 2

(C) Week 3

(D) Week 4

FIGURE B.1 – Weekly load profile samples for each year of the planning horizon considered (illustration of the wide variation in inter-temporal variability considered in the study)

C Complete multi-stage adaptive robust optimization model formulation

C.1 Robust model formulation

Letting $\mathcal{V}_{ys}^{t}$ $(= \{\boldsymbol{L}_{ys}^{t}, \boldsymbol{CF}_{ys}^{t}\}), \forall y \in Y, s \in S, t \in T$, and given that recourse decisions made in a time period t depend on the full history of the load L and IRES-CF CF from the first time period up to t, the formulation of the robust counterpart (RC) is:

$$\min_{\Omega,\Theta} \sum_{y \in Y} (1+DR)^{-y} \cdot \sum_{i \in I^{new}} C_i^{inv} \cdot P_i^{max} \cdot q_{iy} \tag{C.1a}$$

$$+ \sum_{y \in Y} (1+DR)^{-y} \cdot \sum_{s \in S} \cdot \sum_{t \in T} \sum_{i \in I^{th}} \left(C_i^{stup} \cdot z_{iyst} \right) \tag{C.1b}$$

$$+ \sum_{y \in Y} (1+DR)^{-y} \cdot \sum_{i \in I} C_{iy}^{fom} \cdot P_i^{max} \cdot \sum_{l=1}^{y} q_{il} \tag{C.1c}$$

$$+ \max_{\substack{\mathcal{V}_{ys}^{t} \in \mathcal{U}_{ys}^{t} \\ t \in T}} \sum_{y \in Y} (1+DR)^{-y} \cdot \sum_{s \in S} \sum_{t \in T} \left[\sum_{i \in I} \left(C_{iy}^{mrgl} \cdot p_{iyst}(\mathcal{V}_{ys}^{t}) \right) + C^{lns} \cdot lns_{yst}(\mathcal{V}_{ys}^{t}) \right] \tag{C.1d}$$

s.t.

Commissioning and commitment constraints

$$x_{iy} \leq \sum_{l=1}^{y} q_{il}, \forall i \in I^{new}, \forall y \in Y \tag{C.2}$$

$$\sum_{i \in I^{new}} C_i^{inv} \cdot P_i^{max} \cdot q_{iy} \leq B_y^{max}, \forall y \in Y \tag{C.3}$$

$$\sum_{i \in I} \left(P_i^{max} \cdot x_{iy} \right) \geq \left(1 + r^{min} \right) \cdot L^{max}, \forall y \in Y \tag{C.4}$$

$$\sum_{i \in I^{res}} x_{iy} \cdot P_i^{max} \geq Pen_y^{lvl} \cdot \sum_{i \in I} x_{iy} \cdot P_i^{max}, \forall y \in Y \tag{C.5}$$

$$u_{iyst} \leq x_{iy}, \forall i^{th} \in I, y \in Y, s \in S, t \in T \tag{C.6}$$

$$u_{iyst} - u_{iyst-1} = z_{iyst} - v_{iyst}, \forall i \in I^{th}, y \in Y, s \in S, t \in T \setminus \{1\} \tag{C.7}$$

$$u_{iyst} \geq \sum_{\tau \geq t - M_i^u}^{t} z_{iys\tau}, \forall i \in I^{th}, y \in Y, s \in S, t \in T \setminus \{1, ..., M_i^u\} \tag{C.8}$$

$$x_{iy} - u_{iyst} \geq \sum_{\tau \geq t - M_i^d}^{t} v_{iys\tau}, \forall i \in I^{th}, y \in Y, s \in S, t \in T \setminus \{1, ..., M_i^d\} \tag{C.9}$$

Full immunization

$$\forall \mathcal{V}_{ys}^{t} \in \prod_{t' \in [t]} \mathcal{U}_{ys}^{t'}, [t] \triangleq \{1, ..., t\}, \exists p_{iyst}(.), lns_{yst}(.) \in \mathbb{R}_{+}, \forall i \in I, y \in Y, s \in S, t \in T \tag{C.10}$$

Dispatch constraints

$$\sum_{i \in I} p_{iyst}(\mathcal{V}_{ys}^{t}) + lns_{yst}(\mathcal{V}_{ys}^{t}) = L_{yst}, \forall y \in Y, s \in S, t \in T \tag{C.11}$$

$$p_{iyst}(\mathcal{V}_{ys}^{t}) \leq u_{iyst} \cdot P_{i}^{max} \cdot (1 - \epsilon_{i}), \forall i \in I^{th}, y \in Y, s \in S, t \in T \tag{C.12}$$

$$p_{iyst}(\mathcal{V}_{ys}^{t}) \geq u_{iyst} \cdot P_{i}^{min}, \forall i \in I^{th}, y \in Y, s \in S, t \in T \tag{C.13}$$

$$p_{iyst}(\mathcal{V}_{ys}^{t}) \leq x_{iy} \cdot P_{i}^{max} \cdot CF_{iyst}, \forall i \in I^{res}, y \in Y, s \in S, t \in T \tag{C.14}$$

$$p_{iyst}(\mathcal{V}_{ys}^{t}) - p_{iyst-1}(\mathcal{V}_{ys}^{t-1}) \leq u_{iyst-1} \cdot R_{i}^{Umax} + z_{iyst} \cdot P_{i}^{start}, \forall i \in I^{th}, y \in Y, s \in S, t \in T \setminus \{1\} \tag{C.15}$$

$$p_{iyst-1}(\mathcal{V}_{ys}^{t-1}) - p_{iyst}(\mathcal{V}_{ys}^{t}) \leq u_{iyst-1} \cdot R_{i}^{Dmax}, \forall i \in I^{th}, y \in Y, s \in S, t \in T \setminus \{1\} \tag{C.16}$$

$$p_{iyst}(\mathcal{V}_{ys}^{t}), lns_{yst}(\mathcal{V}_{ys}^{t}) \geq 0, \forall i \in I, y \in Y, s \in S, t \in T \tag{C.17}$$

C.2 Solution methodology

Because of the full immunization constraint and the fact that the uncertain parameters are real-valued, the robust counterpart is semi-infinite, in that it has a finite number of decision variables but an infinite number of constraints. Applying linear decision rules on continuous recourse variables, where the recourse variables $\boldsymbol{R}_{yst}(\mathcal{V}_{ys}^{t}) = \boldsymbol{R}_{yst}^{\boldsymbol{0}} + \sum_{t' \in [t]} \boldsymbol{R}_{ystt'}^{\boldsymbol{L}} \cdot L_{yst'} + \sum_{i' \in I^{res}} \sum_{t' \in [t]} \boldsymbol{R}_{i'ystt'}^{\boldsymbol{C}} \cdot CF_{i'yst'}$, where $[t] \triangleq \{1, ..., t\}$ and $(\boldsymbol{R}_{yst}^{\boldsymbol{0}}, \boldsymbol{R}_{ystt'}^{\boldsymbol{L}}, \boldsymbol{R}_{i'ystt'}^{\boldsymbol{C}})$ are the coefficients of the linear decision rule. Then, in the model with linear decision rules, the constraints can be processed into a finite number of linear constraints, relying on a duality-based reformulation to obtain the final MILP problem. the robust counterpart becomes:

$$\min_{\Omega, \Theta} \sum_{y \in Y} (1 + DR)^{-y} \cdot \sum_{i \in I^{new}} C_{i}^{inv} \cdot P_{i}^{max} \cdot q_{iy} \tag{C.18}$$

$$+ \sum_{y \in Y} (1 + DR)^{-y} \cdot \sum_{s \in S} \cdot \sum_{t \in T} \sum_{i \in I^{th}} \left(C_{i}^{stup} \cdot z_{iyst} \right) \tag{C.19}$$

$$+ \sum_{y \in Y} (1 + DR)^{-y} \cdot \sum_{i \in I} C_{iy}^{fom} \cdot P_{i}^{max} \cdot \sum_{l=1}^{y} q_{il} \tag{C.20}$$

$$+ \sum_{y \in Y} Q_{y} \tag{C.21}$$

s.t. first stage constraints (C.2)-(C.9)

$$\text{s.t.} \quad \forall \mathcal{V}_{ys}^{t} \in \prod_{t' \in [t]} \mathcal{U}_{ys}^{t'}, [t] \triangleq \{1, ..., t\}, \exists p_{iyst}(.) \in \mathbb{R}_{+}, lns_{yst} \in \mathbb{R}_{+}, \forall i \in I, y \in Y, s \in S, t \in T \tag{C.22}$$

$$Q_{y} \geq (1 + DR)^{-y} \cdot \sum_{s \in S} \sum_{t \in T} \left[\sum_{i \in I} C_{iy}^{mrgl} \cdot (p_{iyst}^{0} + \sum_{t' \in [t]} p_{iystt'}^{L} \cdot L_{yst'} + \sum_{i' \in I^{res}} \sum_{t' \in [t]} p_{i'iystt'}^{C} \cdot CF_{i'yst'}) \right.$$

$$\left. + C^{lns} \cdot (lns_{yst}^{0} + \sum_{t' \in [t]} lns_{ystt'}^{L} \cdot L_{yst'} + \sum_{i' \in I^{res}} \sum_{t' \in [t]} lns_{i'ystt'}^{C} \cdot CF_{i'yst'}) \right], \forall y \in Y \tag{C.23}$$

$$\sum_{i\in I}\left(p^0_{iyst}+\sum_{t'\in[t]}p^L_{iystt'}\cdot L_{yst'}+\sum_{i'\in I^{res}}\sum_{t'\in[t]}p^C_{i'iytt'}\cdot CF_{i'yst'}\right)+$$
$$\left(lns^0_{yst}+\sum_{t'\in[t]}lns^L_{ystt'}\cdot L_{yst'}+\sum_{i'\in I^{res}}\sum_{t'\in[t]}lns^C_{i'ystt'}\cdot CF_{i'yst'}\right)=L_{yst},\quad \forall y\in Y,s\in S,t\in T \tag{C.24}$$

$$\left(p^0_{iyst}+\sum_{t'\in[t]}p^L_{iystt'}\cdot L_{yst'}+\sum_{i'\in I^{res}}\sum_{t'\in[t]}p^C_{i'iystt'}\cdot CF_{i'yst'}\right)\leq u_{iyst}\cdot P^{max}_i\cdot(1-\epsilon_i),$$
$$\forall i\in I^{th},y\in Y,s\in S,t\in T \tag{C.25}$$

$$\left(p^0_{iyst}+\sum_{t'\in[t]}p^L_{iystt'}\cdot L_{yst'}+\sum_{i'\in I^{res}}\sum_{t'\in[t]}p^C_{i'iystt'}\cdot CF_{i'yst'}\right)\geq u_{iyst}\cdot P^{min}_i,$$
$$\forall i\in I^{th},y\in Y,s\in S,t\in T \tag{C.26}$$

$$\left(p^0_{iyst}+\sum_{t'\in[t]}p^L_{iystt'}\cdot L_{yst'}+\sum_{i'\in I^{res}}\sum_{t'\in[t]}p^C_{i'iystt'}\cdot CF_{i'yst'}\right)\leq x_{iy}\cdot P^{max}_i\cdot CF_{iyst},$$
$$\forall i\in I^{res},y\in Y,s\in S,t\in T \tag{C.27}$$

$$\left(p^0_{iyst}+\sum_{t'\in[t]}p^L_{iystt'}\cdot L_{yst'}+\sum_{i'\in I^{res}}\sum_{j'\in[j]}p^C_{i'iystt'}\cdot CF_{i'yst'}\right)-\left(p^0_{iyst-1}+\sum_{t'\in[t-1]}p^L_{iyst-1t'}\cdot L_{yst'}\right.$$
$$\left.+\sum_{i'\in I^{res}}\sum_{t'\in[t-1]}p^C_{i'iyst-1t'}\cdot CF_{i'yst'}\right)\leq u_{iyst-1}\cdot R^{Umax}_i+z_{iyst}\cdot P^{start}_i,\quad \forall i\in I^{th},y\in Y,s\in S,t\in T\setminus\{1\} \tag{C.28}$$

$$\left(p^0_{iyst-1}+\sum_{t'\in[t-1]}p^L_{iyst-1t'}\cdot L_{yst'}+\sum_{i'\in I^{res}}\sum_{t'\in[t-1]}p^C_{ii'yst-1t'}\cdot CF_{i'yst'}\right)-\left(p^0_{iyst}+\sum_{t'\in[t]}p^L_{iystt'}\cdot L_{yst'}\right.$$
$$\left.+\sum_{i'\in I^{res}}\sum_{t'\in[t]}p^C_{ii'ystt'}\cdot CF_{i'yst'}\right)\leq u_{iyst-1}\cdot R^{Dmax}_i,\quad \forall i\in I^{th},y\in Y,s\in S,t\in T\setminus\{1\} \tag{C.29}$$

$$\left(p^0_{iyst}+\sum_{t'\in[t]}p^L_{iystt'}\cdot L_{yst'}+\sum_{i'\in I^{res}}\sum_{t'\in[t]}p^C_{ii'ystt'}\cdot CF_{i'yst'}\right)\geq 0,\quad \forall i\in I,y\in Y,s\in S,t\in T \tag{C.30}$$

$$\left(lns^0_{yst}+\sum_{t'\in[t]}lns^L_{ystt'}\cdot L_{yst'}+\sum_{i'\in I^{res}}\sum_{t'\in[t]}lns^C_{i'ystt'}\cdot CF_{i'yst'}\right)\geq 0,\quad \forall y\in Y,s\in S,t\in T \tag{C.31}$$

Re-arranging the terms of the the constraint, given that an uncertainty-affected constraint $\text{LHS}_{ys}\leq \text{RHS}_{ys}$, where LHS contains all uncertainty terms and RHS contains the rest, is valid $\forall \mathcal{V}^t_{ys}\in\mathcal{U}^t_{ys},t\in T$, *if*

and only if $\max_{\mathcal{V}^t_{ys}\in\mathcal{U}^t_{ys},t\in T} \text{LHS}_{ys} \leq \text{RHS}_{ys}$. Notice that any ($\geq$) constraint can easily be transformed to a ($\leq$) one and can follow the same above logic. The model, thus, becomes:

$$\min_{\Omega,\Theta} \sum_{y\in Y}(1+DR)^{-y}\cdot\sum_{i\in I^{new}} C^{inv}_i\cdot P^{max}_i\cdot q_{iy} \tag{C.32}$$

$$+\sum_{y\in Y}(1+DR)^{-y}\cdot\sum_{s\in S}\cdot\sum_{t\in T}\sum_{i\in I^{th}}\left(C^{stup}_i\cdot z_{iyst}\right) \tag{C.33}$$

$$+\sum_{y\in Y}(1+DR)^{-y}\cdot\sum_{i\in I} C^{fom}_{iy}\cdot P^{max}_i\cdot\sum_{l=1}^{y} q_{il} \tag{C.34}$$

$$+\sum_{y\in Y} Q_y \tag{C.35}$$

s.t. first stage constraints (C.2)-(C.9)

$$\text{s.t.}\quad \forall\mathcal{V}^t_{ys}\in\prod_{t'\in[t]}\mathcal{U}^{t'}_{ys},[t]\triangleq\{1,...,t\},\exists p_{iyst}(.)\in\mathbb{R}_+, lns_{yst}\in\mathbb{R}_+,\forall i\in I,y\in Y,s\in S,t\in T \tag{C.36}$$

$$\max_{\substack{\mathcal{V}^t_{ys}\in\mathcal{U}^t_{ys}\\ t\in T}}(1+DR)^{-y}\cdot\sum_{s\in S}\sum_{t\in T}\left[\sum_{t'\in[t]}\left(\sum_{i\in I}p^L_{iystt'}+lns^L_{ystt'}\right)\cdot L_{yst'}+\sum_{t'\in[t]}\sum_{i'\in I^{res}}\left(\sum_{i\in I}p^C_{ii'ystt'}+lns^C_{ystt'}\right)\cdot CF_{i'yst'}\right]$$

$$\leq Q_y-(1+DR)^{-y}\cdot\sum_{s\in S}\sum_{t\in T}\left[\sum_{i\in I}\left(C^{mrgl}_{iy}\cdot p^0_{iyst}\right)+\left(C^{lns}\cdot lns^0_{yst}\right)\right],\quad\forall y\in Y. \tag{C.37}$$

$$\left(\sum_{i\in I}p^0_{iyst}+lns^0_{yst}\right)+\sum_{t'\in[t-1]}\left(\sum_{i\in I}p^L_{iystt'}+lns^L_{ystt'}\right)\cdot L_{yst'}+\left(\sum_{i\in I}p^L_{iystt}+lns^L_{ystt}-1\right)\cdot L_{yst}+$$

$$\sum_{i'\in I^{res}}\sum_{t'\in[t]}\left(\sum_{i\in I}p^C_{ii'ystt'}+lns^C_{ystt'}\right)\cdot CF_{i'yst'}=0,\quad\forall\mathcal{V}^t_{ys}\in\mathcal{U}^t_{ys},y\in Y,s\in S,t\in T \tag{C.38}$$

$$\max_{\mathcal{V}^t_{ys}\in\mathcal{U}^t_{ys}}\sum_{t'\in[t]}\left(p^L_{iystt'}\cdot L_{yst'}\right)+\sum_{i'\in I^{res}}\sum_{t'\in[t]}\left(p^C_{ii'ystt'}\cdot CF_{i'yst'}\right)\leq(1-\epsilon_i)\cdot P^{max}_i\cdot u_{iyst}-p^0_{iyst},$$

$$\forall i\in I^{th},y\in Y,s\in S,t\in T \tag{C.39}$$

$$\min_{\mathcal{V}^t_{ys}\in\mathcal{U}^t_{ys}}\sum_{t'\in[t]}\left(p^L_{iystt'}\cdot L_{yst'}\right)+\sum_{i'\in I^{res}}\sum_{t'\in[t]}\left(p^C_{ii'ystt'}\cdot CF_{i'yst'}\right)\geq u_{iyst}\cdot P^{min}_i-p^0_{iyst},$$

$$\forall i\in I,y\in Y,s\in S,t\in T \tag{C.40}$$

$$\max_{\mathcal{V}^t_{ys}\in\mathcal{U}^t_{ys}}\sum_{t'\in[t]}\left(p^L_{iystt'}\cdot L_{yst'}\right)+\sum_{\substack{\{i'\in I^{res},t'\in[t]:\\ i'\neq i,t'\neq t\}}}\left(p^C_{ii'ystt'}\cdot CF_{i'yst'}\right)+\left(p^C_{iiystt}-\cdot x_{iy}\cdot P^{max}_i\right)\cdot$$

$$CF_{iyst}\leq -p^0_{iyst},\quad\forall i\in I^{res},y\in Y,s\in S,t\in T \tag{C.41}$$

$$\max_{\mathcal{V}^t_{ys}\in\mathcal{U}^t_{ys}} \sum_{t'\in[t-1]} \left(p^L_{iystt'} - p^L_{iyst-1t'}\right)\cdot L_{yst'} + p^L_{iystt}\cdot L_{yst} + \sum_{i'\in I^{res}} \Bigg(\sum_{t'\in[t-1]} \left(p^C_{ii'ystt'} - p^C_{ii'yst-1t'}\right)\cdot CF_{i'yst'}$$
$$+ p^C_{ii'ystt}\cdot CF_{i'yst}\Bigg) \le u_{iyst-1}\cdot R^{Umax}_i + z_{iyst}\cdot P^{start}_i - p^0_{iyst} + p^0_{iyst-1}, \forall i\in I^{th}, y\in Y, s\in S, t\in T\setminus\{1\} \tag{C.42}$$

$$\max_{\mathcal{V}^t_{ys}\in\mathcal{U}^t_{ys}} \sum_{t'\in[t-1]} \left(p^L_{iyst-1t'} - p^L_{iystt'}\right)\cdot L_{yst'} - p^L_{iystt}\cdot L_{yst} + \sum_{i'\in I^{res}} \Bigg(\sum_{t'\in[t-1]} \left(p^C_{ii'yst-1t'} - p^C_{ii'ystt'}\right)\cdot CF_{i'yst'}$$
$$- p^C_{ii'ystt}\cdot CF_{i'yst}\Bigg) \le u_{iyst-1}\cdot R^{Dmax}_i - p^0_{iyst-1} + p^0_{iyst} \quad \forall i\in I^{th}, y\in Y, s\in S, t\in T\setminus\{1\} \tag{C.43}$$

$$\min_{\mathcal{V}^t_{ys}\in\mathcal{U}^t_{ys}} \sum_{t'\in[t]} \left(p^L_{iystt'}\cdot L_{yst'}\right) + \sum_{i'\in I^{res}}\sum_{t'\in[t]} \left(p^C_{ii'ystt'}\cdot CF_{i'yst'}\right) \ge -p^0_{iyst}, \quad \forall i\in I, y\in Y, s\in S, t\in T \tag{C.44}$$

$$\min_{\mathcal{V}^t_{ys}\in\mathcal{U}^t_{ys}} \sum_{t'\in[t]} \left(lns^L_{ystt'}\cdot L_{yst'}\right) + \sum_{i'\in I^{res}}\sum_{t'\in[t]} \left(lns^C_{i'ystt'}\cdot CF_{i'yst'}\right) \ge -lns^0_{yst}, \quad \forall y\in Y, s\in S, t\in T \tag{C.45}$$

C.3 Constraint Processing

Dualizing the left-hand side of the constraint and because of strong duality, this set of non-linear inequalities can be replaced by the set of linear inequalities, where π is the vector of dual variables associated with the bounds of the uncertainty set. Below we illustrate how the semi-infinite robust counterpart is converted into a finite mixed integer linear programming problem.

1. Dualizing constraint (C.37):

$$\max_{\substack{\mathcal{V}^t_{ys}\in\mathcal{U}^t_{ys}\\ t\in T}} (1+DR)^{-y}\cdot \sum_{s\in S}\sum_{t\in T}\left[\sum_{t'\in[t]}\left(\sum_{i\in I} p^L_{iystt'} + lns^L_{ystt'}\right)\cdot L_{yst'} + \sum_{t'\in[t]}\sum_{i'\in I^{res}}\left(\sum_{i\in I} p^C_{ii'ystt'} + lns^C_{ystt'}\right)\cdot CF_{i'yst'}\right]$$
$$\le Q_y - (1+DR)^{-y}\cdot\sum_{s\in S}\sum_{t\in T}\left[\sum_{i\in I}\left(C^{mrgl}_{iy}\cdot p^0_{iyst}\right) + \left(C^{lns}\cdot lns^0_{yst}\right)\right], \quad \forall y\in Y.$$

Becomes the set of equations:

$$\sum_{s\in S}\Bigg[\sum_{t'\in T}(\pi^A_{yst'}\cdot\bar{L}_{yst'} - \pi^B_{yst'}\cdot \underline{L}_{yst'}) + \sum_{t'\in T}\sum_{i'\in I^{res}}(\pi^C_{i'yst'}\cdot\bar{CF}_{i'yst'} - \pi^D_{i'yst'}\cdot\underline{CF}_{i'yst'})$$
$$+ \sum_{t'\in T}\left(\pi^E_{yst'}\cdot\Gamma\cdot(\bar{L}_{yst'} - \sum_{i'\in I^{res}}\underline{CF}_{i'yst'})\right)\Bigg] \le Q_y - (1+DR)^{-y}\cdot\sum_{s\in S}\sum_{t\in T}\left[\sum_{i\in I} C^{mrgl}_{iy}\cdot p^0_{iyst} + C^{lns}\cdot lns^0_{yst}\right],$$
$$\forall y\in Y. \tag{C.46a}$$

$$\pi^A_{yst'} - \pi^B_{yst'} + \pi^E_{yst'} \ge (1+DR)^{-y}\cdot\sum_{t=t'}^{T}\left(\sum_{i\in I} C^{mrgl}_{iy}\cdot p^L_{iystt'} + C^{lns}\cdot lns^L_{ystt'}\right),$$
$$\forall y\in Y, s\in S, t'\in T \tag{C.46b}$$

$$\pi^{C}_{i^{'}yst^{'}} - \pi^{D}_{i^{'}yst^{'}} - \pi^{E}_{yst^{'}} \geq (1+DR)^{-y} \cdot \sum_{t=t^{'}}^{T} \left(\sum_{i \in I} C^{mrgl}_{iy} \cdot p^{C}_{ii^{'}ystt^{'}} + C^{lns} \cdot lns^{C}_{ystt^{'}} \right), \quad \forall i^{'} \in I^{res}, y \in Y, s \in S, t^{'} \in T \tag{C.46c}$$

$$\pi^{A}_{yst^{'}}, \pi^{B}_{yst^{'}}, \pi^{C}_{i^{'}yst^{'}}, \pi^{D}_{i^{'}yst^{'}}, \pi^{E}_{yst^{'}} \geq 0, \quad \forall i^{'} \in I^{res}, y \in Y, s \in S, t^{'} \in T \tag{C.46d}$$

2. Constraint (C.38):

$$\left(\sum_{i \in I} p^{0}_{iyst} + lns^{0}_{yst} \right) + \sum_{t^{'} \in [t-1]} \left(\sum_{i \in I} p^{L}_{iystt^{'}} + lns^{L}_{ystt^{'}} \right) \cdot L_{yst^{'}} + \left(\sum_{i \in I} p^{L}_{iystt} + lns^{L}_{ystt} - 1 \right) \cdot L_{yst} +$$
$$\sum_{i^{'} \in I^{res}} \sum_{t^{'} \in [t]} \left(\sum_{i \in I} p^{C}_{ii^{'}ystt^{'}} + lns^{C}_{ystt^{'}} \right) \cdot CF_{i^{'}yst^{'}} = 0, \quad \forall \mathcal{V}^{t}_{ys} \in \mathcal{U}^{t}_{ys}, y \in Y, s \in S, t \in T$$

Becomes the set of equations:

$$\sum_{i \in I} p^{0}_{iyst} + lns^{0}_{yst} = 0, \quad \forall y \in Y, s \in S, t \in T \tag{C.47a}$$

$$\sum_{i \in I} p^{L}_{iystt^{'}} + lns^{L}_{ystt^{'}} = 0, \quad \forall y \in Y, s \in S, t^{'} \in [t-1], t \in T \tag{C.47b}$$

$$\sum_{i \in I} p^{L}_{iystt^{'}} + lns^{L}_{ystt^{'}} = 1, \quad \forall y \in Y, s \in S, t^{'} = t, t \in T \tag{C.47c}$$

$$\sum_{i \in I} p^{C}_{ii^{'}ystt^{'}} + lns^{C}_{ystt^{'}} = 0, \quad \forall i^{'} \in I^{res}, y \in Y, s \in S, t^{'} \in [t], t \in T \tag{C.47d}$$

3. Constraint (C.39):

$$\max_{\mathcal{V}^{t}_{ys} \in \mathcal{U}^{t}_{ys}} \sum_{t^{'} \in [t]} \left(p^{L}_{iystt^{'}} \cdot L_{yst^{'}} \right) + \sum_{i^{'} \in I^{res}} \sum_{t^{'} \in [t]} \left(p^{C}_{ii^{'}ystt^{'}} \cdot CF_{i^{'}yst^{'}} \right) \leq (1-\epsilon_i) \cdot P^{max}_{i} \cdot u_{iyst} - p^{0}_{iyst},$$
$$\forall i \in I^{th}, y \in Y, s \in S, t \in T$$

Becomes the set of linear inequalities:

$$\sum_{t^{'} \in [t]} (\pi^{A2}_{iystt^{'}} \cdot \bar{L}_{yst^{'}} - \pi^{B2}_{iystt^{'}} \cdot \underline{L}_{yst^{'}}) + \sum_{i^{'} \in I^{res}, t^{'} \in [t]} (\pi^{C2}_{ii^{'}ystt^{'}} \cdot \bar{CF}_{i^{'}yst^{'}} - \pi^{D2}_{ii^{'}ystt^{'}} \cdot \underline{CF}_{i^{'}yst^{'}})$$
$$+ \sum_{t^{'} \in [t]} \pi^{E2}_{iystt^{'}} \cdot \Gamma \cdot (\bar{L}_{yst^{'}} - \sum_{i^{'} \in I^{res}} \underline{CF}_{i^{'}yst^{'}}) \leq (1-\epsilon_i) \cdot P^{max}_{i} \cdot u_{iyst} - p^{0}_{iyst},$$
$$\forall i \in I^{th}, y \in Y, s \in S, t \in T \tag{C.48a}$$

$$\pi^{A2}_{iystt^{'}} - \pi^{B2}_{iystt^{'}} + \pi^{E2}_{iystt^{'}} \geq p^{L}_{iystt^{'}}, \quad \forall i \in I^{th}, y \in Y, s \in S, t^{'} \in [t], t \in T \tag{C.48b}$$

$$\pi^{C2}_{ii'ystt'} - \pi^{D2}_{ii'ystt'} - \pi^{E2}_{iystt'} \geq p^{C}_{ii'ystt'}, \quad \forall i^{'} \in I^{res}, i \in I^{th}, y \in Y, s \in S, t^{'} \in [t], t \in T \tag{C.48c}$$

$$\pi^{A2}_{iystt'}, \pi^{B2}_{iystt'}, \pi^{C2}_{ii'ystt'}, \pi^{D2}_{ii'ystt'}, \pi^{E2}_{iystt'} \geq 0, \quad \forall i^{'} \in I^{res}, y \in Y, s \in S, t^{'} \in [t], t \in T \tag{C.48d}$$

4. Constraint (C.40):

$$\min_{\mathcal{V}^t_{ys} \in \mathcal{U}^t_{ys}} \sum_{t' \in [t]} \left(p^{L}_{iystt'} \cdot L_{yst'} \right) + \sum_{i' \in I^{res}} \sum_{t' \in [t]} \left(p^{C}_{ii'ystt'} \cdot CF_{i'yst'} \right) \geq u_{iyst} \cdot P^{min}_{i} - p^{0}_{iyst},$$
$$\forall i \in I, y \in Y, s \in S, t \in T$$

Can be written as:

$$\max_{\mathcal{V}^t_{ys} \in \mathcal{U}^t_{ys}} \sum_{t' \in [t]} \left(-p^{L}_{iystt'} \cdot L_{yst'} \right) + \sum_{i' \in I^{res}} \sum_{t' \in [t]} \left(-p^{C}_{ii'ystt'} \cdot CF_{i'yst'} \right) \leq p^{0}_{iyst} - u_{iyst} \cdot P^{min}_{i},$$
$$\forall i \in I, y \in Y, s \in S, t \in T \tag{C.49a}$$

and becomes the set of linear inequalities:

$$\sum_{t' \in [t]} (\pi^{A3}_{iystt'} \cdot \bar{L}_{yst'} - \pi^{B3}_{iystt'} \cdot \underline{L}_{yst'}) + \sum_{i' \in I^{res}} \sum_{t' \in [t]} (\pi^{C3}_{ii'ystt'} \cdot \bar{CF}_{i'yst'} - \pi^{D3}_{ii'ystt'} \cdot \underline{CF}_{i'yst'})$$
$$+ \sum_{t' \in [t]} \pi^{E3}_{iystt'} \cdot \Gamma \cdot (\bar{L}_{yst'} - \sum_{i' \in I^{res}} \underline{CF}_{i'yst'}) \leq p^{0}_{iyst} - u_{iyst} \cdot P^{min}_{i}, \quad \forall i \in I, y \in Y, s \in S, t \in T \tag{C.49b}$$

$$\pi^{A3}_{iystt'} - \pi^{B3}_{iystt'} + \pi^{E3}_{iystt'} \geq -p^{L}_{iystt'}, \quad \forall i \in I, y \in Y, s \in S, t \in T, t^{'} \in [t] \tag{C.49c}$$

$$\pi^{C3}_{ii'ystt'} - \pi^{D3}_{ii'ystt'} - \pi^{E3}_{iystt'} \geq -p^{C}_{ii'ystt'}, \quad \forall i \in I, i^{'} \in I^{res}, y \in Y, s \in S, t \in T, t^{'} \in [t] \tag{C.49d}$$

$$\pi^{A3}_{iystt'}, \pi^{B3}_{iystt'}, \pi^{C3}_{ii'ystt'}, \pi^{D3}_{ii'ystt'}, \pi^{E3}_{iystt'} \geq 0, \quad \forall i \in I, i^{'} \in I^{res}, y \in Y, s \in S, t \in T, t^{'} \in [t] \tag{C.49e}$$

5. Constraint (C.41):

$$\max_{\mathcal{V}^t_{ys} \in \mathcal{U}^t_{ys}} \sum_{t' \in [t]} \left(p^{L}_{iystt'} \cdot L_{yst'} \right) + \sum_{\substack{\{i^{'} \in I^{res}, t^{'} \in [t]: \\ i^{'} \neq i, t^{'} \neq t\}}} \left(p^{C}_{ii'ystt'} \cdot CF_{i'yst'} \right) + \left(p^{C}_{iiystt} - \cdot x_{iy} \cdot P^{max}_{i} \right) \cdot$$
$$CF_{iyst} \leq -p^{0}_{iyst}, \quad \forall i \in I^{res}, y \in Y, s \in S, t \in T$$

Becomes the set of equations:

$$\sum_{t' \in [t]} (\pi^{A4}_{iystt'} \cdot \bar{L}_{yst'} - \pi^{B4}_{iystt'} \cdot \underline{L}_{yst'}) + \sum_{i' \in I^{res}, t' \in [t]} (\pi^{C4}_{ii'ystt'} \cdot \bar{CF}_{i'yst'} - \pi^{D4}_{ii'ystt'} \cdot \underline{CF}_{i'yst'})$$
$$+ \sum_{t' \in [t]} \pi^{E4}_{iystt'} \cdot \Gamma \cdot (\bar{L}_{yst'} - \sum_{i' \in I^{res}} \underline{CF}_{i'yst'}) \leq -p^{0}_{iyst}, \quad \forall i \in I^{th}, y \in Y, s \in S, t \in T \tag{C.50a}$$

$$\pi^{A4}_{iystt'} - \pi^{B4}_{iystt'} + \pi^{E4}_{iystt'} \geq p^{L}_{iystt'}, \quad \forall i \in I^{th}, y \in Y, s \in S, t^{'} \in [t], t \in T \tag{C.50b}$$

$$\pi^{C4}_{ii'ystt'} - \pi^{D4}_{ii'ystt'} - \pi^{E4}_{iystt'} \geq p^{C}_{ii'ystt'}, \quad \forall\{i^{'} \in I^{res}, j^{'} \in [j] : i^{'} \neq i, j^{'} \neq j\}, i \in I^{res}, j \in J, y \in Y \quad \text{(C.50c)}$$

$$\pi^{C4}_{ii'ystt'} - \pi^{D4}_{ii'ystt'} - \pi^{E4}_{iystt'} \geq p^{C}_{ii'ystt'} - x_{i,y} \cdot P^{max}_{i}, \quad \forall i \in I^{res}, j \in J, y \in Y, i^{'} = i, j^{'} = j \quad \text{(C.50d)}$$

$$\pi^{A4}_{iystt'}, \pi^{B4}_{iystt'}, \pi^{C4}_{ii'ystt'}, \pi^{D4}_{ii'ystt'}, \pi^{E4}_{iystt'} \geq 0, \quad \forall i^{'} \in I^{res}, y \in Y, s \in S, t^{'} \in [t], t \in T \quad \text{(C.50e)}$$

6. Constraint (C.42):

$$\max_{\mathcal{V}^{t}_{ys} \in \mathcal{U}^{t}_{ys}} \sum_{t^{'} \in [t-1]} \left(p^{L}_{iystt'} - p^{L}_{iyst-1t'} \right) \cdot L_{yst'} + p^{L}_{iystt} \cdot L_{yst} + \sum_{i^{'} \in I^{res}} \left(\sum_{t^{'} \in [t-1]} \left(p^{C}_{ii'ystt'} - p^{C}_{ii'yst-1t'} \right) \cdot CF_{i'yst'} \right.$$
$$\left. + p^{C}_{ii'ystt} \cdot CF_{i'yst} \right) \leq u_{iyst-1} \cdot R^{Umax}_{i} + z_{iyst} \cdot P^{start}_{i} - p^{0}_{iyst} + p^{0}_{iyst-1},$$
$$\forall i \in I^{th}, y \in Y, s \in S, t \in T \setminus \{1\}$$

Becomes the set of inequalities:

$$\sum_{t^{'} \in [t]} (\pi^{A5}_{iystt'} \cdot \bar{L}_{yst'} - \pi^{B5}_{iystt'} \cdot \underline{L}_{yst'}) + \sum_{i^{'} \in I^{res}} \sum_{t^{'} \in [t]} (\pi^{C5}_{ii'ystt'} \cdot \bar{CF}_{i'yst'} - \pi^{D5}_{ii'ystt'} \cdot \underline{CF}_{i'yst'})$$
$$+ \sum_{t^{'} \in [t]} \pi^{E5}_{iystt'} \cdot \Gamma \cdot (\bar{L}_{yst'} - \sum_{i^{'} \in I^{res}} \underline{CF}_{i'yst'}) \leq u_{iyst-1} \cdot R^{Umax}_{i} + z_{iyst} \cdot P^{start}_{i} - p^{0}_{iyst} + p^{0}_{iyst-1},$$
$$\forall i \in I^{th}, y \in Y, s \in S, t \in T \setminus \{1\} \quad \text{(C.51a)}$$

$$\pi^{A5}_{iystt'} - \pi^{B5}_{iystt'} + \pi^{E5}_{iystt'} \geq p^{L}_{iystt'} - p^{L}_{iyst-1t'}, \quad \forall i \in I^{th}, y \in Y, s \in S, t^{'} \in [t-1], t \in T \setminus \{1\} \quad \text{(C.51b)}$$

$$\pi^{A5}_{iystt'} - \pi^{B5}_{iystt'} + \pi^{E5}_{iystt'} \geq p^{L}_{iystt'}, \quad \forall i \in I^{th}, y \in Y, s \in S, t^{'} = t, t \in T \setminus \{1\} \quad \text{(C.51c)}$$

$$\pi^{C5}_{ii'ystt'} - \pi^{D5}_{ii'ystt'} - \pi^{E5}_{iystt'} \geq p^{C}_{ii'ystt'} - p^{C}_{ii'yst-1t'}, \quad \forall i \in I^{th}, i^{'} \in I^{res}, y \in Y,$$
$$s \in S, t^{'} \in [t-1], t \in T \setminus \{1\} \quad \text{(C.51d)}$$

$$\pi^{C5}_{ii'ystt'} - \pi^{D5}_{ii'ystt'} - \pi^{E5}_{iystt'} \geq p^{C}_{ii'ystt'}, \quad \forall i \in I^{th}, i^{'} \in I^{res}, y \in Y, s \in S, t^{'} = t, t \in T \setminus \{1\} \quad \text{(C.51e)}$$

$$\pi^{A5}_{iystt'}, \pi^{B5}_{iystt'}, \pi^{C5}_{ii'ystt'}, \pi^{D5}_{ii'ystt'}, \pi^{E5}_{iystt'} \geq 0, \quad \forall i^{'} \in I^{res}, y \in Y, s \in S, t^{'} \in [t], t \in T \quad \text{(C.51f)}$$

7. Constraint (C.43):

$$\max_{\mathcal{V}^{t}_{ys} \in \mathcal{U}^{t}_{ys}} \sum_{t^{'} \in [t-1]} \left(p^{L}_{iyst-1t'} - p^{L}_{iystt'} \right) \cdot L_{yst'} - p^{L}_{iystt} \cdot L_{yst} + \sum_{i^{'} \in I^{res}} \left(\sum_{t^{'} \in [t-1]} \left(p^{C}_{ii'yst-1t'} - p^{C}_{ii'ystt'} \right) \cdot CF_{i'yst'} \right.$$
$$\left. - p^{C}_{ii'ystt} \cdot CF_{i'yst} \right) \leq u_{iyst-1} \cdot R^{Dmax}_{i} - p^{0}_{iyst-1} + p^{0}_{iyst} \quad \forall i \in I^{th}, y \in Y, s \in S, t \in T \setminus \{1\}$$

Becomes the set of inequalities:

$$\sum_{t^{'}\in[t]}(\pi^{A6}_{iystt^{'}}\cdot\bar{L}_{yst^{'}}-\pi^{B6}_{iystt^{'}}\cdot\underline{L}_{yst^{'}})+\sum_{i^{'}\in I^{res}}\sum_{t^{'}\in[t]}(\pi^{C6}_{ii^{'}ystt^{'}}\cdot\bar{CF}_{i^{'}yst^{'}}-\pi^{D6}_{ii^{'}ystt^{'}}\cdot\underline{CF}_{i^{'}yst^{'}})$$
$$+\sum_{t^{'}\in[t]}\pi^{E6}_{iystt^{'}}\cdot\Gamma\cdot(\bar{L}_{yst^{'}}-\sum_{i^{'}\in I^{res}}\underline{CF}_{i^{'}yst^{'}})\leq u_{iyst-1}\cdot R^{Dmax}_{i}-p^{0}_{iyst-1}+p^{0}_{iyst},$$
$$\forall i\in I^{th},y\in Y,s\in S,t\in T\setminus\{1\} \tag{C.52a}$$

$$\pi^{A6}_{iystt^{'}}-\pi^{B6}_{iystt^{'}}+\pi^{E6}_{iystt^{'}}\geq p^{L}_{iyst-1t^{'}}-p^{L}_{iystt^{'}},\quad \forall i\in I^{th},y\in Y,s\in S,t^{'}\in[t-1],t\in T\setminus\{1\} \tag{C.52b}$$

$$\pi^{A6}_{iystt^{'}}-\pi^{B6}_{iystt^{'}}+\pi^{E6}_{iystt^{'}}\geq -p^{L}_{iystt^{'}},\quad \forall i\in I^{th},y\in Y,s\in S,t^{'}=t,t\in T\setminus\{1\} \tag{C.52c}$$

$$\pi^{C6}_{ii^{'}ystt^{'}}-\pi^{D6}_{ii^{'}ystt^{'}}-\pi^{E6}_{iystt^{'}}\geq p^{C}_{ii^{'}yst-1t^{'}}-p^{C}_{ii^{'}ystt^{'}},\forall i\in I^{th},i^{'}\in I^{res},y\in Y,$$
$$s\in S,t^{'}\in[t-1],t\in T\setminus\{1\} \tag{C.52d}$$

$$\pi^{C6}_{ii^{'}ystt^{'}}-\pi^{D6}_{ii^{'}ystt^{'}}-\pi^{E6}_{iystt^{'}}\geq -p^{C}_{ii^{'}ystt^{'}},\quad \forall i\in I^{th},i^{'}\in I^{res},y\in Y,s\in S,t^{'}=t,t\in T\setminus\{1\} \tag{C.52e}$$

$$\pi^{A6}_{iystt^{'}},\pi^{B6}_{iystt^{'}},\pi^{C6}_{ii^{'}ystt^{'}},\pi^{D6}_{ii^{'}ystt^{'}},\pi^{E6}_{iystt^{'}}\geq 0,\qquad \forall i^{'}\in I^{res},y\in Y,s\in S,t^{'}\in[t],t\in T \tag{C.52f}$$

8. Constraint (C.44):

$$\min_{\mathcal{V}^{t}_{ys}\in\mathcal{U}^{t}_{ys}}\sum_{t^{'}\in[t]}\left(p^{L}_{iystt^{'}}\cdot L_{yst^{'}}\right)+\sum_{i^{'}\in I^{res}}\sum_{t^{'}\in[t]}\left(p^{C}_{ii^{'}ystt^{'}}\cdot CF_{i^{'}yst^{'}}\right)\geq -p^{0}_{iyst},$$
$$\forall i\in I,y\in Y,s\in S,t\in T$$

Can be written as:

$$\max_{\mathcal{V}^{t}_{ys}\in\mathcal{U}^{t}_{ys}}\sum_{t^{'}\in[t]}\left(-p^{L}_{iystt^{'}}\cdot L_{yst^{'}}\right)+\sum_{i^{'}\in I^{res}}\sum_{t^{'}\in[t]}\left(-p^{C}_{ii^{'}ystt^{'}}\cdot CF_{i^{'}yst^{'}}\right)\leq p^{0}_{iyst},$$
$$\forall i\in I,y\in Y,s\in S,t\in T \tag{C.53a}$$

and becomes the set of linear inequalities:

$$\sum_{t^{'}\in[t]}(\pi^{A7}_{iystt^{'}}\cdot\bar{L}_{yst^{'}}-\pi^{B7}_{iystt^{'}}\cdot\underline{L}_{yst^{'}})+\sum_{i^{'}\in I^{res}}\sum_{t^{'}\in[t]}(\pi^{C7}_{ii^{'}ystt^{'}}\cdot\bar{CF}_{i^{'}yst^{'}}-\pi^{D7}_{ii^{'}ystt^{'}}\cdot\underline{CF}_{i^{'}yst^{'}})$$
$$+\sum_{t^{'}\in[t]}\pi^{E7}_{iystt^{'}}\cdot\Gamma\cdot(\bar{L}_{yst^{'}}-\sum_{i^{'}\in I^{res}}\underline{CF}_{i^{'}yst^{'}})\leq p^{0}_{iyst},\qquad \forall i\in I,y\in Y,s\in S,t\in T \tag{C.53b}$$

$$\pi^{A7}_{iystt^{'}}-\pi^{B7}_{iystt^{'}}+\pi^{E7}_{iystt^{'}}\geq -p^{L}_{iystt^{'}},\quad \forall i\in I,y\in Y,s\in S,t\in T,t^{'}\in[t] \tag{C.53c}$$

$$\pi^{C7}_{ii^{'}ystt^{'}}-\pi^{D7}_{ii^{'}ystt^{'}}-\pi^{E7}_{iystt^{'}}\geq -p^{C}_{ii^{'}ystt^{'}},\quad \forall i\in I,i^{'}\in I^{res},y\in Y,s\in S,t\in T,t^{'}\in[t] \tag{C.53d}$$

$$\pi^{A7}_{iystt'}, \pi^{B7}_{iystt'}, \pi^{C7}_{ii'ystt'}, \pi^{D7}_{ii'ystt'}, \pi^{E7}_{iystt'} \geq 0, \qquad \forall i \in I, i^{'} \in I^{res}, y \in Y, s \in S, t \in T, t^{'} \in [t] \tag{C.53e}$$

9. Constraint (C.45):

$$\min_{\mathcal{V}^t_{ys} \in \mathcal{U}^t_{ys}} \sum_{t' \in [t]} \left(lns^L_{ystt'} \cdot L_{yst'} \right) + \sum_{i' \in I^{res}} \sum_{t' \in [t]} \left(lns^C_{i'ystt'} \cdot CF_{i'yst'} \right) \geq -lns^0_{yst},$$
$$\forall y \in Y, s \in S, t \in T$$

Can be written as:

$$\max_{\mathcal{V}^t_{ys} \in \mathcal{U}^t_{ys}} \sum_{t' \in [t]} \left(-lns^L_{ystt'} \cdot L_{yst'} \right) + \sum_{i' \in I^{res}} \sum_{t' \in [t]} \left(-lns^C_{i'ystt'} \cdot CF_{i'yst'} \right) \leq lns^0_{yst},$$
$$\forall y \in Y, s \in S, t \in T \tag{C.54a}$$

and becomes the set of linear inequalities:

$$\sum_{t' \in [t]} (\pi^{A8}_{ystt'} \cdot \bar{L}_{yst'} - \pi^{B8}_{ystt'} \cdot \underline{L}_{yst'}) + \sum_{i' \in I^{res}} \sum_{t' \in [t]} (\pi^{C8}_{i'ystt'} \cdot \bar{CF}_{i'yst'} - \pi^{D8}_{i'ystt'} \cdot \underline{CF}_{i'yst'})$$
$$+ \sum_{t' \in [t]} \pi^{E8}_{ystt'} \cdot \Gamma \cdot (\bar{L}_{yst'} - \sum_{i' \in I^{res}} \underline{CF}_{i'yst'}) \leq lns^0_{yst}, \qquad \forall y \in Y, s \in S, t \in T \tag{C.54b}$$

$$\pi^{A8}_{ystt'} - \pi^{B8}_{ystt'} + \pi^{E8}_{ystt'} \geq -lns^L_{ystt'}, \quad \forall y \in Y, s \in S, t \in T, t^{'} \in [t] \tag{C.54c}$$

$$\pi^{C8}_{i'ystt'} - \pi^{D8}_{i'ystt'} - \pi^{E8}_{ystt'} \geq -lns^C_{i'ystt'}, \quad \forall i^{'} \in I^{res}, y \in Y, s \in S, t \in T, t^{'} \in [t] \tag{C.54d}$$

$$\pi^{A8}_{ystt'}, \pi^{B8}_{ystt'}, \pi^{C8}_{i'ystt'}, \pi^{D8}_{i'ystt'}, \pi^{E8}_{ystt'} \geq 0, \qquad \forall i^{'} \in I^{res}, y \in Y, s \in S, t \in T, t^{'} \in [t] \tag{C.54e}$$

Bibliography

[1] Myles R Allen, Vicente R Barros, John Broome, Wolfgang Cramer, Renate Christ, John A Church, Leon Clarke, Qin Dahe, Purnamita Dasgupta, Navroz K Dubash, et al. "IPCC fifth assessment synthesis report-climate change 2014 synthesis report". In: (2014).

[2] IEA. *Global Energy and CO2 Status Report. Allrights reserved*. 2018.

[3] Jennifer Cronin, Gabrial Anandarajah, and Olivier Dessens. "Climate change impacts on the energy system: a review of trends and gaps". In: *Climatic Change* 151.2 (2018), pp. 79–93.

[4] IEA. *Making the energy sector more resilient to climate change. Allrights reserved*. 2015.

[5] Cambridge Institute for Sustainability Leadership. *Climate Change:Implications for the Energy Sector*. 2014.

[6] Reza Hemmati, Rahmat-Allah Hooshmand, and Amin Khodabakhshian. "Comprehensive review of generation and transmission expansion planning". In: *IET Generation, Transmission & Distribution* 7.9 (2013), pp. 955–964.

[7] Pierre Masse and Robert Gibrat. "Application of linear programming to investments in the electric power industry". In: *Management Science* 3.2 (1957), pp. 149–166.

[8] Grigorios A Bakirtzis, Pandelis N Biskas, and Vasilis Chatziathanasiou. "Generation expansion planning by MILP considering mid-term scheduling decisions". In: *Electric Power Systems Research* 86 (2012), pp. 98–112.

[9] Nikolaos E Koltsaklis and Michael C Georgiadis. "A multi-period, multi-regional generation expansion planning model incorporating unit commitment constraints". In: *Applied Energy* 158 (2015), pp. 310–331.

[10] Reza Hemmati, Rahmat-Allah Hooshmand, and Amin Khodabakhshian. "Reliability constrained generation expansion planning with consideration of wind farms uncertainties in deregulated electricity market". In: *Energy Conversion and Management* 76 (2013), pp. 517–526.

[11] Shahab Dehghan, Nima Amjady, and Antonio J Conejo. "Reliability-constrained robust power system expansion planning". In: *IEEE Transactions on Power Systems* 31.3 (2016), pp. 2383–2392.

[12] Xie Min, Chen Jinfu, and Duan Xian Zhong. "Generator maintenance scheduling in the generation expansion planning of interconnected power system". In: *Transmission and Distribution Conference and Exhibition 2002: Asia Pacific. IEEE/PES*. Vol. 3. IEEE. 2002, pp. 1601–1605.

[13] Adelino JC Pereira and João Tomé Saraiva. "A decision support system for generation expansion planning in competitive electricity markets". In: *Electric power systems research* 80.7 (2010), pp. 778–787.

[14] Adelino JC Pereira and João Tomé Saraiva. "Generation expansion planning (GEP)–A long-term approach using system dynamics and genetic algorithms (GAs)". In: *Energy* 36.8 (2011), pp. 5180–5199.

[15] Adelino JC Pereira and João Tomé Saraiva. "A long term generation expansion planning model using system dynamics–Case study using data from the Portuguese/Spanish generation system". In: *Electric Power Systems Research* 97 (2013), pp. 41–50.

[16] Jiraporn Sirikum, Anulark Techanitisawad, and Voratas Kachitvichyanukul. "A new efficient GA-benders' decomposition method: For power generation expansion planning with emission controls". In: *IEEE Transactions on Power Systems* 22.3 (2007), pp. 1092–1100.

[17] Zhigang Lu, Jintao Qi, Bo Wen, and Xueping Li. "A dynamic model for generation expansion planning based on Conditional Value-at-Risk theory under Low-Carbon Economy". In: *Electric Power Systems Research* 141 (2016), pp. 363–371.

[18] J Aghaei, MA Akbari, A Roosta, M Gitizadeh, and T Niknam. "Integrated renewable–conventional generation expansion planning using multiobjective framework". In: *IET generation, transmission & distribution* 6.8 (2012), pp. 773–784.

[19] Yiduo Zhan, Qipeng P Zheng, Jianhui Wang, and Pierre Pinson. "Generation Expansion Planning with Large Amounts of Wind Power via Decision-Dependent Stochastic Programming". In: *IEEE Transactions on Power Systems* (2016).

[20] K Rajesh, A Bhuvanesh, S Kannan, and C Thangaraj. "Least cost generation expansion planning with solar power plant using Differential Evolution algorithm". In: *Renewable Energy* 85 (2016), pp. 677–686.

[21] K Rajesh, S Kannan, and C Thangaraj. "Least cost generation expansion planning with wind power plant incorporating emission using Differential Evolution algorithm". In: *International Journal of Electrical Power & Energy Systems* 80 (2016), pp. 275–286.

[22] Esteban Gil, Ignacio Aravena, and Raúl Cárdenas. "Generation capacity expansion planning under hydro uncertainty using stochastic mixed integer programming and scenario reduction". In: *IEEE Transactions on Power Systems* 30.4 (2015), pp. 1838–1847.

[23] Hatice Tekiner-Mogulkoc, David W Coit, and Frank A Felder. "Mean-risk stochastic electricity generation expansion planning problems with demand uncertainties considering conditional-value-at-risk and maximum regret as risk measures". In: *International Journal of Electrical Power & Energy Systems* 73 (2015), pp. 309–317.

[24] Heejung Park and Ross Baldick. "Stochastic generation capacity expansion planning reducing greenhouse gas emissions". In: *IEEE Transactions on Power Systems* 30.2 (2015), pp. 1026–1034.

[25] Shuya Li, David W Coit, and Frank Felder. "Stochastic optimization for electric power generation expansion planning with discrete climate change scenarios". In: *Electric Power Systems Research* 140 (2016), pp. 401–412.

[26] A Ghaderi, M Parsa Moghaddam, and MK Sheikh-El-Eslami. "Energy efficiency resource modeling in generation expansion planning". In: *Energy* 68 (2014), pp. 529–537.

[27] Andrew Satchwell and Ryan Hledik. "Analytical frameworks to incorporate demand response in long-term resource planning". In: *Utilities Policy* 28 (2014), pp. 73–81.

[28] Hatice Tekiner-Mogulkoc, David W Coit, and Frank A Felder. "Electric power system generation expansion plans considering the impact of Smart Grid technologies". In: *International Journal of Electrical Power & Energy Systems* 42.1 (2012), pp. 229–239.

[29] Francesco Careri, Camillo Genesi, Paolo Marannino, Mario Montagna, Stefano Rossi, and Ilaria Siviero. "Generation expansion planning in the age of green economy". In: *IEEE Transactions on Power Systems* 26.4 (2011), pp. 2214–2223.

[30] Argyris G Kagiannas, Dimitris Th Askounis, and John Psarras. "Power generation planning: a survey from monopoly to competition". In: *International journal of electrical power & energy systems* 26.6 (2004), pp. 413–421.

[31] Reza Hemmati, Rahmat-Allah Hooshmand, and Amin Khodabakhshian. "Comprehensive review of generation and transmission expansion planning". In: *IET Generation, Transmission & Distribution* 7.9 (2013), pp. 955–964.

[32] Hadi Sadeghi, Masoud Rashidinejad, and Amir Abdollahi. "A comprehensive sequential review study through the generation expansion planning". In: *Renewable and Sustainable Energy Reviews* 67 (2017), pp. 1369–1394.

[33] John Kabouris and FD Kanellos. "Impacts of large-scale wind penetration on designing and operation of electric power systems". In: *IEEE Transactions on Sustainable Energy* 1.2 (2010), pp. 107–114.

[34] Bart C Ummels, Madeleine Gibescu, Engbert Pelgrum, Wil L Kling, and Arno J Brand. "Impacts of wind power on thermal generation unit commitment and dispatch". In: *IEEE Transactions on energy conversion* 22.1 (2007), pp. 44–51.

[35] J Charles Smith, Michael R Milligan, Edgar A DeMeo, and Brian Parsons. "Utility wind integration and operating impact state of the art". In: *IEEE transactions on power systems* 22.3 (2007), pp. 900–908.

[36] Matthias Huber, Desislava Dimkova, and Thomas Hamacher. "Integration of wind and solar power in Europe: Assessment of flexibility requirements". In: *Energy* 69 (2014), pp. 236–246.

[37] Michaelangelo D Tabone, Christoph Goebel, and Duncan S Callaway. "The effect of PV siting on power system flexibility needs". In: *Solar Energy* 139 (2016), pp. 776–786.

[38] Germán Morales-España, Jesus M Latorre, and Andres Ramos. "Tight and compact MILP formulation for the thermal unit commitment problem". In: *IEEE Transactions on Power Systems* 28.4 (2013), pp. 4897–4908.

[39] Narayana Prasad Padhy. "Unit commitment-a bibliographical survey". In: *IEEE Transactions on power systems* 19.2 (2004), pp. 1196–1205.

[40] Aidan Tuohy, Peter Meibom, Eleanor Denny, and Mark O'Malley. "Unit commitment for systems with significant wind penetration". In: *IEEE Transactions on Power Systems* 24.2 (2009), pp. 592–601.

[41] Rui Cheng, Zhaofeng Xu, Pei Liu, Zhe Wang, Zheng Li, and Ian Jones. "A multi-region optimization planning model for China's power sector". In: *Applied Energy* 137 (2015), pp. 413–426.

[42] Nikolaos E Koltsaklis, Athanasios S Dagoumas, Georgios M Kopanos, Efstratios N Pistikopoulos, and Michael C Georgiadis. "A spatial multi-period long-term energy planning model: a case study of the Greek power system". In: *Applied Energy* 115 (2014), pp. 456–482.

[43] Christian Barteczko-Hibbert, Ioannis Bonis, Michael Binns, Constantinos Theodoropoulos, and Adisa Azapagic. "A multi-period mixed-integer linear optimisation of future electricity supply considering life cycle costs and environmental impacts". In: *Applied Energy* 133 (2014), pp. 317–334.

[44] Daniel S Kirschen, Juan Ma, Vera Silva, and Régine Belhomme. "Optimizing the flexibility of a portfolio of generating plants to deal with wind generation". In: *Power and Energy Society General Meeting, 2011 IEEE*. IEEE. 2011, pp. 1–7.

[45] Nikolaos E Koltsaklis and Michael C Georgiadis. "A multi-period, multi-regional generation expansion planning model incorporating unit commitment constraints". In: *Applied Energy* 158 (2015), pp. 310–331.

[46] Angela Flores-Quiroz, Rodrigo Palma-Behnke, Golbon Zakeri, and Rodrigo Moreno. "A column generation approach for solving generation expansion planning problems with high renewable energy penetration". In: *Electric Power Systems Research* 136 (2016), pp. 232–241.

[47] JP Deane, Alessandro Chiodi, Maurizio Gargiulo, and Brian P Ó Gallachóir. "Soft-linking of a power systems model to an energy systems model". In: *Energy* 42.1 (2012), pp. 303–312.

[48] Peerapat Vithayasrichareon, T Lozanov, J Riesz, and I MacGill. "Impact of operational constraints on generation portfolio planning with renewables". In: *Power & Energy Society General Meeting, 2015 IEEE*. IEEE. 2015, pp. 1–5.

[49] Andreas Belderbos and Erik Delarue. "Accounting for flexibility in power system planning with renewables". In: *International Journal of Electrical Power & Energy Systems* 71 (2015), pp. 33–41.

[50] Bryan S Palmintier and Mort D Webster. "Impact of operational flexibility on electricity generation planning with renewable and carbon targets". In: *IEEE Transactions on Sustainable Energy* 7.2 (2016), pp. 672–684.

[51] Sérgio Pereira, Paula Ferreira, and AIF Vaz. "Generation expansion planning with high share of renewables of variable output". In: *Applied Energy* 190 (2017), pp. 1275–1288.

[52] Juan Ma, Vera Silva, Régine Belhomme, Daniel S Kirschen, and Luis F Ochoa. "Evaluating and planning flexibility in sustainable power systems". In: *Power and Energy Society General Meeting (PES), 2013 IEEE*. IEEE. 2013, pp. 1–11.

[53] Eamonn Lannoye, Damian Flynn, and Mark O'Malley. "Evaluation of power system flexibility". In: *IEEE Transactions on Power Systems* 27.2 (2012), pp. 922–931.

[54] Andreas Ulbig and Göran Andersson. "Analyzing operational flexibility of electric power systems". In: *International Journal of Electrical Power & Energy Systems* 72 (2015), pp. 155–164.

[55] Juan Ma, Vera Silva, Régine Belhomme, Daniel S Kirschen, and Luis F Ochoa. "Exploring the use of flexibility indices in low carbon power systems". In: *2012 3rd IEEE PES Innovative Smart Grid Technologies Europe (ISGT Europe)*. IEEE. 2012, pp. 1–5.

[56] Jinye Zhao, Tongxin Zheng, and Eugene Litvinov. "A unified framework for defining and measuring flexibility in power system". In: *IEEE Transactions on Power Systems* 31.1 (2016), pp. 339–347.

[57] Yiping Fang and Giovanni Sansavini. "Optimizing power system investments and resilience against attacks". In: *Reliability Engineering & System Safety* 159 (2017), pp. 161–173.

[58] Gerald A Meehl and Claudia Tebaldi. "More intense, more frequent, and longer lasting heat waves in the 21st century". In: *Science* 305.5686 (2004), pp. 994–997.

[59] Selma B Guerreiro, Richard J Dawson, Chris Kilsby, Elizabeth Lewis, and Alistair Ford. "Future heat-waves, droughts and floods in 571 European cities". In: *Environmental Research Letters* 13.3 (2018), p. 034009.

[60] Marc Poumadere, Claire Mays, Sophie Le Mer, and Russell Blong. "The 2003 heat wave in France: dangerous climate change here and now". In: *Risk Analysis: an International Journal* 25.6 (2005), pp. 1483–1494.

[61] Roberto Rocchetta, Yanfu Li, and Enrico Zio. "Risk assessment and risk-cost optimization of distributed power generation systems considering extreme weather conditions". In: *Reliability Engineering & System Safety* 136 (2015), pp. 47–61.

[62] Mathaios Panteli, Cassandra Pickering, Sean Wilkinson, Richard Dawson, and Pierluigi Mancarella. "Power system resilience to extreme weather: Fragility modelling, probabilistic impact assessment, and adaptation measures". In: *IEEE Trans. Power Syst* 32 (2017), pp. 3747–3757.

[63] Francesco Cadini, Gian Luca Agliardi, and Enrico Zio. "A modeling and simulation framework for the reliability/availability assessment of a power transmission grid subject to cascading failures under extreme weather conditions". In: *Applied energy* 185 (2017), pp. 267–279.

[64] Stuart M Cohen, Kristen Averyt, Jordan Macknick, and James Meldrum. "Modeling climate-water impacts on electricity sector capacity expansion". In: *ASME 2014 power conference*. American Society of Mechanical Engineers. 2014, V002T10A007–V002T10A007.

[65] Chengcheng Shao, Mohammad Shahidehpour, Xifan Wang, Xiuli Wang, and Biyang Wang. "Integrated planning of electricity and natural gas transportation systems for enhancing the power grid resilience". In: *IEEE Transactions on Power Systems* 32.6 (2017), pp. 4418–4429.

[66] Xinda Ke, Di Wu, Jennie Rice, Michael Kintner-Meyer, and Ning Lu. "Quantifying impacts of heat waves on power grid operation". In: *Applied energy* 183 (2016), pp. 504–512.

[67] Yixian Liu, Ramteen Sioshansi, and Antonio J Conejo. "Multistage stochastic investment planning with multiscale representation of uncertainties and decisions". In: *IEEE Transactions on Power Systems* 33.1 (2018), pp. 781–791.

[68] Esteban Gil, Ignacio Aravena, and Raúl Cárdenas. "Generation capacity expansion planning under hydro uncertainty using stochastic mixed integer programming and scenario reduction". In: *IEEE Transactions on Power Systems* 30.4 (2015), pp. 1838–1847.

[69] Heejung Park and Ross Baldick. "Stochastic generation capacity expansion planning reducing greenhouse gas emissions". In: *IEEE Transactions on Power Systems* 30.2 (2015), pp. 1026–1034.

[70] Jiaying Shi and Shmuel S Oren. "Stochastic unit commitment with topology control recourse for power systems with large-scale renewable integration". In: *IEEE Transactions on Power Systems* 33.3 (2018), pp. 3315–3324.

[71] Ershun Du, Ning Zhang, Bri-Mathias Hodge, Qin Wang, Zongxiang Lu, Chongqing Kang, Benjamin Kroposki, and Qing Xia. "Operation of a High Renewable Penetrated Power System With CSP Plants: A Look-Ahead Stochastic Unit Commitment Model". In: *IEEE Transactions on Power Systems* 34.1 (2019), pp. 140–151.

[72] Dimitris Bertsimas, David B Brown, and Constantine Caramanis. "Theory and applications of robust optimization". In: *SIAM review* 53.3 (2011), pp. 464–501.

[73] Aharon Ben-Tal and Arkadi Nemirovski. "Robust optimization–methodology and applications". In: *Mathematical Programming* 92.3 (2002), pp. 453–480.

[74] Bo Zeng and Long Zhao. "Solving two-stage robust optimization problems using a column-and-constraint generation method". In: *Operations Research Letters* 41.5 (2013), pp. 457–461.

[75] Aharon Ben-Tal, Alexander Goryashko, Elana Guslitzer, and Arkadi Nemirovski. "Adjustable robust solutions of uncertain linear programs". In: *Mathematical Programming* 99.2 (2004), pp. 351–376.

[76] Aakil M Caunhye and Michel-Alexandre Cardin. "Towards more resilient integrated power grid capacity expansion: A robust optimization approach with operational flexibility". In: *Energy Economics* 72 (2018), pp. 20–34.

[77] Jia Li, Zuyi Li, Feng Liu, Hongxing Ye, Xuemin Zhang, Shengwei Mei, and Naichao Chang. "Robust coordinated transmission and generation expansion planning considering ramping requirements and construction periods". In: *IEEE Transactions on Power Systems* 33.1 (2018), pp. 268–280.

[78] Hongxing Ye and Zuyi Li. "Robust security-constrained unit commitment and dispatch with recourse cost requirement". In: *IEEE Transactions on Power Systems* 31.5 (2016), pp. 3527–3536.

[79] Dimitris Bertsimas, Eugene Litvinov, Xu Andy Sun, Jinye Zhao, and Tongxin Zheng. "Adaptive robust optimization for the security constrained unit commitment problem". In: *IEEE Transactions on Power Systems* 28.1 (2013), pp. 52–63.

[80] Álvaro Lorca, X Andy Sun, Eugene Litvinov, and Tongxin Zheng. "Multistage adaptive robust optimization for the unit commitment problem". In: *Operations Research* 64.1 (2016), pp. 32–51.

[81] Alvaro Lorca and Xu Andy Sun. "Multistage robust unit commitment with dynamic uncertainty sets and energy storage". In: *IEEE Transactions on Power Systems* 32.3 (2017), pp. 1678–1688.

[82] William E Hart, Carl Laird, Jean-Paul Watson, and David L Woodruff. *Pyomo–optimization modeling in python*. Vol. 67. Springer Science & Business Media, 2012.

[83] William E Hart, Jean-Paul Watson, and David L Woodruff. "Pyomo: modeling and solving mathematical programs in Python". In: *Mathematical Programming Computation* 3.3 (2011), pp. 219–260.

[84] Bryan S Palmintier and Mort D Webster. "Heterogeneous unit clustering for efficient operational flexibility modeling". In: *IEEE Transactions on Power Systems* 29.3 (2014), pp. 1089–1098.

[85] Bryan Stephen Palmintier. "Incorporating operational flexibility into electric generation planning: Impacts and methods for system design and policy analysis". PhD thesis. Massachusetts Institute of Technology, 2013.

[86] John Maybee, Paul Randolph, and Noel Uri. "Optimal step function approximations to utility load duration curves". In: *Engineering Optimization* 4.2 (1979), pp. 89–93.

[87] Fernando J De Sisternes and Mort D Webster. "Optimal selection of sample weeks for approximating the net load in generation planning problems". In: *Massachusetts Institute of Technology Engineering Systems Division Working Paper Series*. Vol. 3. 2013, pp. 1–12.

[88] Kris Poncelet, Hanspeter Höschle, Erik Delarue, Ana Virag, and William D'haeseleer. "Selecting representative days for capturing the implications of integrating intermittent renewables in generation expansion planning problems". In: *IEEE Transactions on Power Systems* 32.3 (2017), pp. 1936–1948.

[89] Paul Nahmmacher, Eva Schmid, Lion Hirth, and Brigitte Knopf. "Carpe diem: A novel approach to select representative days for long-term power system modeling". In: *Energy* 112 (2016), pp. 430–442.

[90] Yasuhiro Yamai and Toshinao Yoshiba. "Value-at-risk versus expected shortfall: A practical perspective". In: *Journal of Banking & Finance* 29.4 (2005), pp. 997–1015.

[91] *Available at:* http://clients.rte-france.com. 2017.

[92] IEA/NEA. "Projected costs of generating electricity 2015 edition". In: *OECD* (2015).

[93] Camille Cany, Christine Mansilla, Pascal da Costa, Gilles Mathonnière, Thierry Duquesnoy, and Anne Baschwitz. "Nuclear and intermittent renewables: Two compatible supply options? The case of the French power mix". In: *Energy Policy* 95 (2016), pp. 135–146.

[94] Réseau de transport d'eélectriciteé RTE. *Generation Adequacy Report on the electricity supply-demand balance in France - 2016 Edition*. http://www.rte-france.com. (Accessed on 02-12-2017). 2016.

[95] Dirk Rübbelke and Stefan Vögele. "Impacts of climate change on European critical infrastructures: The case of the power sector". In: *Environmental science & policy* 14.1 (2011), pp. 53–63.

[96] Yannick Rousseau. "Impact of Climate Change on Thermal Power Plants. Case study of thermal power plants in France". PhD thesis. 2013.

[97] Hagen Koch and Stefan Vögele. "Dynamic modelling of water demand, water availability and adaptation strategies for power plants to global change". In: *Ecological Economics* 68.7 (2009), pp. 2031–2039.

[98] Omid Mohseni, Heinz G Stefan, and Troy R Erickson. "A nonlinear regression model for weekly stream temperatures". In: *Water Resources Research* 34.10 (1998), pp. 2685–2692.

[99] Niels Lagergaard Pedersen and Kaj Sand-Jensen. "Temperature in lowland Danish streams: contemporary patterns, empirical models and future scenarios". In: *Hydrological Processes: An International Journal* 21.3 (2007), pp. 348–358.

[100] Jean C Morrill, Roger C Bales, and Martha H Conklin. "Estimating stream temperature from air temperature: implications for future water quality". In: *Journal of Environmental Engineering* 131.1 (2005), pp. 139–146.

[101] DL Elliot. "Adjustment and analysis of data for regional wind energy assessments". In: *Proceedings of the Workshop on Wind Climate*. 1979, pp. 121–131.

[102] Isabelle Tobin, Sonia Jerez, Robert Vautard, Françoise Thais, Erik Van Meijgaard, Andreas Prein, Michel Déqué, Sven Kotlarski, Cathrine Fox Maule, Grigory Nikulin, et al. "Climate change impacts on the power generation potential of a European mid-century wind farms scenario". In: *Environmental Research Letters* 11.3 (2016), p. 034013.

[103] Isabelle Tobin, Robert Vautard, Irena Balog, François-Marie Bréon, Sonia Jerez, Paolo Michele Ruti, Françoise Thais, Mathieu Vrac, and Pascal Yiou. "Assessing climate change impacts on European wind energy from ENSEMBLES high-resolution climate projections". In: *Climatic Change* 128.1-2 (2015), pp. 99–112.

[104] Jan Wohland, Mark Reyers, Juliane Weber, and Dirk Witthaut. "More homogeneous wind conditions under strong climate change decrease the potential for inter-state balancing of electricity in Europe". In: *Earth System Dynamics* 8.4 (2017), pp. 1047–1060.

[105] Sonia Jerez, Isabelle Tobin, Robert Vautard, Juan Pedro Montávez, Jose María López-Romero, Françoise Thais, Blanka Bartok, Ole Bøssing Christensen, Augustin Colette, Michel Déqué, et al. "The impact of climate change on photovoltaic power generation in Europe". In: *Nature communications* 6 (2015), p. 10014.

[106] F Mavromatakis, G Makrides, G Georghiou, A Pothrakis, Y Franghiadakis, E Drakakis, and E Koudoumas. "Modeling the photovoltaic potential of a site". In: *Renewable Energy* 35.7 (2010), pp. 1387–1390.

[107] R Chenni, M Makhlouf, T Kerbache, and A Bouzid. "A detailed modeling method for photovoltaic cells". In: *Energy* 32.9 (2007), pp. 1724–1730.

[108] Laurent Dubus. "Monthly and seasonal forecasts in the French power system". In: *ECMWF Seminar, Personal presentation*. 2012.

[109] Sami I Attia. "The influence of condenser cooling water temperature on the thermal efficiency of a nuclear power plant". In: *Annals of Nuclear Energy* 80 (2015), pp. 371–378.

[110] Abigail González-Díaz, Agustín M Alcaráz-Calderón, Maria Ortencia González-Díaz, Ángel Méndez-Aranda, Mathieu Lucquiaud, and Jose Miguel González-Santaló. "Effect of the ambient conditions on gas turbine combined cycle power plants with post-combustion CO2 capture". In: *Energy* 134 (2017), pp. 221–233.

[111] Karl E Taylor, Ronald J Stouffer, and Gerald A Meehl. "An overview of CMIP5 and the experiment design". In: *Bulletin of the American Meteorological Society* 93.4 (2012), pp. 485–498.

[112] Islam F Abdin and Enrico Zio. "An integrated framework for operational flexibility assessment in multi-period power system planning with renewable energy production". In: *Applied Energy* 222 (2018), pp. 898–914.

Part II

Papers

Paper (i)

Abdin, I. F., & Zio, E. (2018). An integrated framework for operational flexibility assessment in multi-period power system planning with renewable energy production. ***Applied energy*****, 222, 898-914.**

An integrated framework for operational flexibility assessment in multi-period power system planning with renewable energy production

Islam F. Abdin[a], Enrico Zio[a,b,]

[a]*Laboratoire Genie Industriel, CentraleSupélec, Université Paris-Saclay*
3 Rue Joliot Curie, 91190 Gif-sur-Yvette, France.
Chair Systems Science and the Energy Challenge, Fondation Electricité de France (EDF)
[b]*Department of Energy, Politecnico di Milano, Italy*

Abstract

This paper proposes an integrated framework for operational flexibility assessment in power system planning with a significant share of intermittent renewable energy sources (RES). The framework proposed includes: (i) the formulation of an integrated generation expansion planning (GEP) and unit commitment (UC) model accounting for key short-term technical constraints, (ii) the elaboration of accurate and systematic horizon reduction methods to alleviate the computational burden of the resulting large-sized optimization problems and (iii) the definition of suitable metrics for the operational flexibility assessment of the obtained plans. The framework is applied to a ten year planning horizon of a realistically sized case study representing the national power system of France, under several scenarios of RES penetration levels and carbon limits, spanning levels of up to 50%. The importance of incorporating the detailed short-term constraints within long-term planning models is investigated and the results of the assessment clearly show that neglecting them leads to plans significantly short on flexibility, and more so for high renewable energy penetration levels. Moreover, the results highlight the importance of relying on suitable quantitative metrics for operational flexibility assessment in power systems planning rather

Email addresses: islam.abdin@centralesupelec.fr (Islam F. Abdin), enrico.zio@centralesupelec.fr, enrico.zio@polimi.it (Enrico Zio)

than solely relying on generic performance measures, such as system costs and mixes of power plants, which are shown not to sufficiently reflect the flexibility levels of the obtained plans.

Keywords:
Operational Flexibility, Flexibility Metrics, Generation Expansion Planning, Unit Commitment, Renewable Energy Penetration, Optimization

---

List of symbols

Indexes:

i	index of power plant cluster
j	index of sub-periods (hours)
s	index of sub-periods (load-levels)
y	index of planning year

Sets:

I	set of power plant clusters
I^{new}	subset of new power plants cluster
I^{res}	subset of renewable energy units cluster
I^{th}	subset of thermal and nuclear units cluster
J	set of hourly sub-periods
S	set of load-levels sub-periods
Y	set of years in the planning horizon
Θ	set of investment decision variables
Ω	set of operation decision variables

Parameters:

Y^{end}	end year of the planning horizon
Y^{res}	first year during which the RES quota target is binding

$L_{y,*}$	demand at sub-period j or s in year y (MW)
$Dur_{y,s}$	duration of load block s in year y (hours)
P_i^{max}	maximum capacity of power plant i (MW)
P_i^{min}	minimum stable power output of power plant $i \in I^{th}$ (MW/h)
C_i^{inv}	investment cost of unit i (M€)
I_i^{max}	maximum allowable units to be commissioned within the planning horizon
T_i^{life}	expected life-time of new power plant i (years)
T_i^{const}	construction time of power plant i (years)
R_i^{Umax}	maximum upwards ramping capability of power plant $i \in I^{th}$ (MW/h)
R_i^{Dmax}	maximum downwards ramping capability of power plant $i \in I^{th}$ (MW/h)
P_i^{start}	maximum output of power plant $i \in I^{th}$ when started (MW)
$CF_{i,y,*}$	capacity factor of renewable energy sources $i \in I^{res}$ during sub-period j or s, of year y (%)
E_i	amount of carbon emission per MWh of power plant i (tCO_2 / MWh)
E_y^{max}	maximum total allowable emission per year y (tCO_2)
$EFOR_i$	Expected forced outage rate of power plant i (%)
M_i^u	minimum up-time for power plant $i \in I^{th}$ (hours)
M_i^d	minimum down-time of power plant $i \in I^{th}$ (hours)
DR_y	discount rate for year y (%)
$C_{i,y}^{mrgl}$	marginal cost of power plant i including the variable O&M and CO_2 costs, considering inflation (€/ MWh)
C_i^s	start-up cost of power plant i (€)
C^{lns}	cost of load not served (€/ MWh)
C_i^{fom}	fixed O&M costs of power plant i (€)
Pen_y^{level}	annual renewable penetration level requirement (%)
Prr	percentage of the load required to be covered by primary reserve (%)
Srr^{up}	percentage of the load required to be covered by the secondary upwards reserve (%)
Srr^{dn}	percentage of the load required to be covered by the secondary downwards reserve (%)
a^{res}	percentage of the variable generation output covered by secondary reserve (%)

r^{min}	minimum planning reserve margin (MW)

Continuous Variables:

$p_{i,y,*}$	energy output of power plant i at sub-period j or s, during year y (MWh)
$pr_{i,y,j}$	primary reserve of unit i at sub-period j during year y (MWh)
$sr^{up}_{i,y,j}$	secondary upwards reserve of unit i at sub-period j during year y (MWh)
$sr^{dn}_{i,y,j}$	secondary downwards reserve of unit i at sub-period j during year y (MWh)
$lns_{y,*}$	load not served at sub-period j or s, during year y (MW)
$v_{i,y,j}$	shut-down decision of unit i during sub-period j in year y

Discrete Variables:

$x_{i,y}$	availability (commissioning) state of power plant i in year y
$q_{i,y}$	commissioning decision of power plant i in year y
$u_{i,y,j}$	commitment status of power plant i during sub-period j in year y
$z_{i,y,j}$	start-up decision of power plant i during sub-period j in year y

Acronyms:

CF	Capacity Factor
EFS	Expected Flexibility Shortfall
GEP	Generation Expansion Planning
IRRE	Insufficient Ramping Resources Expectation
LDC	Load Duration Curve
LNS	Load Not Served
MILP	Mixed Integer Linear Programming
O&M	Operation and Maintenance
RES	Renewable Energy Sources
UC	Unit Commitment

I. Introduction

Generation expansion planning (GEP) is a well studied techno-economic problem, which relates to determining the optimal of generation technologies mix, their siting and their investment schedules, for ensuring that the electricity demand over a certain time horizon can be satisfied. With the power sector being constantly subjected to changes, driven by economical, technical, social and environmental issues, GEP modeling techniques have continuously evolved to accommodate the newly arising requirements. Such modeling advancements have been covered in recent literature reviews and include, among others (Sadeghi et al., 2017; Oree et al., 2017): improvements in the details considered (e.g. reliability and maintenance), policy developments, such as the restructuring of the power sector, renewable energy sources (RES) integration and support schemes, uncertainty and stochasticity modeling, and the consideration of real-options for adaptive power systems design (Caunhye and Cardin, 2017).

One of the most recent concerns in power systems planning is dealing with the high share of intermittent RES penetration required in the system, driven by strict environmental policies, such as the EU renewable energy directive (European Council, 2009) and its proposed revision (European Council, 2016), and other regional and national targets. The resulting increased variability in the net load (system demand minus RES production) requires that the remainder of the thermal units cope with tighter operational flexibility requirements (Brouwer et al., 2015; Kubik et al., 2015), generally defined as the ability of the system to respond to the inter-temporal variability rising both from intermittent RES production and from variations in electricity demand. In this respect, operational flexibility regards the short-term operation of those generation units and their technical characteristics: ramping rates, unit commitment states, minimum up and down times, start-up times and minimum stable load, to name a few.

From an assessment point of view, accounting for operational flexibility in this new context is a critical element for overall system reliability (see for example Fulli et al. (2017) for a discussion on these requirements in Europe). Whereas reliability relates to the fact

that sufficient firm-capacity[1] is available at each time period to satisfy the system load, as measured by typical metrics, such as loss of load expectation (LOLE) and expected energy not supplied (EENS), operational flexibility considers how a specific operational state of the system at a given period would contribute to (or hinder) its ability to deploy its resources for accommodating variations in subsequent periods: for this, no time period can be assessed in isolation of the others, nor without detailed knowledge of the exact system state and technical characteristics at the given period. Therefore, metrics to describe operational flexibility have been recently proposed in the literature, varying in the degree of complexity and in the data required for their estimation. Lannoye et al. (2012) proposes a probabilistic metric that takes into account key technical characteristics of the generation units, and aggregates them for a system-level assessment. In (Ulbig and Andersson, 2015) a number of interdependent metrics are defined for individual generation units to assess their available flexibility in real time. Oree and Hassen (2016) proposes a composite metric which aggregates a set of the generation units flexibility parameters through normalization, weighting and correlation analysis, while (Zhao et al., 2016) proposes a metric which additionally considers the impacts of the transmission network on the flexibility levels.

With respect to power systems planning, traditional long-term GEP models do not consider the chronological representation of net load variations, nor the short-term technical constraints of the generation units, but rather rely on average system representations. The generation plans obtained are, therefore, not explicitly driven by the requirement to deal with short-term variations. This type of evaluation is, on the contrary, typically performed by the well known unit commitment (UC) problem, which does not consider investment decisions (Abujarad et al., 2017). Accordingly, to account for the operational flexibility aspect, recent planning studies have started to investigate the importance of integrating the short-term constraints within long-term planning models. Belderbos and Delarue (2015) solve a traditional GEP model based on a basic screening curve method and propose a perturbation algorithm with embedded short-term constraints to improve the plans obtained. They show that considering the short-term constraints results in the installation of more

[1] Available generation capacity excluding failed units, units in maintenance, offline units, etc.

mid and peak load capacities than the case of neglecting them. Similar results are reported in (Palmintier and Webster, 2016), who solve a combined GEP-UC model for a single future year, under several wind penetration and carbon pricing scenarios. Additionally they show that neglecting short-term constraints leads to an underestimation of carbon emission and wind curtailment levels of the obtained plans. The same general trends are shown in (Welsch et al., 2014) and (Wierzbowski et al., 2016) for case studies on Ireland and Poland, respectively. For multi-annual planning studies, Koltsaklis and Georgiadis (2015) propose a combined model and use it for the future planning of the Greek power system, while Guo et al. (2017) propose a similar investigation applied to the Chinese power system. In both cases the results revealed the correlation between significant RES penetration with increased amounts of peaking units investments. Finally, Pereira et al. (2017) compare an integrated model to a classical one for a ten year planning period and show that neglecting these constraints underestimates both the investment costs and the emissions levels.

The above studies have investigated the importance of including the short-term constraints within long-term planning models to account for the operational flexibility in power systems planning by analyzing the differences in generation mixes, system costs, curtailment levels, or a combination of these. None of those studies, however, have performed a quantitative assessment using metrics that are specifically designed to evaluate the operational flexibility aspect. Furthermore, the mentioned planning models are computationally intensive, so that different ad-hoc methods for the horizon reduction have been used but neglecting to address the bias that these could introduce on the results of the assessment.

Research objectives and contributions

To overcome these limitations, in this paper we introduce an integrated operational flexibility assessment framework that i) is based on consistent horizon reduction methods driven by an explicit optimization objective to avoid biases that can arise from ad-hoc approximations and ii) adopts suitable metrics to quantitatively assess the flexibility level of the obtained plans.

Within the framework presented, an integrated GEP-UC model is proposed, cast as a mixed integer linear programming (MILP) problem, and we employ the integer clustering

method for handling discrete decision variables (Palmintier and Webster, 2014), which provides a good approximation and a significant reduction of the computational complexity. A 10 years planning horizon is considered based on realistic load and RES capacity factor data obtained for the national system of France. The horizon reduction is systematically dealt with by the implementation of a dynamic programming algorithm that optimizes the step-function approximation of the traditional GEP model and an exhaustive search algorithm for the chronological load approximation of the integrated GEP-UC model. For the quantitative operational flexibility assessment, the probabilistic metric of insufficient ramping resource expectation (IRRE) proposed in (Lannoye et al., 2012) is used. We complement this measure by originally introducing the expected flexibility shortfall (EFS) metric, which indicates the expected load loss when the system is not able to adequately respond to the inter-temporal variability.

The numerical examples consider a single-region green-field planning problem with no generation units existing in the system. On one hand, this is done to avoid any bias those existing units may impose on the expansion plans and, therefore, to focus solely on the models outcomes; on the other hand, it is done to validate the framework capability for efficiently addressing large-sized instances. The framework, however, is straightforwardly applicable to grey-field planning problems and easily extendable to muli-regional planning. A wide range of RES penetration levels (0% to 50%), most notably wind and solar, is considered and the same for carbon emission limits.

The original contributions of the work are:

- The paper contributes to power systems planning with high shares of RES penetration and stringent carbon targets, by proposing a computationally efficient, multi-period integrated GEP-UC model that accounts for key short-term constraints and chronological net load representation. In particular,
    * The importance of considering these constraints to account for operational flexibility under high RES penetration has been demonstrated quantitatively by comparing the output of the integrated model to that of the traditional GEP, which leads to investment decisions based on average system operating condi-

tions.

* For computational tractability, horizon reduction is introduced by systematic optimization, to avoid biases on the results obtained by ad-hoc methods.

- The paper introduces the expected flexibility shortfall (EFS) metric for operational flexibility assessment to capture the expected amount of load loss specifically due to insufficient flexibility. We analyze the complementarity of this metric to other metrics of literature, most notably the insufficient ramping resource expectation (IRRE) proposed in (Lannoye et al., 2012) which considers the expected frequency of flexibility shortage rather than its magnitude.

- The relevance of the overall modeling for real applications is shown by its application to a realistic case study representing the national system of France, with load and RES capacity-factor data spanning a 10-years planning period. Sensitivity to key supply and demand parameters is also performed.

- The results of the paper for a wide range of RES penetration targets and carbon emission limits allows highlighting the importance of relying on suitable metrics for the assessment rather than on quantities typically considered for power system planning, like generation mixes, system costs and amount of renewable curtailment which are not capable to reflect the true flexibility levels of the obtained plans.

For real applications, the integrated framework can be used by power system planners to rapidly and accurately evaluate the impact of different system parameters and policy requirements on the resulting generation expansion plans, most notably in terms of operational flexibility. The planner can, then, adapt the policy requirements to ensure generation plans with an adequate flexibility level or set proper expectations on which levels are attainable under a specific set of parameters and requirements. Moreover, several remarks are highlighted in the relevant sections regarding the proper treatment of RES investments as decision variables within the simplified optimization model as well as the horizon reduction method, which can prove useful for practitioners if similar types of models are to be considered.

II. Operational flexibility assessment framework

A. Overview

The integrated operational flexibility assessment framework proposed is schematically illustrated in Figure (1). For comparison purposes, it will be applied to two types of power system planning models: the traditional GEP model soft-linked with a UC model (denoted S-GEP) and the integrated GEP-UC model solved as a single optimization (denoted C-GEP). Figure (1a) illustrates the assessment framework applied to the former, and Figure (1b) that applied to the latter. The framework stands: i) the formulation of the models, ii) the elaboration of accurate horizon reduction approximation methods and iii) the elaboration of suitable metrics for assessment of the operational flexibility of the of the obtained plans, described in details in the following sections.

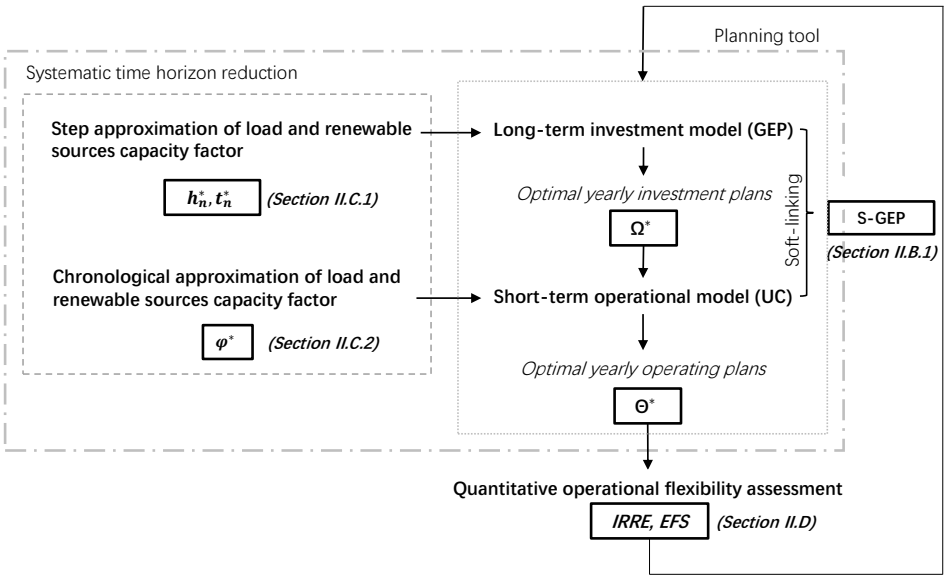

(a) Soft-linked planning models

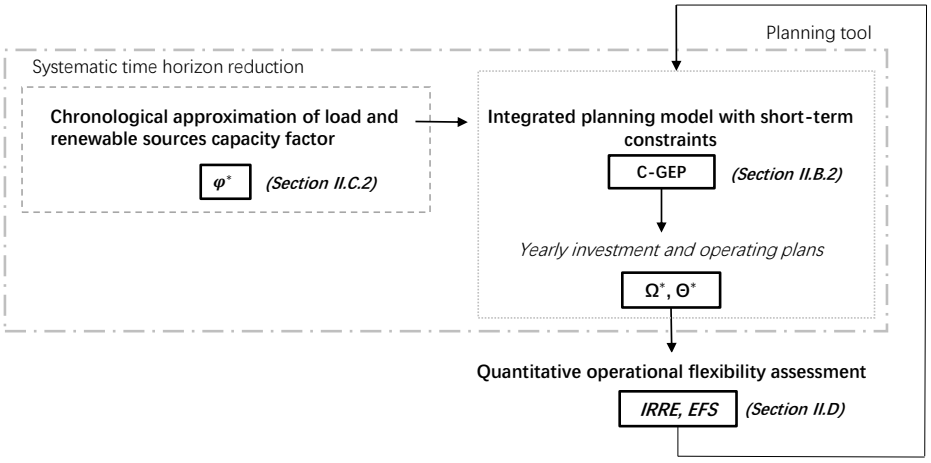

(b) Integrated models

Figure 1: Operational flexibility assessment framework

B. Power system planning models formulation

As previously mentioned, two types of power system planning models are considered for operational flexibility assessment:

B.1. Soft-linked GEP-UC model (S-GEP)

The S-GEP model consists of two mixed integer linear programming problems which are successively solved:

i. A long-term GEP model, which has the objective of minimizing the total discounted cost over the planning horizon under typical long-term simplified constraints. No hourly chronological order is considered and load is represented as load blocks derived from a load-duration curve (LDC) with duration ($Dur_{y,s}$) and levels ($L_{y,s}$). The detailed model formulation can be found in Appendix (A.A)

ii. A short-term UC model, which has the objective of minimizing the short-term operational costs, taking into account the detailed short-term technical capabilities of the units, the chronological demand and RES availability. The detailed model formulation can be found in Appendix (A.B)

The soft linking of the two problems is achieved by:

1. Solving the long-term GEP problem first, under the simplified system representation;
2. Populating the obtained investment plans within the UC problem, which is, then, solved to obtain the detailed operation of these plans.

B.2. Combined GEP-UC model (C-GEP)

The C-GEP model is the straightforward integration of the two models described above into a single optimization model, with the following adjustments:

- The load-duration step representation indexed by (s) in the S-GEP model is replaced by the hourly chronological representation (j), for all parameters and decision variables.
- The detailed operating cost equation of the UC objective function replaces that of the traditional GEP model.

The resulting high resolution MILP problem is known to be computationally challenging, especially when considering a multi-annual planning horizon: (i) the formulation has been, therefore, adapted to handle discrete decision variables by means of the integer clustering method proposed in (Palmintier and Webster, 2014); (ii) and time horizon reduction is introduced systematically, as explained in the next section.

C. Time horizon reduction

The traditional GEP, UC and integrated GEP-UC models have different natures, notably in the time resolution considered for the load and RES capacity factor (CF). Different approximation methods are, therefore, employed for the horizon reduction.

C.1. Load and RES-CF approximations for the GEP model

To obtain the investment decisions in the traditional GEP model, yearly load is typically represented as a load-duration curve (LDC), which is approximated by a step-function, where each step represents an average load-level and duration. This function is typically obtained by deciding in an ad-hoc manner the number of steps and segmenting the LDC accordingly. Depending on the choice of segmentation, the outcome of the model can greatly differ, for instance, if more steps are introduced for the peak load hours or the base ones.

Moreover, in a multi-annual planning context the LDC forecast varies among the different years, so that a segmentation strategy for a year might not be optimal for other years. A consistent method for the LDC approximation is, therefore, necessary.

The seminal work of Maybee et al. (1979) is one of very few studies in power systems planning found to address this issue. We define a similar optimization problem where the objective of the step function approximation is the minimization of the energy mismatch between each approximated step and its actual corresponding segment. The optimization problem can be formulated as:

$$\min_{\mathbf{t}} \sum_{n=1}^{N} \sum_{i=t_{n-1}}^{t_n} \left(F(i) - h_n\right)^2 \tag{1}$$

subject to:

$$h_n = \frac{1}{t_n - t_{n-1}} \cdot \sum_{i=t_{n-1}}^{t_n} F(i), \quad n = 1, 2, ..., N \tag{2}$$

where $F(i)$ represents the actual LDC function, N is the total number of steps specified for the approximation, n is the index of the current approximation step, h_n is the height (load level) of the step function for step n and t_n is the breakpoint at which the step function changes value from step n to step $n+1$. The objective is to find the breakpoints vector $\boldsymbol{t}$ which fully defines the approximated step function and is such to minimize the mismatch of equation (1). This problem can be stated as a dynamic programming problem, where the backward recursive functional equation is defined as:

$$f_n(x) = \min_{x \le t \le T} \left[\sum_{i=x}^{t} \left(F(i) - h_{N-n+1}\right)^2 + f_{n-1}(t) \right], \quad n = 1, 2, ..., N \tag{3}$$

for which h_{N-n+1} can be calculated as given in equation (2).

It is important to note that since we consider the investment in RES capacity as a decision variable, it heavily depends on the average capacity factor (CF) of each RES technology. Neglecting this consideration within the simplified long-term GEP problem is equivalent to assuming that wind and solar technologies are fully dispatchable. Constraint

(A.11) in the Appendix is, therefore, introduced to avoid this inaccuracy. Similar to the LDC approximation, the CF of each RES technology can be approximated by a level and a duration. However, the real average correlation between the load and the RES-CF should be maintained to avoid unrealistic and biased results. An illustration of the approach followed in this work to achieve this is given in Appendix B.

C.2. Load and RES-CF approximations for the UC and GEP-UC models

The horizon reduction for the C-GEP and UC models need to maintain the real hourly chronological order of both the load and the RES-CF. This is typically achieved by approximating the full year to a number of days, weeks or months while preserving the sub-period chronological order. We opt to represent a year by a number of sampled weeks obtained by solving an optimization problem similar to that proposed by De Sisternes and Webster (2013), which reported superior approximations than other ad-hoc methods.

The weeks are selected with the objective of minimizing the energy mismatch between the actual LDC and the approximated one (LDC^{aprox}) obtained through scaling up the weeks sampled to the full year length. Mathematically this is represented by (De Sisternes and Webster, 2013):

$$\phi^* \in arg\min_{\phi} \sum_{i=0}^{T} (LDC_i - LDC_{\phi,i}^{aprox})^2 \tag{4}$$

where T is the total number of hours in each planning year and ϕ is a vector containing the set of indexes of the selected weeks. The optimization can be solved using an exhaustive search that evaluates all possible combinations of the n specified weeks and selects those that minimizes the energy mismatch. Once the optimal weeks are obtained for the load, the same weeks are selected for the RES-CF data to ensure that the correlation between the two is maintained.

D. Flexibility assessment metrics

To quantify the flexibility of the system, we adopt two probabilistic metrics: the insufficient ramping resource expectation (IRRE) proposed in (Lannoye et al., 2012), and the originally introduced expected flexibility shortfall (EFS) metric.

D.1. Insufficient Ramping Resource Expectation (IRRE)

The IRRE is the expected number of instances in which the generation units in a power system cannot answer to the changes in net load. The metric is generally obtained by (Lannoye et al., 2012):

1. Calculating the net load ramping time series for the whole planning horizon in both upwards (up) and downwards (dn) directions.
2. Calculating the up/dn available flexible resources within a specified time horizon of interest (e.g. one hour), given the availability and commitment status of each generation unit, its start-up time, its actual production level and its total upwards or downwards ramping capabilities for the next period.
3. Aggregating all the time series for all resources to obtain the total up/dn available flexibility time series.
4. Calculating the up/dn available flexibility empirical cumulative distribution function from the total available flexibility time series.
5. Calculating the probability of insufficient ramping by substituting the required net load ramping in the obtained distribution function. The sum of the up/down probabilities time series gives the IRRE+/-.

D.2. Expected Flexibility Shortfall (EFS)

While the IRRE indicates the expected frequency for not meeting the flexibility requirements, it does not give any information about how short the system is on average when not able to meet these requirements. This can be calculated through the expected flexibility shortfall (EFS) metric.

The EFS metric builds on the value-at-risk (VaR) measure defined as the "possible maximum loss over a given holding period within a fixed confidence level" (Yamai and Yoshiba, 2005). Mathematically, this is defined as:

$$VAR_{\alpha}(X) = \sup\{x \mid P[X \geq x] > \alpha\} \tag{5}$$

where X in our context is a variable denoting the loss of load due to insufficient flexibility and $\sup\{x \mid P[X \geq x] > \alpha\}$ indicates the highest 100α percentile of the loss distribution.

The expected flexibility shortfall (EFS) is, thus, the conditional expectation of load loss due to insufficient flexibility, given that it is beyond the VaR level, or:

$$EFS_\alpha(X) = E\left[X \mid X \geq VaR_\alpha(X)\right] \tag{6}$$

The EFS is calculated by performing steps (1) to (3) of the IRRE calculations, followed by:

4. Calculating the up/dn losses time series as the absolute difference between the up/dn net load ramping series and the respective total available flexibility resources.
5. Calculating the VaR at the desired $100(1-\alpha)\%$ confidence levels.
6. Calculating the EFS as the average loss for observations exceeding the VaR level, at the respective confidence levels.

III. Numerical Example

A. Test system

For the multi-annual demand representation, we have taken the 10 years load data of France, from 2006 to 2015, which are publicly available at (RTE-France, 2017), to represent a realistic system demand for 10 planning years. We have similarly calculated the RES-CF, namely wind and solar power, from the actual yearly production time series, by dividing each hourly production by the total installed capacity of each technology. This results in the hourly CF time series per renewable technology and for each year.

Table 2 summarizes the technical and cost data for the generation technologies considered in the expansion planning. The cost data and units capacities are obtained from the IEA/NEA Projected Costs of Generating Electricity report (2015 edition) (IEA/NEA, 2015); the remaining technical characteristics are largely based on data described in (Cany et al., 2016) to maintain consistency with characteristics relevant to the French power system. The discount rate is assumed to be 3%, the minimum design reserve margin r^{min} is set to 15% of the maximum annual load, operating reserves are set to cover 1% of the hourly load for primary and secondary reserves, and 10% of the hourly RES production for upwards and downwards secondary reserves. The penalty for not meeting demand (C^{lns}) is set to 4k€/MWh to discourage load shedding. Finally, the construction time of new units is neglected , as we are considering a relatively concise planning horizon.

Table 2: Technical and economic characteristics for the different generation technologies

Technology [i]	P_i^{max} [MW]	P_i^{min} [MW]	R_i^{Umax} [MWh/min]	R_i^{Dmax} [MWh/min]	M_i^u [$hours$]	M_i^d [$hours$]	E_i [tCO_2/MWh]	$EFOR_i$	C_i^{inv} [$M€$]	C_i^{mrgl} [$€/MWh$]	C_i^s [$k€$]
Nuclear	1400	700	$0.5\%P_n$/min	$0.5\%P_n$/min	12	48	0	0.01	3.95	9.33	15.0
Fossil Hard Coal	1100	550	$1.5\%P_n$/min	$1.5\%P_n$/min	6	10	0.96	0.06	2.08	36.67	11.26
Fossil Gas (CCGT)	550	165	$5\%P_n$/min	$5\%P_n$/min	3	5	0.46	0.04	1.02	69.00	7.53
Fossil Gas (OCGT)	270	54	$20\%P_n$/min	$20\%P_n$/min	1	2	0.67	0.08	0.7	110.00	3.79
On-Shore Wind	80	0	/	/	/	/	0	*	1.9	0	/
Solar-PV	60	0	/	/	/	/	0	*	1.5	0	/

B. Implementation notes and remarks

All optimization problems are modeled in the Python programming language. The MILP problems are programmed using the Pyomo software package (Hart et al., 2012, 2011) and solved using IBM ILOG-CPLEX with an optimality gap of 0.1%. It is important to note that for the UC and the GEP-UC models, the yearly demand is approximated by 4 representative weeks and the chronological order within each week is maintained; however, the immediate demand profile change between one week and the next may not reflect the realistic variation that could occur in the system. It is important, therefore, to decouple the operational decision variables from one week to the next, to eliminate any bias from incorrect initialization. In this respect, unit states are constrained to be identical at the beginning and end of each week, which reasonably assumes that each week is followed by a similar one.

IV. Results and discussion

A. RES penetration and carbon emission policy scenarios

We first explore 12 scenarios covering a wide range of RES penetration and carbon emission targets: a base case with no RES nor emission targets, in addition to all remaining combinations of 0%, 25%, 35% and 50% binding RES penetration targets (represented as a percentage of total electricity demand) and 0%, 75% and 50% emission limit (calculated as a percentage of each corresponding no emission limit scenario). We apply the assessment framework on the two types of planning models considered (C-GEP and S-GEP), for comparing the effect of integrating the short-term constraints within the long-term investment

planning problem and primarily in terms of operational flexibility. For the S-GEP model, each annual LDC is approximated by twelve load-duration steps using the dynamic programming optimization described in Section (II.C.1). The normalized root mean squared error (NRMSE) of the energy mismatch for the ten approximated yearly LDC have a mean of 3.91% and a standard deviation of 0.002. For the C-GEP model, each year is approximated by four weeks through the optimization problem described in Section (II.C.2), where within each week, hourly chronological order is maintained. The NRMSE of the 10 approximated yearly loads have a mean of 0.63% and a standard deviation of 0.003.

A.1. Base case

We start by investigating the results of the base case for both S-GEP and C-GEP models. Figure (2) illustrates the total capacity installed of each generation technology, at the end of each year, obtained by each model. The bulk of the investments is done in the first year, where 82.01 GW and 80.59 GW total capacities are installed by the S-GEP and the C-GEP model, respectively, and gradually increase to the end of the planning horizon. The final total capacities installed are 87.14 GW and 85.72 GW for S-GEP and C-GEP, respectively. The additional capacities in both cases are in the Fossil OCGT technology. It can be observed that, in this case with no requirement on RES penetration, the capacity investments given by both models closely resemble to each other.

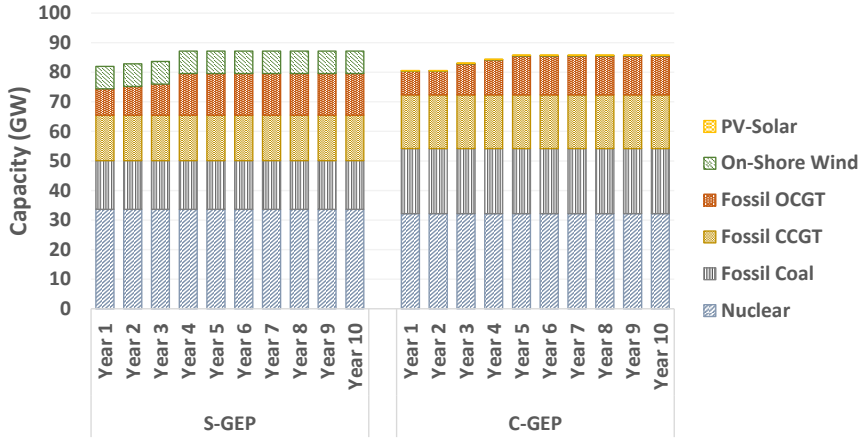

Figure 2: Cumulative yearly installed capacity for the base case obtained through the S-GEP (left) and C-GEP (right) models

Table 3: Results of different performance measures and operational flexibility metrics for the plans obtained through the S-GEP and C-GEP models for the base case (No RES requirement, no carbon limits) (worse performance highlighted).

(a) Installed capacities and generic performance measures results

	S-GEP	C-GEP	
Total RES Installed Capacity [GW]	7.60	0.14	**Difference [%]**
Total Installed Capacity [GW]	87.14	85.72	**(C-GEP relative to S-GEP)**
Total Cost (excluding LNS) [B€]	313.00	310.59	-0.77%
Load Not Served [% of total load]	0.12%	0.01%	-89.38%
RES shedding [% of total RES]	0.00%	0.00%	/
Carbon Emission [Mtons]	1379.60	1699.93	+23.22%

(b) Operational flexibility metrics results

		S-GEP	C-GEP	Difference [%] (C-GEP relative to S-GEP)
IRRE+ (% of upwards ramps)		7.38%	2.20%	-70.13%
EFS+ (MW)	**EFS+ (95%)**	512.70	90.53	-82.22%
	EFS+ (99%)	2402.85	451.31	-38.08%
IRRE- (% of downwards ramps)		0.01%	0.00%	-42.52%
EFS- (MW)	**EFS- (95%)**	0.00	0.00	/
	EFS- (99%)	0.00	0.00	/

To better assess the S-GEP and C-GEP obtained plans, a number of performance measures are compared. Most notably, we compare the amount of load not served (LNS), the amount of RES shedding, the total carbon emission and the total cost (investment + operating costs)[2] of the plans obtained through each model for the whole planning horizon. Table (6a) summarizes the results of the different measures for the base case. The C-GEP model outperforms the S-GEP in the resulting LNS, amounting to only 0.01% of the total load for the former as opposed to 0.12% for the latter. Since only a small fraction of the capacities installed are in RES technologies, no amount of RES shedding was required. Wind and solar shedding would typically be decided if large energy quantities are produced, leading to very large inter-temporal variability so that it becomes more cost effective to shed the cheap RES energy than to adapt the rest of the thermal units (e.g. turn on or shut down some of those units). Regarding carbon emission, operating the C-GEP obtained plan evidently results in higher total emission ($\approx$ 1700 Mtons compared to $\approx$ 1380 Mtons by the

[2]excluding the cost of LNS to avoid redundancy

S-GEP model), which is explained by the overall higher fossil capacities installed. The total investment and operating cost is lower for the C-GEP plan (310.59 Bn€) compared to the S-GEP one (313.00 Bn€). This, together with the lower amount of LNS, indicates that the C-GEP plan is better adapted to satisfy the load at lower cost, but results in higher carbon emission than the S-GEP one.

The operational flexibility assessment of the resulting plans using the proposed metrics is summarized in Table (6b) . The IRRE and EFS results (at the 95% and 99% confidence intervals) are reported for the total increasing (+) and decreasing (-) net load variations. The results show that operating the S-GEP obtained plan is expected not to satisfy 7.38% of the total number of upwards ramps (IRRE+) as opposed to only 2.20% for the C-GEP plan. Moreover, the EFS is more than 5 times higher for the S-GEP plan, averaging around 512.00 MW and 2400 MW, at the 95% and the 99% confidence intervals, respectively, as opposed to an expectation of only 90 MW and 450 MW for the C-GEP obtained plan, at the respective confidence intervals. Regarding the negative ramps, it is shown that the operational flexibility shortages are of much less significance for both models plans, albeit still being slightly worse for the S-GEP one.

A.2. Increased RES penetration and emission limit policies

Table (4) summarizes the results of the different performance measures analyzed for the base-case scenario (top-left corner), along with the different combinations of RES penetration (horizontally) and emission limit (vertically) policies considered. First, we notice how an increased RES penetration requirement leads to a significant difference in the final capacity mix given by the S-GEP and the C-GEP models compared to when such requirement is not imposed. Moving horizontally across the Table, i.e. to higher RES requirements, the "short-term aware" C-GEP model results in mixes with much higher fossil capacities and much less nuclear than to the S-GEP one. These fossil technologies possess overall better short-term dynamic properties, such as ramping capabilities and shorter minimum up and down times. Such an investment choice can be, therefore, attributed to the ability of the integrated C-GEP model to derive decisions better adapted to the increased short-term variations imposed by the RES penetration. Moreover, the total capacity installed increases

significantly for the C-GEP plans compared to the S-GEP ones. The S-GEP model overestimates the actual RES availability since it considers average capacity factor values, so it invests in overall less capacities in the other technologies. This gap increases with higher RES penetration, from around 10 GW difference for the 25% RES cases, to 15 GW for those with 35% RES and up to 30 GW difference for the 50% RES penetration plans. It is clear that such capacity differences are non-negligible and that they would significantly affect the reliability of the power system, if not adequately accounted for.

This becomes even clearer as we consider the resulting LNS percentage. There is a steep increase in the amount of LNS for the S-GEP plans with higher RES levels, from 0.12% of the total load on average and up to 2.7% for the highest RES penetration levels. As predicted from the capacity difference, this represents an unacceptably high level of LNS and defies the security of supply of the plans. The C-GEP plans, on the other hand, maintain a low average LNS percentage of 0.02%, with negligible variation across all scenarios. RES shedding exhibits a similar steep increase with the higher RES penetration levels; however, it remains comparable for both the C-GEP and S-GEP plans with only a few percentage points difference in each respective scenario. As previously explained, shedding decisions are taken when they are more cost effective, the C-GEP model accounts for these sheds when deciding on the investment plans, and ensures that the plans obtained would still meet the RES quota requirements. This is not the case for the S-GEP plans, which could lead to final plans that are theoretically meeting these requirements, but practically are not.

By looking at the differences in the performance measures of the C-GEP and S-GEP plans, especially the total installed capacities, one would expect a much higher total cost (not including LNS cost) for the C-GEP plans compared to the S-GEP ones. This is in fact not the case: while indeed the C-GEP plans with significant RES penetrations result in higher costs, these are not proportional to the additional investments made and the amount of LNS avoided. The maximum cost difference reached at 50% RES penetration averaged around only +6.31% more for the C-GEP plans than for the S-GEP ones, whereas the capacities were on average +20% higher.

Again, the amount of carbon emission is consistently higher for all C-GEP plans com-

pared to the S-GEP ones, which is not surprising as the amount of fossil capacity installed is higher in those plans. This was optimally obtained through the C-GEP model as those units possess faster dynamic capabilities that are needed to counterbalance the higher net load variability as more RES penetrate the system. Furthermore, this leads to the observation that increasing RES penetration levels by itself does not necessarily indicate lower carbon emission levels in the system, since the rest of the investments are counterbalancing with more dynamic yet more emitting units. In this respect, the S-GEP model can be considered to be underestimating the actual emission levels as higher RES penetrate the systems. For our numerical example, these underestimations are found to be in the range of 14% (No RES, 50% emission limit case) to 60% (35% RES, no emission limit case).

Imposing carbon emission limits, as shown by moving vertically across the table does not have a significant impact on most of these measures. It does, however, considerably affect the capacity mix obtained through the different models. Evidently, as more stringent carbon limits are imposed, the capacity mix shifts towards less emitting technologies and, most notably, nuclear. Most of the fossil capacity reduction is in the fossil coal capacity since it is the most emitting one; the total capacity installed, however, remains almost constant. Furthermore, despite the large differences in the capacity mixes, the total costs of the plans do not heavily vary, averaging around +1% increase in most cases, as higher emission limits are imposed.

Table 4: Results of the different performance measures for the plans obtained through the S-GEP and C-GEP models for the range of RES penetration and carbon emission limits considered (worse performance highlighted)

			No RES		25% RES		35% RES		50% RES	
			S-GEP	C-GEP	S-GEP	C-GEP	S-GEP	C-GEP	S-GEP	C-GEP
No emission limit	Installed Capacity (GW)	Nuclear	33.60	32.20	23.80	2.80	19.60	0.00	12.60	0.00
		Fossil Coal	16.50	22.00	15.40	39.60	13.20	37.40	11.00	28.60
		Fossil CCGT	15.40	18.15	13.20	17.05	12.65	18.70	10.45	19.80
		Fossil OCGT	14.04	13.23	17.28	21.06	17.01	22.41	18.09	25.65
		On-Shore Wind	7.60	0.08	56.96	54.48	79.76	75.20	113.92	108.24
		PV-Solar	0.00	0.06	0.00	0.06	0.00	3.12	0.00	18.00
	Total RES Installed Capacity [GW]		7.60	0.14	56.96	54.54	79.76	78.32	113.92	126.24
	Total Installed Capacity [GW]		87.14	85.72	126.64	135.05	142.22	156.83	166.06	200.29
	Load Not Served [%]		0.12%	0.01%	0.61%	0.01%	1.21%	0.02%	1.62%	0.02%
	RES Shedding [%]		0.00%	0.00%	2.31%	0.44%	5.89%	2.48%	12.59%	9.56%
	Carbon Emission [Mtons]		1379.60	1699.93	1177.23	2920.81	1074.35	2648.64	1007.95	1876.63
	Total Cost (excluding LNS) [B€]		313.00	310.59	354.19	359.68	375.28	383.58	409.32	435.14
75% emission limit	Installed Capacity (GW)	Nuclear	37.80	37.80	28.00	11.20	22.40	8.40	15.40	4.20
		Fossil Coal	12.10	17.60	11.00	28.60	8.80	27.50	7.70	16.50
		Fossil CCGT	15.40	16.50	13.20	19.80	14.30	19.80	11.00	28.05
		Fossil OCGT	14.31	14.04	17.28	21.33	17.01	22.95	18.09	25.11
		On-Shore Wind	7.52	0.08	56.96	54.56	79.76	74.88	113.92	107.44
		PV-Solar	0.06	0.06	0.00	0.06	0.00	3.84	0.00	19.02
	Total RES Installed Capacity [GW]		7.58	0.14	56.96	54.62	79.76	78.72	113.92	126.46
	Total Installed Capacity [GW]		87.19	86.08	126.44	135.55	142.27	157.37	166.11	200.32
	Load Not Served [%]		0.11%	0.01%	1.19%	0.02%	2.71%	0.02%	2.71%	0.03%
	RES Shedding [%]		0.00%	0.00%	2.81%	0.91%	6.25%	3.41%	13.06%	9.70%
	Carbon Emission [Mtons]		1047.78	1272.76	890.20	2180.01	857.71	1966.52	831.14	1407.10
	Total Cost (excluding LNS) [B€]		313.63	311.11	355.75	360.35	377.05	385.04	411.22	439.54
50% emission limit	Installed Capacity (GW)	Nuclear	40.60	43.40	30.80	22.40	26.60	18.20	18.20	12.60
		Fossil Coal	5.50	12.10	6.60	20.90	5.50	19.80	4.40	9.90
		Fossil CCGT	18.70	19.80	16.50	15.95	13.20	17.60	11.55	26.40
		Fossil OCGT	14.85	10.80	15.66	21.06	17.28	22.68	17.82	25.11
		On-Shore Wind	7.52	0.16	56.96	54.16	79.76	74.00	113.92	106.40
		PV-Solar	0.06	0.00	0.00	0.06	0.00	4.92	0.00	20.64
	Total RES Installed Capacity [GW]		7.58	0.16	56.96	54.32	79.76	78.92	113.92	127.04
	Total Installed Capacity [GW]		87.23	86.26	126.52	135.07	142.34	157.20	165.89	201.05
	Load Not Served [%]		0.11%	0.02%	0.60%	0.02%	1.19%	0.02%	2.70%	0.01%
	RES Shedding [%]		0.00%	0.00%	3.04%	1.77%	6.72%	4.47%	13.47%	11.34%
	Carbon Emission [Mtons]		737.05	849.79	670.82	1392.25	631.64	1323.82	660.86	937.32
	Total Cost (excluding LNS) [B€]		315.71	312.59	356.99	361.39	379.31	387.85	413.05	442.17

Let us now analyze how increased RES penetration and stringent emission limit policies impact the operational flexibility of the capacity expansion plans. The operational flexibility metrics values for all cases considered are summarized in Table (5)

For the upwards ramping requirements, the results show that the S-GEP plans become significantly short on flexibility as higher percentages of RES penetrate the system. A linear and steep increasing trend of the flexibility shortage, reaching an IRRE+ of up to 47% (for

the 50% RES case), represents a failure to answer to almost half of the number of times the system is expected to provide upwards flexibility. The EFS+ similarly reaches multiples of its value for the plan with lower RES penetrations (e.g. EFS value of 8157.30 MW compared to 2402.85 MW with 99% confidence, for the 50% and 0% RES cases, respectively). For the C-GEP plans, the different metrics indicate very low expected shortages compared to the S-GEP ones. The IRRE+ does not exceed 2.20% for all cases considered and remains almost constant at an average of 1.30%. On the other hand, the EFS+ does not exceed a comparatively smaller value up to the 99% confidence, for all cases considered.

For the downwards ramping requirements, as with the base case, the results are much less significant, with no shortage expected in most of the cases. This is reasonably justified since we consider a single-region planning where as a consequence of considering all generation units sitting at the same region, at any given moment, enough generation units are online and can reduce their production to answer to downward ramps. It is still seen through the IRRE- metric results that systems with very large RES presence would exhibit some flexibility shortage. Generally, it should be noted that the downwards flexibility shortage would become more relevant considering multi-regional planning, since the available downwards resources will be limited to those belonging to the same region.

It is shown that the flexibility shortage of the C-GEP plans remain low and almost constant across all the different cases considered, while that of the S-GEP plans are much more affected by the RES penetration levels than by carbon emission limits. The consistently low C-CEP shortage values do not only indicate this model superior adequacy in accounting for the different RES and carbon requirements, but that it is also able to fully cope to the variations in the different policy requirements, while ensuring adequate operational flexibility levels.

Table 5: Results of the operational flexibility metrics for the plans obtained through the S-GEP and C-GEP models for the range of RES penetration and carbon emission limits considered (worse performance highlighted).

			No RES		25% RES		35% RES		50% RES	
			S-GEP	C-GEP	S-GEP	C-GEP	S-GEP	C-GEP	S-GEP	C-GEP
No emission limit	IRRE+ (% of upwards ramps)		7.38%	2.20%	16.13%	1.20%	26.74%	1.12%	46.71%	1.13%
	EFS+ (MW)	EFS+ (95%)	512.70	90.53	1681.61	34.37	3118.14	38.76	4275.79	70.53
		EFS+ (99%)	2402.85	451.31	5781.33	171.33	8670.87	193.24	8157.30	351.60
		EFS+ (99.9%)	5212.17	3227.19	10704.63	1278.89	17876.77	1602.35	14674.80	2977.76
	IRRE- (% of downwards ramps)		0.01%	0.01%	0.01%	0.01%	0.04%	0.04%	0.23%	0.2%
	EFS- (MW)	EFS- (95%)	0.00	0.00	0.00	0.00	0.00	0.00	0.00	0.00
		EFS- (99%)	0.00	0.00	0.00	0.00	0.00	0.00	0.00	0.00
		EFS- (99.9%)	0.00	0.00	0.00	0.00	0.00	0.00	0.00	0.00
75% emission limit	IRRE+ (% of upwards ramps)		7.27%	2.15%	16.30%	1.07%	26.82%	1.02%	46.86%	1.17%
	EFS+ (MW)	EFS+ (95%)	497.39	84.57	1862.13	24.49	3128.12	35.51	4782.05	77.56
		EFS+ (99%)	2345.28	421.59	6587.33	122.06	8725.54	177.04	8983.71	386.65
		EFS+ (99.9%)	5117.10	3061.18	13561.78	1049.74	19269.63	1521.26	15706.40	3169.95
	IRRE- (% of downwards ramps)		0.01%	0.01%	0.01%	0.01%	0.04%	0.04%	0.23%	0.22%
	EFS- (MW)	EFS- (95%)	0.00	0.00	0.00	0.00	0.00	0.00	0.00	0.00
		EFS- (99%)	0.00	0.00	0.00	0.00	0.00	0.00	0.00	0.00
		EFS- (99.9%)	0.00	0.00	0.00	0.00	0.00	0.00	0.00	0.00
50% emission limit	IRRE+ (% of upwards ramps)		7.24%	2.04%	16.43%	1.37%	27.34%	1.43%	47.56%	1.23%
	EFS+ (MW)	EFS+ (95%)	484.50	75.20	1927.50	37.60	3586.40	179.40	5107.20	132.00
		EFS+ (99%)	2293.33	374.74	6702.66	187.55	9670.93	894.45	9969.54	658.18
		EFS+ (99.9%)	5069.55	2963.69	14665.06	1359.96	20659.63	5378.26	16145.05	3692.00
	IRRE- (% of downwards ramps)		0.01%	0.01%	0.01%	0.01%	0.05%	0.03%	0.22%	0.19%
	EFS- (MW)	EFS- (95%)	0.00	0.00	0.00	0.00	0.00	0.00	0.00	0.00
		EFS- (99%)	0.00	0.00	0.00	0.00	0.00	0.00	0.00	0.00
		EFS- (99.9%)	0.00	0.00	0.00	0.00	0.00	0.00	0.00	0.00

These results are consistent with those of the other studies reviewed. Most notably, in Palmintier and Webster (2016) where an overall similar investigation was conducted to compare two model types similar to those presented in this work. Their investigation over a range of RES and carbon levels revealed the same trends in the capacity mixes obtained, most notably, that with higher RES penetration, the mix shifts to include more units with faster dynamic properties (typically fossil peaking units). They also showed that carbon emission can be underestimated by 30-60% by planning models that do not consider short-term system representation. However, they considered only a single-period optimization problem with wind penetration as an exogenous parameter, and did not consider quantitative metrics for the operational flexibility assessment. The multi-period planning considered here allows more realistic planning paradigms, where investment decisions can be optimally taken at different periods, and allows a wide variation in the system parameters at the

different periods (see for example the wide spectrum of inter-temporal load variations of the four weeks sampled per year in Appendix C). Moreover, it is observed in the results, that although the resulting capacity mixes give an indication of the flexibility levels of the plans obtained, they do not capture to what extent these plans are short on operational flexibility. Which becomes more clear when suitable quantitative metrics are used, as shown in these results.

B. Exploring the effect of fuel cost variation on operational flexibility

The investment plans obtained are evidently dependent on the set of system parameters initially chosen. Since we consider a deterministic problem, the variation in those parameters could admittedly alter the results obtained, most notably, the uncertainties regarding fuel costs and load evolution trend. We, therefore, opt for exploring selected scenarios representing a wide variation in those parameters, and investigating their effect on the operational flexibility levels of the plans obtained. In this section two scenarios of fuel costs (coal and natural gas costs) are explored: 50% increase and 50% decrease, to cover a wide variation of the base case, and consistent with the percentages considered in the IEA report for sensitivity analysis (IEA/NEA, 2015). For clarity, only the results of the C-GEP model are reported for the median 35% RES penetration level. However, all emission limit scenarios are investigated, since it is reasonable to assume that fuel costs could have a higher impact on the plans obtained when combined with stringent emission limits.

The installed capacities for all fuel cost and emission limit scenarios are illustrated in Figure (3). For the highest fuel cost scenario, much of the coal and -to a lesser extent- CCGT capacities are substituted by the less emitting nuclear units, more so as tighter emission limits are enforced. For the lower prices, the coal capacity is still substituted, but this time by the peaking CCGT and OCGT units. The lower emission requirements are attained through progressive substitution of fossil units by nuclear ones, as can be observed within each fuel cost scenario. The total installed capacity across all scenarios, however, remain constant.

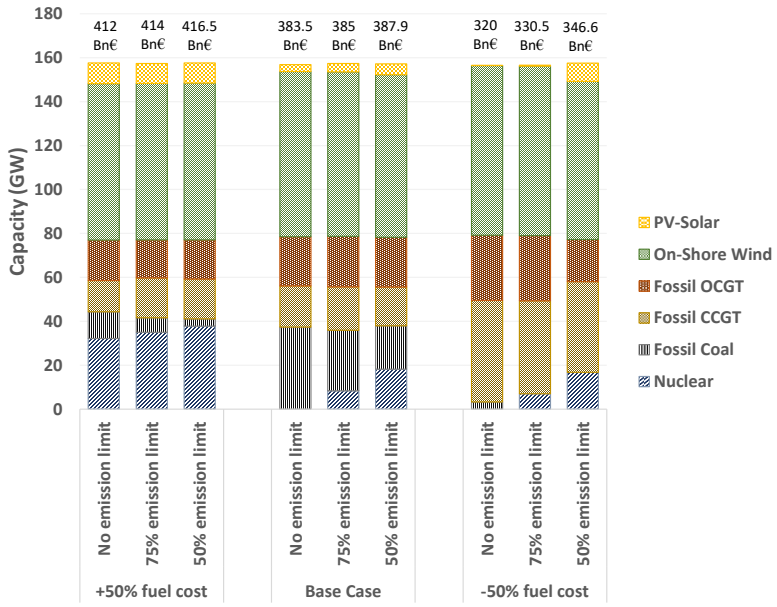

Figure 3: Total installed capacity as given by the C-GEP model under 35% RES penetration for the different fuel cost scenarios

In terms of operational flexibility, Figures (4a) and (4b) illustrate the results for the IRRE+ and EFS+, respectively. As can be expected, plans obtained under the highest fuel cost have the highest expectation of upwards flexibility shortages. This is because much of the fossil units, which possess better dynamic properties, are replaced by the less flexible nuclear ones. The opposite is observed for the plans obtained at the lowest fuel cost driven by the higher capacities of those peaking units. Notice, again, that despite this significant variation in the capacity mix across the different fuel scenarios, the IRRE of the integrated C-GEP model plans did not exceed 2.05% of the total number of upwards ramps, with a quasi-linear decreasing trend as a function of less stringent emission limits and decreasing fuel costs. This remains a very small percentage point relative to any shortage value observed for the S-GEP model under RES penetrations. The EFS+ confirms the trends observed using the IRRE metric, however, at the highest fuel cost scenario it signaled a relatively high shortage expectations that could go up to the order of several GWs at the 99% confidence level. Such a magnitude is significant and would be important to account for, and highlights the complementarity of the two measurement approaches for giving an

accurate assessment.

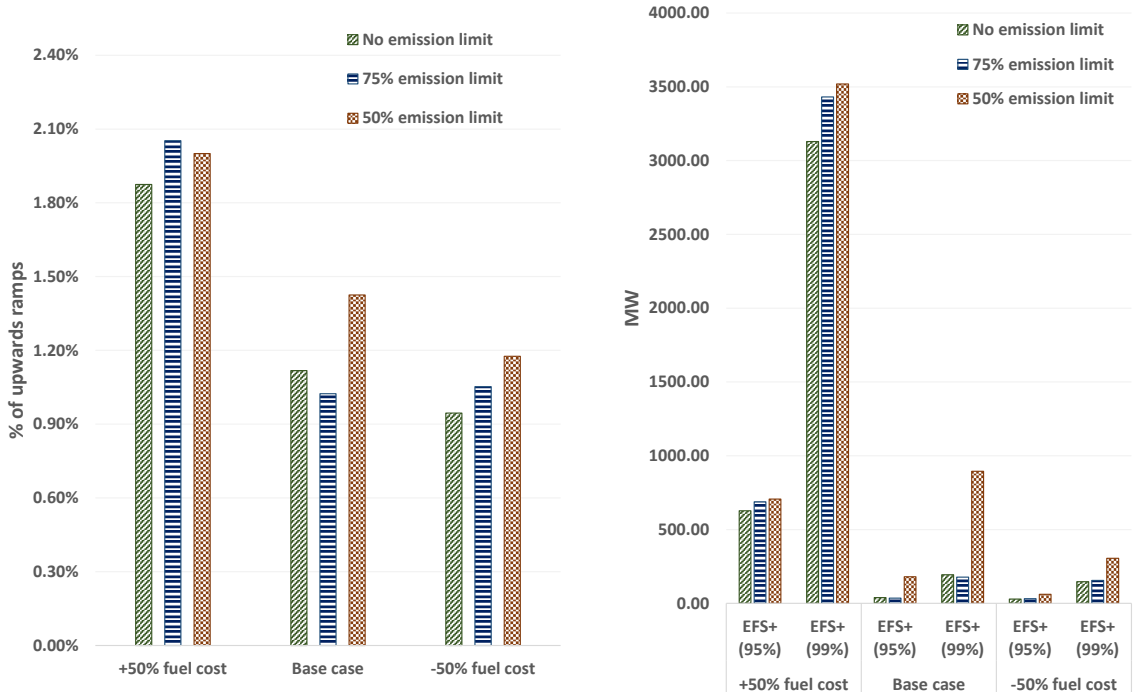

(a) IRRE+ (b) EFS+

Figure 4: Results of operational flexibility assessment on the plans obtained through the C-GEP model under 35% RES penetration and for the different fuel cost scenarios

C. Exploring the effect of load evolution on operational flexibility

The load evolution trends could be another source of influence on the plans obtained. In this respect, in their 2016 "Generation Adequacy Report", RTE (2016) presented future load projections for France and Europe, with high and low growth scenarios of roughly +2% and -1%, respectively, accounting for all different sectors. For the purpose of sensitivity analysis, for the high an low load scenarios, we have amplified these values considering a +20% and a -10% load growth starting of the fifth year of the planning horizon. The negative scenario being a proxy for stringent energy efficiency driven policies. For clarity, only the results of the C-GEP model are reported for the median 35% RES penetration level and for the no emission limit policy. It should also be noted that no changes are assumed for the hourly load patterns compared to the previous cases considered.

The total power generation per technology and per load evolution scenario is illustrated in Figure (5). The Figure shows that, overall, there are no changes in the capacity mixes obtained, but that only the total capacities and production quantities vary per technology. Naturally, the installed capacities and power generation decrease as the total system load decreases. The reduction is mostly in the RES technologies amounting to more than 50% of the total generation decrease across scenarios. This can be explained through two effects: lower load means that less RES is required to satisfy the 35% penetration requirement, and it is more cost efficient (subject to the given assumptions) to reduce the RES levels than to answer to the increased net load variability by cycling thermal units.

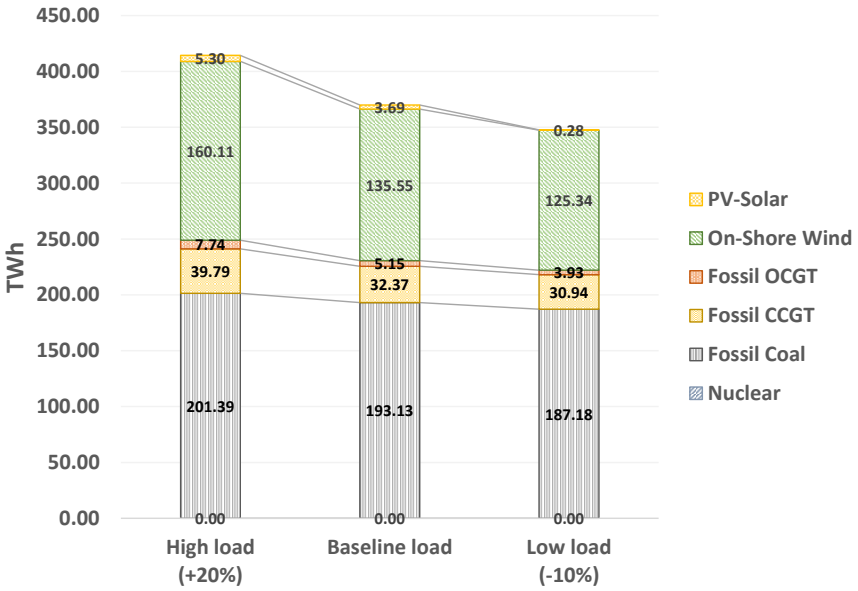

Figure 5: Total energy production per technology for the plans obtained by the C-GEP model under 35% RES penetration for the different load growth scenarios

Regarding how the load evolution trend affects the obtained plans, Table (6a) summarizes the results of some of the performance measures previously considered. Overall, a gradual decreasing trend can be observed in all measurements with respect to the decreasing load scenario. This is also true for the operational flexibility results reported in Table (6b). While the absolute difference in those results would be important to consider for actual system planning, the linear gradual trend found suggests that the overall load

evolution exhibits a less significant effect on the operational flexibility of the plans than the variations in the inter-temporal load patterns.

Table 6: Results of different performance measures and operational flexibility metrics for the plans obtained through the C-GEP models under 35% RES penetration for the different load growth scenarios

(a) Generic performance measures results

	High load (+20%)	Baseline load	Low load (-10%)
Total RES Installed Capacity [GW]	94.24	78.32	69.6
Total Installed Capacity [GW]	188.52	156.83	142.15
Load Not Served [% of total load]	0.02%	0.02%	0.02%
RES shedding [% of total RES]	3.43%	2.48%	2.25%
Carbon Emission [Mtons]	2818.70	2648.64	2555.18
Total Cost [Bn€]	439.67	383.58	357.42%

(b) Operational flexibility metrics results

		High load (+20%)	Baseline load	Low load (-10%)
IRRE+ [% of upwards ramps]		1.16%	1.12%	1.05%
EFS+ [MW]	**EFS+ [95%]**	51.10	38.76	32.30
	EFS+ [99%]	254.70	193.24	161.10
IRRE- [% of downwards ramps]		0.08%	0.04%	0.04%
EFS- [MW]	**EFS- [95%]**	0.00	0.00	0.00
	EFS- [99%]	0.00	0.00	0.00

V. Conclusions

In this work, an integrated framework for the quantitative assessment of operational flexibility in power systems planning has been presented and a realistic size case study has been investigated under several scenarios of renewable energy sources penetration levels and carbon reduction targets. Moreover, an investigation of the effect of varying the fuel costs and load growth has been conducted to comprehensively identify the most significant parameters that can affect the system operational flexibility.

The application of the framework to the case studies has shown its ability to provide transparent and objective results for obtaining and assessing different expansion plans across a wide range of policy requirements. The study has also allowed to highlight the importance of integrating short-term technical constraints and chronological load patterns, within long-term planning models and especially under significant renewable energy penetration levels.

Through the analysis of the results of the case studies considered, the following general conclusions can be drawn:

- The results confirm those presented in other works and, most notably, that neglecting short-term constraints within long-term planning leads to an underestimation of the investment required in peaking fossil units, unrealistic production schedules with high amounts of load not served and an underestimation of carbon emissions.

- Insights were gained by employing quantitative flexibility metrics for the assessment, most notably that expansion plans obtained through the integrated model are robust to the different renewable energy penetration and emission scenario realizations, in terms of flexibility shortage, i.e., they maintain a constant low shortage level regardless of the different requirements imposed.

- On the other hand, flexibility-neglecting generation expansion planning models have shown a linear and significant trend of flexibility shortage with respect to the different renewable energy sources penetration requirements, enough to offset any computational advantage they have when such requirements are binding.

- The complementarity of the two metrics considered, with regards to the frequency of flexibility shortage and its magnitude, is highlighted. It is shown that the sensitivity of one with respect to the different scenarios can be more significant than the other, which is important to consider for real applications.

- Moreover, the results emphasize the importance of the use of suitable quantitative metrics for operational flexibility assessment, as opposed to relying on other generic indicators, such as the generation mix or system costs, which are not capable of reflecting the true flexibility levels of the obtained plans.

Finally, a limitation of the presented work lies in the mixed integer linear optimization models considered. Indeed, the economic planning parameters and the technical behavior of energy generation are affected by nonlinear conditions. For instance, production costs and ramping rates are nonlinear functions of the variations in partial-load levels, while start-up costs and times are nonlinear functions of shut-down duration. These conditions

become particularly relevant when short-term capabilities and operational flexibility are considered in the model. In this regard, future work will be devoted to the extension of the optimization model for accounting of nonlinearities in the system. Moreover, the model can be further extended by considering muti-regional planning, network representation and the uncertainties in the load and renewable energy generation.

VI. References

References

Hadi Sadeghi, Masoud Rashidinejad, and Amir Abdollahi. A comprehensive sequential review study through the generation expansion planning. *Renewable and Sustainable Energy Reviews*, 67:1369–1394, 2017.

Vishwamitra Oree, Sayed Z. Sayed Hassen, and Peter J. Fleming. Generation expansion planning optimisation with renewable energy integration: A review. *Renewable and Sustainable Energy Reviews*, 69:790 – 803, 2017. ISSN 1364-0321.

Aakil M. Caunhye and Michel-Alexandre Cardin. An approach based on robust optimization and decision rules for analyzing real options in engineering systems design. *IISE Transactions*, 49(8):753–767, 2017.

European Council. Directive 2009/28/ec of the european parliament and of the council of 23 april 2009 on the promotion of the use of energy from renewable sources and amending and subsequently repealing directives 2001/77/ec and 2003/30/ec. http://eur-lex.europa.eu/eli/dir/2009/28/oj, 2009. (Accessed on 02-01-2017).

European Council. Proposal for a directive of the european parliament and of the council on the promotion of the use of energy from renewable sources (recast) com/2016/0767 final/2 - 2016/0382 (cod). http://eur-lex.europa.eu/legal-content/EN/ALL/?uri=CELEX:52016PC0767R(01), 2016. (Accessed on 02-01-2017).

Anne Sjoerd Brouwer, Machteld van den Broek, Ad Seebregts, and André Faaij. Operational flexibility and economics of power plants in future low-carbon power systems. *Applied Energy*, 156:107 – 128, 2015. ISSN 0306-2619.

M.L. Kubik, P.J. Coker, and J.F. Barlow. Increasing thermal plant flexibility in a high renewables power system. *Applied Energy*, 154:102 – 111, 2015. ISSN 0306-2619.

Gianluca Fulli, Marcelo Masera, Catalin Felix Covrig, Francesco Profumo, Ettore Bompard, and Tao Huang. The eu electricity security decision-analytic framework: Status and perspective developments. *Energies*, 10(4):425, 2017.

Eamonn Lannoye, Damian Flynn, and Mark O'Malley. Evaluation of power system flexibility. *IEEE Transactions on Power Systems*, 27(2):922–931, 2012.

Andreas Ulbig and Göran Andersson. Analyzing operational flexibility of electric power systems. *International Journal of Electrical Power & Energy Systems*, 72:155–164, 2015.

Vishwamitra Oree and Sayed Z. Sayed Hassen. A composite metric for assessing flexibility available in conventional generators of power systems. *Applied Energy*, 177:683–691, 2016.

Jinye Zhao, Tongxin Zheng, and Eugene Litvinov. A unified framework for defining and measuring flexibility in power system. *IEEE Transactions on Power Systems*, 31(1): 339–347, 2016.

Saleh Y. Abujarad, M.W. Mustafa, and J.J. Jamian. Recent approaches of unit commitment in the presence of intermittent renewable energy resources: A review. *Renewable and Sustainable Energy Reviews*, 70:215 – 223, 2017.

Andreas Belderbos and Erik Delarue. Accounting for flexibility in power system planning with renewables. *International Journal of Electrical Power & Energy Systems*, 71:33–41, 2015.

Bryan S. Palmintier and Mort D. Webster. Impact of operational flexibility on electricity generation planning with renewable and carbon targets. *IEEE Transactions on Sustainable Energy*, 7(2):672–684, 2016.

Manuel Welsch, Paul Deane, Mark Howells, Brian Ó Gallachóir, Fionn Rogan, Morgan Bazilian, and Hans-Holger Rogner. Incorporating flexibility requirements into long-term

energy system models–a case study on high levels of renewable electricity penetration in ireland. *Applied Energy*, 135:600–615, 2014.

Michal Wierzbowski, Wojciech Lyzwa, and Izabela Musial. Milp model for long-term energy mix planning with consideration of power system reserves. *Applied Energy*, 169:93 – 111, 2016. ISSN 0306-2619.

Nikolaos E. Koltsaklis and Michael C. Georgiadis. A multi-period, multi-regional generation expansion planning model incorporating unit commitment constraints. *Applied Energy*, 158:310–331, 2015.

Zheng Guo, Rui Cheng, Zhaofeng Xu, Pei Liu, Zhe Wang, Zheng Li, Ian Jones, and Yong Sun. A multi-region load dispatch model for the long-term optimum planning of china's electricity sector. *Applied Energy*, 185:556 – 572, 2017. ISSN 0306-2619.

Sérgio Pereira, Paula Ferreira, and AIF Vaz. Generation expansion planning with high share of renewables of variable output. *Applied Energy*, 190:1275–1288, 2017.

Bryan S. Palmintier and Mort D Webster. Heterogeneous unit clustering for efficient operational flexibility modeling. *IEEE Transactions on Power Systems*, 29(3):1089–1098, 2014.

John Maybee, Paul Randolph, and Noel Uri. Optimal step function approximations to utility load duration curves. *Engineering Optimization*, 4(2):89–93, 1979.

Fernando J De Sisternes and Mort D Webster. Optimal selection of sample weeks for approximating the net load in generation planning problems. In *Massachusetts Institute of Technology Engineering Systems Division Working Paper Series*, volume 3, pages 1–12, 2013.

Yasuhiro Yamai and Toshinao Yoshiba. Value-at-risk versus expected shortfall: A practical perspective. *Journal of Banking & Finance*, 29(4):997–1015, 2005.

RTE-France. Available at:. `http://clients.rte-france.com`, 2017. (Accessed on 20-12-2016).

IEA/NEA. Projected costs of generating electricity 2015 edition. *OECD*, 2015.

Camille Cany, Christine Mansilla, Pascal da Costa, Gilles Mathonnière, Thierry Duquesnoy, and Anne Baschwitz. Nuclear and intermittent renewables: Two compatible supply options? the case of the french power mix. *Energy Policy*, 95:135 – 146, 2016.

William E Hart, Carl Laird, Jean-Paul Watson, and David L Woodruff. *Pyomo–optimization modeling in python*, volume 67. Springer Science & Business Media, 2012.

William E Hart, Jean-Paul Watson, and David L Woodruff. Pyomo: modeling and solving mathematical programs in python. *Mathematical Programming Computation*, 3(3):219–260, 2011.

Réseau de transport d'eélectriciteé RTE. Generation adequacy report on the electricity supply-demand balance in france - 2016 edition. http://www.rte-france.com/en/article/forecast-assessment-electricity-supply-demand-balance, 2016. (Accessed on 02-12-2017).

Appendix A. Models formulation

A. Long-term GEP model with no short-term constraints

The model is formulated as a mixed integer linear program (MILP), with the main characteristics that no hourly chronological order is considered and demand is represented as load blocks derived from a load-duration curve with durations ($Dur_{y,s}$) and levels ($L_{y,s}$).

GEP objective function

The objective is the minimization of the total discounted costs over the planning horizon. Equation (A.1) represents the total investment costs in new units, equation (A.2) represents the total production costs calculated on the basis of the yearly load-duration curves, and equation (A.3) represents the fixed operation and maintenance (O&M) costs:

$$\min_{cost} \sum_{y \in Y} (1 + DR)^{-y} \cdot \sum_{i \in I} C_i^{inv} \cdot P_i^{max} \cdot q_{i,y} \tag{A.1}$$

$$+\sum_{y\in Y}(1+DR)^{-y}\cdot\sum_{s\in S}Dur_{y,s}\cdot\left[\sum_{i\in I}\left(C_{i,y}^{marginal}\cdot p_{i,y,s}\right)+C^{lns}\cdot lns_{y,s}\right] \tag{A.2}$$

$$+\sum_{y\in Y}(1+DR)^{-y}\cdot\sum_{i\in I}C_{i,y}^{fom}\cdot P_i^{max}\cdot\sum_{l=1}^{y}q_{i,l} \tag{A.3}$$

GEP constraints

1. Units commissioning and construction time:

$$x_{i,y}=\sum_{l=1}^{y}q_{i,l-T_i^{const}+1}\qquad\forall i\in I^{new},y\in Y \tag{A.4}$$

2. Annual budget constraint:

$$\sum_{y\in Y}q_{i,y}\leq I_i^{max}\qquad\forall i\in I^{new} \tag{A.5}$$

3. Lifetime of new units:

$$\sum_{\tau=y-T_i^{life}+1}^{y}q_{i,\tau}=x_{i,y}\qquad\forall i\in I^{new},y\in Y \tag{A.6}$$

4. Supply-demand balance constraint:

$$Dur_{y,s}\cdot\left(\sum_{i\in I}p_{i,y,s}+lns_{y,s}\right)=Dur_{y,s}\cdot L_{y,s}\qquad\forall s\in S,y\in Y \tag{A.7}$$

5. Maximum generation output levels:

$$p_{i,y,s}\leq(1-EFOR_i)\cdot P_i^{max}\cdot x_{i,y}\qquad\forall i\in I^{thermal},s\in S,y\in Y \tag{A.8}$$

6. Adequacy reserve margin:

$$\sum_{i\in I}(P_i^{max}\cdot x_{i,y})\geq\left(1+r^{min}\right)\cdot\max_{s}(L_{y,s}),\qquad\forall y\in Y \tag{A.9}$$

7. Minimum annual renewable penetration:

$$\sum_{i\in I^{res}}\sum_{s\in S}(Dur_{y,s}\cdot p_{i,y,s})\geq Pen_y^{level}\cdot\sum_{s\in S}(Dur_{y,s}\cdot L_{y,s}),\qquad\forall y\in[Y^{res},Y^{end}] \tag{A.10}$$

8. Renewable energy production: RES production is typically represented through an hourly availability or hourly capacity factor (CF). Since in the S-GEP problem no chronological hourly representation is considered, an approximation method is used

to obtain what we refer to as the RES capacity factor duration curve (RES-CFDC), described in details in Appendix B:

$$Dur_{y,s} \cdot p_{i,y,s} \leq x_{i,y} \cdot P_i^{max} \cdot Dur_{y,s} \cdot CF_{i,y,s} \quad \forall i \in I^{res}, s \in S, y \in Y \tag{A.11}$$

9. Allowable emission:

$$\sum_{i \in I} \left(E_i \cdot \sum_{s \in S} (Dur_{y,s} \cdot p_{i,y,s}) \right) \leq E_y^{max}, \qquad \forall y \in Y \tag{A.12}$$

B. Short-term operational model with no design variables (UC)

For the UC model, all the commissioning decisions are considered to have been taken beforehand (from the GEP model) and the model seeks only to find the optimal short-term system operation.

UC objective function

The objective is the minimization of the total discounted operating costs of the systems, including variable production cost, start-up cost and LNS cost:

$$\min_{cost} \sum_{y \in Y} (1 + DR)^{-y} \cdot \sum_{j \in J} \left[\sum_{i \in I} \left(C_{i,y}^{marginal} \cdot p_{i,y,j} + C_i^s \cdot z_{i,y,j} \right) + C^{lns} \cdot lns_{y,j} \right] \tag{A.13}$$

UC constraints

1. Only units commissioned can be operated: this constraint represents the link between the long-term investment and the operating decisions:

$$u_{i,y,j} \leq x_{i,y} \qquad \forall i \in I^{thermal}, j \in J, y \in Y \tag{A.14}$$

2. Supply-demand balance constraint:

$$\sum_{i \in I} p_{i,y,j} + lns_{y,j} = L_{y,j} \qquad \forall j \in J, y \in Y \tag{A.15}$$

3. Unit-commitment constraint:

$$u_{i,y,j} - u_{i,y,j-1} = z_{i,y,j} - v_{i,y,j} \qquad \forall i \in I^{th}, j \in J/\{1\}, y \in Y \tag{A.16}$$

4. Minimum up-time (A.17) and down-time (A.18) of generation units:

$$u_{i,y,j} \geq \sum_{\tau \geq j - M_i^u}^{j} z_{i,y,\tau} \qquad \forall i \in I^{th}, j \in J, y \in Y \tag{A.17}$$

$$x_{i,y} - u_{i,y,j} \geq \sum_{\tau \geq j - M_i^d}^{j} v_{i,y,\tau} \qquad \forall i \in I^{th}, j \in J, y \in Y \tag{A.18}$$

5. Upwards (A.19) and downwards (A.20) ramping capabilities of generation units:

$$p_{i,y,j} - p_{i,y,j-1} \leq u_{i,y,j-1} \cdot R_i^{Umax} + z_{i,y,j} \cdot P_i^{start} \qquad \forall i \in I^{th}, j \in J/\{1\}, y \in Y \tag{A.19}$$

$$p_{i,y,j-1} - p_{i,y,j} \leq u_{i,y,j-1} \cdot R_i^{Dmax} \quad \forall i \in I^{th}, j \in J/\{1\}, y \in Y \tag{A.20}$$

6. Maximum (A.21) and minimum (A.22) output levels of generation units:

$$p_{i,y,j} + pr_{i,y,j} + sr_{i,y,j}^{up} \leq (1 - EFOR_i) \cdot P_i^{max} \cdot u_{i,y,j} \qquad \forall i \in I^{th}, j \in J, y \in Y \tag{A.21}$$

$$p_{i,y,j} \geq u_{i,y,j} \cdot P_i^{min} + sr_{i,y,j}^{dn} \qquad \forall i \in I^{th}, j \in J, y \in Y \tag{A.22}$$

7. Operating reserves: three types of operating reserves are considered, according to a defined percentage of hourly load and of renewable generation: those are primary reserve (A.23), secondary upwards reserve (A.24), and secondary downwards reserve (A.25):

$$\sum_{i \in I^{th}} pr_{i,y,j} \geq Prr \cdot L_{y,j} \qquad \forall j \in J, y \in Y \tag{A.23}$$

$$\sum_{i \in I^{th}} sr_{i,y,j}^{up} \geq Srr^{up} \cdot L_{y,j} + \sum_{i \in I^{res}} (a^{res} \cdot p_{i,y,j}) \qquad \forall j \in J, y \in Y \tag{A.24}$$

$$\sum_{i \in I^{th}} sr_{i,y,j}^{dn} \geq Srr^{dn} \cdot L_{y,j} + \sum_{i \in I^{res}} (a^{res} \cdot p_{i,y,j}) \qquad \forall j \in J, y \in Y \tag{A.25}$$

8. Renewable energy production:

$$p_{i,y,j} \leq x_{i,y} \cdot P_i^{max} \cdot CF_{i,y,j} \quad \forall i \in I^{res}, j \in J, y \in Y \tag{A.26}$$

Appendix B. RES-CF approximation for the long-term GEP model

One way to approximate the RES-CF is to re-order the chronological CF values in descending order and divide them into CF-blocks, each having a level and duration. A fundamental problem with this approach is that it presumes that the highest RES-CF is concurrent with the highest load level and, analogously, the lowest RES-CF is concurrent with the lowest load level. This imposes a significant and unrealistic bias in the results. We, thus, propose to approximate the RES capacity factor duration curve (RES-CFDC) in a way that maintains the real hourly correlation between the load and the RES availability, when both chronological time-series are available.

This can be best illustrated by means of an example: consider a 6 weeks representation of hourly load and solar CF time series, such as that shown in Figure (B.6). This can be a forecasted time-series or historically monitored data. Each hourly load level corresponds to a specific solar CF for the same hour. When the load is re-ordered in descending order into a LDC, the solar-CF is re-ordered by maintaining each CF respective value relative to its original hourly load level. When the LDC is, then, approximated by a step-function to obtain average load levels and durations, the same duration blocks are used to segment and find corresponding average values for the solar CF time-series.

(a) LDC step function approximation

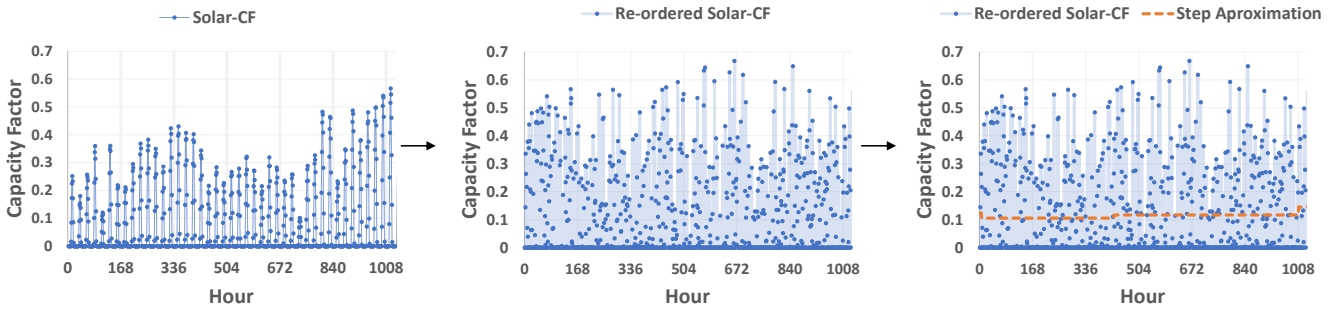

(b) Solar-CF step function approximation

Figure B.6: 6 weeks representation of load and Solar CF yearly data and their step function approximation

Appendix C. Load profiles

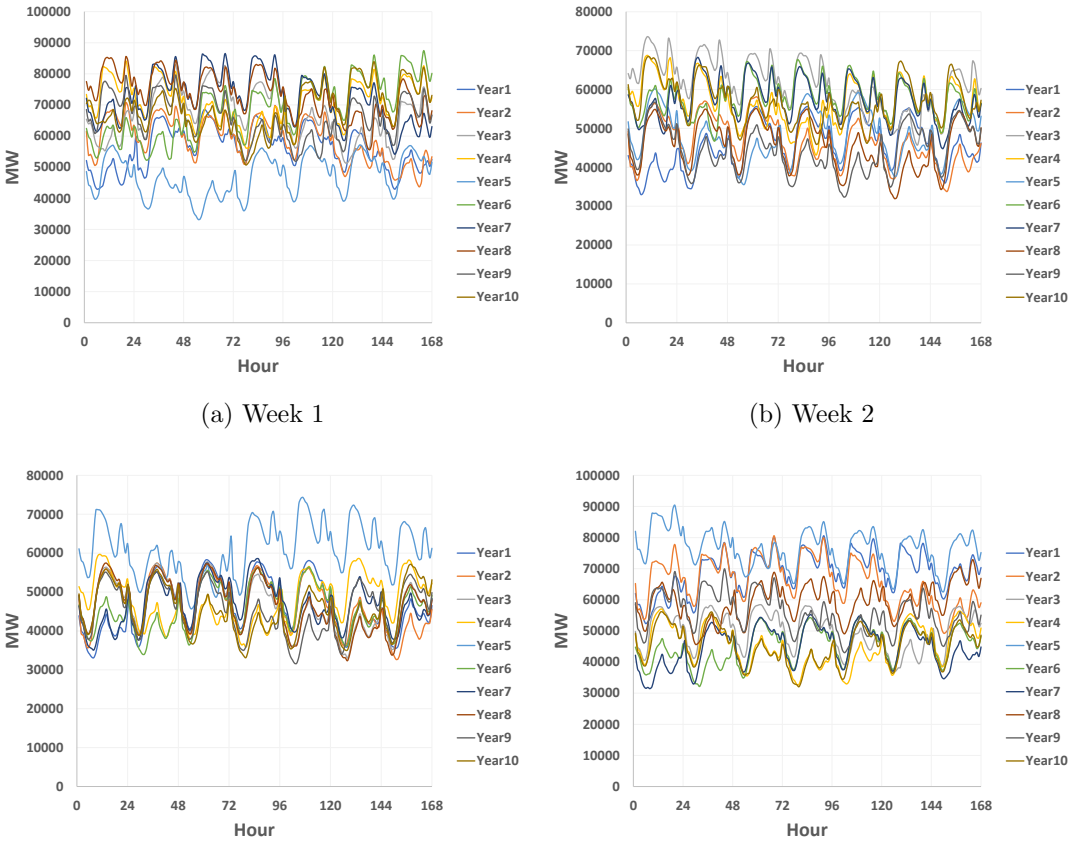

(a) Week 1

(b) Week 2

(c) Week 3

(d) Week 4

Figure C.7: Weekly load profile samples for each year of the planning horizon considered (illustration of the wide variation in inter-temporal variability considered in the study)

Paper (ii)

Abdin, I.F., Fang, Y.-P., Zio, E., (UNDER REVISION). A modeling and optimization framework for power system design with operational flexibility and resilience against extreme weather events. ***Renewable and Sustainable Energy Reviews*****.**

A modeling and optimization framework for power system design with operational flexibility and resilience against extreme weather events

Abdin, I.F.[a], Fang, Y.-P.[a], Zio, E.[b,c,*]

[a] *Laboratoire Genie Industriel, CentraleSupélec, Université Paris-Saclay*
3 Rue Joliot Curie, 91190 Gif-sur-Yvette, France.
Chair Systems Science and the Energy Challenge, Fondation Electricité de France (EDF)
[b] *Mines ParisTech, PSL Research University, CRC, Sophia Antipolis, France*
[c] *Department of Energy, Politecnico di Milano, Italy*

Abstract

Operational flexibility is an integral part of the design of power systems with a high share of renewable energy sources. Resilience against severe weather is also becoming an important concern. In this paper, we propose a comprehensive framework for power systems planning which considers both flexibility and resilience against extreme weather events. A set of piece-wise linear models are developed to calculate the impact of extreme heat waves and drought events on the performance of the power generation units and on the system load. We analyze the results obtained on a case study under real future climate projections from the Coupled Model Intercomparison Project phase 5 and compare them to those from conventional planning methods.

Highlights

- A quantitative modeling framework for extreme heat wave and drought events
- An optimization model for resilient power system design against extreme weather impact

*Corresponding author
Email addresses: islam.abdin@centralesupelec.fr (Abdin, I.F.), yiping.fang@centralesupelec.fr (Fang, Y.-P.), enrico.zio@polimi.it (Zio, E.)

- High shares of renewables improve the system resilience against extreme heat wave events
- Investigation of the interaction between the flexibility and resilience of power systems

Keywords

Power system design; renewable energy penetration; operational flexibility; extreme weather events; power system resilience

Nomenclature

Abbreviations

CF	Capacity Factor
CLC	Closed-Loop Cooling
CMIP5	Coupled Model Intercomparison Project phase 5
CP	Conventional Planning
EAC	Equivalent Annual Cost
EFS	Expected Flexibility Shortfall
HUA	Hourly Unit Availability
IGEP	Integrated Generation Expansion Planning
IRES	Intermittent Renewable Energy Sources
LNS	Load Not Served
MILP	Mixed Integer Linear Programming
O&M	Operation and Maintenance
OTC	Once-Through Cooling
PV	Photo Voltaic
RCP	Representative Concentration Pathway
RP	Resilient Planning
VaR	Value at Risk

Indexes:

i	index of power plant cluster
j	index of sub-periods (hours)
w	index of sub-periods (weeks)
y	index of planning year

Sets:

I	set of power plant per technologies
I^{new}	subset of new power plants technologies available
I^{res}	subset of renewable energy units
I^{th}	subset of thermal and nuclear units
T	set of hourly sub-periods
W	set of weekly sub-periods
Y	set of years in the planning horizon

Parameters:

C_i^{inv}	investment cost of unit i (M€)
C^{lns}	cost of load not served (€/ MWh)
$C_{i,y}^{marg}$	marginal cost of power plant i including the variable O&M and CO_2 costs, considering inflation (€/ MWh)
C_i^{OM}	fixed O&M costs of power plant i (€)
C_i^{stup}	start-up cost of power plant i (€)
$Capt_i^{max}$	maximum capacity of power plant in technology cluster i (MW)
$CF_{i,y,w,t}$	capacity factor of renewable energy sources $i \in I^{res}$ during hourly sub-period t of week w, of year y (%)
DR_y	discount rate for year y (%)
$EFOR_i$	Expected forced outage rate of power plant i (%)
$Load_{y,w,t}$	system load at hour j, week w in year y (MWh)
$Maxbudget_y$	maximum budget available for investment in generation expansion for year y (in M€)
M_i^{up}	minimum up-time for power plant $i \in I^{th}$ (hours)
M_i^{dn}	minimum down-time of power plant $i \in I^{th}$ (hours)
P_i^{min}	minimum stable power output of power plant in technology cluster $i \in I^{th}$ (MW/h)
$Penlevel$	renewable penetration level requirement (%)
Pwr_i^{start}	maximum output of power plant $i \in I^{th}$ when started (MW)
$Resv^{min}$	minimum planning reserve margin (MW)
Rmp_i^{Dnmax}	maximum downwards ramping capability of power plant $i \in I^{th}$ (MW/h)
Rmp_i^{Upmax}	maximum upwards ramping capability of power plant $i \in I^{th}$ (MW/h)
T_i^{const}	construction time of power plant i (years)
T_i^{life}	expected life-time of new power plant i (years)

Continuous Variables:

$lns_{y,w,t}$	load not served at hourly sub-period t of week w, during year y (MW)
$pwrgen_{i,y,w,t}$	energy output of power plant i at hourly sub-period t of week w, during year y (MWh)
$shtdn_{i,y,w,t}$	shut-down decision of unit i during hourly sub-period t of week w in year y

Discrete Variables:

$avail\_unt_{i,y}$	availability (commissioning) state of power plant i in year y
$inv_{i,y}$	commissioning decision of power plant i in year y
$unt\_cmt_{i,y,w,t}$	commitment status of power plant i during hourly sub-period t of week w in year y
$strtup_{i,y,w,t}$	start-up decision of power plant i during hourly sub-period t of week w in year y

1. Introduction

Reliability and security of supply are central considerations for power systems design, and are key to regional and global energy-related policies [1]. Methods for power systems planning have typically ensured key reliability aspects under normal operating conditions and in response to anticipated demand variability and supply disruptions, e.g. due to errors in load forecasts and to unexpected generation units outages. Solutions have been commonly built on capacity adequacy and operating reserves requirements.

Recent objectives of environmental sustainability and the threats coming from severe weather events are challenging in various ways the reliability requirements of power systems design:

- On one hand, low carbon power systems with a high share of intermittent renewable energy sources (IRES) are characterized by a sharp increase in inter-temporal net-load variability. The associated difficulty in anticipating short-term variations brings the need to consider *operational flexibility* as a critical design concern of future power systems [2]. Power systems operational flexibility under a large share of IRES penetration

have received attention in recent years. Various studies proposed flexibility metrics [3–6] and planning models [7–11].

- On another hand, increasingly frequent and extreme weather events, such as heat waves, droughts, floods and storms, significantly affect the operational status of power systems. Evidence of power generation disruptions due to such events highlights the fragility of the existing systems. This leads to the need of considering *resilience* in the planning of future power systems [12], most notably with respect to events such as extreme heat waves, which affect both power load and generation units. Heat waves are among the most worrying weather extremes, due to the expected increase in their frequency and severity in the 21st century [13, 14]. For example, France was particularly impacted by the 2003 summer heat wave, which caused an excess of about 15,000 deaths from 4th to 18th August directly attributable to the heat [15]. By combining peaks of extreme temperature and severe soil and hydrological droughts, this event also affected significantly the energy production sector (mainly via the cooling process of thermal power plants). These last years, numerous regions of the world experienced severe heat waves with comparable effects: Russia in 2010, Texas in 2011, Australia in 2012, India and Southern Pakistan in 2015. Therefore, it is of great importance to design the ability of the energy systems for coping with heat waves in the future.

Recent research has been dedicated to studying the impacts of extreme weather events on power systems. Rocchetta et al. [16] presents a multi-objective optimization of distributed power generation systems considering extreme wind and lightning events. Panteli et al. [17] proposes a probabilistic methodology to assess the resilience degradation of transmission networks subject to extreme wind events. In Cadini et al. [18], an extreme weather stochastic model is applied to a realistic cascading failure simulator of power grids, accounting for the operating conditions that a repair crew may encounter during an extreme weather event. The impacts of water availability on the generation capacity expansion planning is investigated in Cohen et al. [19], and the electricity sector growth is compared under different scenarios

of water rights. Shao et al. [20] proposes an integrated electricity and natural gas planning model taking into consideration the power grid resilience against storms, earthquakes and floods. Ke et al. [21] studies the potential impacts of heat waves on power grid operation, by quantifying the capacity of thermal power plants as a function of ambient temperature. Whereas most of those studies focus on evaluating the impact of extreme weather threats on the operation of power systems, there exist very few studies that incorporate resilience within the power system design problem itself.

With regards to the above, sustainable and resilient power system design calls for 1) developing integrated flexibility and resilience frameworks for future investment planning on power systems with a high share of IRES penetration and 2) assessing different strategies to mitigate the natural threats and improve system performance. With this perspective, in this work we extend a previously proposed integrated framework for flexible power systems planning [11] to include resilience against extreme weather events. In particular, we consider extreme heat waves and droughts events, and propose systematic methods for assessing their impact on the design and operation of the system. The main contributions of this work are:

- Proposing a set of piece-wise linear models to describe the impact of different scenarios of extreme heat waves and water availability on the derating of thermal power units operation, renewable generation production and system load.

- Explicitly incorporating the extreme weather impact in a modified mixed integer linear programming (MILP) power system planning model to derive adequate system investment decisions.

- Extending our previously proposed quantitative framework for operational flexibility assessment of power systems with a high share of IRES penetration (presented in [11]) to also include their resilience against extreme heat waves and drought events.

- Applying the framework to a practical sized power system planning problem with realistic future climate projections, for demonstrating the relevance of the proposed planning approach in terms of system costs and technology choices.

The rest of the paper is organized as follows. In Section (2), the piece-wise linear model for describing the impact of extreme heat waves and drought events is described and incorporated into the power system planning problem. A practical size case study generically based on the southern French power system is presented under different climate projections and IRES penetration levels in Section (3). The results shown in Section (4) quantify the impact of the climate change events from the viewpoints of system costs, flexibility and resilience of energy supply. Section (5) presents concluding remarks.

2. Methodology

Extreme heat waves affect thermal power plants by reducing their efficiency due to the derating of their cooling capabilities during the event. Load is sensitive to heat waves as it can significantly increase during periods of high temperatures due to increased air conditioning usage. The following section describes a set of piece-wise linear models to quantify these impacts and integrate them within the power system design problem.

2.1. Piece-wise linear models of the impact of extreme weather events (high temperature and water availability)

2.1.1. Basic model of thermal power plant cooling systems

Different cooling technologies exist for thermal power generation units. In the event of extreme heat waves, the impact on the different technologies can be different. Since in a power systems planning model the choice among the different cooling systems is a decision variable, it is important to model the specific attributes of each technology separately. In this study, we consider two main cooling technologies:

- Once-through Cooling (OTC) system: the heated cooling water is returned to the water source. A large volume of water from the water source is required.

- Closed-loop cooling (CLC) system: water is circulated in the cooling loop including a cooling tower, where a small portion of cooling water evaporates and is released to atmosphere. Only a small volume of water has to be withdrawn from the water source.

The required volume of cooling water V^{req} for operating a thermal power plant at its maximum capacity P^{max} is proportional to P^{max} and inversely proportional to the increase of the temperature in the cooling water ΔT [22–24], as follows:

$$V^{req} \propto \frac{P^{max}(1-\alpha)}{\Delta T} \tag{1}$$

$$\Delta T = max\left(min\left(T^{out\_max} - T^{in\_w}, \Delta T^{max}\right), 0\right) \tag{2}$$

where α is the share of waste heat released into air [%]; this share is small for OTC systems ($\alpha \to 0$) whereas it is large for CLC systems ($\alpha \to 1$); the permissible temperature increase of the cooling water ΔT is limited by: 1) the regulated maximum permissible temperature increase of the cooling water ΔT^{max}, and 2) the regulated maximum permissible temperature of the discharged cooling water T^{out_max} [22].

We can see that when $T^{in\_w} \leq T^{out\_max} - \Delta T^{max}$, the maximum permissible temperature increase of the cooling water is only limited by ΔT^{max}, and the required volume of cooling water V^{req} is, thus, a constant value ($V^{req} = V^*$) for $\Delta T = \Delta T^{max}$. However, a high value of T^{in_w} generally leads to an increase in V^{req} for operating the plant at its maximum capacity. This increase is significant for OTC systems, whereas it is moderate for CLC systems.

For thermal power plants with CLC systems, it is acceptable to assume that such plants are robust to water shortages and are independent from water availability [22, 23]. Also, the dependency to source water temperature can be neglected since any rise in the water temperature can be compensated by increasing the volume of cooling water V^{req} [23]. Instead, CLC systems are mainly affected by the temperature of cooling water circulated back to the condenser, T^{in_c}, which can be assumed to be close to air temperature [23].

2.1.2. Extreme weather event impact model

We consider extreme heat waves and drought events during summer time (JJAS, 21 June-20 September) that may force thermal power plants to reduce production owing to scarcity and high temperature of the cooling water. The intensity of the extreme weather event (ewe)

of heat wave and drought is modeled by:

$$ewe = [T_{it}, A_{it}], \forall i \in I, t \in T \tag{3}$$

where T_{it} is the hourly air temperature at plant i, from which we can calculate the related stream temperature $T_i^{in\_w}$ based on air-water interaction as follows [24]:

$$T_{it}^{in\_w} = t^{min} + \frac{t^{max} - t^{min}}{1 + e^{\gamma(t^{ip} - T_{it})}} \tag{4}$$

The parameters for the air/water temperature relationship are derived from the literature [22, 25, 26]: the minimum stream temperature is assessed to be $t^{min} = 0°C$, the maximum stream temperature to be $t^{max} = 30.4°C$, the steepest slope to be $\gamma = 0.14$ and the air temperature at the inflection point to be $t^{ip} = 16.5°C$ [27]. The parameter of the extreme weather event A_{it} represents the hourly availability (percentage) of intake cooling flow at plant i, time t and is defined by:

$$A_{it} = \frac{\min(V_{it}^{src}, V_i^{cpty})}{V_i^*} \tag{5}$$

where V_{it}^{src} is the permissible amount of water flow that can be taken from the water source at plant i at time t, V_i^{cpty} represents the water extraction capacity of the plant and V_i^* is the constant amount of the required volume of intake cooling water for plant i when the intake water temperature $T_{it}^{in\_w} \leq T^{out\_max} - \Delta T^{max}$, as previously explained in Section (2.1.1).

For thermal power plants using the OTC system, $\forall i \in I^{th\_otc}$, the ratio of P_{it}^{usable} to P_i^{max} as a function of T_{it} and A_{it} can be expressed by the following piece-wise linear equations for different ranges of T_{it}:

$$z_{it}^{ewe} = \begin{cases} P_{it}^{usable}/P_i^{max} = min(1, A_{it}), & T_{it}^{in\_w} \leq T_{health} \\ \min(1, A_i) \cdot \left[1 - \beta \cdot \left(T^{in\_w} - T_{health}\right)\right], & T_{health} \leq T_{it}^{in\_w} \leq T_{risk} \\ \min(1, A_{it}) \cdot \delta \cdot \dfrac{(T^{out\_max} - T_{it}^{in\_w})}{\Delta T^{max}}, & T_{risk} \leq T_{it}^{in\_w} \leq T_{shutdown} \\ 0, & T_{it}^{in\_w} \geq T_{shutdown} \end{cases} \tag{6}$$

where β is the efficiency degrading rate when T^{in_w} is in the range of $[T_{health}, T_{risk}]$ and T_{risk} is defined to represent the temperature when the actual maximum discharge of waste of heat

is equal to the designed value and is given by:

$$T_{risk} = T^{out\_max} - \Delta T^{max} \cdot \frac{1}{A_{it}} \tag{7}$$

Coefficient δ can be calculated based on the continuation of the piece-wise linear functions (6) at $T_{it}^{in\_w} = T_{risk}$ and is given by:

$$\delta = A_{it} + \beta \cdot \Delta T^{max} - \beta \cdot A_{it} \cdot (T^{out\_max} - T_{health}) \tag{8}$$

The above piece-wise linear equations (6) hold when $T_{risk} \geq T_{health}$, i.e., $A_i \geq \Delta T^{max}/(T^{out\_max} - T_{health})$. For the case where $T_{risk} \leq T_{health}$, i.e., $A_i \leq \Delta T^{max}/(T^{out\_max} - T_{health}) \triangleq A_{it}^{shtg}$, we can simplify the piece-wise linear functions (6) as follows:

$$z_{it}^{ewe} = \begin{cases} \min(1, A_{it}), & T_{it}^{in\_w} \leq T_{health} \\ \min(1, A_{it}) \cdot A_{it}^{shtg} \cdot \dfrac{(T^{out\_max} - T_{it}^{in\_w})}{\Delta T^{max}}, & T_{health} \leq T_{it}^{in\_w} \leq T_{shutdown} \\ 0, & T_{it}^{in\_w} \geq T_{shutdown} \end{cases} \tag{9}$$

For a thermal plant using the CLC system, $\forall i \in I^{th\_clc}$, the following piece-wise linear functions are used to describe the impact of the air temperature ($T_{it} \approx T_{it}^{in\_c}$) on the usable power capacity:

$$z_{it}^{ewe} = \begin{cases} 1, & T_{it} \leq T_{health\_air} \\ 1 - \rho \cdot (T_{it} - T_{health\_air}), & T_{it} \geq T_{health\_air} \end{cases} \tag{10}$$

For renewable generation units, wind power and solar photovoltaic (PV) systems do not require water to generate electricity and, thus, the capacity of renewable generation will not be affected largely by an extreme heat wave and drought event. To obtain the future PV and wind power potential capacity factor (CF), we use the recent CMIP5 data of high-resolution climate projections (fully described in section (3.2)), together with the wind and PV power production models proposed in the literature.

Since the wind speed at the turbine height is not a standard output of the climate projection model, we use near-surface wind speeds at 10 meters V_{10m} and assume a power-law relationship for extrapolating the vertical wind profile [28, 29]. The velocity at hub

height H is calculated as:

$$V_H = V_{10m} \cdot \left(\frac{H}{10}\right)^{\frac{1}{7}} \tag{11}$$

Then, the wind speed V_H is converted into turbine-generated electric power capacity factor z_{it}, $\forall i \in I^{res-wind}, t \in T$ using a standard power curve, described as follows:

$$\forall i \in I^{res-wind} z_i = \begin{cases} 0, & \text{if } V_H < V_l \text{ or } V_H > V_0 \\ \dfrac{V_H^3 - V_l^3}{V_R^3 - V_l^3}, & \text{if } V_l \leq V_H < V_R \\ 1, & \text{if } V_R \leq V_H < V_0 \end{cases} \tag{12}$$

where V_l, V_R and V_0 are the cut-in, rated and cut-out velocity of a wind turbine, respectively. Wind power capacity factor is calculated at the grid cell level (defined in the climate projection model) assuming a unique turbine model for all grid cells ($H = 80$ m, $V_l = 3.5$ m/s, $V_R = 12$ m/s, $V_0 = 25$m/s), as in [30, 31]

PV power generation potential depends on solar irradiance, named surface-downwelling shortwave (i.e., wavelength interval 0.2-4.0 μm) radiation (R_{sds}) in the climate models, and other atmospheric variables affecting panel efficiency, i.e., surface air temperature (Tas) and surface wind velocity (V_{10m}). The PV power generation can be expressed as [32, 33]:

$$\forall i \in I^{res-pv}, z_i = \left[1 + \gamma \ \left(T_{cell} - T^0\right)\right] \cdot \frac{R_{sds}}{R^0_{sds}} \tag{13}$$

where the upper script 0 refers to standard test conditions for which the nominal capacity of a PV device is determined as its measured power output ($R^0_{sds} = 1000$ Wm^{-2}, $T^0 = 25$°C). Parameter γ is set at -0.005°C^{-1}, considering the typical temperature efficiency of monocrystalline silicon solar panels [32]. Finally, the PV cell temperature T_{cell} is obtained as:

$$T_{cell} = c_1 + c_2 T_{as} + c_3 R_{sds} + c_4 V_{10m} \tag{14}$$

where $c_1 = 4.3$°C, $c_2 = 0.943$, $c_3 = 0.028$°Cm^{2}W^{-1} and $c_4 = $ -1.528°Csm^{-1} [32, 34].

After obtaining the grid cell level renewable (wind and PV) power capacity factors, then, the regional renewable power potentials can be obtained by averaging all the grid cell levels inside a given region.

Power demand is usually sensitive to climatic conditions. To capture this, the power demand in the extreme weather event is represented by:

$$L_t^{ewe} = l_t + C^l \cdot (\overline{T}_t - \overline{T}_t^{ref}) \tag{15}$$

where C^l is the temperature sensitivity coefficient of power load, e.g., it is around $+500MW/+1°C$ during the summer time in France [35]. Here $\overline{T}_t$ and $\overline{T}_t^{ref}$ represent the geographical average values of the projected air temperature and historical reference air temperature, respectively.

2.2. Power system planning model with short-term operational constraints

Operational flexibility in long term planning should be accounted for by considering the short-term technical constraints of the generating units, such as the unit commitment of generation units, their ramping capabilities and minimum up and down times, to name a few [11]. We refer to this class of planning models as the integrated generation expansion planning (IGEP) models, since it combines both long-term investment constraints and short-term unit commitment constraints within a single optimization. The multi-period IGEP planning model used here seeks to minimize the total discounted system cost over the whole time horizon. These costs include: annualized equivalent investment costs, fixed operation and maintenance costs, and variable operation costs of the power system (fuel cost, start-up costs and cost of load not served). The plans obtained are subject to long-term constraints including the budget limit, adequacy requirement, renewable penetration level, and short-term constraints including supply-demand balance, generation limits, unit commitment decisions, ramping limits and minimum up and down times. The model is formulated as a mixed integer linear program (MILP) considering annual long-term generation expansion planning constraints and hourly short-term unit commitment decisions.

2.2.1. Objective function

The objective is the minimization of the total discounted costs over the planning horizon. Equation (16) represents the total investment costs in new units, equation (17) represents the total production costs including start-up costs and cost of LNS, and equation (18) represents the fixed operation and maintenance (O&M) costs. It should be noted that the investment

cost considered in this model is the Equivalent Annual Cost (EAC) that is obtained by using the $AnnuityFactor_i$ calculated as: $AnnuityFactor_i = \dfrac{1-(1+DR)^{-Tlife_i}}{DR}$. This ensures the proper relationship between the annual investment and operational costs and the correct evaluation of the different investment options having different life spans $Tlife_i$

$$\min_{cost} \sum_{y \in Y} (1+DR)^{-y} \cdot AnnuityFactor_i \cdot \sum_{i \in I^{new}} C_i^{inv} \cdot Capt_i^{max} \cdot inv_{i,y} \tag{16}$$

$$+ \sum_{y \in Y} (1+DR)^{-y} \cdot \sum_{w \in W} Weight \cdot \sum_{t \in T} \Bigg[\sum_{i \in I} \left(C_{i,y}^{marg} \cdot pwrgen_{i,y,w,t} \right)$$
$$+ \sum_{i \in I^{th}} \left(C_i^{stup} \cdot stup_{i,y,w,t} \right) + C^{lns} \cdot lns_{y,w,t} \Bigg] \tag{17}$$

$$+ \sum_{y \in Y} (1+DR)^{-y} \cdot \sum_{i \in I} C_{i,y}^{OM} \cdot Capt_i^{max} \cdot \sum_{l=1}^{y} inv_{i,l} \tag{18}$$

2.2.2. Constraints

Since we consider a multi-period planning horizon, Eq. (19) keeps track of the investment decisions made in year y taking into account the construction time of the unit following:

$$avail\_unt_{i,y} = \sum_{l=1}^{y} inv_{i,l-T_i^{const}+1}, \quad \forall i \in I^{new}, y \in Y \backslash [T_i^{const} - 1] \tag{19}$$

The maximum allowable discounted investment budget is limited in Eq (20) such as:

$$(1+DR)^{-y} \cdot \sum_{i \in I^{new}} C_i^{inv} \cdot Capt_i^{max} \cdot inv_{i,y} \leq Maxbudget_y, \quad \forall y \in Y \tag{20}$$

Eq (21) ensures that the adequacy level requirement is met by ensuring enough firm capacity to satisfy a reserve margin above the maximum predicted load:

$$\sum_{i \in I^{th}} (Capt_i^{max} \cdot avail\_unt_{i,y}) \geq \left(1 + Resrv^{min}\right) \cdot \max_{w,t}(Load_{y,w,t}), \quad \forall y \in Y \tag{21}$$

The renewable penetration level required in the system is set through Eq (22):

$$\sum_{i \in I^{res}} avail\_unt_{i,y} \cdot Capt_i^{max} \geq Penlevel \cdot \sum_{i \in I} avail\_unt_{i,y} \cdot Capt_i^{max}, \quad \forall y \in Y \tag{22}$$

Eq (23) ensures the coupling between investment and operational decisions:

$$unt\_cmt_{i,y,w,t} \leq avail\_unt_{i,y} \quad \forall i \in I^{thermal}, t \in T, w \in W, y \in Y \tag{23}$$

The hourly supply and demand balance as well as the amount of LNS is constrained by Eq (24):

$$\sum_{i \in I} pwrgen_{i,y,w,t} + lns_{y,w,t} = Load_{y,w,t} \quad \forall t \in T, w \in W, y \in Y \tag{24}$$

Eq (25) constraints the hourly unit commitment decisions by the startup and shutdown decisions:

$$unt\_cmt_{i,y,w,t} - unt\_cmt_{i,y,w,t-1} = stup_{i,y,w,t} - shtdn_{i,y,w,t}, \quad \forall i \in I^{th}, t \in T/\{1\}, \\ w \in W, y \in Y \tag{25}$$

The hourly maximum and minimum production levels for thermal units are given in Eq (26) and Eq (27), respectively:

$$pwrgen_{i,y,w,t} \leq (1 - EFOR_i) \cdot Capt_i^{max} \cdot unt\_cmt_{i,y,w,t}, \quad \forall i \in I^{th}, t \in T, w \in W, y \in Y \tag{26}$$

$$pwrgen_{i,y,w,t} \geq P^{min} \cdot unt\_cmt_{i,y,w,t} \quad \forall i \in I^{th}, t \in T, w \in W, y \in Y \tag{27}$$

The renewable sources production is limited by the hourly capacity factor CF as given in Eq (28):

$$pwrgen_{i,y,w,t} \leq avail\_unt_{i,y} \cdot Capt_i^{max} \cdot CF_{i,y,w,t}, \quad \forall i \in I^{res}, t \in T, w \in W, y \in Y \tag{28}$$

Eq (29) and Eq (30) constraint the hourly upwards and downwards ramping capabilities for thermal units, respectively:

$$pwrgen_{i,y,w,t} - pwrgen_{i,y,w,t-1} \leq unt\_cmt_{i,y,w,t-1} \cdot Rmp_i^{upmax} + strtup_{i,y,w,t} \cdot Pwr_i^{start}, \\ \forall i \in I^{th}, t \in T \backslash \{1\}, w \in W, y \in Y \tag{29}$$

$$pwrgen_{i,y,w,t-1} - pwrgen_{i,y,w,t} \leq unt\_cmt_{i,y,w,t-1} \cdot Rmp_i^{Dnmax}, \\ \forall i \in I^{th}, t \in T \backslash \{1\}, w \in W, y \in Y \tag{30}$$

Finally, Eq (31) and Eq (32) ensures that the minimum allowable up and down times for thermal units are respected:

$$unt\_cmt_{i,y,w,t} \geq \sum_{\tau=t-M_i^{up}}^{t} strtup_{i,y,w,\tau} \quad \forall i \in I^{th}, t \in T \backslash [M_i^{up}], w \in W, y \in Y \tag{31}$$

$$avail\_unt_{i,y} - unt\_cmt_{i,y,w,t} \geq \sum_{\tau=t-M_i^{dn}}^{t} shtdn_{i,y,w,\tau}, \quad \forall i \in I^{th}, t \in T \backslash [M_i^{dn}], \; w \in W, y \in Y \tag{32}$$

2.2.3. Integrating resilience requirement into system design

The impact of an extreme weather event to the power generation system is measured by the decrease of the generation capacity of affected thermal and PV plants, and the increase of power demand, as given above. Then, the power generation system resilience is evaluated by a deterministic metric, which is referred to as the total load not served (LNS) during the period of the extreme weather event, and is defined as:

$$LS_{yt}^{ewe} = \left(Load_{yt}^{ewe} - \sum_{i \in I} pwrgen_{iyt}^{ewe} \right), \quad \forall y \in Y, t \in T^{ewe} \tag{33}$$

$$pwrgen_{iyt}^{ewe} \leq z_{iyt}^{ewe} \cdot Capt_i^{max} \cdot unt\_cmt_{iyt}, \quad \forall i \in I, y \in Y, t \in T^{ewe} \tag{34}$$

$$\sum_{t \in T^{ewe}} LS_{yt}^{ewe} \leq LS^{max}, \quad \forall y \in Y \tag{35}$$

where unt_cmt_{iyt} is the unit commitment state of generation units of technology i at time t in year y, and z_{iyt}^{ewe} is the efficiency factor of the generation units of technology i during the extreme weather event, calculated using the above piece-wise linear equations (6)-(14), and T^{ewe} is the total duration of the event. Equation (33) calculates the total amount of load shedding LS in each year y during the extreme weather event as the difference between the hourly demand and the total power generation from all power units. Equation (34) limits the power generation output $pwrgen$ of generation units of technology i at year y during the extreme weather event $t \in T^{ewe}$ to the efficiency factor z_{iyt}^{ewe}. Finally, constraint (35) limits

the amount of load shedding allowed during the extreme weather event LS_{yt}^{ewe} to a maximum limit LS^{max}.

It should be noted that the resilience metric used here is focused on the ability of the power system to mitigate the impact of the extreme heat wave and drought events and not on the recovery from those events. This is because in these specific extreme weather events the main action is to reduce the thermal units production levels or to shut them down completely to avoid overheating and further damages to the units, so that recovery of normal operation is immediate once weather conditions go back to normal.

2.2.4. Assessing the flexibility of the power system design

High shares of IRES production increase the inter-temporal variability of the remaining net system load. Enough available thermal units, then, need to be operational and sufficiently flexible to cope with these variations and ensure production reliability. Proper metrics are needed to evaluate the operational flexibility of the plans obtained under different weather and IRES scenarios.

In this work, we adopt the Expected Flexibility Shortfall (EFS) metric presented in [11]. This probabilistic metric takes into account detailed technical and temporal attributes of the thermal units to quantify the system ability to meet inter-temporal variations. Figure (1) shows a schematic illustration of the EFS calculation method.

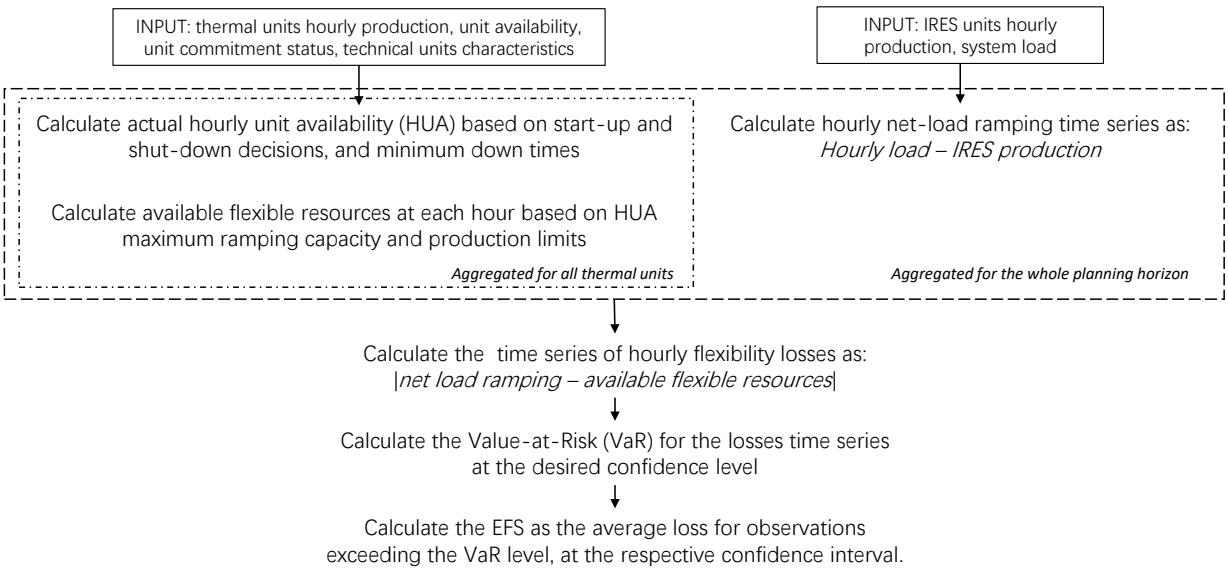

Figure 1: EFS calculation

3. Power system characteristics and climate scenarios

3.1. Power system modeling

We consider a multi-annual planning horizon representing the period between the year 2041 to 2046. Linear regression is used to obtain the system hourly load from the historical electricity load time series of France from the year 2008 to 2012 (publicly available at [36]), assuming a growth of 1% to 1.5% from the beginning to the end of the planning horizon. The cost data for the generation technologies considered for the expansion planning are based on the IEA/NEA Projected Costs of Generating Electricity report (2015) [37]; the remaining technical characteristics are assumed based on values found in the literature and are summarized in Table (1).

Table 1: Technical parameters for power generation technologies

Technology	Nuclear	Coal	CCGT	Solar-PV	On-shore Wind
Maximum Capacity per installed unit $[MW]$	1400	1100	550	60	80
Minimum stable load $[MW]$	700	550	165	0	0
Maximum upward ramping $[MWh/min]$	$0.5\%P_n$/min	$1.5\%P_n$/min	$5\%P_n$/min	/	/
Maximum downward ramping $[MWh/min]$	$0.5\%P_n$/min	$1.5\%P_n$/min	$5\%P_n$/min	/	/
Minimum up time $[hours]$	12	6	3	/	/
Minimum down time $[hours]$	24	10	5	/	/
Start-up cost [k€]	15.0	11.26	7.53	/	/

Thermal generation units can be equipped with one of two different cooling technologies, that have different cost and technical characteristics. Under normal conditions, cooling towers with recirculating water (CLC) reduce the overall efficiency of power plants by $2-5\%$ compared to once-through use of water from seas, lakes or large streams (OTC). Thus, these towers are associated with larger operational/marginal costs compared to OTC systems. Moreover, the investment costs of CLC systems are around 20% higher than those for OTC systems. Table (2) summarizes the specific technical and cost parameters of the generation units equipped with each cooling technology [23, 38, 39].

Table 2: Technical and economic characteristics for the different generation technologies

Technology $[i]$	$\beta/\rho/\ C^{pv}$ [%]	$T_{health}/T_{health\_air}/T^{ref\_pv}$ $[^\circ C]$	$T_{shutdown}$ $[^\circ C]$	T^{out_max} $[^\circ C]$	ΔT^{max} $[^\circ C]$	C_i^{inv} $[M€/MW]$	C_i^{mrgl} $[€/MWh]$
Nuclear-OTC	0.44	15	32	32	10	3.95	13.84
Nuclear-CLC	0.44	10	/	/	/	4.74	14.11
Coal-OTC	0.97	15	32	32	10	2.08	38.97
Coal-CLC	0.94	10	/	/	/	2.60	39.75
CCGT-OTC	0.31	15	32	32	10	1.02	70.16
CCGT-CLC	0.30	10	/	/	/	1.22	71.50
Solar-PV	0.50	25	/	/	/	1.5	1.71
On-Shore Wind	/	/	/	/	/	1.9	2.16

Within the optimization planning framework, the investment decisions are grouped by technology option using the unit clustering method proposed in [40]. The yearly load is optimally approximated by four representative weeks as proposed in [41] and the chronological order within each week is maintained. This is especially important for correctly capturing the operational flexibility attributes of the system while ensuring the computational tractability of the optimization problem. An additional week corresponding to the one containing the

peak summer load is, then, added to simulate the impact of the heat wave and drought events during summer time.

3.2. Climate projections data of heat wave and drought events

Historical baseline temperature as well as future temperature projections for the years 2041 to 2046 are based on data obtained from the Coupled Model Intercomparison Project (CMIP5) experiments [42]. Similarly, wind speeds and solar irradiance data used to calculate the wind and solar CF are obtained from the CMIP5 experiments, following the models presented in section (2.1.2). We consider three Representative Concentration Pathways (RCPs) that cover the impact of different trajectories of greenhouse gas concentration on future climate, compared to pre-industrial levels. In particular, we consider the RCP 8.5, RCP 4.5 and RCP 2.6, which represent an increased in radiative forcing of +8.5 Wm^{-2}, +4.5 Wm^{-2} and +2.6 Wm^{-2} respectively, compared to pre-industrial values. Table (3) summarizes the details of the CMIP5 experiments used for the different climate projections.

Table 3: Details of the experiments used for the historical and projected temperature scenarios

Experiment type	Modeling Center (or group)	Institute ID	Model Name	Experiment	Period	Variable	Frequency
Historical (baseline)	Meteorological Research Institute	MRI	MRI-CGCM3	historicalEXT	2008-2012	tas	3hr
Projection	Centre National de Recherches Mtorologiques	CNRM	CNRM-CM5	rcp85, rcp45, rcp26	2041-2046	tas	3hr
Projection	Meteorological Research Institute	MRI	MRI-CGCM3	rcp85, rcp45, rcp26	2041-2046	uas, vas, rsds	3hr

Since we are primarily interested in extreme weather scenarios related to the region of southern France, the climate data considered have been limited to the geographical scope of interest: that is, data spanning the longitudinal and latitudinal scope of approximately ($W2°35'00'' - E8°10'00''$) and ($N46°06'00'' - N41°19'00''$), respectively. To quantify the impact of an extreme heat wave, the average temperature time series as well as the average wind and solar CF are, then, computed for the geographical area considered, for each pro-

jected climate scenarios. Regarding water availability levels, different water level scenarios during the heat wave events are assumed to cover: high availability levels (A $>$ 1), normal levels (A $=$ 1) and low availability levels (A $<$ 1).

4. Results and discussion

4.1. Impact of extreme heat wave and drought events on system load and efficiency of power generation

We start our investigation with a focus on future climate parameters obtained from the RCP 8.5 experiments, which is the representative concentration pathway assuming no decrease in current carbon emission trends throughout the 21st century. Significant temperature increase during the summer period is observed under the Representative Concentration Pathway (RCP 8.5), compared to the historical baseline scenario. The impact of this temperature increase on the load and power generation units are computed for a typical summer week for each year of the planning horizon. As an example, Figure (2) illustrates the projected temperature increase and its impact on system load during the period between the 30th of July and the 6th of August for the year 2041 in southern France, compared to the historical average levels in the same period and location. The temperature difference is seen to reach levels of +9.2°C, while its impact on the system load (calculated as per the proposed impact model) can increase up to +1840 MWh. Similar order of differences are observed for the other planning years considered.

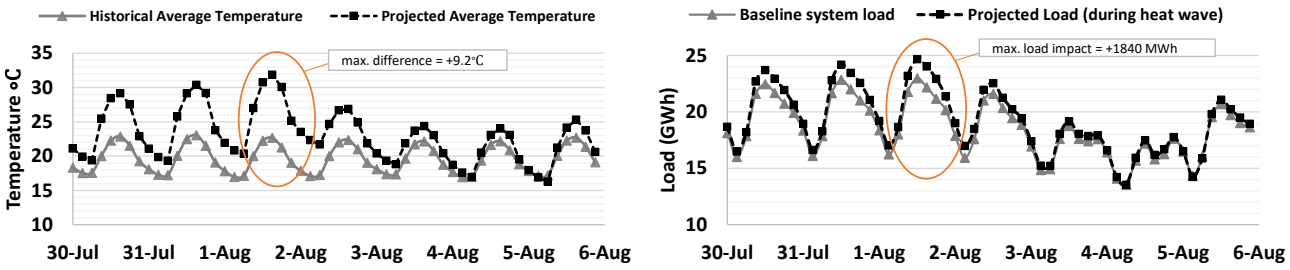

(a) Temperature difference

(b) Load difference

Figure 2: Temperature difference and its impact on system load during the period between the 5th and the 12th of August, for both the baseline and the projected scenarios

The effect of heat wave and water shortages on the efficiency of thermal units depends on the cooling technology deployed. We consider three different levels of water availability and calculate their impact on the efficiency of thermal units during the heat wave event. Figure (3) illustrates the resulting efficiency for nuclear power plants during a heat wave and under different water availability levels, using data for the year 2041. It can be seen that OTC-based generators are highly affected by water shortages, compared with CLC units, which are impacted by the heat wave but maintain the same efficiency levels regardless of the water availability level.

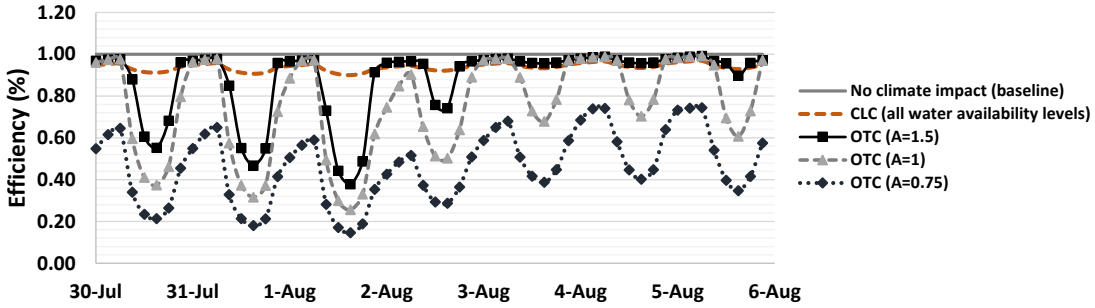

Figure 3: Example of nuclear generation units efficiency derating during a heat wave event for different cooling technologies (OTC and CLC) and under different water availability scenarios (high availability: A $>$ 1, normal availability: A = 1, low availability A $<$ 1)

4.2. Resilient power system planning vs conventional planning

Resilient power systems planning should account for the impact of extreme weather events as an integral part of the planning problem, as discussed in the previous sections. We compare the resilient plans (denoted RP) to conventional plans (CP), obtained assuming no climate impact on the efficiency of the generation units. CP future investment plans are, then, used to simulate operation under different realizations of climate scenarios, to assess operational performance. We focus first on the results obtained under no IRES penetration level requirements.

The total amount of load not served (LNS) during the heat wave period is taken as the primary performance measure for the plans obtained. Figure (4) illustrates the resulting LNS for both RP and CP under the extreme weather events. The results show a significant

load loss for the conventionally planned systems, that sharply increases with the worsening of the climate conditions. The loss reaches up to 851 GWh under the worst scenario of climate impact. This is not the case for the RP, which are shown to suffer an LNS significantly lower than CP, with a maximum of 17 GWh under the worst scenario of climate impact.

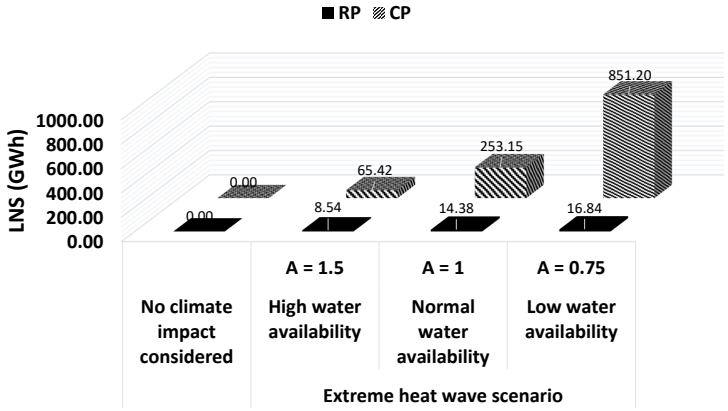

Figure 4: LNS during different extreme weather events. Comparison between RP and CP under no IRES penetration.

In terms of system costs, RP have overall higher annualized investment and operational costs compared to CP, as can be seen in Figure (5). This is directly related to the fact that for RP the extreme weather impact on the power system is taken into account and so the plan compensates the lower thermal units efficiency by investing in more and better performing units. The slightly higher investment and operational costs, however, are fully offset by the reductions in LNS costs, as can be seen in Figure (5). The maximum difference between the total annualized investment and operation costs of the RP compared to the CP is equal to 1.23 B€ (low water availability scenario in Figure (5)), while the LNS cost saving for the same scenario is around 9.52 B€.

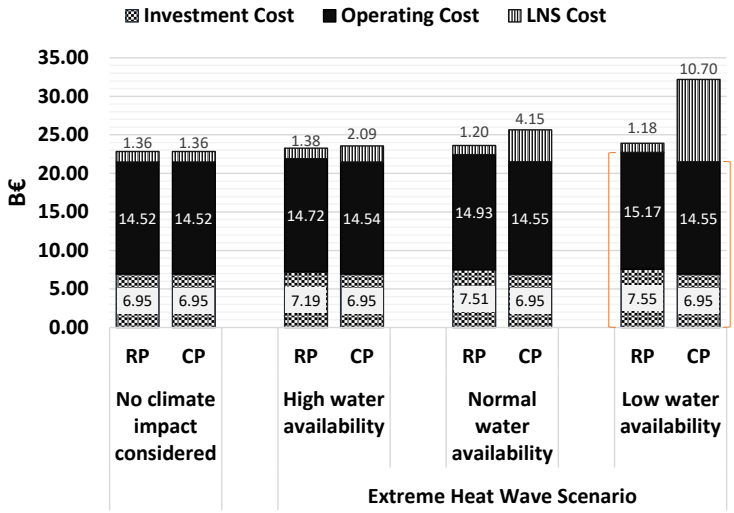

Figure 5: Comparison between RP and CP costs subject to different extreme weather events under no IRES penetration.

Next, we extend the analysis to evaluate the impact of increasing IRES penetration levels on the system performance. Most notably we consider 0%, 25% and 50% IRES energy penetration levels (percentages of total system load) and solve the optimization problems under all extreme weather events, for both the RP and CP.

Figure (6) shows the impact of the increasing share of IRES levels on the LNS of the system during the extreme weather events, for RP and CP. Higher IRES penetration has a clear effect on reducing the amount of LNS during the extreme events. RP maintain low LNS levels in all cases considered, and slightly improves with increasing IRES levels, while CP show a significant decrease in LNS as IRES power compensates for the lack of system resilience.

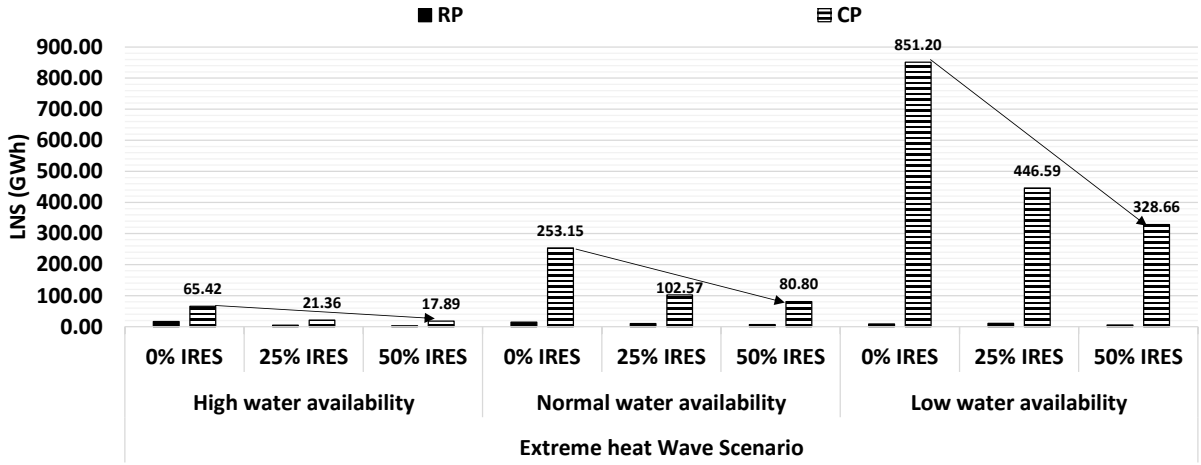

Figure 6: Impact of high IRES penetration on LNS during different extreme weather events.

Moreover, it is shown that the increased IRES capacity reduces the gap between RP and CP, in terms of annualized investment and operational costs. For example, the difference in the total annualized investment and operation costs between the RP and CP plans decreases from +5.70% to +1.60% under the 0% and 50% IRES levels respectively, under the "Extreme heat wave - Low water availability" scenario in Table (4). The same trends are also found under the other extreme weather scenarios considered.

			Annualized Investment Cost [BEuro]			Operating Cost (excluding LNS) [BEuro]			Total inv + op costs [BEuro]		
			RP	CP	Difference (% wrt CP)	RP	CP	Difference (% wrt CP)	RP	CP	Difference (% wrt CP)
Extreme heat wave scenario	High water availability	0% IRES	7.19	6.95	3.52%	14.72	14.54	1.20%	21.91	21.49	1.95%
		25% IRES	9.37	9.37	0.05%	14.12	13.99	0.95%	23.49	23.35	0.59%
		50% IRES	12.92	12.92	0.04%	14.29	14.14	1.03%	27.21	27.06	0.56%
	Normal water availability	0% IRES	7.51	6.95	8.02%	14.93	14.55	2.57%	22.43	21.50	4.33%
		25% IRES	9.55	9.37	2.00%	14.13	14.00	0.95%	23.69	23.37	1.37%
		50% IRES	13.05	12.92	0.99%	14.30	14.15	1.04%	27.34	27.07	1.01%
	Low water availability	0% IRES	7.55	6.95	8.63%	15.17	14.55	4.30%	22.72	21.50	5.70%
		25% IRES	9.66	9.37	3.09%	14.30	14.01	2.03%	23.95	23.38	2.46%
		50% IRES	13.17	12.92	1.92%	14.35	14.17	1.32%	27.52	27.08	1.60%

Table 4: Comparison of RP and CP costs under different IRES penetration levels and extreme weather events.

4.3. Impact of extreme weather events on technology choice and system flexibility

The previous section has illustrated how power system RP cope with the detrimental impact of extreme weather events, with no significant increase in the system cost. We analyze

in details the choices in the RP under the different scenarios. Most notably, the generation technology choice and capacity installed are major contributors to the system performance. Figure (7) summarizes the investment capacities and technologies choices under the different extreme weather events and IRES penetration levels. For clarity, the results illustrate the total capacity installed per each cooling technology type (OTC-based capacity vs CLC-based capacity) summed over all thermal power plants installed, under each scenario.

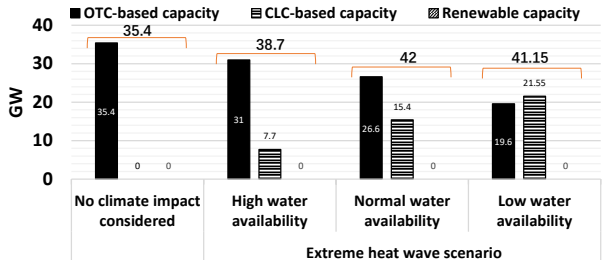

(a) 0% IRES penetration

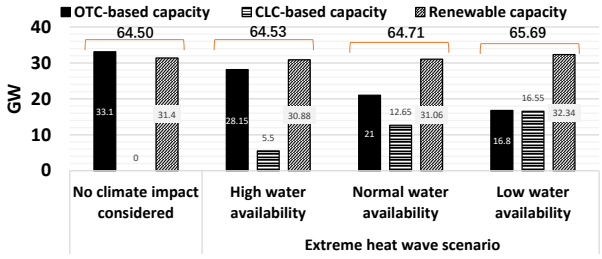

(b) 25% IRES penetration

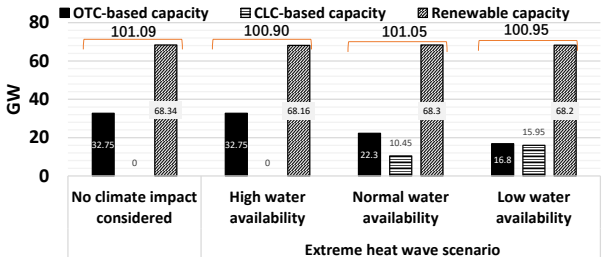

(c) 50% IRES penetration

Figure 7: RP technology choice and capacity installed under different IRES penetration levels and extreme weather events.

The results show a clear shift from (the cheaper) OTC-based capacities to the (more expensive) CLC-based technology when the heat wave event is accounted for, primarily as a result of internalizing in the system design the impact of the extreme event. This shift to CLC-based units further increases considering lower water availability levels during the heat wave event. The results also show that the total capacity of all technologies installed does not in fact vary in response to different extreme weather events but is rather significantly impacted by the amount of IRES penetration in the system, for an average of 39.3GW,

64.8GW and 101GW for the 0%, 25% and 50% IRES penetration scenarios, respectively, with low standard deviations of 2.9, 0.5 and 0.08 within each IRES scenario. On the other hand, the significant increase of capacity installed across different IRES penetration scenarios is directly attributed to the increased capacity required to satisfy the operational flexibility needs of the system under these scenarios, as has been discussed in previous work [11].

We finally explore how the operational flexibility of the RP and CP plans are affected by the different extreme climate events. Table (5) summarizes the EFS results at the 99% confidence level, for all IRES and climate scenarios. It can be seen that when the extreme weather events are not taken into account in the planning phase (as per the CP), the operational flexibility shortage is multiple times that of its RP counterpart under the same extreme weather events. This flexibility shortage difference further increases considering higher levels of IRES penetration. For instance, the EFS reaches approximately 7355 MW for CP compared to 27655 MW for RP, during the extreme weather event for a system with 50% share of IRES capacity. The flexibility shortages, however, are significantly lower than the load losses for the CP due to the lack of resilience, which were shown to be in the order of several hundred GWh in the previous sections. This is important to note since both RP and CP accommodate the operational flexibility attribute.

			EFS [MW] (99% condifdence level)	
			RP	CP
Extreme heat wave scenario	0% IRES	High water availability	28.84	3359.03
		Normal water availability	785.57	4588.56
		Low water availability	1933.98	5375.94
	25% IRES	High water availability	752.57	1732.63
		Normal water availability	1472.30	5050.12
		Low water availability	1621.71	4435.47
	50% IRES	High water availability	618.18	1281.81
		Normal water availability	1038.70	3981.68
		Low water availability	2655.01	7354.27

Table 5: Expected Flexibility Shortfall (EFS) of RP under different IRES penetration levels and climate scenarios.

4.4. Sensitivity of the results for different climate projections (RCP8.5, RCP4.5 and RCP2.6)

In the previous sections, we have shown the improvements achieved by RP which account for extreme heat waves and drought events. Both RP and CP were optimized and/or evaluated under the climate parameters of the RCP 8.5, that is the most pessimistic radiative concentration pathway for the 21st century. In this section, we perform a sensitivity analysis considering other RCP projections from the CMIP5 climate experiments to confirm the relevance of the planning framework proposed under less pessimistic concentration pathways.

RCP 2.6 and 4.5 climate data are used to calculate future power system operating conditions. Most notably, solar irradiance and wind speed data are used to obtain wind and solar-PV CF, and temperature data during the summer period are used to simulate the future heat wave scenarios and their impact on thermal generators. We, then, use the RP and CP under the RCP 8.5 scenario to check their operational performance under the other RCP scenarios.

Figure (8) shows the performance of the RP and CP obtained under the RCP 8.5, in terms of LNS during the extreme heat event under all RCP pathways considered. The values shown are the average LNS amounts for all water availability scenarios per each RCP. The results confirm the consistently lower LNS for the RP under all RCP scenarios and for all IRES penetration levels. In addition, as expected, the LNS decreases as less pessimistic RCP scenarios are considered. For example, the average LNS for the RP under 0% IRES penetration decreases from 10 GWh for the RCP 8.5 to 0.05 GWh for the RCP 2.6 scenarios.

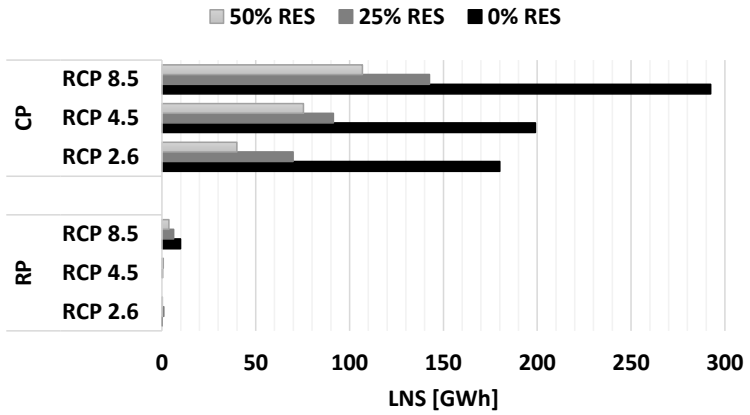

Figure 8: Average amount of LNS under each RCP scenario (8.5, 4.5 and 2.6) and IRES penetration levels (0%, 25% and 50%). Comparison between the results for RP and CP.

With regards to the operational flexibility, the results reported in Figure (9) show the average EFS of the plans obtained under all extreme weather events for different IRES penetration levels. Less obvious trends can be found for the operational flexibility levels of the obtained plans across the different RCPs, as measured by the EFS metric. It can be confirmed, however, that RP consistently outperform CP also in terms of flexibility, as can be seen in the overall lower shortage levels illustrated in Figure (9). The improved flexibility performance of the RP highlights an important interaction between the resilience of the system and its flexibility, and the compound impact of failing to consider either aspect in the power system design phase.

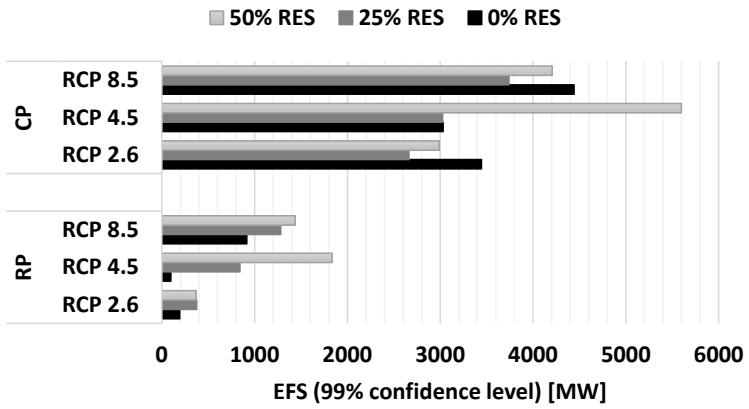

Figure 9: Average amount of EFS under each RCP scenario (8.5, 4.5 and 2.6) and IRES penetration levels (0%, 25% and 50%). Comparison between the results for the RP and CP.

5. Conclusions

In this work, we propose a framework for power systems planning considering operational flexibility and resilience against extreme weather events. Specifically, we propose a set of piece-wise linear models to quantify the impact of extreme heat waves and drought events, and propose methods to integrate their impacts within the power system planning models.

We investigate a practically sized case study based on realistic climate projections and system attributes representatives of the southern French geographical area. Several extreme climate scenarios related to heat waves and water shortages are investigated and the results are compared between the resilience-driven planning framework proposed and the conventional planning results.

The results show that significant improvements in terms of load supply during an extreme heat wave and drought events can be achieved under the resilient planning framework compared to conventional planning. It is also shown that although these improvements come at higher investment and operational costs, they are fully offset by the economic savings achieved by reducing the amount of load loss during those events. In terms of system flexibility, the results further show that although the plans obtained have higher flexibility shortage levels, they keep at least an order of magnitude lower than the load losses due

to the lack of system resilience. This further highlights the advantage of adopting such comprehensive planning framework.

The modeling and optimization framework presented here can be directly extended to multi-regional planning, to account for the differences in weather conditions across the different regions. Moreover, since extreme weather events are uncertain and stochastic in nature, the presented deterministic framework for resilient power system design can be improved by accounting for the uncertainties within a probabilistic framework.

References

[1] Gianluca Fulli, Marcelo Masera, Catalin Felix Covrig, Francesco Profumo, Ettore Bompard, and Tao Huang. The eu electricity security decision-analytic framework: Status and perspective developments. *Energies*, 10(4):425, 2017.

[2] MI Alizadeh, M Parsa Moghaddam, N Amjady, P Siano, and MK Sheikh-El-Eslami. Flexibility in future power systems with high renewable penetration: A review. *Renewable and Sustainable Energy Reviews*, 57:1186–1193, 2016.

[3] Eamonn Lannoye, Damian Flynn, and Mark O'Malley. Evaluation of power system flexibility. *IEEE Transactions on Power Systems*, 27(2):922–931, 2012.

[4] Juan Ma, Vera Silva, Régine Belhomme, Daniel S Kirschen, and Luis F Ochoa. Evaluating and planning flexibility in sustainable power systems. In *Power and Energy Society General Meeting (PES), 2013 IEEE*, pages 1–11. IEEE, 2013.

[5] Andreas Ulbig and Göran Andersson. Analyzing operational flexibility of electric power systems. *International Journal of Electrical Power & Energy Systems*, 72:155–164, 2015.

[6] Jinye Zhao, Tongxin Zheng, and Eugene Litvinov. A unified framework for defining and measuring flexibility in power system. *IEEE Transactions on Power Systems*, 31 (1):339–347, 2016.

[7] Daniel S Kirschen, Juan Ma, Vera Silva, and Régine Belhomme. Optimizing the flexibility of a portfolio of generating plants to deal with wind generation. In *Power and Energy Society General Meeting, 2011 IEEE*, pages 1–7. IEEE, 2011.

[8] Nikolaos E Koltsaklis and Michael C Georgiadis. A multi-period, multi-regional generation expansion planning model incorporating unit commitment constraints. *Applied energy*, 158:310–331, 2015.

[9] Andreas Belderbos and Erik Delarue. Accounting for flexibility in power system planning with renewables. *International Journal of Electrical Power & Energy Systems*, 71:33–41, 2015.

[10] Bryan S Palmintier and Mort D Webster. Impact of operational flexibility on electricity generation planning with renewable and carbon targets. *IEEE Transactions on Sustainable Energy*, 7(2):672–684, 2016.

[11] Islam F Abdin and Enrico Zio. An integrated framework for operational flexibility assessment in multi-period power system planning with renewable energy production. *Applied Energy*, 222:898–914, 2018.

[12] Yiping Fang and Giovanni Sansavini. Optimizing power system investments and resilience against attacks. *Reliability Engineering & System Safety*, 159:161–173, 2017.

[13] Gerald A Meehl and Claudia Tebaldi. More intense, more frequent, and longer lasting heat waves in the 21st century. *Science*, 305(5686):994–997, 2004.

[14] Selma B Guerreiro, Richard J Dawson, Chris Kilsby, Elizabeth Lewis, and Alistair Ford. Future heat-waves, droughts and floods in 571 european cities. *Environmental Research Letters*, 13(3):034009, 2018.

[15] Marc Poumadere, Claire Mays, Sophie Le Mer, and Russell Blong. The 2003 heat wave in france: dangerous climate change here and now. *Risk Analysis: an International Journal*, 25(6):1483–1494, 2005.

[16] Roberto Rocchetta, Yanfu Li, and Enrico Zio. Risk assessment and risk-cost optimization of distributed power generation systems considering extreme weather conditions. *Reliability Engineering & System Safety*, 136:47–61, 2015.

[17] Mathaios Panteli, Cassandra Pickering, Sean Wilkinson, Richard Dawson, and Pierluigi Mancarella. Power system resilience to extreme weather: Fragility modelling, probabilistic impact assessment, and adaptation measures. *IEEE Trans. Power Syst*, 32: 3747–3757, 2017.

[18] Francesco Cadini, Gian Luca Agliardi, and Enrico Zio. A modeling and simulation framework for the reliability/availability assessment of a power transmission grid subject to cascading failures under extreme weather conditions. *Applied energy*, 185:267–279, 2017.

[19] Stuart M Cohen, Kristen Averyt, Jordan Macknick, and James Meldrum. Modeling climate-water impacts on electricity sector capacity expansion. In *ASME 2014 power conference*, pages V002T10A007–V002T10A007. American Society of Mechanical Engineers, 2014.

[20] Chengcheng Shao, Mohammad Shahidehpour, Xifan Wang, Xiuli Wang, and Biyang Wang. Integrated planning of electricity and natural gas transportation systems for enhancing the power grid resilience. *IEEE Transactions on Power Systems*, 32(6):4418–4429, 2017.

[21] Xinda Ke, Di Wu, Jennie Rice, Michael Kintner-Meyer, and Ning Lu. Quantifying impacts of heat waves on power grid operation. *Applied energy*, 183:504–512, 2016.

[22] Dirk Rübbelke and Stefan Vögele. Impacts of climate change on european critical infrastructures: The case of the power sector. *Environmental science & policy*, 14(1): 53–63, 2011.

[23] Yannick Rousseau. *Impact of Climate Change on Thermal Power Plants. Case study of thermal power plants in France.* PhD thesis, 2013.

[24] Hagen Koch and Stefan Vögele. Dynamic modelling of water demand, water availability and adaptation strategies for power plants to global change. *Ecological Economics*, 68 (7):2031–2039, 2009.

[25] Omid Mohseni, Heinz G Stefan, and Troy R Erickson. A nonlinear regression model for weekly stream temperatures. *Water Resources Research*, 34(10):2685–2692, 1998.

[26] Niels Lagergaard Pedersen and Kaj Sand-Jensen. Temperature in lowland danish streams: contemporary patterns, empirical models and future scenarios. *Hydrological Processes: An International Journal*, 21(3):348–358, 2007.

[27] Jean C Morrill, Roger C Bales, and Martha H Conklin. Estimating stream temperature from air temperature: implications for future water quality. *Journal of Environmental Engineering*, 131(1):139–146, 2005.

[28] DL Elliot. Adjustment and analysis of data for regional wind energy assessments. In *Proceedings of the Workshop on Wind Climate*, pages 121–131, 1979.

[29] Isabelle Tobin, Sonia Jerez, Robert Vautard, Françoise Thais, Erik Van Meijgaard, Andreas Prein, Michel Déqué, Sven Kotlarski, Cathrine Fox Maule, Grigory Nikulin, et al. Climate change impacts on the power generation potential of a european mid-century wind farms scenario. *Environmental Research Letters*, 11(3):034013, 2016.

[30] Isabelle Tobin, Robert Vautard, Irena Balog, François-Marie Bréon, Sonia Jerez, Paolo Michele Ruti, Françoise Thais, Mathieu Vrac, and Pascal Yiou. Assessing climate change impacts on european wind energy from ensembles high-resolution climate projections. *Climatic Change*, 128(1-2):99–112, 2015.

[31] Jan Wohland, Mark Reyers, Juliane Weber, and Dirk Witthaut. More homogeneous wind conditions under strong climate change decrease the potential for inter-state balancing of electricity in europe. *Earth System Dynamics*, 8(4):1047–1060, 2017.

[32] Sonia Jerez, Isabelle Tobin, Robert Vautard, Juan Pedro Montávez, Jose María López-Romero, Françoise Thais, Blanka Bartok, Ole Bøssing Christensen, Augustin Colette, Michel Déqué, et al. The impact of climate change on photovoltaic power generation in europe. *Nature communications*, 6:10014, 2015.

[33] F Mavromatakis, G Makrides, G Georghiou, A Pothrakis, Y Franghiadakis, E Drakakis, and E Koudoumas. Modeling the photovoltaic potential of a site. *Renewable Energy*, 35(7):1387–1390, 2010.

[34] R Chenni, M Makhlouf, T Kerbache, and A Bouzid. A detailed modeling method for photovoltaic cells. *Energy*, 32(9):1724–1730, 2007.

[35] Laurent Dubus. Monthly and seasonal forecasts in the french power system. In *ECMWF Seminar, Personal presentation*, 2012.

[36] RTE-France. Available at:. `http://clients.rte-france.com`, 2017. (Accessed on 20-12-2016).

[37] IEA/NEA. Projected costs of generating electricity 2015 edition. *OECD*, 2015.

[38] Sami I Attia. The influence of condenser cooling water temperature on the thermal efficiency of a nuclear power plant. *Annals of Nuclear Energy*, 80:371–378, 2015.

[39] Abigail González-Díaz, Agustín M Alcaráz-Calderón, Maria Ortencia González-Díaz, Ángel Méndez-Aranda, Mathieu Lucquiaud, and Jose Miguel González-Santaló. Effect of the ambient conditions on gas turbine combined cycle power plants with post-combustion co2 capture. *Energy*, 134:221–233, 2017.

[40] Bryan S Palmintier and Mort D Webster. Heterogeneous unit clustering for efficient operational flexibility modeling. *IEEE Trans. Power Syst*, 29(3):1089–1098, 2014.

[41] Fernando J de Sisternes and Mort D Webster. Selection of sample weeks for approximating the net load in generation planning problems. Technical report, ESD Working Paper, Massachusetts Institute of Technology, 2013.

[42] Karl E Taylor, Ronald J Stouffer, and Gerald A Meehl. An overview of cmip5 and the experiment design. *Bulletin of the American Meteorological Society*, 93(4):485–498, 2012.

Paper (iii)

Abdin, I.F., Caunhye, A., Zio, E., (UNDER REVISION). Multi-stage adaptive robust optimal power system planning considering operational flexibility. ***IEEE Transactions on Power Systems*****.**

Multi-stage Adaptive Robust Optimal Power System Planning Considering Operational Flexibility

Islam F. Abdin[a], Aakil Cauhnye[1], Enrico Zio[b,c,*]

[a] *Laboratoire Genie Industriel, CentraleSupélec, Université Paris-Saclay*
3 Rue Joliot Curie, 91190 Gif-sur-Yvette, France.
Chair Systems Science and the Energy Challenge, Fondation Electricité de France (EDF)
[b] *Mines ParisTech, PSL Research University, CRC, Sophia Antipolis, France*
[c] *Department of Energy, Politecnico di Milano, Italy*

Abstract

This paper presents a multi-stage adaptive robust power system planning model, which accounts for detailed short-term unit commitment and ramping constraints. The uncertainty of electricity demand and renewable power generation is taken into account through distribution-free bounded intervals, with parameters that permit control over the level of conservatism of the solution. A solution method based on linear decision rules and information-level approximation is also presented. The importance of considering detailed short-term ramping constraints in ensuring proper operational flexibility of power system plans is shown with a realistic-size case study. The results confirm the effectiveness of the proposed approach in coping with multi-fold ramping uncertainties for power systems planning.

Keywords: Adaptive robust optimization, Affine policies, Renewable energy uncertainty, Operational flexibility, Unit commitment

Nomenclature

Indexes:

i index of power plant technology

*Corresponding author
Email addresses: islam.abdin@centralesupelec.fr (Islam F. Abdin), aakil.caunhye@ (Aakil Cauhnye), enrico.zio@polimi.it (Enrico Zio)

s index of sub-periods (days or weeks)

t index of sub-periods (hours)

y index of planning year

Sets:

I set of power plant technologies

I^{res} subset of renewable energy power plants

I^{th} subset of thermal and nuclear power plants

S set of daily or weekly sub-periods

T set of hourly sub-periods

Y set of years in the planning horizon

Parameters:

$\bar{P}_i$ maximum output of power plant belonging to technology i (MW)

$\bar{R}_i^{Dn}$ maximum downwards ramping capability of power plant $i \in I^{th}$ (MW/h)

$\bar{R}_i^{Up}$ maximum upwards ramping capability of power plant $i \in I^{th}$ (MW/h)

B_y^{max} maximum budget available for investment in generation expansion for year y (in M€)

C^{lns} cost of load not served (€/ MWh)

$C_{i,y}^{marg}$ marginal cost of power plant technology i including the variable O&M cost (€/ MWh)

C_i^{FOM} fixed O&M costs of power plant belonging to technology i (€)

C_i^{inv} investment cost of technology i (M€)

C_i^{stup} start-up cost of power plant belonging to technology i (€)

CF_{iyst} capacity factor of renewable energy sources $i \in I^{res}$ during hourly sub-period t of day or week s, of year y (%)

DF^y discount factor for year y (%)

ϵ_i Expected forced outage rate of power plant belonging to technology i (%)

L_{yst} system load at hour t, day or week s in year y (MWh)

M_i^d minimum down-time of power plant of technology $i \in I^{th}$ (hours)

M_i^u minimum up-time for power plant of technology $i \in I^{th}$ (hours)

P_i^{min} minimum stable power output of power plant of technology $i \in I^{th}$ (MW/h)

P_i^{start} maximum output of power plant of technology $i \in I^{th}$ when started (MW)

r^{min} minimum adequacy reserve margin

RES^{lvl} renewable penetration level requirement (%)

Continuous Variables:

lns_{yst} load not served at hourly sub-period t of day or week s, during year y (MW)

p_{iyst} energy output of power plants belonging to technology i at hourly sub-period t of day or week s, during year y (MWh)

v_{iyst} shut-down decision of units belonging to technology i during hourly sub-period t of day or week s in year y

Discrete Variables:

q_{iy} commissioning decision of power plant of technology i in year y

u_{iyst} commitment status of power plant of technology i during hour t of day or week s in year y

x_{iy} availability (commissioning) state of power plant of technology i in year y

z_{iyst} start-up decision of power plant of technology i during hour t of day or week s in year y

1. Introduction

Planning power systems to properly accommodate the rapid growth of intermittent renewable energy sources (IRES), such as wind and solar power, has received extensive attention in recent years. The challenges brought by the variability of IRES production emphasize the need to account for operational flexibility as an integral part of power systems planning models [1]. Operational flexibility is a time-and-state specific attribute of the power system that most notably relates to its short-term ramping abilities. Methods have been proposed to account for this attribute in power system planning, among which, a new class of integrated generation expansion planning (GEP) and unit commitment (UC) models (IGEP-UC) [2]. These models combine long-term investment decisions and short-term UC constraints within a single optimization framework to explicitly ensure that ramping requirements are respected. However, because of the computational complexity of the resulting problems, most of the applications have been limited to deterministic instances.

Accounting for the inherent uncertainty in IRES supply and system load, however, is another significant concern for ensuring adequate system flexibility. Two popular approaches have been often applied to address these uncertainties for the GEP and UC problems, separately. One is stochastic optimization (SO) [3–7], which models uncertain parameters by means of scenarios generated from probability distribution functions. This method may be suitable if the probability functions are available, which is not always the case, and especially when considering long-term uncertainties such as in a GEP problem. Moreover, SO does not guarantee the feasibility of the solution for all possible uncertainty realizations, which is a significant limitation in addressing the operational flexibility issue. The other popular approach is robust optimization (RO) [8], which models uncertain parameters by means of distribution-free bounded intervals. RO is attractive in that it avoids the above-mentioned

limitations of SO, but, it has been often criticized for resulting in over-conservative solutions and for being computationally intensive. State-of-the art RO methods deal with these problems by introducing an uncertainty budget parameter to control the conservatism of the solution and by resorting to efficient solution methods (such as Column and Constraint Generation (CCG) [9] or affine simplification of the recourse action [10]) to accelerate the solution.

Some research works have focused on RO-based approaches to handle uncertainties and address operational flexibility in power systems planning and operation. In [11], a two-stage adaptive RO model is proposed for long term generation and transmission expansion under generator output uncertainties but with no explicit consideration of the ramping requirements. Ramping was considered in [12] for power system planning but only through an approximated hourly load ramping uncertainty that is based on average net-load levels. Detailed ramping constraints were considered in robust unit commitment models such as in [13–16], but without considering the impact on power systems planning. Moreover, [15] has demonstrated how the two-stage robust UC model can lead to infeasibility in the dispatch problem when the generation ramping capability is limited. This showed the importance of considering non-anticipativity constraints in power systems operations within a multistage robust optimization. Yet these results were not extended to investigate their impact on the power systems investment decisions. In this work, we confirm these results and further extend the analysis showing how investment decisions for power systems planning can widely vary as a result of accounting for detailed ramping uncertainties. The main contributions of this work are:

1) A multiperiod multi-stage affinely adjustable robust optimization (AARO) model is formulated for long term integrated generation expansion planning and unit commitment to explicitly account for operational flexibility in power system planning. The uncertainty characterization of the system load and IRES capacity factor (IRES-CF) takes the form of a deterministic uncertainty set with a controllable level of conservatism. The dimensionality problem of the fully adjustable model is discussed along with the concept of "information

basis level" of the resulting problem.
2) To resolve the dimensionality issue, an approximation method is proposed by introducing a new parameter which controls the level of affine dependency (information level) of the problem. We conduct a sensitivity analysis on this parameter and show that significant computational gains can be achieved while keeping the significance of the results.
3) The proposed approach is applied for investment decisions in a practical-sized case study with a high share of IRES penetration, under realistic assumptions. The importance of explicitly considering the detailed ramping constraints for robust long-term planning is shown and discussed in details. The superiority of considering multi-stage AARO over other methods to account for operational flexibility in power systems planning with high shares of IRES production is demonstrated.

The rest of the paper is organized as follows. In Section (2) the deterministic IGEP-UC model as a mixed integer linear programming problem is introduced. In Section (3) the full description of the multi-stage AARO formulation is presented. The solution method is proposed in Section (4). The results of the case study are presented and discussed in Section (5). Section (6) offers some concluding remarks on the work.

2. Deterministic model

The multi-period power system planning model used here seeks to minimize the total discounted system cost over the whole time horizon. These costs include: annualized equivalent investment costs (1a), start-up cost. (1b), fixed operation and maintenance costs (1c) and variable operation costs of the power system (fuel cost, start-up costs and cost of load not served (LNS)) (1d). The objective function to minimize is, then, written as:

Objective function

$$\min_{total\ cost} \sum_{y \in Y} DF^y \cdot \sum_{i \in I^{new}} C_i^{inv} \cdot \bar{P}_i \cdot q_{iy} \tag{1a}$$

$$+ \sum_{y \in Y} DF^y \cdot \sum_{s \in S} \sum_{t \in T} \sum_{i \in I^{th}} \left(C_i^{stup} \cdot z_{iyst} \right) \tag{1b}$$

$$+\sum_{y\in Y} DF^{y}\cdot\sum_{i\in I} C_{iy}^{FOM}\cdot\bar{P}_{i}\cdot\sum_{l=1}^{y} q_{il} \tag{1c}$$

$$+\sum_{y\in Y} DF^{y}\cdot\sum_{s\in S}\sum_{t\in T}\left[\sum_{i\in I}\left(C_{iy}^{marg}\cdot p_{iyst}\right)+C^{lns}\cdot lns_{yst}\right] \tag{1d}$$

The minimization of the objective function is subject to long-term commissioning constraints, and short-term commitment and dispatch constraints as follows:

Commissioning and commitment constraints

$$x_{iy}\leq\sum_{l=1}^{y} q_{il},\forall i\in I^{new},\forall y\in Y \tag{2a}$$

$$\sum_{i\in I^{new}} C_{i}^{inv}\cdot\bar{P}_{i}\cdot q_{iy}\leq B_{y}^{max},\forall y\in Y \tag{2b}$$

$$\sum_{i\in I}\left(\bar{P}_{i}\cdot x_{iy}\right)\geq\left(1+r^{min}\right)\cdot L^{max},\forall y\in Y \tag{2c}$$

$$\sum_{i\in I^{res}} x_{iy}\cdot\bar{P}_{i}\geq Res^{lvl}\cdot\sum_{i\in I} x_{iy}\cdot\bar{P}_{i},\forall y\in Y \tag{2d}$$

$$u_{iyst}\leq x_{iy},\forall i^{th}\in I,y\in Y,s\in S,t\in T \tag{2e}$$

$$u_{iyst}-u_{iyst-1}=z_{iyst}-v_{iyst},\forall i\in I^{th},y\in Y,s\in S,t\in T\setminus\{1\} \tag{2f}$$

$$u_{iyst}\geq\sum_{\tau\in[t]\setminus[t-M_{i}^{u}-1]} z_{iys\tau},\forall i\in I^{th},y\in Y,s\in S,t\in T\setminus[M_{i}^{u}] \tag{2g}$$

$$x_{iy}-u_{iyst}\geq\sum_{\tau\in[t]\setminus[t-M_{i}^{d}-1]} v_{iys\tau},\forall i\in I^{th},y\in Y,s\in S,t\in T\setminus[M_{i}^{d}] \tag{2h}$$

Eq. (2a) keeps track of the investment decisions made in year y throughout the planning horizon. The maximum allowable budget is limited in Eq (2b). Eq (2c) ensures the adequacy reserve margin. The IRES level required in the system is ensured through Eq (2d). Eq (2e) ensures the coupling between investment and operational decisions. Eq (2f) constrains the hourly unit commitment decisions by the startup and shutdown decisions. Finally, Eq. (2g) and Eq. (2h) ensure that the minimum allowable up- and down-times for thermal units are respected:

Dispatch constraints

$$\sum_{i\in I} p_{iyst}+lns_{yst}=L_{yst},\forall y\in Y,s\in S,t\in T \tag{3a}$$

$$p_{iyst} \leq u_{iyst} \cdot \bar{P}_i \cdot (1 - \epsilon_i), \forall i \in I^{th}, y \in Y, s \in S, t \in T \tag{3b}$$

$$p_{iyst} \geq u_{iyst} \cdot P_i^{min}, \forall i \in I^{th}, y \in Y, s \in S, t \in T \tag{3c}$$

$$p_{iyst} \leq x_{iy} \cdot \bar{P}_i \cdot CF_{iyst}, \forall i \in I^{res}, y \in Y, s \in S, t \in T \tag{3d}$$

$$p_{iyst} - p_{iyst-1} \leq u_{iyst-1} \cdot \bar{R}_i^{Up} + z_{iyst} \cdot P_i^{start}, \forall i \in I^{th}, y \in Y, s \in S, t \in T \setminus \{1\} \tag{3e}$$

$$p_{iyst-1} - p_{iyst} \leq u_{iyst-1} \cdot \bar{R}_i^{Dn}, \forall i \in I^{th}, y \in Y, s \in S, t \in T \setminus \{1\} \tag{3f}$$

Regarding power dispatch, the hourly supply and demand balance is ensured by Eq. (3a). The hourly maximum and minimum production levels for thermal units are given in Eq (3b) and Eq. (3c), respectively. IRES production is limited by the hourly capacity factor CF as given in Eq (3d). Finally, Eq. (3e) and Eq. (3f) constrain the hourly upwards and downwards ramping capabilities for thermal units, respectively.

3. Robust optimization formulation

As previously mentioned, this paper proposes a distribution-free characterization of both load and IRES supply uncertainties. The sub-period load vector, $\boldsymbol{L}$, takes on a range of possible values given by $\underline{\boldsymbol{L}} \leq \boldsymbol{L} \leq \bar{\boldsymbol{L}}$ and the capacity factor, $\boldsymbol{CF}$, which models IRES supply uncertainty, varies in the range $\underline{\boldsymbol{CF}} \leq \boldsymbol{CF} \leq \bar{\boldsymbol{CF}}$. A polyhedral uncertainty characterization is defined as follows:

$$\mathcal{U}_{yst}(\Gamma) = \Bigg\{ L_{yst} \in \mathbb{R}_+, \boldsymbol{CF}_{yst} \in \mathbb{R}_+^{|I^{res}|} : \underline{\mathrm{L}}_{yst} \leq L_{yst} \leq \bar{L}_{yst}, \underline{\mathrm{CF}}_{iyst} \leq CF_{iyst} \leq \bar{CF}_{iyst},$$

$$\forall i \in I^{res}, L_{yst} - \sum_{i \in I^{res}} CF_{iyst} \leq \Gamma \cdot (\bar{L}_{yst} - \sum_{i \in I^{res}} \underline{\mathrm{CF}}_{iyst}) \Bigg\}, \forall y \in Y, s \in S, t \in T \tag{4}$$

where $\Gamma(\leq 1)$, represents the level of conservatism of the decision maker. It is clear that when $\Gamma = 1$, the load and IRES-CF can take on their full range of possible values. When $\Gamma < 1$, the uncertainty set excludes the absolute worst-case situation, which is where all sub-period loads are at their highest values and all IRES-CF are at their lowest values. Indeed, by varying Γ, the decision maker can control the level of conservatism in planning. Moreover, the uncertainty set is non-anticipative, in the sense that in sub-period t of year y

the decision maker only has information about current and past uncertainty realizations. The lower bound of the uncertainty budget Γ can be easily derived to show that it is equivalent to:

$$\Gamma \geq \max_{y\in Y, s\in S, t\in T} \left\{ \frac{\underline{\mathrm{L}}_{yst} - \sum_{i\in I^{res}} \bar{CF}_{iyst}}{\bar{L}_{yst} - \sum_{i\in I^{res}} \underline{\mathrm{CF}}_{iyst}} \right\}. \tag{5}$$

3.1. Robust Model Formulation

The model under uncertainty is represented by a multistage adaptive robust optimization model, where decisions related to unit commitment, commissioning and start-up are *here-and-now* decisions made robust to uncertainty realizations and the dispatch decisions are *wait-and-see* decisions made subject to (and thus, flexible to) uncertainty realizations. The objective of the model is to minimize the total cost of here-and-now decisions plus the worst-case total cost of wait-and-see decisions, also known as recourse decisions. Another important component of the model is full immunization, meaning the maintenance of feasibility over all possible uncertainty realizations in the polyhedral uncertainty sets. Letting $\mathcal{V}^t_{ys}$ $(= \{\boldsymbol{L}^t_{ys}, \boldsymbol{CF}^t_{ys}\})$, $\forall y \in Y, s \in S, t \in T$, and given that recourse decisions made in a time period t depend on the full history of the load L and IRES-CF CF from the first time period up to t, the formulation of the robust counterpart (RC) is:

$$\min_{total\ cost} \text{(1a)-(1c)} + \max_{\substack{\mathcal{V}^t_{ys}\in\ \mathcal{U}^t_{ys} \\ t\in T}} \sum_{y\in Y} DF^y \cdot \sum_{s\in S}\sum_{t\in T}$$
$$\left[\sum_{i\in I} \left(C^{marg}_{iy} \cdot p_{iyst}(\mathcal{V}^t_{ys}) \right) + C^{lns} \cdot lns_{yst}(\mathcal{V}^t_{ys}) \right] \tag{6}$$

s.t. first stage constraints (2a)-(2h)

s.t. $\forall \mathcal{V}^t_{ys} \in \prod_{t'\in[t]} \mathcal{U}^{t'}_{ys}, [t] \triangleq \{1, ..., t\}, \exists p_{iyst}(.), lns_{yst}(.) \in \mathbb{R}_+, \forall i \in I, y \in Y,$

$s \in S, t \in T$ (7a)

$$\sum_{i\in I} p_{iyst}(\mathcal{V}^t_{ys}) + lns_{yst}(\mathcal{V}^t_{ys}) = L_{yst}, \forall y \in Y, s \in S, t \in T \tag{7b}$$

$$p_{iyst}(\mathcal{V}^t_{ys}) \leq u_{iyst} \cdot \bar{P}_i \cdot (1-\epsilon_i), \forall i \in I^{th}, y \in Y, s \in S, t \in T \tag{7c}$$

$$p_{iyst}(\mathcal{V}^t_{ys}) \geq u_{iyst} \cdot P^{min}_i, \forall i \in I^{th}, y \in Y, s \in S, t \in T \tag{7d}$$

$$p_{iyst}(\mathcal{V}^t_{ys}) \leq x_{iy} \cdot \bar{P}_i \cdot CF_{iyst}, \forall i \in I^{res}, y \in Y, s \in S, t \in T \tag{7e}$$

$$p_{iyst}(\mathcal{V}^t_{ys}) - p_{iyst-1}(\mathcal{V}^{t-1}_{ys}) \leq u_{iyst-1} \cdot \bar{R}^{Up}_i + z_{iyst} \cdot P^{start}_i,$$
$$\forall i \in I^{th}, y \in Y, s \in S, t \in T \setminus \{1\} \tag{7f}$$

$$p_{iyst-1}(\mathcal{V}^{t-1}_{ys}) - p_{iyst}(\mathcal{V}^t_{ys}) \leq u_{iyst-1} \cdot \bar{R}^{Dn}_i, \forall i \in I^{th}, y \in Y, s \in S, t \in T \setminus \{1\} \tag{7g}$$

$$p_{iyst}(\mathcal{V}^t_{ys}), lns_{yst}(\mathcal{V}^t_{ys}) \geq 0, \forall i \in I, y \in Y, s \in S, t \in T \tag{7h}$$

3.2. Multistage affinely adjustable robust counterpart

Because of the full immunization constraint (7a) and the fact that the uncertain parameters are real-valued, the robust counterpart is semi-infinite. We propose to consider linear decision rules to make the problem tractable. This method, which results in what is known as a multistage affinely adjustable robust counterpart (AARC), is appealing in that it results in a linear model that can be solved using over-the-counter solvers and does not require significant tailor-made implementation efforts. The AARC is obtained by replacing the vector of recourse variables using the following affine relationship:

$$\boldsymbol{R}_{yst}(\mathcal{V}^t_{ys}) = \boldsymbol{R}^{\boldsymbol{0}}_{yst} + \sum_{t' \in [t]} \boldsymbol{R}^{\boldsymbol{L}}_{ystt'} \cdot L_{yst'} + \sum_{i' \in I^{res}} \sum_{t' \in [t]} \boldsymbol{R}^{\boldsymbol{C}}_{i'ystt'} \cdot CF_{i'yst'} \tag{8}$$

where $[t] \triangleq \{1, ..., t\}$ and $(\boldsymbol{R}^{\boldsymbol{0}}_{yst}, \boldsymbol{R}^{\boldsymbol{L}}_{ystt'}, \boldsymbol{R}^{\boldsymbol{C}}_{i'ystt'})$ are the coefficients of the linear decision rule. Then, in the model with linear decision rules, the constraints can be processed into a finite number of linear constraints, relying on a duality-based reformulation to obtain the final MILP problem. Below we illustrate how the processing is achieved for one equality and one inequality constraint.

Equality constraint: Consider the supply-demand equality constraint (7b). Replacing the uncertainty dependent variables $p_{iyst}(\mathcal{V}^t_{ys})$ and $lns_{yst}(\mathcal{V}^t_{ys})$ following equation (8), and re-arranging the terms, we obtain:

$$\left(\sum_{i \in I} p^0_{iyst} + lns^0_{yst}\right) + \sum_{t' \in [t-1]} \left(\sum_{i \in I} p^L_{iystt'} + lns^L_{ystt'}\right) \cdot L_{yst'} + \left(\sum_{i \in I} p^L_{iystt} + lns^L_{ystt} - 1\right)$$

$$\cdot L_{yst} + \sum_{i' \in I^{res}} \sum_{t' \in [t]} \left(\sum_{i \in I} p^{C}_{ii'ystt'} + lns^{C}_{ystt'} \right) \cdot CF_{i'yst'} = 0, \forall \mathcal{V}^{t}_{ys} \in \mathcal{U}^{t}_{ys}, y \in Y, s \in S, t \in T \tag{9a}$$

From this we know that equality (9a) is valid *if and only if* equations (9b)-(9e) are satisfied.

$$\sum_{i \in I} p^{0}_{iyst} + lns^{0}_{yst} = 0, \forall y \in Y, s \in S, t \in T \tag{9b}$$

$$\sum_{i \in I} p^{L}_{iystt'} + lns^{L}_{ystt'} = 0, \forall y \in Y, s \in S, t^{'} \in [t-1], t \in T \tag{9c}$$

$$\sum_{i \in I} p^{L}_{iystt'} + lns^{L}_{ystt'} = 1, \forall y \in Y, s \in S, t' = t, t \in T \tag{9d}$$

$$\sum_{i \in I} p^{C}_{ii'ystt'} + lns^{C}_{ystt'} = 0, \forall i^{'} \in I^{res}, y \in Y, s \in S, t^{'} \in [t], t \in T \tag{9e}$$

Inequality constraint: Consider the maximum production limit inequality (7c). The constraint, after applying the affine relationship (8), becomes:

$$\left(p^{0}_{iyst} + \sum_{t' \in [t]} p^{L}_{iystt'} \cdot L_{yst'} + \sum_{i' \in I^{res}} \sum_{t' \in [t]} p^{C}_{i'iystt'} \cdot CF_{i'yst'} \right) \leq u_{iyst} \cdot P^{max}_{i} \cdot (1 - \epsilon_i), \forall i \in I^{th},$$

$$y \in Y, s \in S, t \in T \tag{10a}$$

Re-arranging the terms of the the constraint, given that an uncertainty-affected constraint $\text{LHS}_{ys} \leq \text{RHS}_{ys}$, where LHS contains all uncertainty terms and RHS contains the rest, is valid $\forall \mathcal{V}^{t}_{ys} \in \mathcal{U}^{t}_{ys}, t \in T$, *if and only if* $\max_{\mathcal{V}^{t}_{ys} \in \mathcal{U}^{t}_{ys}, t \in T} \text{LHS}_{ys} \leq \text{RHS}_{ys}$. Notice that any ($\geq$) constraint can easily be transformed to a ($\leq$) one and can follow the same above logic. Applying this logic to inequality (10a) we get:

$$\max_{\mathcal{V}^{t}_{ys} \in \mathcal{U}^{t}_{ys}} \sum_{t' \in [t]} \left(p^{L}_{iystt'} \cdot L_{yst'} \right) + \sum_{i' \in I^{res}} \sum_{t' \in [t]} \left(p^{C}_{ii'ystt'} \cdot CF_{i'yst'} \right) \leq (1 - \epsilon_i) \cdot P^{max}_{i} \cdot u_{iyst} - p^{0}_{iyst},$$

$$\forall i \in I^{th}, y \in Y, s \in S, t \in T \tag{10b}$$

Dualizing the left-hand side of the constraint and because of strong duality, this set of non-linear inequalities can be replaced by the set of linear inequalities (10c)-(10f), where $\boldsymbol{\pi}$ is the vector of dual variables associated with the bounds of the uncertainty set (4). Applying the same principle to all inequality and equality constraints, the semi-infinite robust counterpart is converted into a finite mixed integer linear programming problem.

$$\sum_{t^{'}\in[t]}(\pi^{A}_{iystt^{'}}\cdot\bar{L}_{yst^{'}}-\pi^{B}_{iystt^{'}}\cdot\underline{L}_{yst^{'}})+\sum_{t^{'}\in[t]}\sum_{i^{'}\in I^{res}}(\pi^{C}_{ii^{'}ystt^{'}}\cdot\bar{CF}_{i^{'}yst^{'}}-\pi^{D}_{ii^{'}ystt^{'}}\cdot\underline{\mathrm{CF}}_{i^{'}yst^{'}})+$$
$$\sum_{t^{'}\in[t]}\pi^{E}_{iystt^{'}}\cdot\Gamma\cdot(\bar{L}_{yst^{'}}-\sum_{i^{'}\in I^{res}}\underline{\mathrm{CF}}_{i^{'}yst^{'}})\leq(1-\epsilon_i)\cdot P^{max}_{i}\cdot u_{iyst}-p^{0}_{iyst},$$

$$\forall i\in I^{th},y\in Y,s\in S,t\in T \tag{10c}$$

$$\pi^{A}_{iystt^{'}}-\pi^{B}_{iystt^{'}}+\pi^{E}_{ystt^{'}}\geq p^{L}_{iystt^{'}},\forall i\in I^{th},y\in Y,s\in S,t^{'}\in[t],t\in T \tag{10d}$$

$$\pi^{C}_{ii^{'}ystt^{'}}-\pi^{D}_{ii^{'}ystt^{'}}-\pi^{E}_{ystt^{'}}\geq p^{C}_{ii^{'}ystt^{'}},\forall i^{'}\in I^{res},i\in I^{th},y\in Y,s\in S,t^{'}\in[t],t\in T \tag{10e}$$

$$\pi^{A}_{iystt^{'}},\pi^{B}_{iystt^{'}},\pi^{C}_{ii^{'}ystt^{'}},\pi^{D}_{ii^{'}ystt^{'}},\pi^{E}_{iystt^{'}}\geq 0,\forall i^{'}\in I^{res},i\in I^{th},y\in Y,s\in S,t^{'}\in[t],t\in T \tag{10f}$$

4. Solution method

4.1. Problem dimensionality issues

As shown in the previous section, recourse decisions made in a time period, t, depend on $\mathcal{V}^t\,(=\{\mathcal{V}_1,...,\mathcal{V}_t\})$, i.e., the history of load and IRES-CF realizations from the first time period up to t. The duality-based approach used to define the equivalent deterministic problem, therefore, leads to an extremely large MILP reformulation. Take for example the maximum production limit constraint (7c): in the deterministic formulation, this constraint would have a dimension of $\mid I^{th} \mid \times \mid Y \mid \times \mid S \mid \times \mid T \mid$, which we can denote as $\mid det. \mid$. On the other hand, the set of inequalities defining the AARC of this constraint (i.e., inequalities (10c)-(10f)) have a dimension of $\mid det. \mid \times \left(1+\frac{|T|+1}{2}\cdot(1+\mid I^{res} \mid)\right)$, according to the definition of the uncertainty set (4). That is, the dimension of each robust constraint is multiplied by a strictly positive factor which is a function of the number of time periods T and number of IRES units I^{res}, considered. Even for a moderate size problem, this can quickly lead to extremely large and intractable MILP instances. For example, if we consider a time periods set T with a magnitude of 24 hours and an RES units set I^{res} with a magnitude of 2 (e.g. wind and solar), the number of AARC constraints would be 38.5 multiples of the same set of constraints in the original deterministic formulation. The same applies for

the number of variables, were each AARC constraints set would require an additional $5 \times \left(|I|+|Y|+|S|+\frac{|T|(|T|+1)}{2}\right) + 2|I^{res}|$ dual variables and an additional $|I|\times|Y|\times|S|\times\frac{|T|(|T|+1)}{2} \times (1 + |I^{res}|)$ affine coefficient variables, compared to the original deterministic constraint formulation.

4.2. Information basis approximation

Notice that one of the most important contributors to the above dimensionality issue is the appearance of the triangular number $\frac{|T|\cdot(|T|+1)}{2}$ which exponentially increases with the number of periods considered. This factor arises since in the defined linear decision rule, the recourse variables depend on the entire history of realized uncertainty at every time period up to t, $\forall t \in T$. Following [10], we call this full affine dependency the "on-line information basis" since it -reasonably- considers that the decision maker takes into account all historical information revealed about the uncertainty realizations to adapt the recourse decision variables at the current time period.

We propose and investigate a solution method based on information basis level approximation, where, instead of considering the full affine dependency, only the most recent uncertainty realizations are taken into account to adjust the recourse variables at the current time period t. For this, we introduce a new parameter representing the information level, denoted h ($\leq |T|$), which will allow us to control how *early* the model accounts for information on uncertainty realization, to adjust the recourse variable at the current period. In this sense, the h parameter represents the number of most recent time periods that will be taken into account in the linear decision rule. If $h = |T|$, the full historical periods will be taken into account, which is equivalent to full affine dependency. If $h < |T|$, both the size of the equivalent AARC set of constraints, the associated dual variables and the affine coefficient variables will be reduced.

To implement this approximation method, the running index $[t]$ needs to be re-defined such as: $[t] \triangleq \begin{cases} \{1, ..., t\}, & \text{if } t \leq h \\ \{t-h, ..., t\}, & \text{if } t > h \end{cases}$. As an example, the number of AARC constraints

defining inequalities (10c)-(10f) will have a dimension of: $\mid det. \mid \times\Bigg(1 + 1/|T|\cdot(h+1)\cdot\left(|T|-\frac{h}{2}\right)\cdot(1+|I^{res}|)\Bigg)$, compared to the previously calculated value. This leads to a reduction in the number of constraints by a total of: $|det.|\times|I^{res}|\times\left((0.5|T|-h-0.5)+\frac{h^2+h}{2|T|}\right)$ constraints, for each robust constraint reformulation. The same calculations can be made for the reduction in the number of variables. Notice that, as logical, the reduction in the number of constraints (and variables) increases as h decreases, i.e. as we take into account less historical information. However, the relationship is non-linear and indeed is negligeable for h values that are close to $|T|$, and is only significant around low values of h. Hence, there is a clear trade-off in the level of adjustability of the recourse variables and the computational complexity. This might lead to the expectation that using this method, we considerably sacrifice optimality for computational simplicity. Indeed, we show in the next section that this is not necessarily the case: by conducting a sensitivity analysis on the quality of solutions obtained by varying the h parameter, we show that significant computational gains can be achieved while still maintaining high quality of the solution.

5. Case Study

5.1. Power system description and implementation notes

The multi-annual planning horizon covers 5 years from 2041 to 2046. The hourly system load is obtained through linear regression of the historical load time series of France for the years 2008 to 2012 (publicly available at [17]), assuming a growth of 1.5% throughout the planning years. Wind and Solar-PV capacity factors (CF) are calculated from the wind speeds and solar irradiance data obtained from the CMIP5 experiments [18] for the same time period. The cost data for the power generation technologies are based on the IEA/NEA Projected Costs of Generating Electricity report (2015) [19]. Table (1) summarizes the costs considered and the remaining technical characteristics of the power generation units.

To solve the multi-annual IGEP-UC model, each full year is approximated by 4 days optimally obtained using the method proposed in [20]. Hourly load uncertainty is set to

Table 1: Technical and economic characteristics for the different generation technologies

Technology [i]	$\bar{P}_i$ [MW]	P_i^{min} [MW]	$\bar{R}_i^{Up}$ [MWh/min]	$\bar{R}_i^{Dn}$ [MWh/min]	M_i^u [hrs]	M_i^d [hrs]	ϵ_i	C_i^{inv} [M€/MW]	C_i^{marg} [€/MWh]	C_i^s [k€]
Nuclear	1400	700	$0.5\%\bar{P}$/min	$0.5\%\bar{P}$/min	12	48	0.01	3.95	9.33	15.0
Coal	1100	550	$1.5\%\bar{P}$/min	$1.5\%\bar{P}$/min	6	10	0.06	2.08	36.67	11.26
CCGT	550	165	$5\%\bar{P}$/min	$5\%\bar{P}$/min	3	5	0.04	1.02	69.00	7.53
On-Shore Wind	240	0	/	/	/	/	0	1.9	0	/
Solar-PV	180	0	/	/	/	/	0	1.5	0	/

vary within 10% of the nominal values, while hourly IRES uncertainty is set to vary within 20% around the nominal values. The MILP optimization models are developed in the Python programming language using the Pyomo software package [21] and solved on a PC with Intel Core i7 at 3.2GHz and 8GB memory using IBM ILOG-CPLEX with an optimality gap of 0.01%. Experimental testing showed that the interior-point method (Barrier algorithm) should be used to find the root relaxation of the MILP, to avoid primal-dual degeneracy.

5.2. Sensitivity analysis on information basis approximation

We start with a reduced-size instance to conduct a sensitivity analysis on the impact of varying the information level parameter h on the planning problem solution time and quality. The horizon considered for this purpose covers only two planning years, each represented by 4 days of 24 hours. The parameter h, therefore, can vary from 1 to 24, representing the lowest to the highest information levels taken into account in the linear decision rule, respectively. Furthermore, since the ramping up and down constraints (7f) and (7g) are the only second-level constraints that are time-coupling, and where the full value of considering detailed commitment decisions appear, we compare two variations of the problems solution: one where we relax the ramping constraints and conduct the sensitivity, and the other where the ramping constraints are enforced. To ensure the proper evaluation of the quality of the solutions obtained, the integer-relaxed, fully affine dependent problem is solved as a guaranteed lower bound solution for both the ramping-relaxed and ramping-enforced MILP problems. A schematic description of how the optimality gap is compared for the purpose of the sensitivity analysis is shown in Fig. (1).

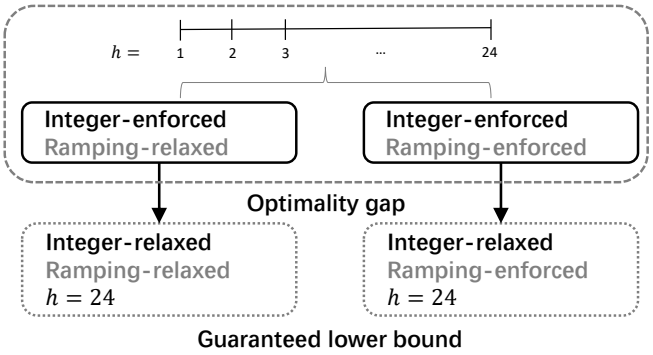

Figure 1: Schematic illustration of the process for calculating the optimality gap for both ramping-relaxed and ramping-enforced MILP problems.

Table (2) shows the optimality gap obtained for solving the problem under different values of information level parameter h, for both the ramping-relaxed and the ramping-enforced MILP problems. It is shown that in all cases, the objective function (total cost) gap is at most 1%, which is an indicator of a strong performance even for low values of h. These results are consistent with the investment decisions obtained as is shown in Table (3). These decisions are identical for the solution under the lowest ($h = 1$) and the highest ($h = 24$) information basis levels. Moreover, the standard deviation of these investment decisions across all instances is very low, indicating the consistency of these results across all problem instances. Moreover, we have found that these observations hold across the h sensitivity variations performed under different values of uncertainty budget (Γ). With respect to the computational performance, Figure (2) shows that indeed the computational time significantly decreases as we consider lower values of h. For both ramping-relaxed and ramping-enforced cases, the solution for the lowest h values is obtained within 10 to 40 seconds. Notice that this range remains consistent for the ramping-relaxed problem across all values of h, slightly increasing to a maximum of 38 seconds. For the ramping-enforced problem, a clear and significant solution time increase can be observed. For the fully adjustable problem ($h = 24$), the solution time is 4375 seconds, compared to 11, 15 and 31 seconds for the three lowest h values considered, respectively. This confirms that significant improvements can be gained in computational time while maintaining good results by using

the proposed approximated linear decision rule.

Table 2: Guaranteed optimality gap for the solutions obtained with respect to the sensitivity on the h parameter, for both the ramping-relaxed and the ramping-enforced MILP problems.

Information level (h)	1	2	3	4	5	6	7	8	9	10	11	12
Ramping-relaxed	0.37%	0.36%	0.70%	0.24%	0.40%	0.75%	0.75%	0.75%	0.16%	0.06%	0.87%	0.88%
Ramping-enforced	0.94%	0.95%	0.31%	0.50%	0.23%	0.05%	0.04%	0.49%	0.04%	0.48%	0.51%	0.26%
Information level (h)	13	14	15	16	17	18	19	20	21	22	23	24
Ramping-relaxed	0.47%	0.95%	0.80%	1.01%	0.53%	0.11%	0.26%	0.92%	0.54%	0.62%	0.40%	0.40%
Ramping-enforced	0.01%	0.03%	0.95%	0.48%	0.67%	0.61%	0.95%	0.50%	0.02%	0.97%	0.03%	0.03%

Table 3: Number of units installed as per the ramping-enforced robust MILP problem under the lowest and highest information levels h.

	Number of units			
	$h = 1$	$h = 24$	all h	
Technology			Mean	Std. dev.
Nuclear Units	31	31	31	0
Coal Units	12	12	12	0
CCGT Units	27	27	27	0
Wind Units	298	298	298.8	3.97
Solar Units	0	0	0.33	0.48

It should be noted that the variation in the solution time across different information level (h) problems is not strictly increasing. This is due to the differences in the time taken for the generic solver to solve the MILPs. Many factors, other than the problem size, can impact the solution time; for example the quality of the initial heuristic solution and the quality of the cuts generated by the solver. Notice also how by considering the ramping constraints, the computational time of the problem increases significantly even for these reduced case studies. It is, then, worthy to investigate what value are these constraints adding to the solutions of the robust power system planning problem.

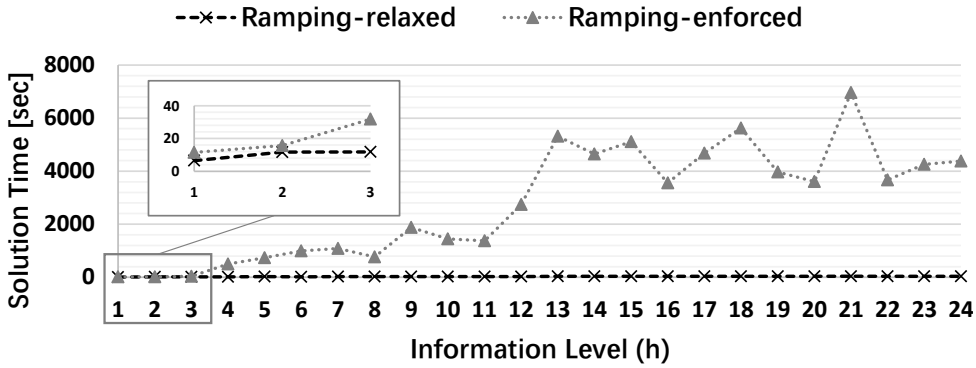

Figure 2: Impact of varying h on the computational time of the ramping-relaxed and ramping-enforced robust MILP problems.

5.3. Worst-case analysis for robust power systems planning with ramping constraints

Notice that according to the definition of the uncertainty set (4) and letting the uncertain parameters take on their full range of values ($\Gamma = 1$), the robust solution should be expected to be trivial and simply equivalent to the worst-case deterministic solution. This is since any solution that satisfies the highest hourly load ($\bar{L}$) and lowest IRES-CF ($\underline{\text{C}}\text{F}$) should be -readily- feasible to satisfy any combination of lower load and higher IRES-CF in the uncertainty range. We show that this is, indeed, the case if the time-coupling ramping constraints are ignored. However, enforcing the ramping constraints implicitly re-defines the worst-case dispatch decisions in the AARC problem so that they are no longer simply satisfying the worst load and IRES-CF, but rather also ensuring the ramping feasibility under all other uncertainty realizations of those parameters. A simple example for this effect would be to satisfy the ramping between the lowest load ($\underline{\text{L}}_t$) at t and the successive highest load ($\bar{L}_{t+1}$) at $t+1$, if the uncertainties are to be realized in such a way. More complex interactions would occur if, in addition, we consider the uncertainty of the IRES-CF. In this case, unlike the AARC method, no straightforward method exists to ensure the feasibility of these complex interactions within the deterministic nor the stochastic models.

To illustrate this effect on the system investment and operation decisions, we will consider the whole 5 years planning horizon previously described for the case study and analysis. To further highlight the impact of the detailed ramping constraints on the robust solution

obtained, we expand the hourly uncertainty of load and RES-CF to be within 20% and 50% of their nominal values, respectively. Finally, we will deploy the information basis approximation method described in the previous section to find the solution to the AARC problem. The results will be compared to the worst-case deterministic problem solution (denoted WCD), both for the ramping-relaxed and ramping-enforced cases.

Let us first consider the ramping-relaxed case; as expected, both WCD and worst-case AARC solutions are identical. The total objective value in both cases amounts to 63.36Billion€. The breakdown of the (annualized) investment, operational and load not served (LNS) costs is shown in Fig. (3). By enforcing the ramping constraints, indeed, we find that the solutions of both problems are no longer identical. Clearly, the WCD objective value in this case is higher than the one with no ramping considered. Yet, interestingly, these values are even higher for the AARC worst-case solution with a +3.10% and +12.43% increase in the investment and operational costs, respectively, and a −17.25% decrease in the LNS cost, compared to the WCD solution, as shown in Fig. (3). It is clear that properly accounting for the uncertainty withing the AARC model significantly increases the investment and operational costs of the system because of the "implicit" worst-case ramping requirements.

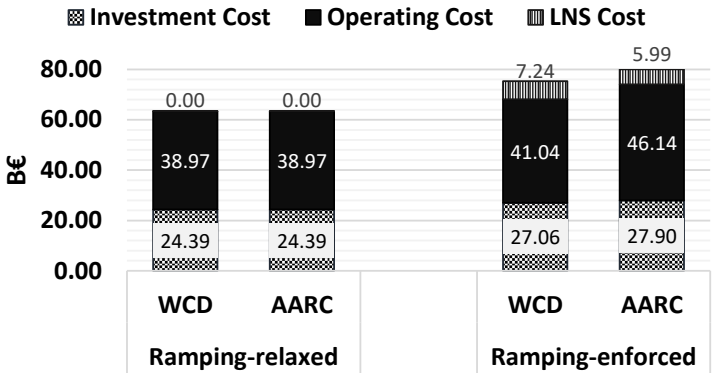

Figure 3: Breakdown of (annualized) investment, operational and LNS solution costs for the ramping-relaxed and ramping-enforced problems. Comparison between the WCD and AARC solutions.

To further understand how the uncertainties are driving the investment decisions within the ramping-enforced problems, Table (4) compares the total capacities installed per tech-

nology type for all cases considered. First, it is shown that the capacities installed are identical for both WCD and AARC solutions when the ramping is relaxed. Then, enforcing the ramping constraints leads to a clear shift in the installed capacities under the WCD solution, most notably, a shift from the least flexible nuclear capacity, to the most flexible CCGT capacity. However, the ramping-enforced AARC solution confirms that neglecting the load and RES-CF uncertainties underestimates the actual flexible capacity needed to account for the implicit worst case rampings. This is verified as per the investment decisions in a lower nuclear capacity and higher coal and CCGT ones, compared to the WCD solution.

Table 4: Breakdown of total installed capacity per technology type for the ramping-relaxed and ramping-enforced problems. Comparison between the WCD and AARC solutions.

	Capacity Installed [GW]			
	Ramping-relaxed		Ramping-enforced	
Technology	WCD	AARC	WCD	AARC
Nuclear capacity	67.2	67.2	64.4	56
Coal capacity	7.7	7.7	6.6	15.4
CCGT capacity	12.1	12.1	20.3	25.3
Wind capacity	1.68	1.68	61.7	78.9
Solar capacity	85.32	85.32	29.7	19.62

Another indicator of the superiority of the AARC solution in accounting for ramping uncertainty, is the amount of RES shedding attained for the worst-case solution. This is because RES shedding is another mean for managing inter-temporal ramping variability next to thermal units ramping capacity and load shedding. Notice in Table (5) how the WCD and AARC shedding amounts are identical for the ramping-relaxed case, and the improved RES shedding amounts as given by the AARC (total of 0.76%) compared to WCD solution (total of 4.47%), for the ramping-enforced case.

We finally discuss the solution times taken for the WCD and AARC problems. The WCD problem takes few seconds to be solved, whereas, even for a moderate h value ($h = 8$), the AARC problem can take several hours as can be seen in Table (6). Clearly, accounting for the uncertainties under the AARC approach comes at a significant computational price. It

Table 5: Breakdown of RES shedding for the ramping-relaxed and ramping-enforced problems. Comparison between the WCD and AARC solutions.

	Ramping-relaxed		Ramping-enforced	
	WCD	AARC	WCD	AARC
Wind power shedding	2.15%	2.15%	3.02%	0.82%
Solar power shedding	1.47%	1.47%	8.67%	0.56%
Total RES shedding	1.49%	1.49%	4.47%	0.76%

is important to note, however, how the proposed information basis approximation method proposed allows for tractable and high-quality solutions, whereas considering the full AARC formulation for the ramping-enforced case does not allow us to find a root-relaxation solution even after 40 hours of run-time.

Table 6: Computational time for the ramping-relaxed and ramping-enforced problems. Comparison between the WCD and AARC solutions.

	Ramping-relaxed		Ramping-enforced	
	WCD	AARC ($h = 8$)	WCD	AARC ($h = 8$)
Computation time [sec]	12	3060	13.3	25657.8

6. Conclusions

The uncertainty and intermittency of high shares of renewable energy production presents major challenges to the operational flexibility requirements in power systems expansion planning. Existing planning methods that do not explicitly consider the ramping events fail to estimate to which extent the uncertainties in system load and renewable production impact those flexibility requirements. To address this issue, this paper presents a multi-stage adaptive robust power system planning model which accounts for detailed short-term unit commitment and ramping constraints. The model accounts for the *here-and-now* commissionning and commitment decisions made robust against load and renewable generation

uncertainties, and *wait-and-see* dispatch decisions subject to uncertainty realization. To alleviate the computational burden, a solution method based on linear decision rules approximation is proposed and a sensitivity analysis is performed to confirm the effectiveness of this solution approach. A realistic-size case study is investigated and the results show how considering the detailed ramping constraints within a multistage robust model significantly improves the plans obtained in terms of operational flexibility. This is because those uncertainties re-define the worst-case ramping requirements in such a way that would not be captured within stochastic or non-causal planning models.

Acknowledgment

The authors would like to thank Dr. Elizaveta Kuznetsova and Prof. Michel-Alexandre Cardin for their contributions in the early stages of the work. This work is partially supported by the Future Resilient Systems project at the Singapore-ETH Centre (SEC), which is funded by the National Research Foundation of Singapore (NRF), Prime Minister's Office, Singapore, under its Campus for Research Excelence and Technological Enterprise (CREATE) programme. The project is administered by the National University of Singapore (NUS) under grants WBS R-266-000-089-592 and R-266-000-070-281.

References

[1] MI Alizadeh, M Parsa Moghaddam, N Amjady, P Siano, and MK Sheikh-El-Eslami. Flexibility in future power systems with high renewable penetration: A review. *Renewable and Sustainable Energy Reviews*, 57:1186–1193, 2016.

[2] Islam F Abdin and Enrico Zio. An integrated framework for operational flexibility assessment in multi-period power system planning with renewable energy production. *Applied Energy*, 222:898–914, 2018.

[3] Yixian Liu, Ramteen Sioshansi, and Antonio J Conejo. Multistage stochastic investment planning with multiscale representation of uncertainties and decisions. *IEEE Transactions on Power Systems*, 33(1):781–791, 2018.

[4] Esteban Gil, Ignacio Aravena, and Raúl Cárdenas. Generation capacity expansion planning under hydro uncertainty using stochastic mixed integer programming and scenario reduction. *IEEE Transactions on Power Systems*, 30(4):1838–1847, 2015.

[5] Heejung Park and Ross Baldick. Stochastic generation capacity expansion planning reducing greenhouse gas emissions. *IEEE Transactions on Power Systems*, 30(2):1026–1034, 2015.

[6] Jiaying Shi and Shmuel S Oren. Stochastic unit commitment with topology control recourse for power systems with large-scale renewable integration. *IEEE Transactions on Power Systems*, 33(3):3315–3324, 2018.

[7] Ershun Du, Ning Zhang, Bri-Mathias Hodge, Qin Wang, Zongxiang Lu, Chongqing Kang, Benjamin Kroposki, and Qing Xia. Operation of a high renewable penetrated power system with csp plants: A look-ahead stochastic unit commitment model. *IEEE Transactions on Power Systems*, 34(1):140–151, 2019.

[8] Aharon Ben-Tal and Arkadi Nemirovski. Robust optimization–methodology and applications. *Mathematical Programming*, 92(3):453–480, 2002.

[9] Bo Zeng and Long Zhao. Solving two-stage robust optimization problems using a column-and-constraint generation method. *Operations Research Letters*, 41(5):457–461, 2013.

[10] Aharon Ben-Tal, Alexander Goryashko, Elana Guslitzer, and Arkadi Nemirovski. Adjustable robust solutions of uncertain linear programs. *Mathematical Programming*, 99(2):351–376, 2004.

[11] Aakil M Caunhye and Michel-Alexandre Cardin. Towards more resilient integrated power grid capacity expansion: A robust optimization approach with operational flexibility. *Energy Economics*, 72:20–34, 2018.

[12] Jia Li, Zuyi Li, Feng Liu, Hongxing Ye, Xuemin Zhang, Shengwei Mei, and Naichao Chang. Robust coordinated transmission and generation expansion planning considering ramping requirements and construction periods. *IEEE Transactions on Power Systems*, 33(1):268–280, 2018.

[13] Hongxing Ye and Zuyi Li. Robust security-constrained unit commitment and dispatch with recourse cost requirement. *IEEE Transactions on Power Systems*, 31(5):3527–3536, 2016.

[14] Dimitris Bertsimas, Eugene Litvinov, Xu Andy Sun, Jinye Zhao, and Tongxin Zheng. Adaptive robust optimization for the security constrained unit commitment problem. *IEEE Transactions on Power Systems*, 28(1):52–63, 2013.

[15] Álvaro Lorca, X Andy Sun, Eugene Litvinov, and Tongxin Zheng. Multistage adaptive robust optimization for the unit commitment problem. *Operations Research*, 64(1):32–51, 2016.

[16] Alvaro Lorca and Xu Andy Sun. Multistage robust unit commitment with dynamic uncertainty sets and energy storage. *IEEE Transactions on Power Systems*, 32(3):1678–1688, 2017.

[17] RTE-France. Available at:. http://clients.rte-france.com, 2017. (Accessed on 20-10-2018).

[18] Karl E Taylor, Ronald J Stouffer, and Gerald A Meehl. An overview of cmip5 and the experiment design. *Bulletin of the American Meteorological Society*, 93(4):485–498, 2012.

[19] IEA/NEA. Projected costs of generating electricity 2015 edition. *OECD*, 2015.

[20] Kris Poncelet, Hanspeter Höschle, Erik Delarue, Ana Virag, and William D'haeseleer. Selecting representative days for capturing the implications of integrating intermittent renewables in generation expansion planning problems. *IEEE Transactions on Power Systems*, 32(3):1936–1948, 2017.

[21] William E Hart, Carl Laird, Jean-Paul Watson, and David L Woodruff. *Pyomo–optimization modeling in python*, volume 67. Springer Science & Business Media, 2012.

Titre : Modélisation technico-économique et optimisation robuste de la planification des systèmes de production électrique sous une large part de sources d'énergie renouvelables et d'événements climatiques extrêmes.

Mots clés : Modélisation technico-économique, optimisation robuste, énergie renouvelables, incertitudes de provision, flexibilité opérationnelle, résilience, changements climatiques.

Résumé : Les objectifs récents en ce qui concerne la durabilité des systèmes électriques et l'atténuation des menaces liées au changement climatique modifient la portée des exigences de planification de ces systèmes. D'une part, les systèmes durables d'énergie à faible émission de carbone qui comportent une part élevée de sources d'énergie renouvelables intermittentes (IRES) se caractérisent par une forte augmentation de la variabilité intertemporelle et nécessitent des systèmes flexibles capables d'assurer la sécurité de l'approvisionnement électrique. D'autre part, la fréquence et la gravité accrues des phénomènes climatiques extrêmes menacent la fiabilité du fonctionnement des réseaux électriques et exigent des systèmes résilients capables de résister à ces impacts potentiels. Tout en s'assurant que les incertitudes inhérentes au système sont bien prises en compte directement au moment de la prise des décisions de planification à long terme.

Dans ce contexte, la présente thèse vise à développer une modélisation technico-économique et un cadre d'optimisation robuste pour la planification des systèmes électriques multi-périodes en considérant une part élevée d'IRES et la résilience aux phénomènes climatiques extrêmes. Le problème spécifique de planification considéré est celui du choix de la technologie, de la taille et du programme de mise en service des unités de production conventionnelles et renouvelables sous des contraintes techniques, économiques, environnementales et opérationnelles. Dans le cadre de ce problème, les principales questions de recherche à aborder sont : (i) l'intégration et l'évaluation appropriées des besoins de flexibilité opérationnelle en raison de la variabilité accrue des parts élevées de la production d'IRES, (ii) la modélisation et l'intégration appropriées des exigences de résilience contre les phénomènes climatiques extrêmes dans la planification du système électrique et (iii) le traitement des incertitudes inhérentes de l'offre et la demande dans ce cadre de planification. En résumé, les contributions originales de cette thèse sont :

- Proposer un modèle de planification du système électrique intégré multi période avec des contraintes dynamiques et en considérant un pourcentage élevé de pénétration des énergies renouvelables.
- Introduire la mesure du déficit de flexibilité prévu pour l'évaluation de la flexibilité opérationnelle.
- Proposer un ensemble de modèles linéaires pour quantifier l'impact des vagues de chaleur extrêmes et de la disponibilité de l'eau sur le déclassement des unités de production d'énergie thermique et nucléaire, la production d'énergie renouvelable et la consommation électrique du système.
- Présenter une méthode permettant d'intégrer explicitement l'impact des phénomènes climatiques extrêmes dans le modèle de planification du système électrique.
- Traiter les incertitudes inhérentes aux paramètres de planification du système électrique par la mise en œuvre d'un nouveau modèle d'optimisation adaptatif robuste à plusieurs phases.
- Proposer une nouvelle méthode de solution basée sur l'approximation des règles de décision linéaires du modèle de planification robuste.
- Appliquer le cadre proposé à des études de cas de taille pratique basées sur des projections climatiques réalistes et selon plusieurs scénarios de niveaux de pénétration des énergies renouvelables et de limites de carbone pour valider la pertinence de la modélisation globale pour des applications réelles.

Title : Techno-economic modeling and robust optimization of power systems planning under a high share of renewable energy sources and extreme weather events.

Keywords : Techno-economic modeling, robust optimization, renewable energy, supply uncertainties, operational flexibility, resilience, climate change.

Abstract : Recent objectives for power systems sustainability and mitigation of climate change threats are modifying the breadth of power systems planning requirements. On one hand, sustainable low carbon power systems which have a high share of intermittent renewable energy sources (IRES) are characterized by a sharp increase in inter-temporal variability and require flexible systems able to cope and ensure the security of electricity supply. On the other hand, the increased frequency and severity of extreme weather events threatens the reliability of power systems operation and require resilient systems able to withstand those potential impacts. All of which while ensuring that the inherent system uncertainties are adequately accounted for directly at the issuance of the long-term planning decisions.

In this context, the present thesis aims at developing a techno-economic modeling and robust optimization framework for multi-period power systems planning considering a high share of IRES and resilience against extreme weather events. The specific planning problem considered is that of selecting the technology choice, size and commissioning schedule of conventional and renewable generation units under technical, economic, environmental and operational constraints. Within this problem, key research questions to be addressed are: (i) the proper integration and assessment of the operational flexibility needs due to the increased variability of the high shares of IRES production, (ii) the appropriate modeling and incorporation of the resilience requirements against extreme weather events within the power system planning problem and (iii) the representation and treatment of the inherent uncertainties in the system supply and demand within this planning context.

In summary, the original contributions of this thesis are:

- Proposing a computationally efficient multi-period integrated generation expansion planning and unit commitment model that accounts for key short-term constraints and chronological system representation to derive the planning decisions under a high share of renewable energy penetration.
- Introducing the expected flexibility shortfall metric for operational flexibility assessment.
- Proposing a set of piece-wise linear models to quantify the impact of extreme heat waves and water availability on the derating of thermal and nuclear power generation units, renewable generation production and system load.
- Presenting a method for explicitly incorporating the impact of the extreme weather events in a modified power system planning model.
- Treating the inherent uncertainties in the electric power system planning parameters via a novel implementation of a multi-stage adaptive robust optimization model.
- Proposing a novel solution method based on ``information basis" approximation for the linear decision rules of the affinely adjustable robust planning model.
- Applying the framework proposed to a practical size case studies based on realistic climate projections and under several scenarios of renewable penetration levels and carbon limits to validate the relevance of the overall modeling for real applications.

Université Paris-Saclay
Espace Technologique / Immeuble Discovery
Route de l'Orme aux Merisiers RD 128 / 91190 Saint-Aubin, France